



**Understanding Poly(2-hydroxyethyl methacrylate)
(PHEMA) Hydrogel as a Multifunctional Membrane
in Microfluidic Cell Culture Platform**

by

Weiwei Zhao

A Doctoral Thesis

Submitted in partial fulfilment of the requirements
for the award of
Doctor of Philosophy of Loughborough University

June 2014

© by Weiwei Zhao, 2014

Abstract

Cell culture technology developed at the turn of 20th century using Petri dish, which is not able to consider the microenvironment that the cells experience in vessels, has remained virtually unchanged for almost a century. However, such microenvironment associated with cell culture which usually consists of soluble factors, extracellular matrix cues, and cellular networks is difficult to reproduce experimentally with the traditional approach. In order to further elaborate complex mechanisms of cell biology through mimicking such microenvironment *in vivo*, the technical approaches together with developed microdevices are highly demanded within such a context. Microfluidic devices have been extensively developed and used for cell culture in the last two decades, which offer numerous advantages and a great potential for accurate and efficient control of the complex culturing microenvironment at cellular length scale. However, these devices are relatively complex in their fabrication and integration to fulfil multifunctional tasks for cell culture and drug testing simultaneously, which for example requires a membrane between the culture chamber and drug delivery reservoir to control microenvironment at cellular scale. This thesis is to primarily focus on the feasibility and reliability in the attempt of using poly(2-hydroxyethyl methacrylate) (PHEMA) hydrogel as an inserted membrane, based on its permeable and flexible tissue-like properties. PHEMA membrane is able to serve dual purposes in the microfluidic systems in cell culture: i) exchanging nutrients between culture chamber and drug delivery reservoir; and ii) sealing the microchannel circuits. To understand the characteristics of PHEMA hydrogel, this research particularly considered the following interconnected aspects which are likely to be encountered in the manufacturing and uses of PHEMA hydrogel as a multifunctional membrane:

- 1) Material properties:** The cytotoxicity and adhesion strength of PHEMA to cells as well as diffusion characteristics of solvable molecules (*e.g.* glucose) inside PHEMA must be experimentally examined to evaluate its bio-related properties, thereby to assess the suitability of PHEMA hydrogel as a membrane. On the other hand, an investigation on mechanical-related properties of PHEMA hydrogel, in particular its responses to uniaxial compression conditions, is also important, for instance of using numerical simulations based on hyperelastic theories, which have to be subsequently verified by experimental study.

- 2) Packaging and assembly:** This considered the practical aspects in the uses of PHEMA hydrogel as a multifunctional membrane being incorporated into a microfluidic device to evaluate its feasibility and reliability through mechanical fastening assembly process. It has been particularly concerned that the strains induced in the hydrogel membrane due to compression can be critical, and the stress concentrations in PHEMA membrane which is inevitable can cause potential failure in contact with microchannels or culture chamber under the compression.
- 3) Optimum device design:** A systematic study on the PHEMA hydrogel in the use as a membrane is necessary to determine the various factors that may be applied on cells in the microfluidic device, e.g. nutrient supply and hydrodynamic shear, which can allow identification of optimum parameters in the design and fabrication of microfluidic devices. Numerical modelling as a useful approach is able to assist the determination of various dimensional parameters associated with culture chamber and microchannel in the consideration of optimum design of such devices, where the PHEMA hydrogel can be inserted as a multifunctional membrane.

In this thesis, both experimental studies and numerical simulations have been undertaken to evaluate the characteristics of PHEMA hydrogel as a multifunctional membrane which can be potentially incorporated in the microfluidic cell culture device. From simulations, an appropriate model based primarily on Mooney-Rivlin hyperelastic theory has been established and utilised to understand the mechanical behaviour of PHEMA hydrogel when it is subject to a compressive stress. From both modelling and experimental work, the packaging and integration of microfluidic devices through mechanical fastening technique have been investigated in connection with the use of PHEMA hydrogel as a membrane. The optimum design of the microfluidic device for cell culture has therefore been proposed based on the intensive simulations and experimental validation. It is envisaged that the results from this thesis can ultimately facilitate an applicable tool set to enable bespoke microfluidic devices through optimum design and manufacturing.

Keywords: Cell culture, Microfluidic device, PHEMA hydrogel, Membrane, Hyperelastic deformation, Mechanical fastening.

List of Publications

1. **Zhao W.**, Santaniello T., Webb P., Lenardi C., Liu C.. 'A new approach towards an optimum design and manufacture of microfluidic devices based on ex situ fabricated hydrogel based thin films' integration', in *Electronic Components and Technology Conference*, May 29th ~ June 1st, 2012, San Diego, CA, USA. pp. 1997-2004.
2. **Zhao W.**, Liu C., Lenardi C., Santaniello T., Wu F.. 'Mechanical fastening to enable room temperature packaging for LOCs based on biocompatible hydrogel thin film'. *Proceedings of the 14th International Conference on Electronics Materials and Packaging*. December 13~16th, 2012, Hongkong, China, pp. 316-320.
3. **Zhao W.**, Lenardi C., Webb P., Liu C., Santaniello T., Gassa F.. 'A methodology to analyse and simulate mechanical characteristics of poly(2-hydroxyethyl methacrylate) hydrogel', *Polymer International*, 2013; **62**: 1059-1067. DOI: 10.1002/pi.4392.
4. **Zhao W.**, Liu C., Wu F., Lenardi C.. 'An investigation on the mechanical behaviour of poly(2-hydroxyethyl methacrylate) hydrogel membrane under compression in the assembly process of microfluidic system', *Journal of Polymer Science Part B: Polymer Physics*, 2014; **52**: 485–495. DOI: 10.1002/polb.23449.

Pending:

5. **Zhao W.**, Shi Z., Chen X., Yang G., Lenardi C., Liu C.. 'Mechanical characterisation of PHEMA-based natural nanofibre-reinforced hydrogel under compression'. 2014.
To be submitted to *Nanoscale*.

Acknowledgement

The path towards this thesis spans three and a half years of work and many people have been involved and contributed to the presented ideas and understanding gained. I would like to take this opportunity to express my sincere thanks to the various people who have helped me in the process of my research.

I owe my deepest gratitude to Prof. Changqing Liu and Dr. Cristina Lenardi, my supervisors, for providing me the opportunity to work in this exciting project. Their expert academic advice, continuous support and constructive comments have been a great value for creating an enthusiastic environment to carry out my work efficiently. It was a great pleasure and privilege for me to have pursued my PhD under their supervision. I also wish to thank immensely Dr. Patrick Webb from the Manufacturing Technology Centre (the-mtc), who was one of my supervisors during my first year, for his valuable suggestions and helpful ideas on the overview of the project.

I would also like to acknowledge Prof. Fengshun Wu, Prof. Guang Yang, Dr. Weisheng Xia, Dr. Zhijun Shi and Ms. Xiuli Chen based at Huazhong University of Science and Technology, Dr. Federico Gassa and Dr. Tommaso Santaniello from the University of Milan, for their kind support and advice during the Marie Curie International Research Staff Exchange Scheme (IRSES) Project (Grant No. PIRSES-GA-2010-269113). Without their crucial help and collaboration, this work would have been unsuccessful.

My thanks are also due to the Engineering and Physical Sciences Research Council (EPSRC) and the Wolfson School of Mechanical and Manufacturing Engineering of Loughborough University in support of my studentship to undertake this research.

Finally, I also wish to thank my parents, my fiancée for their love and support over the years. Their belief that I can achieve my ambition has been my incentive to work hard on this thesis.

Loughborough, Leicestershire

Weiwei Zhao

Table of Content

Abstract.....	I
List of Publications	III
Acknowledgement	IV
Table of Content.....	V
List of Tables.....	X
List of Figures.....	XI
List of Abbreviations	XX
Chapter 1. Introduction	1
1.1 Background, Research Motivation and Considerations	1
1.2 Aims and Objectives of the Thesis	4
1.3 Structure of the Thesis	6
Chapter 2. Context and Literature Review: Hydrogel-based Microfluidic System.....	10
2.1 Microfluidic Technology for Lab-on-Chip Applications	10
2.1.1 Microfluidic Systems and Their Applications	10
2.1.2 Materials for Microfluidic Device	11
2.1.3 Fabrication of Microfluidic Device	12
2.1.4 Packaging of Microfluidic Device	14
2.2 Hydrogel-based Microfluidic System for Cell Culture.....	16
2.2.1 Hydrogel and Its Classifications.....	16
2.2.2 Properties of Hydrogels	19
2.2.3 Applications of Hydrogels for Bio-purposes	21
2.2.3.1 2D or 3D Cell Culture in Microfluidic System	21
2.2.3.2 Perfusion Cell Culture	22
2.3 Summary and Thesis Tasks.....	23
Chapter 3. Research Methodology	25
3.1 Theories and Tools for Modelling	25
3.1.1 Material Characteristics and Simulation Theories	25
3.1.1.1 Mechanical Deformation Models	25
3.1.1.2 Diffusion Mechanism Models	28

3.1.2 COMSOL Multiphysics.....	30
3.2 Equipment and Experiments	30
3.2.1 Equipment and Testing Techniques.....	30
3.2.2 Synthesis and Preparation of PHEMA Hydrogel	32
3.2.3 Swelling and Drying of PHEMA Hydrogel	35
3.2.3.1 Swelling and Washing of PHEMA Hydrogel.....	35
3.2.3.2 Drying of PHEMA Hydrogel	38
Chapter 4. Diffusion and Biocompatible Properties of PHEMA Hydrogel	41
4.1 Introduction	41
4.2 Diffusion Properties of Swollen PHEMA Hydrogel	42
4.2.1 Kinetic Theories of Diffusion	42
4.2.2 Experimental Methods	43
4.2.3 Results and Discussion	45
4.2.3.1 Glucose Release Rate.....	45
4.2.3.2 Capacity of Absorption.....	47
4.3 Cytotoxicity effect of PHEMA on cells.....	48
4.3.1 Principle and Methods	48
4.3.1.1 Live/Dead Cell Staining Imaging.....	48
4.3.1.2 Cell Viability Measurement	49
4.3.2 Preparation of PHEMA Substrates and Cells.....	50
4.3.3 Results and Discussions.....	52
4.4 Adhesion Strength of Cell-PHEMA.....	54
4.4.1 Principle and Method.....	54
4.4.2 Details of the Agitator and Experimental Set-ups.....	57
4.4.3 Results and Discussions.....	60
4.5 Summary	62
Chapter 5. Mechanical Characteristics of PHEMA Hydrogel under the Compression	64
5.1 Introduction	64
5.2 Theoretical Basis in Simulation	64
5.2.1 Mooney-Rivlin Model	64

5.2.2 Neo-Hookean Model.....	67
5.3 Mechanical Behaviour of Fully Swollen PHEMA Hydrogel.....	68
5.3.1 Uniaxial Compressive Test to Determine the Coefficients for Simulation	68
5.3.1.1 Apparatus and Experimental Approach	68
5.3.1.2 Uniaxial Compressive Test Results	69
5.3.2 Simulations of Mechanical Behaviour of Fully Swollen PHEMA Hydrogel.....	73
5.3.3 Fully Swollen PHEMA Hydrogels under the Cycling Compressive Loads	77
5.3.3.1 Experimental Approach	77
5.3.3.2 Test Results and Discussions.....	79
5.4 Mechanical Behaviour of Partially Swollen PHEMA Hydrogel	83
5.4.1 Uniaxial Compressive Test on Specimens with Different Degree of Swelling	83
5.4.1.1 Experimental Approach	83
5.4.1.2 Test Results and Discussions.....	83
5.4.2 Simulations of Mechanical Behaviour of Partially Swollen PHEMA Hydrogel	85
5.5 Summary	86
Chapter 6. Assembly Process with PHEMA Membrane under Mechanical Fastening	87
6.1 Introduction	87
6.2 Determination of Critical Leakage Pressure by Simulation	88
6.2.1 Principle Basis and Model Building.....	88
6.2.2 Simulation Results and Discussions	89
6.3 Determination of Critical Leakage Pressure by Experiments	91
6.3.1 Design and Manufacturing of Testing Chip	91
6.3.2 Leakage Testing Device (LTD) Assembly and Installations	93
6.3.3 Experimental Results and Discussions	96
6.3.3.1 Material Failure Due to Fastening.	96
6.3.3.2 Determination of Maximum Allowed Fluid Pressure (P_f).....	97
6.4 Mechanical Behaviour of Hydrogel Membrane in Microchannel	100
6.4.1 Simulation of the Mechanical and Geometrical Response of Membrane.....	101
6.4.2 Experimental Validation for the Simulation of Membrane.....	108
6.4.3 Passable Rate and Optimum Design of Microfluidic Channels.....	111

6.5 Mechanical Behaviour of Hydrogel Membrane in Culture Chamber	113
6.5.1 Installation of PHEMA Membrane	114
6.5.2 Drastic Stress Distribution on PHEMA Membrane in Culture Chamber.....	115
6.6 Summary	119
Chapter 7. Dynamic Perfusion Process in Microfluidic Culture System.....	121
7.1 Introduction	121
7.2 Theoretical Basis	121
7.2.1 Fluid Dynamics	121
7.2.2 Diffusion in Hydrogel.....	122
7.2.3 Diffusion and Reaction in Solution	123
7.3 Simulation Details	124
7.3.1 Geometry Building	124
7.3.2 Determination of Input Parameters	125
7.4 Results in Culture Chamber	127
7.4.1 Nutrient Supply to Cells	127
7.4.2 Fluidic Shear Stress on Cells.....	130
7.4.3 Determination of Inflow Velocity for Perfusion Culture	132
7.4.4 Dimensional Effects on Nutrient Supply	133
7.4.5 Dimensional Effects on Fluidic Shear Stress	135
7.4.6 Effect of Location of the Microchannel on Shear Stress.....	136
7.5 Results in Whole System	139
7.5.1 Glucose from Culture Chamber to Drug Delivery Reservoir	139
7.5.2 Testing Drug from Delivery Reservoir to Culture Chamber	141
7.6 Discussions.....	143
7.6.1 Optimum Design of the Culture Chamber	143
7.6.2 Experimental Validation of Simulations	144
7.7 Summary	146
Chapter 8. Conclusions, Recommendations and Future Works.....	148
8.1 Main Conclusions.....	148
8.1.1 Properties of PHEMA Hydrogel Material.....	148

8.1.2 Packaging for PHEMA-Based Microfluidic Device	149
8.1.3 Cell Culture in PHEMA-Based Microfluidic Device	150
8.2 Recommendations for Optimum Design of Microfluidic Device	151
8.3 Future Work	152
References	154
Appendices	169
A1 Dimensions of Connector and Chips	169
A2 Calibration Certificate for Compressive Testing Machine	172
A3 Chemicals Sheets	176

List of Tables

1-1 Requirements of microfluidic devices according to biological users	2
3-1 Summary of diffusion models and their corresponding hydrogels	28
3-2 Dimensions of PHEMA specimens	34
4-1 Process of the cumulative release experiment to determine diffusion characteristics of glucose in PHEMA	43
4-2 Process of the cumulative release experiment to determine the capacity of absorption of PHEMA hydrogel on glucose molecules	44
4-3 Geometric information of the specimens used in the cumulative release experiment (Purpose II) and the capacity of absorption	48
4-4 Summary of results and conclusions in Chapter 4	63
5-1 Summary of the RMS method applied to different sizes of PHEMA specimens based on Mooney-Rivlin and neo-Hookean model simulation analysis	76
5-2 Mooney-Rivlin coefficients for PHEMA specimens with various degree of swelling	85
6-1 List of P_f with respect of P_d from numerical simulation	90
6-2 Various values of compressive strains used in this study, in terms of combinations of spacers and PHEMA membrane with different thickness	94
6-3 Comparison of P_f values from simulation and experiment	100
6-4 Material properties and modelling setup used in the simulation	102
6-5 Geometric parameters of microchannels and compressive strains assigned in the simulations	102
6-6 Protrusion [μm] versus variable depth of channel, from simulation	108
7-1 Summary of glucose concentration inside and outside of cells from literature of Foley <i>et al.</i> and the assumption in this work	125
7-2 Summary of the parameters in simulation	127
7-3 Averaged concentration of testing drug with respect to culture chamber inflow velocity	143

List of Figures

1-1 Schematic diagram of the microdevice used to culture cells. Three layers, two thermoplastic layer and one hydrogel membrane, make up the device as two closed microfluidic system, culture chamber at top and drug delivery reservoir at bottom. Cells are cultured in the culture chamber. The molecules exchange between culture chamber and drug delivery reservoir are taking place all the time, through diffusion in hydrogel membrane material.	3
1-2 Overview of the thesis structure. The relationships between chapters are illustrated in the flow chart, especially the inter-correlations between the original research chapters (Chapter 4, 5, 6 and 7). It depicts that the results from Chapter 4, 5 and 6 are contributing to the simulation work in Chapter 7.....	7
2-1 (a) Molecule of HEMA in chemical formula, and simplification of its chemical formula. (b) The schematic diagram of the process of two HEMA molecules merged together through reaction. (c) The structure of polymer chain. (d) Molecule of EGDMA in chemical formula. (e) Structure of polymer chains connected by crosslinker EGDMA. (f) 2D schematic diagram of the network structure of the polymers/hydrogels.	17
3-1 (a) Stress-strain correlation for elastic-plastic material, e.g. metal. (b) Stress-strain correlation for hyperelastic material, e.g. hydrogel or rubber. (c) Stress-strain correlation for viscoelastic material, e.g. amorphous polymers, semicrystalline polymers.	26
3-2 Schematic diagram of the fabrication process of a PHEMA membrane. (a) Settings of the mould; (b) Injection of the polymerising mixture solution; (c) Assembly by compressing, forms a closed chamber for polymerisation of PHEMA; (d) and (e) Disassembly of the mould and extract PHEMA after polymerisation completed.	33
3-3 Swelling and washing process for PHEMA hydrogel. The ideal process of changing the ethanol concentration outside the PHEMA specimen is not achievable, and the actual swelling process is an approaching replica process to the ideal process, which obeys Fick's diffusion law.	36
3-4 (a) Experimental data record on the Degree of Swelling of PHEMA specimen against time under drying environment with 60 Celsius degrees. (b) The pictures of the PHEMA cylindrical specimen in swollen status and dried status. These two specimens have same initial dimensions after synthesis.	38

4-1 (a) Release profile of glucose from PHEMA hydrogel in PBS buffer solution at 37 Celsius degree for 24 hours. (b) linear plot of $\ln(M_t/M_\infty)$ versus $\ln(t)$, to determine the diffusion exponent. The equation of the linear fit of the data is shown. Each set of data was the value averaged from four parallel experiments.	46
4-2 Bar graph of the amount of glucose detected from the PBS buffer solution versus the time. Sum the amount of glucose from all the refresh PBS buffer solutions, the amount of glucose absorbed by PHEMA hydrogel specimen can be obtained.	47
4-3 Schematic diagram of culturing of cells on PHEMA hydrogel substrate in culturing well of a 96-well plate. The thickness of PHEMA hydrogel membrane is 1 mm. Cells are incubated upon the surface of the PHEMA membrane. Culturing media is filled in the whole chamber.	50
4-4 Image of fibroblasts cultured on PHEMA membrane over 24 hours, observed by optical microscope (Olympus IX71). (b) Image of fibroblasts cultured on PHEMA membrane over 24 hours, in same visual range and same scale of the image of (a), which is observed by fluorescence microscope (Olympus DP71, TH4-200). Colour reference: Green for live cell. ...	52
4-5 SEM photographs of fibroblasts which are cultured on PHEMA membrane. (a) Image of highly differentiated active fibroblast and an inactive fibroblast seed. The magnification is 2000x. (b) Image of an active fibroblast with two branched cytoplasm. The magnification is 4000x.	53
4-6 Cell viability test on HUVECs for 24 hours and 48 hours, was conducted using CCK-8 assay. Cells are incubated on PHEMA substrate in PHEMA group, and incubated normally (without PHEMA) in Control group. All incubation of cells was performed under 37°C and 5.0% CO ₂ atmosphere. The error bar of each group consists of the results from three parallel tests.	54
4-7 Schematic flow chart of the principle of the experiments to examine the cell-PHEMA adhesion strength. (a) HUVECs spread and occupy the surface of PHEMA membrane after at least 24 hours incubation. (b) Urging the culturing media flows rotationally at the speed of ω , shear stress with gradient (linear increasing) is formed and applied on cells. (c) Stop rotation and remove the culturing media with detached cells after 5 mins rotation, cells in a circle with radius of $R_{critical}$ will remain on the PHEMA surface..	55
4-8 (a) Schematic diagram of the set-ups of rotated fluid flow. Agitator rotates at a certain speed of ω , it forces the culture medium rotate due to fluidic viscosity. Thus the fluidic shear stress τ will be applied on cells with linear gradient, which is depicted in (b), the top view of the PHEMA	

substrate with rotational flow. (c) Domain of fluid flow in the gap between the bottom of the agitator and the cells.	56
4-9 (a) Circuit diagrams of the agitator, aiming to achieve the rotation at a constant speed. (b) Photograph of the assembly of the agitator, on the basis of the electronic circuit diagram.	58
4-10 (a-f) images of PHEMA membrane after shear testing from optical microscope. This set of images were taken through the same magnification. (g) shows the location of the images (a-f) where they were taken.	61
5-1 Schematics of experimental setup: Water in the container offered the proper aqueous environment for hosting the PHEMA hydrogel specimens during the whole testing process. ..	68
5-2 (a) Uniaxial compressive stress vs. compressive strain plots of five specimens in size of Ø32 mm testing group. (b) Error Bar Graph plot of ultimate strain of PHEMA specimens for both testing group including original specimen failure data points, marked as [].	70
5-3 Difference in compression behaviour (compressive load versus compressive extension) between specimens with different dimensions: same height, different diameter.....	70
5-4 Difference in compression behaviour (stress <i>versus</i> strain) between specimens with different dimensions: same height, different diameter. (a) Engineering stress <i>versus</i> engineering strain. (b) True stress <i>versus</i> true strain.	71
5-5 (a) Barrelling effect in the compressive tests. Lubricant was used in the test to reduce the barrelling effect on specimens. (b) Mooney-Rivlin analysis by operating a linear programming of $\sigma/2(\lambda-\lambda^{-2})$ and $1/\lambda$ on the initial stage of deformation in order to extract the Mooney-Rivlin coefficients. The data from initial stage of deformation has minimum effect by barrelling due to friction	72
5-6 (a) Schematic diagram of the 2D-axisymmetric model for Ø32 mm PHEMA specimens. (b) Simulation result in terms of displacement gradient for the Ø32 mm PHEMA specimens based on Mooney-Rivlin theory, compressive strain is 20%.	74
5-7 Comparison of experiment and simulation based on the Mooney-Rivlin (MR) model and the neo-Hookean (NH) model in (a) PHEMA specimens of Ø18 mm and (b) PHEMA specimens of Ø32 mm.	75
5-8 Flowchart of cycling compressive tests setup.	78

5-9 (a),(c),(e) corresponding to Displacement-Time graph, Velocity-Time graph and Phase space portrait, are the graphs for the actuator motion on PHEMA specimen up to 20% compressive strain. (b), (d) and (f) are the graphs for PHEMA specimen up to 30% compressive strain.....	80
5-10 (a) Initial 50 seconds of stress response to the cycling compression for PHEMA specimen. (b) Stress-strain curves for PHEMA specimen. 100 cycles of compression under the strain rate of 0.017 s^{-1}	81
5-11 (a) Schematic diagram of stress-strain behaviour for material with significant hysteresis effect. Loading and Unloading area are indicated in the diagram. (b) Ratio between Unloading area and Loading area with respect to cycle numbers, for the PHEMA specimen under cycling compression.	82
5-12 Initial Elastic Modulus for PHEMA specimen in variable degree of swelling ranging from 1 to 1.45. Trendline to indicate the general.	84
5-13 Compressive stress-strain curves of PHEMA specimen in different values of degree of swelling (DOS) at 1.1, 1.3, 1.35, 1.45, respectively. The compressive tests were performed perpendicular to the longitudinal direction of the cylindrical PHEMA specimen. The solvent for swelling is distilled water.	84
5-14 Compressive stress-strain curves of PHEMA specimen from experiments (solid curves) and simulations (dashed curves) versus degree of swelling (DOS) at 1.1, 1.3, 1.35, 1.45. The simulations established based on Mooney-Rivlin theory with coefficients C_{01} and C_{10} which are shown in Table 5-2.	85
6-1 (a) Schematic diagram of device cross-sectional packaging structure. (b) Packaging pressures general distribution on the structure during operating condition. (c) Schematic diagram of liquid leakage situation due to high fluid pressure.	88
6-2 The dark areas are the force applied area, pressure direction is shown along the arrows. (a) Distribution pressure applied (Cover). (b) Fluid pressure applied (Fluid). (c) Fixed area (Substrate). All dimensions in mm.	89
6-3 Displacement of central point s [μm] versus fluid pressure P_f [kPa]. Under mechanical compression of $P_d=5$ kPa, the displacement ' s ' reaches zero when the fluid pressure is 9.922 kPa.	90
6-4 Schematic diagram of a microfluidic circuit in a stacked, PHEMA thin film sealed PMMA chip. 91	

6-5 Overview of PMMA chip. Each independent channel consists of ports, T-Channel and L-Channel, used as in/outlet, testing channel and leakage indicative channel respectively.	92
6-6 (a) Cross-section of the channel in PMMA substrate; depth ranges from 200 μm to 1000 μm on each channel sets. (b) Cutter geometry of the micro-milling machine used in Testing Chip manufacturing.	93
6-7 Two parameters have to be measured to calculate the compressive strain of the hydrogel membrane: t_{spacer} and t_{PHEMA} . (a) All components are assembled before the fastening process. PHEMA membrane covers all the channels and is inserted between the two PMMA plate. (b) The microfluidic system is completely assembled by fastening the screws. The fluid inside the microchannels is sealed by membrane which has a protrusion into the cavity of the channels.	94
6-8 Assembly process of the leakage testing device. (a) PHEMA film is positioned over the flat PMMA surface in the region defined by the metallic spacer and (b) top PMMA layer is positioned; the micro-milled fluidic circuits cover the whole hydrogel membrane. [(c) and (d)] Top aluminium jig is positioned and then controlled compression is applied [(e) and (f)].	95
6-9 Schematic diagram of the flow measurement setup.	96
6-10 (a) Failed PHEMA hydrogel membrane, uninstalled from 30% compressive strain. Cracks traced on microchannel edges, especially on the ports. (b) Optical microscope image of the membrane crack on the channel. (c) Normal PHEMA membrane surface image from optical microscope, act as reference when comparing with (b).	97
6-11 Images of the status (Sealed or leaked) of microchannel/port from optical microscope, taken under room temperature. (a) and (c) Microchannel/port operation without leakage, empty in L-Channel. (b) and (d) Microchannel/port operation with leakage, L-Channel filled with red liquids. (e) Schematic diagram for sensor pressure reading changes with time during leakage testing, the peak value of pressure donates the critical fluid pressure, which followed by a pressure collapse due to leakage.	98
6-12 Error bar graph of ultimate fluid pressure value on compressive strain of (a) 10%, (b) 20% in different depth of microchannels. (c) The median of data plot on 10% and 20% strain versus various depths of microchannels.	99

6-13 Distribution of membrane displacements (a) and (c) in millimetre, and Von Mises stress distributions (b) and (d) in Pascal, under the compressive strain of 10% for (a) and (b), and 20% for (c) and (d) is 20%. The depth of channel is 0.6 mm, dip angle is 15°.	103
6-14 Internal stress distributions in Pascal due to different dip angle of channel at 0° (a,c) and 30° (b,c) under the compressive strain of 10%(a,b), 20%(c,d).The depth of channel is 0.6mm, width of channel is 0.55 mm.	104
6-15 Internal stress distributions in Pascal with respect to different width of channel at 0.55 mm (a,c), and 1.20 mm (b,d) under the compressive strain of 10% (a,b), and 20% (c,d). The depth of channel is 0.6 mm, dip angle is 15°.	105
6-16 Membrane protrusion and Von Mises stress near the edge of channel as a function of width of channel under 10% compressive strain. The protrusion of membrane in channel refers to the value of 'r' in Fig.6-18; The Von Mises stress on membrane is selected near the edge of the microchannel (without numerical stress singularity), based on the location shown in Fig.6-13.	106
6-17 Schematic diagram of a microfluidic circuit in a stacked format, PHEMA thin film (membrane) is used to sealed PMMA chip. Cross-section inserted allows for a clear observation of the mechanical behaviour of PHEMA hydrogel membrane in microchannels.	108
6-18 Cross-section's view of PHEMA hydrogel membrane packed in LOC, (a) channel depth 600 μm , compressive strain 10%; (b) channel depth 600 μm , compressive strain 20%; (c) channel depth 500 μm , compressive strain 10%, with membrane failure; (d) channel depth 300 μm , compressive strain 20%, with microchannel blocked.	109
6-19 Membrane protrusion versus the microchannel depth under the compressive strain of 10% and 20%. The solid curve is based on the simulation under 10% compressive strain and the dashed curve is based on the simulation under 20% compressive strain.	111
6-20 Passable rates as function of aspect ratio of microchannel obtained from simulation: inclusion is a schematic diagram of channel with protruded membrane to illustrate the passable rate. .	112
6-21 Schematic diagram to define the three types of constraint for PHEMA membrane (inserted blue rectangle): 1) Two-sides constraint 2) One side constraint; and 3) Free-standing.	114

6-22 (a) The culturing well in multi-layered microfluidic device (half structure). Schematic diagram of modelling setups in 2D (c) which is extracted from 3D geometric modelling (b) to simulate the behaviour of PHEMA membrane under the mechanical fastening bonding.	115
6-23 (a) Simulation setup on PHEMA membrane to analyse stress drop. (b) Two-dimensional plot with colour bar, in terms of distribution of Von Mises stress in PHEMA hydrogel membrane under 10% strain. (c) The graph under the model shows the stress tensor versus top boundary of PHEMA membrane when membrane compressed by 10% strain.	116
6-24 (a) Two-dimensional plot with colour range bar, indicating the distribution of stress on longitudinal direction 'z'. (b) Curves of stress vector on longitudinal direction 'z' versus distribution at the cross-sectional length of the PHEMA under 10%, 20%, 30% compressive strains. Approximate 1 mm length of 'stress buffer area' (2mm-3mm) can be determined by the stress distribution, which connects the compressed PHEMA and free standing PHEMA.....	117
6-25 (a) Two-dimensional plot with colour range bar, indicating the distribution of stress on longitudinal direction 'r'. (b) Curves of stress vector on radial direction 'r' versus distribution at the cross-sectional length of the PHEMA under 10%, 20%, 30% compressive strains. Approximate 1 mm length of 'stress buffer area' (2mm-3mm) can be determined by the stress distribution, which connects the compressed PHEMA and free standing PHEMA.....	118
7-1 (a) Fluid domain in the microdevice, culture chamber and drug delivery reservoir, built in 3D in simulation. (b) Culture chamber after symmetric transform. The hydrogel membrane on the bottom of the culture chamber has been highlighted in blue.	124
7-2 (a) Colour range: distribution of glucose in the equilibrium state under the conditions of $c_{in}=25$ mol/m ³ , $v_{in}=0.1$ mm/s. Isosurface of glucose concentration in the equilibrium state, maximum concentration at inlet then gradually decrease towards the bottom of the chamber, which is the location of cells. (c) Streamlines of fluid flow in the culture chamber.	128
7-3 (a) Correlation between minimum glucose concentration around cells (c_g) and inflow velocity (v_{in}), from simulation. (b) Correlation between glucose consumption rate for single cell ($R_{glucose}$) and inflow velocity (v_{in}), based on Eqn.7-6. (c) Enlarged plotted data from (b)	129
7-4 (a) Velocity gradient of the fluid in culture chamber, when inflow velocity is 0.5 mm/s. (b) Field of hydrodynamic shear stress in culture chamber, when inflow velocity is 0.5 mm/s. The white arrows in (a) and (b) indicates the velocity field of fluid in chamber. (c) Enlarged graph of fluidic	

shear stress gradient and the velocity streamline at the bottom of chamber. The plot is the shear stress along the central line of the bottom of chamber, maximum stress at inlet, minimum stress at centre.	131
7-5 The correlation between maximum shear stress around cells (τ_{max_cell}) and inflow velocity (v_{in}), obtained from modelling. The maximum adhesion strength is tested in Section 4.6 of this thesis. Cell type: HUVECs. Substrate: PHEMA hydrogel.	132
7-6 The dimensional effects of culture chamber (radius and height) on the glucose concentration around cells, based on the configuration of culture chamber which is shown in Fig.7-1b. The inflow glucose concentration is 25 mol/m ³ due to the properties of culture medium. The inflow velocity is assigned as 0, because it gives minimum glucose concentration around cells according to Fig.7-3a.	134
7-7 The relationship of maximum shear stress around cells (τ_{max_cell}) and inflow velocity (v_{in}), with respect to (a) the height of chamber h , when $r=2.5$ mm; and (b) the radius of chamber r , when $h=1.5$ mm. Increase of h , or decrease of r , can result in larger maximum allowed inflow velocity (v_{high}).	135
7-8 (a) Original design of the culture chamber with channels. (b) Definition of ' d ', the distance of channel to the surface of cells.	137
7-9 The fluid velocity (arrows) and velocity streamlines (black curves) in vary value of ' d ', which is ranging from 0.5 to 5.5 mm. Vortex flow can be found in (c), (d), and (e) at the corner of the chamber.	137
7-10 (a)~(f) Spatial distribution of shear stress on the bottom of the culture chamber. (g) The schematic diagram of the settings of the simulation. Scale bar of the distribution is given, red for maximum shear stress, blue for minimum shear stress. (h) The relationship between the maximum shear stress around cells (τ_{max_cell}) and the distance between channel and cells d	138
7-11 Sectional view of all the fluidic domains including culture chamber, membrane and drug delivery reservoir. The colour illustrates the distribution of glucose concentration in the whole system under the equilibrium. The initial constraints at inlets are indicated at the corresponding places. The glucose concentration in cells is 8 mol/m ³ . Glucose transport from culture chamber to drug delivery reservoir through diffusion by PHEMA hydrogel membrane.	140

7-12 Sectional view of all the fluidic domains including culture chamber, membrane and drug delivery reservoir. The colour illustrates the distribution of testing drug concentration in the whole system under the equilibrium. The initial constraints at inlets indicated that the corresponding places. Drug molecules are transported from drug delivery reservoir to culture chamber through diffusion by PHEMA hydrogel membrane.	141
7-13 Sectional-inside view of the fluidic domains. Colour map shows the distribution of testing drug concentration with respect to the various inflow velocities at <i>Inlet 1</i>	142
7-14 (a) The original structural design of the multi-layers microfluidic device, which is illustrated in the Chapter 1. (b) the optimised structure of the device which satisfies the required values of the distance (d) between channels and cells. r is the radius of the culture chamber, h is the height of the culture chamber, h_c is the height of microchannel.	144
7-15 Schematic diagram of the prototype system to verify the function of culture chamber. PHEMA membrane is used to seal the microchannel system, and PHEMA substrate is used to replicate the environment for cells which is shown in Fig.7-14b. Fluid flow rate in the whole system is controlled by the micropump.	145

List of Abbreviations

APS	- Ammonium Persulfate
CCK-8	- Cell Counting Kit-8 assay
CFD	- Computational Fluid Dynamics
CNC	- Computer Numerical Control
COD	- Coefficient of Determination
DC	- Direct Current
DMEM	- Dulbecco's Modified Eagle Medium
DOS	- Degree of Swelling
ECM	- Extracellular Matrix
EGDMA	- Ethylene glycol dimethacrylate
FBS	- Fetal Bovine Serum
FEA	- Finite Element Analysis
HEMA	- 2-Hydroxyethyl methacrylate
hMSCs	- Human Mesenchymal Stem Cells
HUVECs	- Human umbilical vein endothelial cells
MUMPs	- Multifrontal Massively Parallel Solver
MTS	- 3-(4,5-dimethylthiazol-2-yl)-5-(3-carboxymethoxyphenyl)-2-(4-sulfophenyl)-2H-tetrazolium
MTT	- 3-(4,5-dimethylthiazol-2-yl)-2,5-diphenyltetrazolium bromide
PBS	- Phosphate Buffered Saline
PC	- Polycarbonates
PDE	- Partial Differential Equation

PDMS	- Poly(dimethylsiloxane)
PEG	- Poly(ethylene glycol)
PHEMA	- Poly(2-hydroxyethyl methacrylate)
PMMA	- Poly(methyl methacrylate)
PNIPAAm	- Poly(N-isopropylacrylamide)
PVA	- Poly(vinyl alcohol)
RMS	- Root Mean Square
SEM	- Scanning Electron Microscope
TCPS	- Tissue Culture Polystyrene
TEMED	- N,N,N',N'-Tetramethylethylenediamine
UV	- Ultra Violet
VPTT	- Volume Phase Transition Temperature
vol.%	- Volume Percentage
wt.%	- Weight Percentage
XTT	- 2,3-bis-(2-methoxy-4-nitro-5-sulfophenyl)-2H-tetrazolium-5-carboxanilide

Chapter 1. Introduction

1.1 Background, Research Motivation and Considerations

Cell culture techniques, developed at the turn of the 20th century, are still today a fundamental tool in the study of cell function, tissue engineering and pharmacology. However, for almost a century, the traditional cell culture technology, consisting of plating cells in vessels with a homogeneous substrate, media and reagents, has remained virtually unchanged [1]. To further investigate the complex mechanisms of cell biology, a better technique, which is able to mimic the cell microenvironment *in vivo*, is needed. This microenvironment consists of soluble factors, extracellular matrix cues, and cellular networks that have proven difficult to reproduce experimentally using conventional techniques [2]. This level of control of microenvironment is potentially achievable by exploiting micro-technology, such as microfluidics. Microfluidics is a technology of fluid control at micro- or nano- volumes in fluidic networks or channels, which are fabricated onto glass, silicon or polymer substrates. Generally, microfluidic system can provide the microenvironment at cellular scale with closely mimicked *in vivo* environment through spatial and temporal control of solution flow and concentration distributions [3]. In the past ten years, more and more literature about cell culture device, which is fabricated using microtechnology, are reported. Despite these successful developments, culturing cell on microdevice remains a major challenge. For instance, the operation of devices integrating multi-functions is complex to use, thus it restricts the fully access of end-users to the microdevice performance. To address such kind of challenges, the vision of this work is to design and develop a highly integrated multi-material microfabricated platform of highly functional but simple to be operated by a biologist who has no background or expertise of microfabrication. This has to be involved with handling of multi-materials to enable integration of different fabrication strategies and technologies by utilising different types of materials.

Hydrogels possess many characteristics that mimic biological systems and microenvironments, such as the cross-linked nature of the extracellular matrix (ECM), and tissue-like properties, such as water content and permeability to oxygen and metabolites. Using hydrogel as one of the components of the microdevice, allows the cell adhesion and proliferation occur on the hydrogels. Thus, the microdevice that uses hydrogels as a functional interface can take many advantages both

from optimum design of microfluidic structure (polymer, e.g. PMMA) and hydrogel materials, where material properties of hydrogel such as cellular scale network topography and mimicked microenvironment for cells may be exploited.

This study also considers the needs of a microfluidic device for automatic culturing cell at long-term period, inputting testing drugs simply and individually and being reused through disassembly and reassembly routines. By using this device, it will highly reduce the difficulties and complexities that may be preset to the end-users who is investigating the effects of various drugs on living cells. Requirements from the biological end-users, which are based on the desire of people from the biomedical group of University of Milan, were collected and listed in Table 1-1. Thus, the design of microfluidic culture platform in this study has to meet the requirements such as simple and easy to operate, low fabrication cost and high capability.

Biological User Requirements	Importance
1. Reduced inspection labour (around 1.5 hours for 96 standard procedure)	High
2. Long-term culture possible up to 30 days	High
3. Space for 50,000 cells/well (Approximately at least 3mm diameter)	High
4. Simple to use, e.g. only operation for user is pipetting steps	High
5. If not self contained, it has to be fit into an incubator	High
6. Disposable, low cost or reusable	Medium
7. No use of extra equipment unfamiliar to biologists	Medium
8. Reduced culture fluid replenishment labour over 96 well plate	Medium
9. Can handle non-adherent and adherent cells	Low
10. Allow optical observation	Low

According to these requirements listed in Table 1-1, a multi-layer structured hydrogel-based microfluidic platform for cell culture is proposed and shown in Fig.1-1. Two microfluidic chips with culture chamber and drug delivery reservoir, which are made of thermoplastic (Poly(methyl methacrylate) (PMMA)), are assembled with an inserted hydrogel membrane (Poly(2-hydroxyethyl methacrylate) (PHEMA)). The packaging technology is required to hold the assembly together and provide a reliable fluid seal.

Such designed device is able to fulfil the following tasks: 1) cells will be kept and cultured in the culture chamber (upper chamber) at the thermoplastic top layer, surrounded with dynamic culture

medium which is carrying oxygen, glucose and other necessary nutrients. 2) The culturing of cells will be achieved by controlling and adjusting the fluid flow or perfusion time of the culture system in upper chamber, independent to the aqueous environment chamber (lower chamber) in bottom layer. 3) Solution containing drug or other small molecules, for the purposes of testing the reaction of cells to these molecules, is perfused into the drug delivery reservoir through microchannels. 4) These drugs will be delivered into the culture chamber through the hydrogel membrane thanks to the diffusion characteristics of hydrogel materials.

Therefore, the characteristics of such device design can be summarised as follows:

- System can treat culturing of cells and testing of cells individually, without any interruption, which is offering a single variable environment for research on cells.
- Based on microfluidic structure, the usage of solutions is at small amount, thus highly reduced the consumption of culture medium and other expensive growing factors for cells.
- Using the diffusion properties of hydrogels to delivery drugs into the culture chamber and deliver the excreta of cells out of the culture chamber.
- Using hydrogels' rubber-like mechanical property for sealing the device to achieve a reliable bonding and closed microfluidic environment when system operating.
- The novel packaging method, e.g. through mechanical fastening, enables disassembly and reassembly bonding in room temperature, without the assistance of heating source or adhesives.

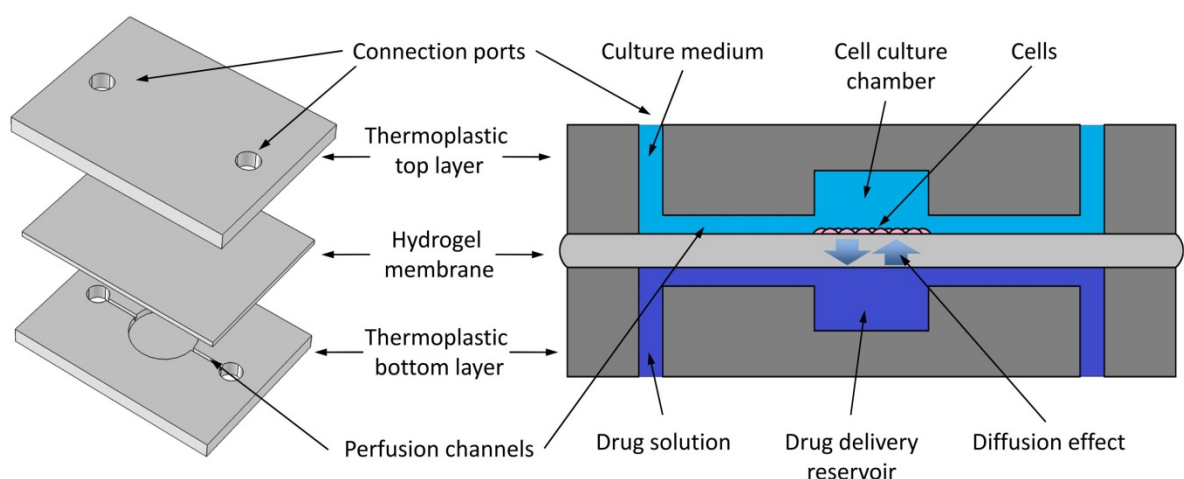


Fig.1-1. Schematic diagram of the microdevice used to culture cells. Three layers, two thermoplastic layer and one hydrogel membrane, make up the device as two closed microfluidic system, culture chamber at top and drug delivery reservoir at bottom. Cells are cultured in the culture chamber. The molecules exchange between culture chamber and drug delivery reservoir are taking place all the time, through diffusion in hydrogel membrane material.

1.2 Aims and Objectives of the Thesis

The primary aim of this thesis is to design and develop a multi-material microfluidic platform, which is made of thermoplastic polymers (e.g. PMMA) and hydrogels, in order to establish a fabrication approach and applicable device for complex hybrid microplatforms for cell culture and incubation. Combining the different materials and processing methods, to develop a complex microdevice which can break the barriers between microfabrication and biological application, is the major challenge in this work that has to be addressed.

Based on the concept design of the device as described in Fig.1-1, the work has inevitably to deal with the determination of the parameters of the hydrogel-based microfluidic device, such as device dimensional parameters (e.g. dimensions of culture chamber or microchannels) and performance determining parameters (e.g. inflow velocity, nutrient concentration and fluidic shear stress). Thus, the fundamental issues, including material property of hydrogel, suitable packaging method for hydrogel-based device, and characteristics or set-ups of perfusion culture device, have to be properly addressed in advance in the course of development of the hydrogel-based microfluidic device. Accordingly, the research in this thesis is divided into following aspects:

- **Research on material:** To investigate the possibility of utilising hydrogel to integrate into microfluidic device for biological purpose, e.g. cell culture. This is primarily focusing on the research of the biocompatibility of hydrogels, including diffusion characteristics, cytotoxicity and cell adhesion.
- **Research on packaging:** To study the feasibility and reliability of the novel packaging method which enables disassembly and re-assembly for the hydrogel-based microfluidic device. It consists of fundamental research on the behaviour of hydrogel membrane in microfluidic channels, in order to achieve a reliable packaging method through optimising the microchannel and selecting the appropriate packaging conditions, e.g. fastening strain.
- **Research on the parameters of device/system:** To determine the parameters for the hydrogel-based microfluidic device to enable suitable conditions for cell culture and to achieve better functional capability for culturing cells. This applies a systematic research on the influence of the dimensional parameters of culture chamber and the environmental conditions on cells during the culturing process in the microfluidic device.

Both experiments and numerical simulations are implemented as research methods or tools to develop the hydrogel-based microfluidic device in this study. The objectives that have been identified for the specific tasks described above can thus be given as follows:

1. Basic property research or verification of PHEMA hydrogel materials, including synthesis, swelling and diffusion characteristics .
2. Designs and experiments to investigate the effect of PHEMA hydrogel on cells, such as experimental approaches to study of the cytotoxicity and cell adhesion on PHEMA.
3. Modelling of PHEMA hydrogel materials on its mechanical deformation, in order to achieve a proper theoretical model to describe and predict the mechanical behaviour of this hydrogel.
4. Experimental approaches to determine the bounds or limits of the microfluidic system, such as ultimate fluidic pressure to guarantee a reliable sealing of the device or the ultimate fastening strain on the hydrogel membrane which can achieve proper sealing without inducing any material failure.
5. Optimum design of microchannels' geometry and the packaging conditions (e.g. compressive strain), aiming to obtain a feasible and reliable packaging for the assembly of multi-material microfluidic device.
6. Research on the capacity of the microfluidic device as a whole system, including the range inflow rate, inflow nutrient concentration and the perfusion time.
7. Optimum design of the culture chamber (bioreactor), through varying the dimensional parameters of the chamber to determine suitable geometry of bioreactor for incubating and testing cells.

Due to the unique interdisciplinary nature, the current work was collaboratively carried out at three locations in UK, Italy and China during the three years of the PhD research life of the author. This has been achieved through strategically taking advantages of the technical capability of each collaborated research team and facilities. Owing to the expertise based on the Wolfson School of Mechanical and Manufacturing Engineering of Loughborough University, most numerical simulated designs, optimizations and predictions were built and developed at the Loughborough University in UK. Within the Interdisciplinary Centre for Nanostructured Materials and Interfaces (CIMaINa) in

Italy, the materials preparation was conducted, where the hydrogels used in this research were synthesised based on the standard procedures thanks to their expertise on hydrogel used as cell culture substrates [4,5]. The experimental study including the manufacturing of PMMA substrate for the hydrogel-based microfluidic device and the testing of the sealing reliability of fluidic system were mostly undertaken at the College of Materials Science and Engineering of Huazhong University of Science and Technology (HUST) in China, using their experimental equipment and the high efficiency of the testing or measuring process. In addition, the experiments related to cell culture were conducted at the biomedical department of HUST, through a strong mutual collaboration with the WUHAN Union Hospital (Wuhan, China) and Peking Union Medical College Hospital (Beijing, China), as such the cell lines can be gained from their source and the incubation/testing of cells can be successfully implemented.

1.3 Structure of the Thesis

This thesis contains eight chapters. The introduction to the current research for the definition of the problems and identification of research objectives is presented in Chapter 1: this includes background of study, research motivation, and initial conceptual design of the device, aims and objectives of thesis, plus this section giving the structure of the thesis. It has briefly articulated the challenges of microtechnology which is used in the biological field, and explains why the current research is important.

In Chapter 2, a literature review is undertaken to gain firm knowledge of microfluidic technology, hydrogel materials, as well as a number of successful examples of microfluidic device embedded with hydrogel materials. The advantages and disadvantages of the common techniques of fabrication or bonding of microfluidic devices are summarised, in order to emerge the strengths and novel features of the technique developed in this thesis. Also, the foundational backgrounds for the material, theory and techniques for the following chapters are reviewed in detail.

Chapter 3 describes the main methodology which has been employed to address the theoretical models used for simulations, and the equipment and testing method used for experiments in this thesis. COMSOL Multiphysics which is the simulating tool used for the simulation work has also been briefly introduced. This chapter also reviews the models that developed by researchers and defines the reason that hyperelastic model and Fickian diffusion

model are chosen to simulate the mechanical behaviour and diffusion mechanism of hydrogels respectively. In addition, the apparatus and manufacturing and testing procedures, including the synthesis, preparation and swelling/drying of PHEMA hydrogel, are depicted in details.

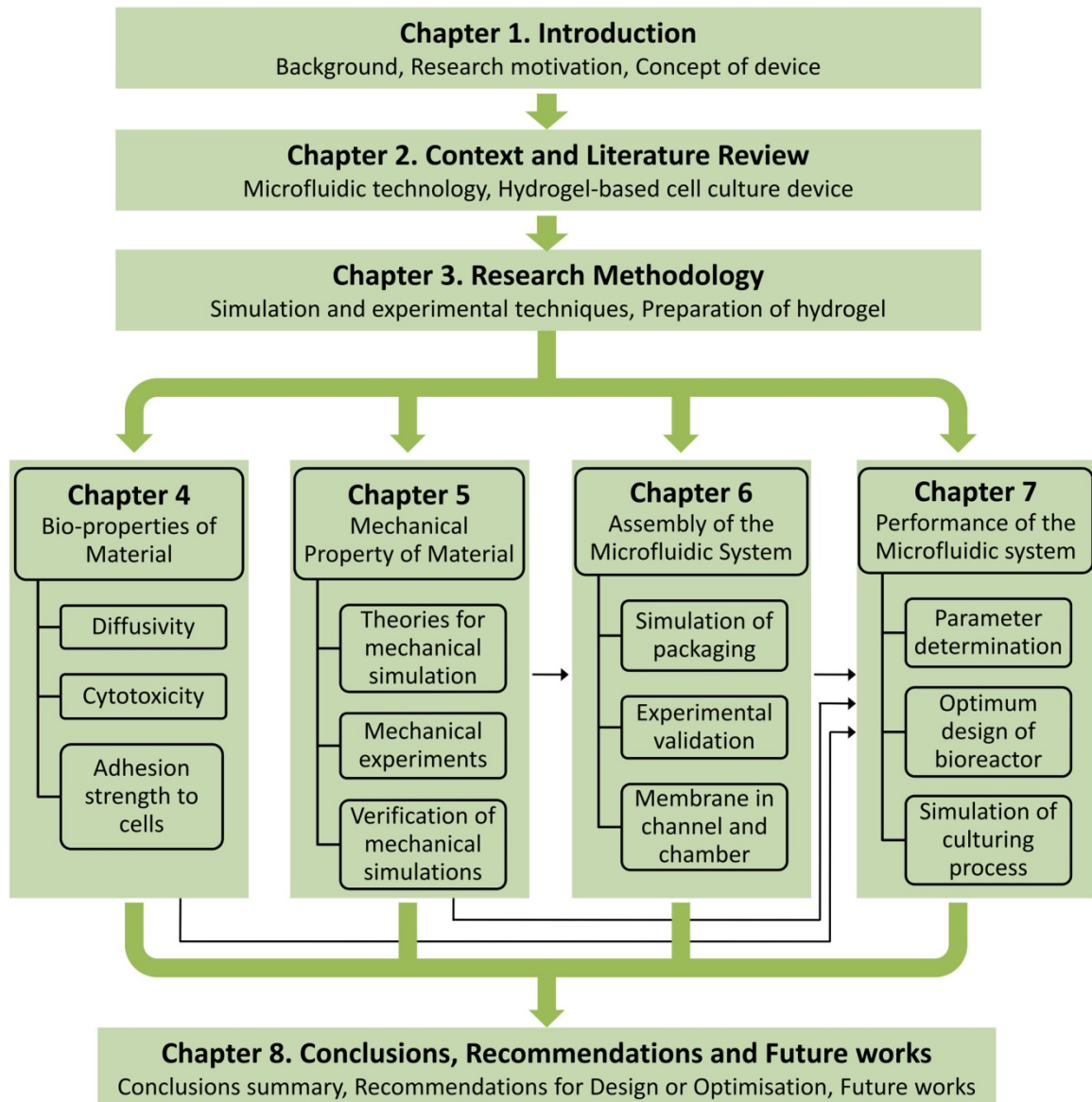


Fig.1-2. Overview of the thesis structure. The relationships between chapters are illustrated in the flow chart, especially the inter-correlations between the original research chapters (Chapter 4, 5, 6 and 7). It depicts that the results from Chapter 4, 5 and 6 are contributing to the simulation work in Chapter 7.

Chapter 4 details the experimental research on the PHEMA hydrogel material, including the diffusion behaviour of glucose in PHEMA, cytotoxicity of PHEMA to common cell models (*i.e.* HUVECs and fibroblasts), and adhesion strength of cells to PHEMA substrate. The objectives 1 and 2 listed in Section 1.2 (at page 5) are focused and elaborated in this chapter. The results presented

in this Chapter 4 will be inter-related with, thereby utilised in the system performance simulation included in Chapter 7.

The theoretical basis of the mechanical deformation of PHEMA hydrogel is reported and verified by experimental work in Chapter 5, initially through establishment of the deformation models of PHEMA hydrogel based on two theories: Mooney-Rivlin and neo-Hookean model. The two models are selected to estimate the dependence of the compressive strain and stress applied on the PHEMA specimen. The model, which can better show the consistence between experimental data and numerical simulation data based on such model, is selected to represent and to predict the mechanical behaviour for both fully swollen and partially swollen PHEMA hydrogel. The results from this chapter will be used in predicting the stress distribution of hydrogel membrane in culture chamber under the compression, and stress concentration or deformation of hydrogel membrane in microchannel in Chapter 6. This chapter presents the results to address the objective number 3.

In Chapter 6, both the experimental and numerical investigations are conducted to understand feasibility and reliability of the mechanical fastening process for the assembly of the microfluidic system, including the determination of maximum pressure in the system, protrusion of membrane in the cavity of microchannel, ultimate compressive strain of the fastening process and stress concentration of hydrogel membrane in the culture chamber. The combination of simulation and experimental work is another validation of numerical simulation, although the theory of modelling has been verified by the uniaxial compressive experiment in Chapter 5. Also, a feasible and reliable packaging method which enables disassembly and reassembly routines of the multi-material microfluidic device is described. In this chapter, the objectives 4 and 5 are attained.

After the research on the material and packaging method presented in Chapter 4, 5, 6, the work presented in Chapter 7 is focusing on the function of the microfluidic system, the cell culture and ECM control. The parameters of this perfusion culture microfluidic device, such as inflow rate, inflow nutrient concentration and perfusion time, are determined according to the requirement of cells culture. The dimensional parameters of the culture chamber, including diameter, height and location of the inflow entrance, are determined by selecting the values which can obtain the best performance of this microfluidic device, *e.g.* being capable of incubate various kinds of cells which require different ECM microenvironment. The numerical simulation in this chapter is established based on the experimental results obtained from the previous chapters, including adhesion strength

of cell to PHEMA substrate (in Chapter 4), the diffusion behaviour of glucose molecules in PHEMA hydrogel (in Chapter 4), the structural design of the multi-material microfluidic device (in Chapter 5&6). The objectives 6 and 7 are the main focuses and have been achieved in this chapter.

Finally, the Chapter 8 summarises the main findings of the work presented in this thesis and the recommendations for optimum design of microchannels, culture chambers, parameters of packaging and perfusion process of the microfluidic device. An outlook on further developments is also provided. The outcomes and the recommendations are expected to serve as a guideline for the researchers who may continue to consider further optimization or development of the hydrogel-based perfusion cell culture microfluidic system.

Chapter 2. Context and Literature Review: Hydrogel-based Microfluidic systems

2.1 Microfluidic Technology for Lab-on-Chip Applications

2.1.1 Microfluidic Systems and Their Applications

Microfluidics represents a series of science and technology of systems that manipulate or deal with small amounts of fluids (10^{-3} ~ 10^{-6} mL), through microchannels at the dimensions ranging from 1 μm to 10 mm [3]. The microfluidic devices are capable of using very small quantities of samples or reagents to carry out reactions or detections with high sensitivity. The obvious advantages of microfluidics are attributed to their small size, low cost, rapid analysis, and convenience to produce the device, etc. [6].

According to the applications of microfluidics, they can be divided into four categories: conditions screening, manipulation of multiphase flow, microanalytical system and cell biology. Firstly, the highly developed microfluidic applications are utilised to screen conditions, including pH, concentration, composition [3]. For examples, large numbers of conditions are compared and analysed to select the best growth of protein crystals [7,8,9]; and high-throughput screening systems are established in drug development [10,11]. Secondly, its application of manipulation of multiphase flow are capable of precisely handling the bubbles [12,13] or droplets [14,15,16] in a continuous liquid stream. For example, in the microfluidic device developed by Garstecki *et al.* [12], streams of liquid and gas are mixed in monodisperse, and the device enables the controlling of the size of the bubbles by controlling the inflow rate or pressure of gas. Thirdly, owing to the small size of microfluidics, the practical microanalytical systems [17,18] which can enable rapid bio-analysis are another focus of the application of microfluidics, such as blood analyse in a portable device within a limit time (e.g. several minutes) [19]. Finally, cell biology is an essential area of research which can be investigated using microfluidic systems. Microfluidic systems enable the fundamental studies of spatial and temporal control of molecules or cells in micrometre scale (0.1~100 μm), in order to investigate the living condition or survival criteria of cells.

2.1.2 Materials for Microfluidic Devices

Microfluidic devices would not be developed so quickly without the significant development of polymer technology. The polymers are suitable materials for fabrication of microfluidic devices including thermosets, thermoplastics and elastomers.

Thermoset polymers consist of numerous crosslinked monomers forming a giant molecule, which are usually hard and fragile. They are usually in a form of liquid with high viscosity before curing. After a chemical reaction or suitable irradiation within an environment over 200 °C, the irreversible curing can take place, which makes the thermoset polymer become solid state being stronger than thermoplastics. Once curing is completed, the thermoset polymers cannot be reheated and melted to be re-shaped. Due to this property, very few thermoset has been used as substrate for microfluidic device.

Thermoplastic is a plastic material with relatively weak crosslink of monomers, such as polystyrene, polycarbonates (PC) or poly(methyl methacrylate) (PMMA). At the temperature above their Glass Transition Temperature (T_g), thermoplastic polymers become plastic which can be moulded into specific shapes. When cooling them below T_g , it causes the curing of thermoplastic material. There are a large number of microfluidic devices which are built using thermoplastic as their substrates. For example, Hupert *et al.* [20] manufactured spiral channels 50 μm wide and 150 μm deep on polycarbonates using hot embossing technique. And Ueda *et al.* [21] produced microchannel with 1 mm diameter and 100 μm deep on poly(methyl methacrylate) using lithography.

Significant research on microfluidic systems have been established based on elastomer, poly(dimethylsiloxane) (PDMS), which possesses the properties of soft, transparent, elastic deformation behaviour and convenient to be synthesised. It is one of the most common polymer materials for making microfluidic devices in lab nowadays [22]. Many microfluidic devices made by PDMS can be found in literature, for instance, 25 nL of chamber has been manufactured on PDMS by Yu *et al.* [23], which was prepared using injection moulding technique; 100 μm deep and wide microchannels were fabricated on PDMS using soft lithography, which is done by Fukuba *et al.* [24]. However, PDMS tends to have problems when it is used as substrate for microfluidic system. Because PDMS is still a polymer which is formed by crosslinked chains, the small molecules in microchannels or chambers may be sank to the PDMS material which may fundamentally affect the biological results. This absorbance of small molecules into PDMS is dependent of the pH value of

the solution which is in contact with PDMS directly [25].

2.1.3 Fabrication of Microfluidic Devices

According to the literature about manufacture of microfluidic devices, the technologies which are frequently used to fabricate microfluidic devices can be summarised into five classes in terms of their manufacturing processes: micro-milling, hot embossing, injection moulding, lithography and laser ablation.

Micro-milling. Milling is a traditional fabrication process in macro-world. The micro-milling technology is developed in the last 15 years, which was applied in watch making, optics apparatus and MEMS manufacturing fields. It is a machining process using micro-machine-tools equipped with tiny cutters. The key components of the micro-milling machine are the cutter and motion controller. Currently, the size of the cutter for a micro-milling machine is ranging from 10 μm to 10 mm [26]. The speed of the spindle is ranging from 2000 rpm to 160000 rpm. High speed of spindle will lead to high temperature induced around the cutting area on the material during manufacturing. Thus, high speed manufacturing using micro-milling technique is not suitable for thermoplastic materials because the high temperature induced by high speed spindle may heat the surrounding material over their glass transition temperature T_g and cause damage of the designed geometry. For the motion controller, CNC (Computer Numerical Control) technology makes the micro-machine tools becoming a fast and powerful controlling system, which enables the accurate and efficient fabrication of the samples in small scale.

Using micro-milling technology for the fabrication of devices such as MEMS or microfluidics is convenient, portable and easily maintained, and reconfigured [26]. However, the vibration of the spindle during manufacturing, which is one of the major problems for this technology, can affect the fabrication accuracy or even destroy the microstructures. Moreover, it is only suitable for unit production which requires several pieces (1~100) of sample only, because it is a time-consuming process.

Hot Embossing. Hot embossing is one of the widely used methods for fabricating polymeric microstructures in academic research and industry [27,28,29,30]. The process of hot embossing can be summarised into following steps:

- 1) Heat the thermoplastic material substrate that are used to make the components over its glass transition temperature T_g , in vacuum environment.
- 2) Heat the master (as mould) with structured patterns on the surface to the temperature of T_g at the same time.
- 3) Press the master onto the thermoplastic substrate by applying a pressure over 500 N/cm² [31] generally.
- 4) Cool both for master and thermoplastic substrate below T_g temperature and then extract the sample from mould.

The primary merit of hot embossing is that their high replication accuracy enables the reliable fabrication of structures in the range of 1~1000 μm [32,33]. The challenges of this kind of fabrication process are that it is difficult to induce the uniform temperature distribution across the master structure and it is not easy to prevent trapped air from forming bubbles during the compress step (step 3).

Injection Moulding. Another commonly used fabrication process for microfluidic device with high efficiency is injection moulding. The injection moulding process, in general, consists of filling, packing, cooling and releasing polymer into a mould. As a preparation step, a microstructure is pre-machined on the surface of a metal mould which has the reverse image of object to be moulded. At the filling and packing step, the thermoplastic material is heated and melted into liquid with high viscosity, then the melted thermoplastic is injected and pressurized to fill the cavity in the mould. Then the injection moulded thermoplastic with designated shape and surface patterns is released from the mould after being cooled and solidified. The primary advantage of injection moulding is that it is capable of building 3D objects in one step. For instance on microfluidic devices, the integration of fluidic interconnects or through-holes can be fabricated in one-step moulding [27,28]. However, the manufacturing of the mould for injection moulding is a high-cost process, so that it will be very costly when only a small amount of samples are to be produced. Owing to its convenience of replication, injection moulding is usually used in industry extensively for high throughput productions.

Lithography. In the micro-fabrication processes, lithography includes photolithography and stereolithography for fabricating 2D and 3D structure respectively. The material used in this technique is called SU-8 as its monomer contains eight epoxy groups. If the material is exposed

under UV light or X-Ray radiation, strong crosslinking will take place between the monomers in the process of cationic polymerisation. This leads to the production of small parts or patterns with main advantages of SU-8, e.g. high mechanical, thermal and chemical stability. However, SU-8 can be difficult to process, because it generates large internal stresses in the film during the polymerisation, which may cause unexpected structural deformation or fracture of the specimen. In addition, due to its strong adhesive property, cured SU-8 can be difficult to remove from a substrate, particularly from a three-dimensional structure with large contact surface to its substrate [34].

Laser Ablation. Another method for the rapid prototyping of microfluidic structures is laser ablation. A high-intensity laser beam can be focused onto the material surface, and the concentrated energy of the beam evaporates the material at the focal point simultaneously. The geometry can be fabricated by using a mask to protect the area which is designed to not be evaporated, or by moving the laser beam to generate the desired structures. Normally, laser ablation is used to fabricate structures on thermoset polymers [35,36]. One of the critical features of laser ablation is that the interaction of the material with the intense laser light may change the chemical properties of the material [37,38]. This effect is difficult to be controlled or avoided. It may cause variations of surface properties especially in some surface sensitive applications, thereby care should be taken to ensure the performance of the device.

2.1.4 Packaging of Microfluidic Devices

As introduced in last section, the microfluidic chips after the fabrication process are not yet a closed fluidic structure which is ready for initiating fluid flow. To complete the device as a functional microfluidic system, the packaging process is equally essential to the fabrication process. The techniques for packaging or bonding to form a functional microfluidic device can be summarised into five groups from the basis of literatures: adhesives and solvent bonding, adhesion and surface modification, thermal pressure bonding, ultrasonic welding and laser welding.

Adhesives and Solvent Bonding. The most common bonding methods to join the polymer parts together are the adhesives bonding [39,40] and solvent bonding [41,42]. The similarity of the principles of these two methods is generally seen by placing adhesives or glues between the two polymer parts followed by urging the solidification of adhesives or glues by heating or pressing, thus

form the chemical bond within the interface of polymer parts. A critical aspect of these two bonding methods is the difficulties to prevent the microstructure from being damaged or blocked by the adhesives. For instance, the adhesives or solvent materials may fill the cavity of microchannels or other microstructures during the forming of chemical bonding at the interface, thus causes the blockage of the microchannel or damage of the microstructure after packaging process and leads to malfunction of the device.

Adhesion and Surface Modification. The surface adhesion for most polymers (e.g. PDMS) is sufficient to create a tight seal, if the bonding process takes place in a very clean environment. For the polymers which have less adhesion properties on their surface, the adhesion can be improved by plasma exposure or surface coating, e.g. with hydrophobic ink [43]. The applications based on this kind of surface chemical modification can be found at literatures [44,45]. However, it is not a stable bonding for long-term packaging solution [45].

Thermal pressure bonding. Chips made of thermoplastic can be bonded together by applying the heating and pressure [46,47,48]. If the two parts are individually made of thermoplastic materials with different T_g , the thermal pressure bonding can be the best choice of packaging, because only one of the chip plate can be melted during the bonding process. For example, the microfluidic chips can be both made of PMMA but different polymer molecular weight [49]. It has to be noted that the 'melting' plate is better to be the chip without surface microstructures, in order to avoid or reduce the possibility of damage of the microstructures.

Ultrasonic welding. Similar as the thermal pressure bonding, the chips made of thermoplastic materials can be bonded by melting them to form a reliable bonding through input of ultrasonic energy. The ultrasonic welding differs from the thermal pressure bonding in that the thermal energy in ultrasonic welding is ultrasonically induced and applied only at the interface of two polymer chips [50,51]. This bonding method is valuable in many cases where solvents or other kind of contaminations are not allowed at the interface due to the integration of biomedical materials. However, the ultrasonic welding is limited by the resolution of ultrasonic welding machine. For instance, ultrasonic energy may not be entirely concentrated on the designated region thereby cause damage of the microstructure on the polymer substrates, if using low resolution machine for ultrasonic welding.

Laser welding. As it is understood from its name, the thermal energy which presents at the interface between the polymer chips in this case is induced by laser radiation [52,53,54]. This bonding technique requires the two target polymer plate possess different absorption coefficients towards laser radiation, thus it can melt only one plate during the bonding process. This technique enables rapid bonding, such as high quality bonding can be achieved within 3 seconds, reported by Kim *et al.* [55].

2.2 Hydrogel-based Microfluidic System for Cell Culture

2.2.1 Hydrogels and Its Classifications

Hydrogels represent a series of three-dimensional crosslinked polymer, with rubber-like mechanical properties. They are similar to natural tissues when hydrated [56]. Hydrated hydrogels contain mostly water, because the crosslinked networks absorb substantial amounts of aqueous solutions. Accordingly, hydrogels are also defined as a colloidal gel in which water is the dispersion medium [57]. At microscale, hydrogel is like a three-dimensional network, constructed by carbon chains which are tangled with each other and connected by chemical permanent junctions. The gaps between chains are filled with water molecules thanks to the hydrophilic property of the carbon chains, when hydrogel at its swollen state [58]. In contrast, the gaps between carbon chains become hollow space, when hydrogel under drying conditions.

To understand the fundamental structure of hydrogels, PHEMA (poly (2-hydroxyethyl methacrylate)), which plays an important role in this thesis, is chosen as an example for clarification. Fig.2-1 illustrates the process of synthesis of PHEMA hydrogel at molecular scale. PHEMA hydrogel is constructed through repetition of a same units, monomer of HEMA. The molecular structure of the monomer of HEMA is shown in Fig.2-1a in chemical structural expression, e.g. Skeletal formula [59]. In these chemical structural expressions, every bond between different atoms is made of two electrons, a single bond (single dash) is made of 2 electrons which are tightly bound together and difficult to be broken. Moreover, a double bond (double dash) is formed of one simple bond and one bond which is not so resistant. Therefore, a double bond is very active that it gives origin to 2 single electron when it is break down (pink points in Fig.2-1b represent electrons). For the monomer of HEMA, the double dash (green) of the molecule is the active part of the monomer which is able to construct carbon chains to form the network structure of PHEMA. The blue region of the HEMA

monomer keeps stable during the polymerisation, thus can be simplified as 'R' group. Different 'R' group leads to various hydrophilic behaviours or other physical properties of polymerised polymer. There is only a hydroxyl in the 'R' group of the HEMA monomer, which makes the polymer hydrophilic similar to alcohol (ethanol or methanol). As it is shown in Fig.2-1b, two similar monomers with two electrons are merged together to form a new single bond (pink dash) by sharing one of their own electrons during polymerising reaction. In reality, such polymerising reaction takes place radically and results in a long chain-like molecule made by the repetition of single monomer (see Fig.2-1c) because there is large number of HEMA monomers in the solution which are available for reaction. This chain-like molecule is named polymer chain.

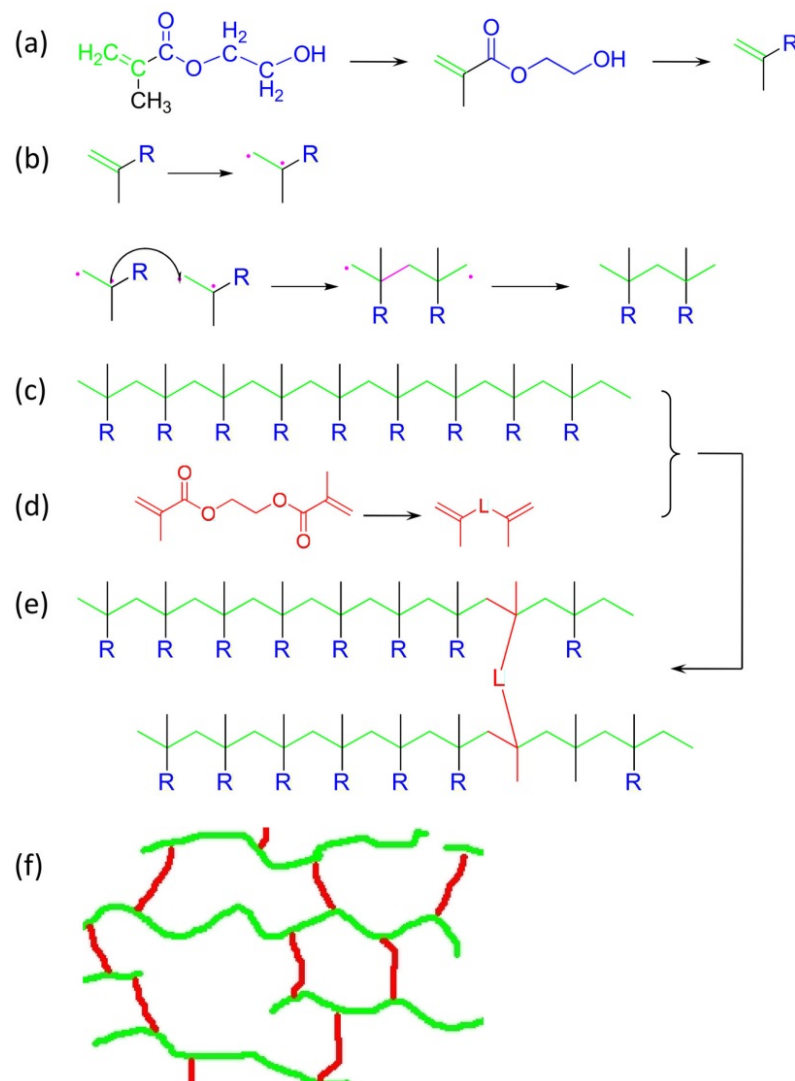


Fig.2-1. (a) Molecule of HEMA in chemical formula, and simplification of its chemical formula. (b) The schematic diagram of the process of two HEMA molecules merged together through reaction. (c) The structure of polymer chain. (d) Molecule of EGDMA in chemical formula. (e) Structure of polymer chains connected by crosslinker EGDMA. (f) 2D schematic diagram of the network structure of the polymers/hydrogels.

The molecules which are used to link the polymer chains with each other and form inter-crossed junctions are named reticulating agent or crosslinker. The crosslinker used to form reticulated structure of PHEMA in this study, is Ethylene Glycole Di Methyl Acrylate (EGDMA). The molecular structure of EGDMA and its simplified molecular structure are described in Fig.2-1d in red. During the polymerisation of PHEMA, two double bonds of the crosslinker are activated and merged together with the polymer chains. The schematic process is illustrated in Fig.2-1e, two individual polymer chains are bonded together by inserting the activated double bonds of crosslinker (red) into the middle of polymer chains. A large number of such reactions are undertaken enabling a reticulate structure constructed by the polymer chains and the crosslinker molecules, such as the two-dimensional schematic diagram shown in Fig.2-1f.

Generally speaking, hydrogels can be categorized in two groups based on their natural or synthetic origins. Natural hydrogels are expensive because they are derived from animals or other natural source. For the purpose of culturing cells, there is a risk of using natural hydrogels as a substrate/scaffold that may carry unknown disease from animal source because they are from natural source. However, the cells grow well on/in them also because they are from natural source. Conversely, artificial hydrogels are cheap, and the components to construct artificial hydrogels are easy to be controlled. Meanwhile, the major disadvantage of artificial hydrogels is that their biocompatibility is not as good as the natural hydrogels when they are used in biological applications, such as cell culture.

Natural hydrogels. Natural hydrogels are good candidate materials for biomedical engineering applications. One of the most popular applications for hydrogels in biomedical engineering is culturing cells in microfluidic devices which are made of or embedded with hydrogels [60]. Due to the characteristics of cells, they are highly sensitive to their micro-environment in their original body, which is known as *in vivo* environment. Under *in vivo* environment, cells grow in a complex bioactive scaffold which provides mechanical support for cell adhesion, differentiation and gene expression. This environment around cells is called extracellular matrix (ECM) [61]. The ECM for incubating cells outside their original body, which is called *in vitro* environment, should reproduce the *in vivo* environment as closely as possible. For the purpose of incubating cells, natural hydrogels can act as suitable substrate for the device, such as collagen [62], fibrin [63], hyaluronic acid [64] from animal source, and chitosan [65], alginate [66], or silk fibrils [67,68] from botanic

sources. These hydrogels have excellent biocompatibility and bioactivity because they are derived from natural sources [69].

However, the growth of internal structures of such cell for promoting hydrogels are complex, which causes difficulties for researchers in determining correlations of communication signals and cellular function [70]. Also, the natural hydrogel can be degraded quickly when extracted from their original natural source, and form a risk of contamination, possibly carrying disease from the natural source to another. Thus, the advantages of artificial hydrogels can be obviously in these aspects.

Artificial hydrogels. Hydrogels can be synthesised from purely artificial molecules such as poly (ethylene glycol) (PEG) [71], poly (vinyl alcohol) (PVA) [72], and poly (2-hydroxyethyl methacrylate) (PHEMA) [73]. The viability of cells has been evaluated when cells are cultured on PEG [74]. The work demonstrated that synthetic hydrogels are similar to the ECM in the *in vivo* environment, so that they can be an incubating platform for cells. Besides, using artificial hydrogels for culturing cells is much cheaper than using natural hydrogels, as such artificial hydrogels are highly reproducible. Moreover, it is possible to modify their specific physical properties through changing the type or amount of the monomer which artificial hydrogels are constructed. These controllable properties contribute to the advantages of artificial hydrogels upon natural hydrogels.

Noticeably, artificial hydrogels have a serious flaw for biological applications as they are lack of bioactivity to promote cell behaviour, such as allowing cells to act as a template to permit cell function [69]. Fortunately, the bioactivity of artificial hydrogels can be improved by further modifying their surfaces or their inner properties, such as coating with a layer of gelatin. For this reason, the artificial hydrogels are still widely used in applications of biological engineering, tissue engineering or regenerative medicine.

2.2.2 Properties of Hydrogels

Young's modulus is always utilised to indicate the initial resistance to stresses, which are induced by compression or tension. Most of hydrogels have small Young's modulus, leading to their rubber-like mechanical characteristics. If using hydrogel to produce a device, soft is obviously a merit that the device will not break easily like that devices which are made of glass or plastic, e.g. polystyrene or PMMA.

The densities of hydrogels are mostly smaller than or close to that of water, because the

hydrogel is partially filled with water molecules at its swollen state [75]. Generally speaking, the amount of water in hydrogel is at least 20 wt%. But for superabsorbent hydrogels, the percentage of water can reach up to 95 wt% [76]. Owing to the large number of water molecules, hydrogels can be utilised as a semi-permeable membrane for separation processes [77], or as biomaterials for transporting bioactive agents within tissues [78,79]. Such applications experimentally examined the ability of hydrogel to restrict or allow the movement of a solute. The molecular structure of hydrogels is usually described as a three-dimensional mesh with a random distribution of water-filled nanopores allowing permeation of molecules between polymer chains [80]. The movements through which the solute molecules can be transported through hydrogel take place mostly via the water-filled nanopores. The permeability of hydrogel is dependent on the size of the pores, the size of the solute molecules, and the diffusion coefficient of the solute molecules in water [80]. The size of nanopores is determined by the variety of hydrogels, which can be as large as $\text{\AA}100$ nm that allows protein molecules pass through, or can be small enough to restrict the passage of inorganic molecules.

Hydrogels usually works in room temperature ($20\text{ }^{\circ}\text{C}$) or body temperature ($37\text{ }^{\circ}\text{C}$), which are lower than their Glass Transition Temperature (T_g). Under these environmental conditions, there are two temperature-dependending physical states of a hydrogel: hydrophilic when dehydrated (dried state) and hydrophobic when hydrated (swollen state). These two states are interchangeable from each other, such as swelling automatically when hydrogels are sank into water, or drying by heating over the Volume Phase Transition Temperature (VPTT) [81]. Accordingly, the state of hydrogel (Dried or Swollen) can be determined by controlling the temperature near hydrogel. For instance, it is reported that a self-cleaning behaviour to growing and releasing cells from their substrate is achieved by utilising the thermoresponsive property of PNIPAAm (poly(N-isopropylacrylamide)) hydrogel [82]. Generally, the VPTT of thermoresponsive hydrogels is ranging from $32\text{ }^{\circ}\text{C}$ to $34\text{ }^{\circ}\text{C}$, which is below the temperature *in vivo*, $37\text{ }^{\circ}\text{C}$. Thus, when hydrogel is implanted into *in vivo* environment, they are under its dehydrated state but behave as hydrophobic all the time [83].

In this study, the PHEMA hydrogel which is used as a membrane is not a thermoresponsive hydrogel. Hence, the swelling state of PHEMA hydrogel is not dependent on the temperature, though the working temperature of the device embedded with PHEMA membrane is body temperature in this case because of the requirements of cell culture.

2.2.3 Applications of Hydrogels for Bio-purposes

Hydrogels possess many characteristics that potentially make them ideal biomaterials. The major striking advantages of hydrogels are their high water content and the good biocompatibility when compared with plastic or silicon [84]. Successful examples include contact lenses [85,86], wound dressings [87,88], super absorbents [89,90,91], and drug delivery systems [92,93]. The high impact applications of hydrogels are cell-based therapeutics [94,95] and soft tissue engineering [67,96]. For instance, the most common used biomaterial for growing skin product is collagen hydrogel [97]; Bertagnoli *et al.* performed a mechanical test of a novel hydrogel which can be implanted as the replacement of nucleus pulposus [98]. These bio-purpose applications are on the foundation of the similarity of hydrogels and real tissues: they both are hydrophilic, resistant to fatigue, and possess similar density.

2.2.3.1 2D or 3D Cell Culture in Microfluidic System

Microfluidic system is able to handle or perform the reaction or detection of very small samples (*e.g.* germ or cells) and rapidly induce the results with high resolution. Hydrogels possess the properties of biocompatible, molecules diffusible (especially for small molecules, *e.g.* oxygen or glucose) and easy to be synthesised. Therefore, microfluidic system and hydrogels are a perfect couple to cope with cellular biology or other bio-related investigation, such as cells culture.

Culture of cells *in vitro* provides a defined platform for investigating the physical behaviour of cells and tissue outside the organism. Traditionally, the culturing of single cell group is achieved by using two dimensional (2D) substrates, such as tissue culture polystyrene (TCPS). In the 2D culture, cells experience the equivalent concentrations of nutrients, growing factors from the culture medium to the *in vivo* environment to simulate the ECM environment in their original body. For instance, with the technology of microfluidic systems, culturing of mammalian cells (such as liver [99], kidney [100] and other common cells [101,102,103]), stem cells [104], for tissue engineering [105,106] have been reported. When hydrogels are integrated into microfluidic system, *e.g.* act as a culturing substrate, a number of advantages emerged and better biocompatibility of such system can be achieved. For example, Engler *et al.* demonstrated that the differentiation of human mesenchymal stem cells (hMSCs) is dependent of the mechanical stiffness of substrate of the system [107,108]. In this perspective, hydrogels which have good biocompatibility and flexible property are the best

choice for mimicking the ECM for culturing cells. However, the communication among cells is quite different between the culture of cells *in vitro* or *in vivo*, because the microenvironments (especially the structure) at these two conditions are diverse [109]. The typical example to evaluate such differences can be found in the contrast experiments that culturing neural cells in 2D platform (coated surface) and 3D scaffold (PEG hydrogel) [110]. With the integration of hydrogels, 3D cell culture becomes possible and convenient over the past few decades. For instance, Liu *et al.* produced 3D hepatic tissues by photopatterning of poly(ethylene glycol) (PEG) hydrogels containing cells [111]. They incorporated cell-adhesive peptides, representing specific ECM proteins, in the hydrogels to support hepatocyte survival.

2.2.3.2 Perfusion Cell Culture

Not only can 2D/3D cell culture platform be built through hydrogel-based microfluidic technique, but also the process of cell culture, such as perfusion culture, can be achieved using hydrogel-based microfluidic device. Microfluidic perfusion culture enables the controlling of delivery or removal of the molecules (*i.e.* drug/solute) in the extracellular microenvironment, and it is also able to offer the controlling of the hydrodynamic stress which is applied on cells by modifying the fluid flow rate. All these controls can be done with the assistance of numerical control (NC) system, thus enable the fully automatic microfluidic perfusion culture as a long-term process. For such long-term automatic culture, there are some successful examples that Tourovskaia *et al.* developed a long-term (>2 weeks) perfusion culture system to incubate muscle cells, and observed that the differentiation process from myoblasts to myotubes [112]; Korin *et al.* developed a periodic 'flow-stop' perfusion culture system for incubating human embryonic stem cell in long term (a week) [113]. Moreover, with the advantages being the low cost and low culture medium consumption, using microfluidic systems to culture cells also provides an opportunity to incubate mammalian cells in a chip with small size and make cells to be operated fully automatically [114]. To achieve such automatic perfusion culture system, two key conditions have to be carefully designed: hydrodynamic shear stress on cells and nutrient supply for cells.

Hydrodynamic shear. Fluid flow in perfusion culture systems leads to the transport of molecules and also results in uneven distribution of hydrodynamic shear stress in the system. The maximum shear stress in the culture system has to be limited, because large shear stress may

cause the cells to detach from their substrate. In human body, a wide range of fluid velocities exist. For instance, the velocity in large blood vessels may measure up to 300 mm/s [115], but the speed slows down immensely since the vascular network expands over the entire volume of the body at the capillary level. Interstitial flow from the vascular system to the lymphatic system is normally in the range of 0.1-1 $\mu\text{m/s}$ [116].

Nutrient supply. Nutrients, such as glucose, oxygen and carbon dioxide, are all necessary growing factors for culturing cells. Glucose is the primary nutrient as well as energy for growth, differentiation and proliferation of cells. Oxygen and carbon dioxide are the necessary nutrient and metabolite for cells, respectively. To mimic the ECM environment for the perfusion culture system, the concentrations of these nutrients have to be individually controlled in a certain range suitable for the cells, and to dynamically adjust the increasing density of cells in the culture chamber, in order to meet the consumption requirements of cells which are growing all the time [117].

2.3 Summary and Thesis Tasks

The state of the art and the definitions of the scientific terms, which are correlated to the topic or work of this thesis, are addressed in this chapter. A number of literatures have been referenced and briefly introduced, in order to lay clear and solid foundations for the materials and technologies which are related to the simulations and experiments in the following chapters, including mechanical properties of hydrogels, fabrication and packaging techniques of microfluidic devices and principle of hydrogel-based microfluidic system. Although there have been extensive works studying on both hydrogel and microfluidic system, as are reviewed in this section, successful examples of applications of hydrogel-based microfluidic system for cell culture are still very problematic. This has presented the challenges for the development of a feasible and reliable packaging process to integrate the hydrogel and microfluidic system forming a multifunctional cell culture device.

To address the challenges, the factors which are not fully understood based on literatures but essential to enable future applications turns to the tasks for this thesis:

- (1) Mechanism of diffusion of glucose in PHEMA hydrogel
- (2) The cytotoxicity of PHEMA hydrogel to cells
- (3) The adhesion strength of cells to PHEMA hydrogel substrate
- (4) The theoretical model to represent the mechanical behaviour of PHEMA hydrogel

(5) Packaging method which enables assembly and disassembly routines

(6) Investigation of the dynamic performance of the perfusion culture device

The first three factors are related to the bio-properties of PHEMA hydrogel, which have been experimentally evaluated and described in the Chapter 4 of this thesis: i) The characteristics of diffusion of glucose defines the molecule transportation between culture chamber and the drug delivery reservoir. ii) The cytotoxicity of PHEMA hydrogel has big impact on cells because of the direct contact of PHEMA hydrogel and cells. iii) The adhesion strength of cells to PHEMA substrate indicates the maximum fluidic shear stress on cells, thereby determines the maximum fluid flow rate within the perfusion culture device.

The following two factors (4 and 5) are utilised to develop a novel packaging method, as it has yet to find a commonly used packaging method that enables assembly and disassembly routines. In this thesis, the mechanical fastening process is investigated to provide such reliable packaging method for microfluidic device. Mechanical fastening is a conventional assembly technique, which has been extensively utilised in various industrial applications, in particular for large components construction (e.g. aircrafts). It has presented a number of advantages over other assembly/bonding methods, such as low processing (e.g. ambient) temperature, easy-to-repair or replacement, low costs and possibilities of multiple disassembly. Using mechanical fastening process to bond microfluidic device offers a number of merits, such as room temperature bonding, recycle enabled, no glue or heating needed, and low cost for whole process. This challenge has been elaborated in the Chapter 5 and Chapter 6 in the thesis.

After the Chapter 4, 5 and 6, the hydrogel-based microfluidic device is thereby constructed as a perfusion cell culture system. The parameters of such microfluidic device are determined using CFD (Computational Fluid Dynamics) simulations to study the characteristics of transportation of nutrient molecules or fluid molecules during the operation of the system. Guidelines for optimising the dimensions of culture chamber can then be proposed. These systematic simulations, in correspondence with the investigation of the dynamic performance of the perfusion culture device, have been implemented in the Chapter 7 of the thesis.

Chapter 3. Research Methodology

3.1 Theories and Tools for Modelling

3.1.1 Material Characteristics and Simulation Theories

3.1.1.1 Mechanical Deformation Models

Hydrogel materials may be stressed when they are embedded in a microfluidic device. Potential failure of such hydrogel component is likely to occur if the stress is high enough, due to its soft and rubber-like property. Therefore, it is important to understand and simulate the mechanical behaviour of hydrogels in the device, since mechanical properties of hydrogels are sensitive to devices in some specific applications, *e.g.* perfusion culture. For instance, the wall of microchannels of a perfusion culture device which is made of hydrogel must endure forces imposed by the flow of an aqueous solution, their responses to the liquid pressure and to the hydrodynamic stress are the key factors to determine the dimensions of device [118]. According to the literatures, the mechanical behaviour of hydrogels can be well described using the theories of rubber elasticity and viscoelasticity, which is based on time-independent and time-dependent recovery of the polymer chains, respectively.

According to the behaviour of hydrogel specimens from mechanical tensile or compressive test, it demonstrates that the response of hydrogel to stress is nearly instantaneous and the deformation induced by stress is fully reversible unless material failure occurs. It is easy to notice that the mechanical response of hydrogel to stress is similar to that of rubbers, as hydrogels and rubbers have similar structure at molecular scale. The microstructure of hydrogels at swollen state is crosslinked networks with free volume between chains. This structure allows the deformation undertaken when external stress is applied and deformation recovered rapidly if external stress is removed. Such response to external stress can be characterised by three theories: elastic-plasticity, hyperelasticity and viscoelasticity. The stress-strain curves for the materials in terms of these theories are schematically shown in Fig.3-1.

Elastic-plasticity. Elastic-plasticity is widely used to depict the mechanical behaviour of common materials in daily life, *e.g.* metals. In this theory, strain ascends linearly with the increasing of stress at the beginning (see Fig.3-1a). Within the linear region, the deformation is fully reversible if the external stress is released, which describes the elasticity of the material. When the stress

keeps increasing beyond the elastic region of the material, the irreversible deformation is caused even if the external stress is removed (see dash line in Fig.3-1a). The slope of the linearity quantitatively depicts the relationship between stress and strain, and the value of such slope is known as Young's modulus or initial tangent modulus. Young's moduli of different hydrogels are experimentally examined by several research groups [85,119,120]. However, in room temperature or body temperature, most of hydrogels exhibits mechanical behaviour similar to rubbers [121], which is understood as hyperelasticity [122,123] (see Fig.3-1b). If the temperature is low enough, hydrogel can lose their rubber elastic properties but exhibit characteristics of viscoelasticity (Fig.3-1c). Obviously, using the Young's modulus, elasticity can only approximately describe the initial part of deformation behaviour (stress-strain relationship) based on hyperelasticity or viscoelasticity, which cannot satisfy the needs to elaborate the deformation of hydrogels at all range of strains.

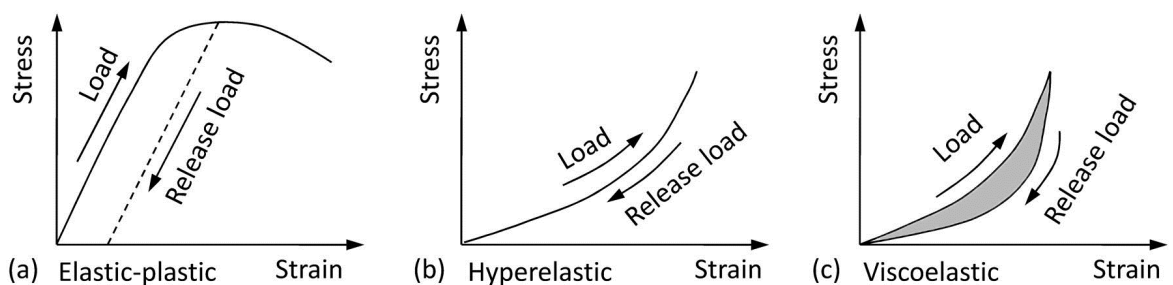


Fig.3-1. (a) Stress-strain correlation for elastic-plastic material, *e.g.* metal. (b) Stress-strain correlation for hyperelastic material, *e.g.* hydrogel or rubber. (c) Stress-strain correlation for viscoelastic material, *e.g.* amorphous polymers, semicrystalline polymers.

Hyperelasticity. As is illustrated in Fig.3-1b, the deformation of hyperelastic materials is fully reversible at all range of strains before reaching the failure point of material. Theoretically, there are two types of descriptions for hyperelastic deformation behaviour: phenomenological descriptions and mechanistic descriptions [124]. Phenomenological description of hyperelastic behaviour includes three main models, Mooney-Rivlin model, Bada model and Ogden model. Mooney-Rivlin model is the first hyperelastic model which is developed by Ronald Rivlin [125] and Melvin Mooney [126]. This model can predict the deformation of material under strain of 100%. Ogden model, a model that is suitable for the prediction of large deformation of rubber-like material (larger than 700% strain), is developed by R.W. Ogden in 1972 [122]. A unique model has also been proposed by Bada and Chevalier [127] who linked the Gent and Thomas model [128] with Ogden model to achieve the theoretical prediction in both small and large strain range, *e.g.* 0~700% strain. For

mechanistic description, neo-Hookean model [129] and Arruda-Boyce model [130] are the most common models accepted. Neo-Hookean model is able to predict the deformation under 100% strain. Beyond this strain point, the disagreement between the stress-strain curves from theoretical simulation and experimental testing becomes obvious. Unlike others, there is no range limit of the strain for Arruda-Boyce model.

According to the ultimate strain that PHEMA hydrogel can resist (60% strain), the Mooney-Rivlin model and neo-Hookean model are capable of describing and predicting the deformation behaviour of PHEMA hydrogel in this study. By utilising PHEMA hydrogel as a sealing membrane for microfluidic device packaging using mechanical fastening technique, compressive load is the external stress that hydrogel membrane has to withstand. Hence, the response of PHEMA hydrogel to compressive load is investigated in Chapter 5 on the basis of Mooney-Rivlin model and neo-Hookean model.

Viscoelasticity. If an external stress is applied to the viscoelastic material, a time-dependent response can take place [131], as such several unique phenomena during the load or unload process are observed which can be depicted as follow [132]:

- If a constant stress is applied on the material, the response of strain will gradually increase with time.
- If a constant strain is applied on the material, the response of stress will gradually decrease with time.
- If periodic load is applied on the material, hysteresis (a phase lag) occurs. The grey area in Fig.3-1c is the hysteresis loop and shows the amount of energy lost in a loading and unloading cycle.

In this case, the working temperature of the PHEMA hydrogel is body temperature (37°C), the required temperature for cell culture. Thus, deformation behaviour of PHEMA hydrogel can be regarded as hyperelasticity instead of viscoelasticity, because the recovery of the deformation is undertaken and completed straight away under such temperature. Furthermore, PHEMA hydrogel membrane is designed to be compressed at all the working time within the microfluidic system, in order to offer a reliable sealing for the microchannels. Hence, there is no movement for PHEMA membrane when it is sealed and bonded in the microfluidic system under its working conditions. Thus, there is no impact of viscoelasticity on the use of the PHEMA hydrogel membrane.

As a brief summary, the investigation of PHEMA hydrogel mechanical properties should only be considered as hyperelastic behaviour, e.g. Mooney-Rivlin model and neo-Hookean model. The

feasibility of using hyperelastic theory to represent the mechanical behaviour of PHEMA hydrogel is examined in detail at Section 5.3.3.

3.1.1.2 Diffusion Mechanism Models

The diffusion of solute molecules in hydrogels is an essential physical phenomenon in many biotechnology fields. Generally speaking, the behaviour of diffusion in hydrogels can be defined as three models: hydrogel free volume, enhanced hydrodynamic drag on the solute, and increased path length due to obstruction. These models are suitable for two types of hydrogels: flexible polymer chains (*i.e.* homogeneous hydrogels) and rigid polymer chains (*i.e.* heterogeneous hydrogels). The diffusion behaviour in homogeneous hydrogels can be precisely described using several diffusion theories, but the behaviour in heterogeneous hydrogels is usually examined by experimental testing.

Table 3-1. Summary of diffusion models and their corresponding hydrogels

Model	Expression	Reference	Hydrogel Class
Free volume theory	$\frac{D_g}{D_0} = (1 - k_1 r_s \varphi^{0.75}) \exp(-k_2 r_s^2 (\frac{\varphi}{1 - \varphi}))$	Lustig <i>et al.</i> [135]	homogeneous
Hydrodynamic	$\frac{D_g}{D_0} = \exp(-k_c r_s^2 \varphi^{0.75})$	Cukier [136]	homogeneous
Hydrodynamic	$\frac{D_g}{D_0} = \left[1 + \left(\frac{r_s^2}{k} \right)^{0.5} + \frac{r_s^2}{3k} \right]^{-1}$	Phillips <i>et al.</i> [137]	heterogeneous
Obstruction	$\frac{D_g}{D_0} = \exp[-(r_s + r_f)/r_f \sqrt{\varphi}]$	Ogston <i>et al.</i> [138]	heterogeneous
Obstruction	$\frac{D_g}{D_0} = \exp(-0.84 \alpha^{1.09})$	Johansson <i>et al.</i> [139]	heterogeneous

D is diffusion coefficient, *k* is constants, *r* is radius of solutes or fibres, φ is the volume fraction of polymer in gel.

Free Volume Theory. The model for free volume theory is based on the diffusion process of solute in liquid. The solute in the medium moves into the hollow space between polymer chains in hydrogel due to random thermal motion, and this movement causes the redistribution of the concentration of the solute in both medium and hydrogel. The diffusion will be stopped if the equilibrium reached [133]. Yasuda *et al.* [134] were the first ones to apply this theory to describe the solute diffusion in hydrogels. Another version of diffusion behaviour description based on this theory is developed by Lustig and Peppas [135]. They proposed the concept of the scaling correlation length between crosslinkers. However, these models (shown in Table 3-1) are based on the

assumption that the sieving is independent of polymer volume fraction which limits that the assumption is only applicable under the low polymer volume fractions.

Hydrodynamic Theory. The Stokes-Einstein equation for diffusion process of solute is the theoretical key of transport behaviour of solute molecules for hydrodynamic theory. It assumes the solute molecules as large rigid spheres which contain all the possible locations of the molecule due to their thermal motion. These 'large sphere molecules' moves only by the friction drag force due to the movement of the solvent. According to this assumption, Cukier *et al.* [136] has proposed an equation for investigating the diffusion behaviour in homogeneous hydrogels. Meanwhile, Phillips *et al.* [137] calculated the frictional coefficient to predict the diffusion behaviour in heterogeneous hydrogels (Table 3-1).

Obstruction Theory. This theory is based on the assumption that the polymer chains act as obstructions in the transport of solute molecules, thereby cause the increase in the distance of diffusion transport. Ogston *et al.* [138] assumed that the crosslinked polymer exists as a random network formed with straight long fibres which are crossed with each other, while the solute molecule is considered to be a hard sphere. Although this assumption is phenomenological reasonable, their prediction results based on this assumption can only provide a qualitative agreement to the experimental observation. Johansson *et al.* [139] developed an obstruction model regarding hydrogels as separated cylindrical meshes, and each single mesh consists of infinite polymer rod of solvent. The average diffusivity of the solute in the mesh obeys the Fickian theory. This hypothesis is similar to the finite element analyse method (FEA) which is widely used in numerical simulation.

According to the work done by Brian Amsden [80] who summarised most of the solute diffusion mechanisms and models for hydrogels, one can conclude i) the free volume theory is strictly valid only for hydrogel in the diluted solute system because it regards both water and polymer as a same function that contributes to transport behaviour of solute. ii) In concentrated solute system, the hydrodynamic model by Cukier [136] is reasonable to describe homogeneous hydrogels than the free volume models. iii) The obstruction models and hydrodynamic models used to predict the behaviour of heterogeneous hydrogels is less accurate and can only give a qualitative description of the diffusion properties of hydrogel.

In this study, free volume theory has been utilised to explain the diffusion mechanism of

glucose in PHEMA hydrogel, because they form a diluted solute system. The accuracy of such explanation is verified by the free volume theory which is elaborated by Peppas *et al.* [140]. On the basis of these fundamental validations, diffusivity of glucose molecules in PHEMA hydrogel has been experimentally examined, which obeys the Fickian diffusion mechanism. These results are presented in Chapter 4.

3.1.2 COMSOL Multiphysics

Finite Element Analysis (FEA), also known as Finite Element Method (FEM), is a numerical technique for finding approximate solutions of partial differential equations (PDE) and integral equations [141]. On the foundation of FEA technique, it is capable of simulating the behaviour of a structure, electromagnetic fields, fluid flow or thermal flow. The modelling has a high accuracy in description of the systems by reducing the governing partial differential equations for the system to groups of linear algebraic equations [142,143].

COMSOL Multiphysics is typical solver software based on FEA technique, which is able to simulate various physics and engineering applications, in particular, multiphysics phenomena. This software consists of modules to cover different application fields, including electrical, mechanical, fluid chemical and interfacing etc. Moreover, the number of available modules is increasing with the periodic updates made by the company [144]. The modules of COMSOL, which are used to obtain the simulations results in this thesis, include structural mechanics (to validate and predict the mechanical deformation of hydrogel), CFD (to study the behaviour of fluid flow) and chemical reactions (to investigate the mechanism of diffusion and reaction).

3.2 Equipment and Experiments

3.2.1 Equipment and Testing Techniques

Various types of equipment were used in the experimental studies of this thesis. According to their uses and applications, they are briefly described in this section.

For investigating the diffusion property of PHEMA hydrogel, the molecules of glucose diffuse out from the PHEMA hydrogel and spread into the PBS (Phosphate Buffered Saline) buffer solution which acts as the receptor of the glucose. To determine the amount of the glucose within the PBS buffer solution at a certain time point, ICB SBA-90 laboratory glucose meter was used. The glucose

meter is capable of detecting the concentration of glucose as low as 0.01 g/L.

For the purpose of examining the cytotoxicity of the PHEMA to cells, microplate reader (Tecan infinite F50), fluorescence microscope (Olympus DP71, TH4-200), optical microscope (Olympus IX71) and field emission scanning electron microscope (SEM JEOL JSM-7600F) were employed. They were employed based on three different methods used to evaluate the cytotoxicity of PHEMA to cells. Microplate reader (Tecan infinite F50) was utilised to evaluate the optical density of testing assay which can quantitatively measure the colour of formazan product from CCK-8 assay. The fluorescence microscope (Olympus DP71, TH4-200) and optical microscope (Olympus IX71) were able to detect the living cells and all the cells (both live and dead) respectively. The SEM (JEOL JSM-7600F) was applied to reveal the shape and status of cells which were cultured on PHEMA substrate for a long period.

In the investigation of adhesion strength of cells to PHEMA hydrogel, a self-built agitator was specially designed and assembled (details see Section 4.4.2, Page 57-59). It can achieve steady rotating speed (± 0.1 r/min) at the range of 100~150 r/min. This self-built agitator was able to offer a steady rotation to the ECM of the cells which can facilitate a designed hydrodynamic stress field.

To produce the partially swollen PHEMA specimen, GENLAB laboratory oven MINO/50 was used to dry the fully swollen PHEMA specimen to achieve specimens with various degree of swelling (DOS, defined by Eqn.3-1 at page 38).

All the mechanical compressive tests on PHEMA specimens were induced by the Instron Series 3366 Model universal testing machine, equipped with i) 10 kN load cell which was used for measuring the mechanical responses of PHEMA hydrogel under compression, including the failure of material; and ii) 50 N load cell which was used to employ the cycling compressive loads.

As for fabrication of microfluidic structure on the PMMA substrate, a circuit board engraving machine (Create-DCM3030) with a $30^\circ/0.1$ mm cutter (Fig.6-6b) was employed. The accuracy of the engraving machine was approximate 5 μm of the depth of microchannel, and the speed of spindle during manufacturing was set to be 1500 rpm.

Keyence VHX1000 Series digital confocal microscopy system equipped with 100X-1000X universal zoom lens was used to examine the cross-section of the multi-layered microfluidic structure, in order to visualise the membrane protrusion in the cavity of microchannels which induced by mechanical fastening technique.

3.2.2 Synthesis and Preparation of PHEMA Hydrogel

The polymerisation of hydrogels is a free radical induced catalysis which has been reported in literatures [145, 146, 147]. It is synthesised through the polymerisation using a homogeneous aqueous solution of the monomer HEMA (70 wt%), water solvent (30 wt%), crosslinker EGDMA (0.1 mol% of HEMA), catalyser TEMED (1.4% weight of HEMA) and initiator of the reaction ammonium persulphate APS (20% weight of water). The reaction of polymerisation is completed by 60% within 1 hour after mixing the chemicals in the mould [148]. The catalyser TEMED and the initiator of the reaction APS are fully consumed during the formation of the chains of PHEMA network, while the crosslinker EGDMA can provide the structural interconnections among the polymer chains, thus forming the stable chemical matrix in molecular scale.

For a given hydrogel at a fixed temperature, if the degree of crosslinker in the hydrogel is increased, the internal stress among polymer chains may be increased [149], and multiphase of hydrogels may be formed, thereby causing various mechanical properties of the hydrogel. Degree of crosslinker indicates that the amount of crosslinker agents in the hydrogel mixture solution. Higher degree of crosslinker in the hydrogel before polymerisation leads to smaller space between network junctions in the hydrogel after polymerisation, as a result of this, smaller degree of swelling of hydrogel is presented. For these reasons, the quantity of crosslinker agents (*e.g.* HEMA, EGDMA and any other components) was strictly controlled by using micropipettes, and the polymerisation of PHEMA specimen was carried out in this study at a fixed temperature by employing a thermostatic water bath, in order to keep side reactions to minimum and avoid a multiphase network structure formed inside the PHEMA during the specimen preparation.

PHEMA specimens are produced with required dimensions by using pre-shaped silicone mould in this work. Generally speaking, the geometry control of the PHEMA specimens during their polymerisation can be divided into three main steps: i) injecting the polymerising liquid mixture into silicone moulds (PDMS) for polymerisation; ii) waiting for the completion of polymerisation reaction; iii) extracting the PHEMA specimen from the silicone mould.

Fig.3-2 illustrates the procedures to fabricate the PHEMA hydrogel into required geometry with specific dimensions. PDMS (poly(dimethylsiloxane)) is used to make the silicone mould enabling self-adhesive property which can offer a proper sealing to prevent the polymerising PHEMA mixture leaking from the mould. Two flat polished aluminium dies are employed to close the system on both

sides. Aluminium is chemically stable during reaction of polymerisation, such chemical stability allow PHEMA specimen to be easily detached from the aluminium substrate at the extraction step (*d* to *e* in Fig.3-2). A copper spacer with certain thickness is assembled to determine the equilibrium thickness of the PHEMA hydrogel specimens. The polymerising liquid mixture is injected into the moulds within 5 minutes after the mixing of the initiator. It is then sealed and pressed by the aluminium plate covers to avoid leakages and constrain final geometry of the PHEMA samples (*b* to *c* in Fig.3-2). The polymerisation of the material should complete within 24 hours [119]. After that, the solid hydrogel can be extracted from the mould, which has to be washed with acetone enabling the removal of adhesive particles or contaminations.

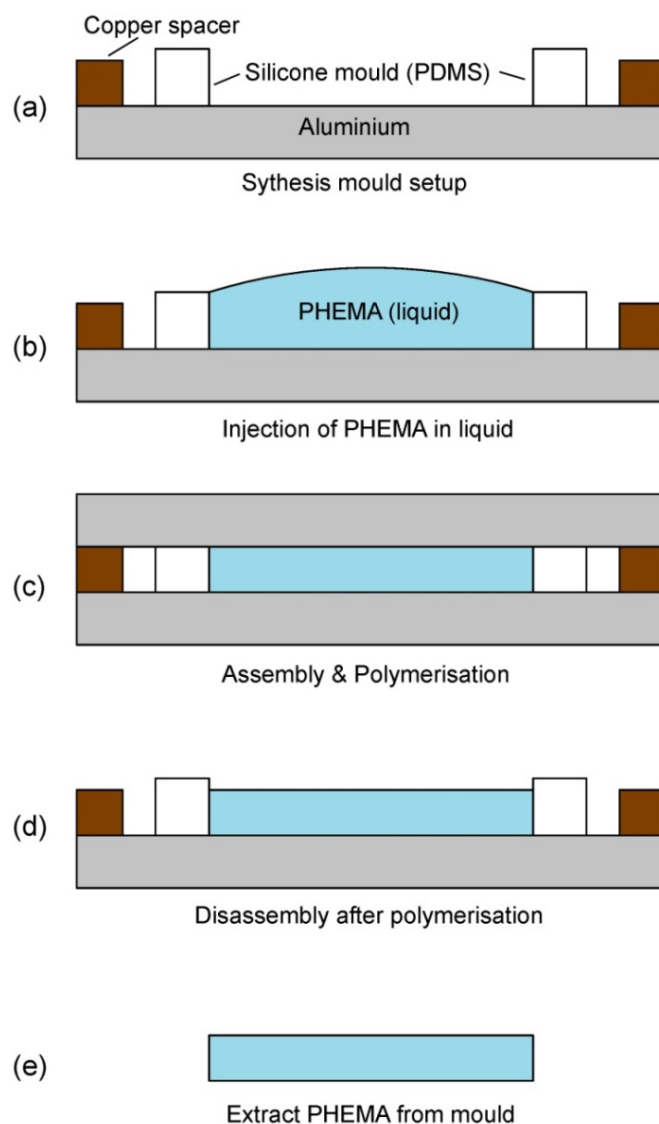


Fig.3-2. Schematic diagram of the fabrication process of a PHEMA membrane. (a) Settings of the mould; (b) Injection of the polymerising mixture solution; (c) Assembly by compressing, forms a closed chamber for polymerisation of PHEMA; (d) and (e) Disassembly of the mould and extract PHEMA after polymerisation completed.

PHEMA specimens have been fabricated in two types of geometry, *i.e.* cylinder and membrane, by modifying the shape of PDMS mould. For compressive test which aims to investigate the mechanical properties of PHEMA, the dimension of specimen in the direction of compressive load cannot be smaller than 5 mm. Otherwise, the range of compressive displacement is too small to be measured by the displacement acquisition system of the compressive testing machine. Therefore, cylindrical PHEMA specimens, with height of 12.5 mm, diameter of 18 mm and 32 mm, are synthesised, aiming to conduct the uniaxial compressive tests (see Chapter 5.3). Meanwhile, PHEMA membranes with thickness less than 1 mm have been fabricated, and used to conduct the experiments to evaluate the reliability of sealing of microfluidic system by PHEMA membrane. All the dimensions of the PHEMA specimens which are used in this thesis, are listed in the Table 3-2. The dimensions of the small PHEMA specimen, 9 mm diameter with 7 mm height, are used in the cycling compressive load test (Chapter 5.4), which is determined by the load cell (maximum 50 N) installed in the compression testing machine. The load cell with capacity of maximum 50 N is capable of cycling compressive load test which requires more sensitive measurement of stress than uniaxial compressive test, and the load cell with smaller measuring range (*e.g.* 50 N in compare with 10 kN load cell) can detect smaller change of load. Meanwhile, the large specimen with diameter of 29 mm and height of 26 mm are used in the diffusion test, because the bigger sample it is, the more molecules of solute it can absorb. For the PHEMA membrane specimens, the dimensions are determined by the customer designed microfluidic testing rig (described in Chapter 6), and are restricted by the Corning® Costar® multi-well plate for the cytotoxicity test (96-well plate, in Chapter 4.3) and ultimate fluidic shear stress test (6-well plate, in Chapter 4.4).

Table 3-2. Dimensions of PHEMA specimens

Geometry	Cylinder			Membrane	
Testing	Uniaxial compression	Cycling compression	Diffusion test	Sealing of microfluidic system	Cell culture substrate
Dimensions [mm]	Ø18, h12.5 Ø32, h12.5	Ø9, h7	Ø29, h26	28x38, h1 28x38, h0.8	Ø6.5, h1 Ø34, h1

Ø: Diameter. h: Height.

3.2.3 Swelling and Drying of PHEMA Hydrogel

After the PHEMA hydrogel is synthesised, a washing process has to be undertaken enabling the removal of the water-soluble contaminations or incomplete reacted molecules using ethanol aqueous solution. Within the same process, the take-up of water in the PHEMA can be gradually increased by reducing the concentration of ethanol in the solution, which can allow the immersed PHEMA to reach its fully saturated status prior to the fastening assembly process. However, different swelling conditions of PHEMA specimens are required for investigating the effect of degree of swelling on its mechanical properties. In such case, an additional drying process of the swollen PHEMA specimen is carried out to achieve various degree of swelling of PHEMA specimen.

As a network structural material, PHEMA hydrogel possesses the properties of interactive exchange between external molecules and the crosslinker agents of the material. Thus, for the types of the interactive exchange behaviours between external molecules (e.g. liquid or solutes) and the hydrogel material, the swelling process and the drying process follow physically-reversed mechanisms: i) Swelling, defined as the liquid molecules diffuse into the dried material, is usually occurs during the process of hydrogel in prepared state (Fig.3-2e) to the swollen state of hydrogel [150]. ii) Drying, depicted as the liquid molecules diffuse out from the swollen material, is used to achieve different degree of swelling of PHEMA hydrogel in this study. These two types of interactive exchange behaviours are experimentally investigated in the following sub-sections.

3.2.3.1 Swelling and Washing of PHEMA Hydrogel

Swelling of the hydrogel is a process that allows hydrogel to reach its hydrophilic/hydrophobic balance status (equilibrium swelling) from its dry status [151]. The equilibrium status of hydrogel can be achieved when the osmotic force of driving solvent into the hydrogel is identical to the elastic force between the stretched hydrogel chains [152]. The equilibrium swelling, which reflects the dimensional change of the material and the patterns of releasing drugs from the material, is controlled by the degree of crosslinker and the interaction between hydrogel chains and solvent molecules. At microscale, the hydrogel chains are pushed apart by the solvent molecules during swelling. Meanwhile, the solvent molecules attached on hydrogel chains and occupied the space between the hydrogel chains, which made the volume of swollen hydrogel larger than that of dry hydrogel.

During the swelling process, the solvent molecules enter into hydrogel material from outside to inside. It leads to the different degree of swelling in the hydrogel, which is higher at the outside layer and lower at the inside core. As a consequence, distributed dimensional change which is caused by the different degree of swelling can result in an internal stress inside the hydrogel specimen. The fracture of specimens can be potentially resulted from the internal stresses due to a rapid change of concentration gradient between the inside (glassy core) and outside (swollen surface) of the PHEMA material. In order to avoid the fracture of PHEMA specimen in this study, ethanol solution is used as a buffer to reduce the internal stresses during the swelling process of PHEMA specimens by gradually decreasing the concentration of ethanol in the solution for immersion of PHEMA specimen. The ideal process of changing the ethanol concentration guaranteeing PHEMA specimens have no internal crack during swelling, which is obtained based on empirical process by researchers in University of Milan, is depicted as the dashed curve in Fig.3-3a. However, such ideal process of ethanol concentration replacement cannot be achieved because the mechanism of the swelling of PHEMA obeys the Fick's law [153] because the swelling is the process that the solvent molecules diffuse into the network structure of PHEMA material.

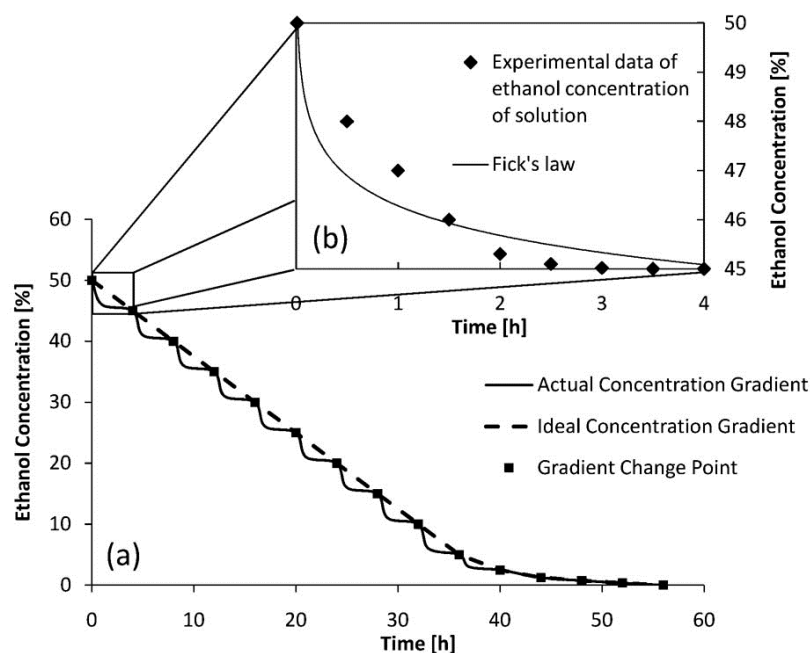


Fig.3-3. Swelling and washing process for PHEMA hydrogel. The ideal process of changing the ethanol concentration outside the PHEMA specimen is not achievable, and the actual swelling process is an approaching replica process to the ideal process, which obeys Fick's diffusion law.

On the basis of Fick's law, the diffusion flux of molecules is given by $flux = -P\Delta c$, where P is the permeability that does not change at a given temperature (e.g. room temperature), and the Δc is the

difference of the concentration of molecules between the inside and outside of the PHEMA specimen. Thus, the diffusion flux decreases with the decreasing of Δc , and the diffusion stops when the equilibrium is reached, e.g. concentration inside and outside of PHEMA specimen are same. Hence, when the PHEMA specimen is initially immersed into aqueous solution of 45 vol% ethanol solution after removed from 50 vol% ethanol solution, the change of the ethanol concentration inside the PHEMA specimen is obeying the diffusion mechanism which is described by Fick's law (Fig.3-3b).

To approach the ideal process of change of the ethanol concentration outside of PHEMA specimen, the periodic replacement of the ethanol aqueous solution is made (see the solid curve in Fig.3-3a). The PHEMA hydrogel specimen were firstly immersed into one litre of 50 vol% ethanol aqueous solution for 4 hours which can allow the PHEMA hydrogel being almost saturated with the 50 vol% ethanol solution. The PHEMA specimens were then removed from the 50 vol% solution and immediately transferred into the 45 vol% ethanol solution for another 4 hours to dilute the ethanol sucked in the specimens, which can serve the dual purposes: i) cleansing the residuals remained inside the PHEMA, and ii) reducing the ethanol content inside the specimens. This process was repeated by decreasing the concentration of ethanol solution by 5 vol% each time until ethanol content in the solution reached 5 vol%. After that, the ethanol content in the solution was reduced to 2.5 vol% and 1.25 vol% for further 8 hours before they were finally transferred into pure deionized water for 5 times to ensure the minimal ethanol content remaining inside the PHEMA specimens prior to the uses of such PHEMA specimens. It is understood that the handling of the PHEMA specimens at the final stage of treatment can be critical, thereby a smaller reduction (e.g. 2.5 or 1.25 vol%) of the ethanol concentration had to be applied to ensure no damages such as fracture can occur.

Therefore, compared with the ideal process of change of the ethanol concentration, the actual process which is implemented in this study shows a 'dip' in Fig.3-3 between every two concentration change points, but overall it still follows the trend of the ideal wash curve. This swelling and washing procedures of hydrogel materials take up to 3 weeks in total, and it shows a novel preparation process for hydrogels, which has similar time consumption but quite a different route of the preparation process from literature [154].

3.2.3.2 Drying of PHEMA Hydrogel

Drying of the hydrogel is a reverse process to swelling, which aims to evaporate solvent molecules out of the network structure of hydrogel. Drying of the PHEMA hydrogel in this study is used to obtain PHEMA hydrogel specimens in different degree of swelling (DOS) from their swollen status, in order to investigate the effect of DOS on the mechanical properties of PHEMA hydrogel.

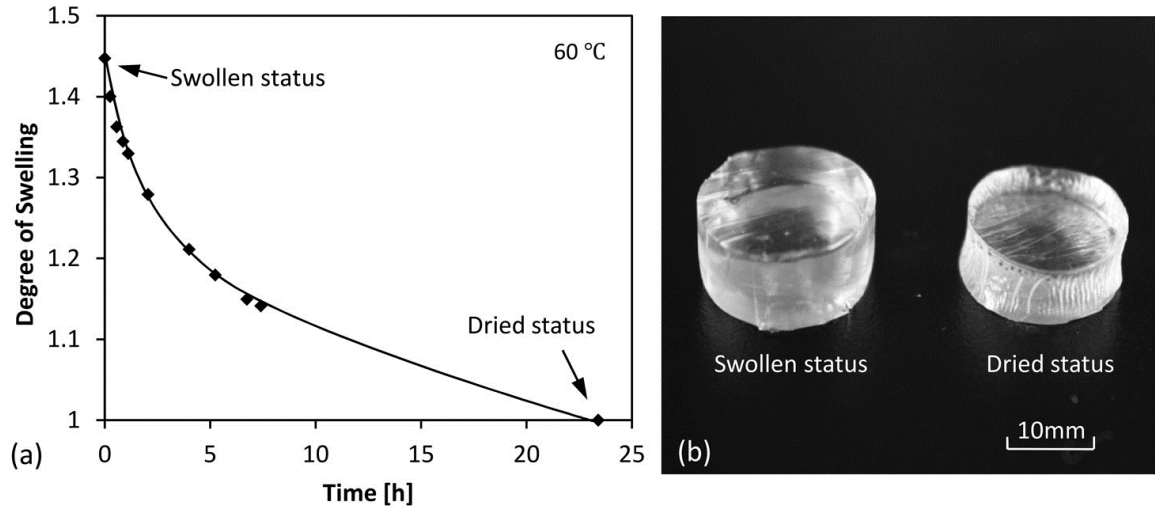


Fig.3-4. (a) Experimental data record on the DOS of PHEMA sample against time under drying environment with 60 Celsius degrees. (b) The pictures of the PHEMA cylindrical specimen in swollen status and dried status. These two specimens have same initial dimensions after synthesis.

Degree of swelling is defined as the ratio of mass of swollen polymer to mass of dried polymer, or the ratio of volume of swollen polymer to volume of the dried polymer [155]. For certain hydrogel specimen, the error of measuring the volume is usually larger than measuring the mass, this geometric error (e.g. non-parallelism of the surface on a cylindrical specimen) of specimen may thereby cause the inaccurate calculation of volumetric value. However, the mass of the specimen can be precisely measured (± 0.0001 g) by using an analytical weighing balance. Therefore, the ratio of mass of swollen PHEMA specimen (m_c) to mass of dried PHEMA (m_d) of the corresponding specimen is chosen to represent the degree of swelling of PHEMA specimen (q) in this study. Thus the expression of degree of swelling is given by

$$q = m_c/m_d \quad \text{Eqn.3-1}$$

where, m_c is the current weight of the PHEMA specimen on a certain time point, m_d is the weight of the dried PHEMA specimen. GENLAB laboratory oven MINO/50 has been used to dry the swollen PHEMA specimens to obtain specimens with different degree of swelling in this study. It offers a drying environment condition of 60 °C, which is higher than the VPTT for PHEMA hydrogel thus

allow the drying process of hydrogel to carry out. The drying speed of PHEMA specimen under 60 °C, which is obtained by measuring the current weight of the specimen over time, is illustrated in Fig.3-4a in terms of the DOS of PHEMA specimen against the drying time. The DOS decreases rapidly during the initial 2 hours of drying. The decreasing speed slows down with the increasing of time (2~8 hours), and reaches a constant value after 8 hours. It took approximate 24 hours for the hydrogel ultimately reach its dried status.

A method which refers to the drying speed graph (Fig.3-4a) is developed to estimate the dried weight of PHEMA specimen before reaching their dried status. For instance, if the PHEMA specimen with DOS of 1.2 is desired, the first step is to estimate the drying time. The DOS at 1.2 of PHEMA specimen corresponds to approximate 4 hours' drying time according to the curve in Fig.3-4a. Thus, the PHEMA specimen has to be placed in the oven under 60 °C for 4 hours. However, the value of DOS of such specimen after this process is still an approximated value, because that the precise dried weights of PHEMA hydrogel specimen (m_d) is yet to know before reaching its dried status, due to slight dimensional difference among the specimens. The procedures for acquiring the PHEMA specimens which can be used for mechanical test with precise values of DOS are developed and recorded as follows:

- 1) Measure the dimensions and weight (m_e) of a PHEMA specimen at its equilibrium swollen status.
- 2) Check the estimate drying time according to Fig.3-3a to obtain the desire degree of swelling. Place the specimen into oven (60 °C) and start time counting.
- 3) Extract the specimen out of oven after reaching the drying time, and cool the specimen down to room temperature. Then measure the weight (m_c) of the specimen.
- 4) Perform the mechanical test, *i.e.* uniaxial compression or cycling compressive test.
- 5) Collect the specimen after mechanical test, and place the specimen back into oven for further drying.
- 6) Remove the specimen from the oven after 24 hours, then measure the weight of the specimen (m_d).
- 7) The precise value of DOS for the PHEMA specimen which was employed in the mechanical test can be calculated using Eqn.3-1.

As a result, PHEMA specimens with the values of DOS at 1.1, 1.3, 1.35 and 1.45 are prepared according to such drying procedures, to investigate the effect of DOS on mechanical characteristics of PHEMA hydrogel, which is reported in Chapter 5.4 in details.

Chapter 4. Diffusion and Biocompatible Properties of PHEMA Hydrogel

4.1 Introduction

The characteristics of diffusion of glucose molecules in poly(2-hydroxyethyl methacrylate) (PHEMA) hydrogel have been investigated in this chapter, because PHEMA hydrogel membrane acts as a molecule transport media in the designed microfluidic device (see Fig.1-1) according to its diffusion property. The reasons that glucose is chosen to be the transport molecule in these experiments are: i) Glucose, one of the basic monosaccharide, is the main energy source that cells need during culturing. ii) Comparing with other necessary molecules for cell culture, *e.g.* oxygen or carbon dioxide, glucose is more convenient to be detected within the solution. The test of the diffusion property of PHEMA hydrogel consists of two experiments: (a) the first one aims to evaluate the speed of glucose diffuses out from PHEMA specimen, such as the release rate of glucose from PHEMA hydrogel. On the basis of the kinetic theories of diffusion and the experimental results, the characteristics of diffusion of glucose molecules in PHEMA hydrogel can be quantitatively determined. (b) The second one aims to determine the absorb capacity PHEMA hydrogel to glucose in terms of the maximum glucose that a PHEMA specimen can absorb under the current chemical environment.

Another factor which can indicate the feasibility of integrating PHEMA in microfluidic devices for bioengineering purposes is the interactive effects of PHEMA to cells, *e.g.* cytotoxicity or biocompatibility. According to literatures, PHEMA hydrogel has been used in bio-purpose applications, such as contact lens [85,86]. It can be regarded as a biocompatible material, but the quantitative measurements of such biocompatibility are rarely reported. Thus, cytotoxicity and the adhesion strength of PHEMA to cells are experimentally evaluated in this study. Both HUVECs (Human umbilical vein endothelial cells) and fibroblasts are employed as target cells and cultured on the PHEMA substrate, in order to obtain the influence of PHEMA substrate to the cells' viability in terms of determination of the cytotoxicity of PHEMA. These two kinds of cells are the most popular models to investigate the effect of ECM (extracellular matrix) to cells. In the experiment to evaluate the adhesion strength of PHEMA to cells, a fluidic viscous force is applied on HUVECs to mimic the

fluid flow above cells in perfusion microfluidic device, after that they are seeded on the PHEMA substrate and formed a strong adhesion on the substrate. Under such fluidic viscous force induced by hydrodynamic shear, cells may be detached from the PHEMA substrate if the fluidic viscous force is high enough. Therefore, the value of adhesion strength of the PHEMA substrate to cells can be derived according to the minimum value of fluidic viscous force that can make cells detached. The value of such adhesion strength provides a reference to design the maximum flow rate for the perfusion culture device.

4.2 Diffusion Properties of Swollen PHEMA Hydrogel

4.2.1 Kinetic Theories of Diffusion

When a swollen hydrogel is sank into buffer solution, the exchange of molecules between hydrogel and its external environments starts immediately. In this study, cylindrical PHEMA hydrogel specimen, which is fully swollen by glucose solution (200 g/L), is placed into PBS buffer (Phosphate Buffered Saline) to investigate the kinetics of diffusion of PHEMA hydrogel to glucose, including diffusion speed, diffusion mechanism and capacity of absorption. PBS buffer is a kind of common used buffer solution in biological research which can mimic the environment of inside human body, because the pH value, osmolarity and ion concentrations of PBS buffer are identical to the isotonic environment of human body.

To analyse the characteristics of molecules diffusion in PHEMA hydrogel, a time dependent model, which is based on an empirical power equation, was developed by Peppas *et al.* [140]:

$$\frac{M_t}{M_\infty} = kt^n, \quad \text{Eqn.4-1}$$

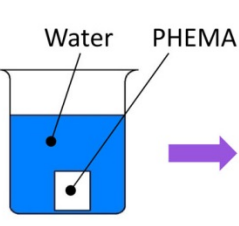
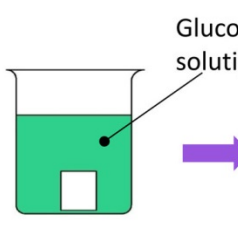
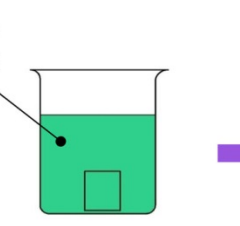
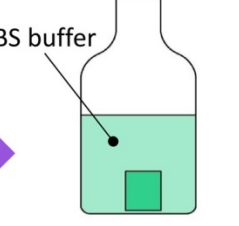
where M_t and M_∞ denote the absolute cumulative amounts of molecule released from the hydrogel at time t and at the equilibrium respectively; k is a constant related to the properties of hydrogel network, *e.g.* structure, degree of crosslinker. And n is the diffusion exponent. According to the literature [156], three models which are dependent of the numerical range of the diffusion exponent n , can indicate the characteristics of releasing molecules from hydrogel material: (1) Fickian diffusion ($n=0.5$), diffusion controlled release process; (2) Zero-order model ($n=1$), swelling controlled release process; (3) Ritger-Peppas's empirical model ($0.5 < n < 1$), anomalous release with respect to the applicability. According to Eqn.4-1, it is easy to notice that the relationship between

$\ln(M_t/M_\infty)$ and $\ln(t)$ is linear, with slope n and intercept k . Meanwhile, the values of M_t/M_∞ and t can be obtained from the cumulative release experiment. The value of diffusion exponent n can be determined based on the results from cumulative release experiment, to indicate which kind of kinetics model can best describe the diffusion characteristics of glucose in PHEMA hydrogel.

4.2.2 Experimental Methods

Two cumulative release experiments are conducted, with the purposes of i) investigating the diffusion characteristics of PHEMA, when it is interacted with glucose molecules; ii) studying the capacity of absorption of PHEMA hydrogel to glucose.

Table 4-1. Process of the cumulative release experiment to determine diffusion characteristics of glucose in PHEMA.

			
Step 1	Step 2:	Step 3:	Step 4:
PHEMA specimen swollen in water	Diffuse in glucose solution	Glucose completely diffused in PHEMA	Diffuse glucose out in PBS buffer
Conditions: <ul style="list-style-type: none"> • Diluted water • Swell for 72 hours 	Conditions: <ul style="list-style-type: none"> • 200 g/L glucose solution • 37 °C, 100r/min stirring • Swell for 72 hours 		Conditions: <ul style="list-style-type: none"> • 300 ml PBS buffer • 37 °C, 100 r/min stirring • Swell for 24 hours • Extract 3 ml sample at certain time point

For the first type of cumulative release experiment (Purpose I), the experimental set-ups, conditions and descriptions are illustrated in the Table 4-1. Step 1, 2 and 3 are the preparing procedures, aiming to fabricate the PHEMA specimen which is filled with glucose molecules. 72 hours of stirring ensure that the glucose concentration inside the PHEMA specimens saturates completely. The step 4 aims to obtain the speed that glucose molecules diffuse out from the PHEMA specimen, by monitoring the glucose concentration in the PBS buffer over time. The constant environment for the diffusion experiment under 37 °C and 100 r/min stirring are maintained in water bath and using a magnetic stirring system.

According to the step 4 in Table 4-1, 3 ml solution is withdrawn from the PBS buffer solution outside the PHEMA specimen and immediately replaced by 3 ml fresh 37 °C PBS buffer solution at the designated time interval points (t_x). The samples of such withdrawn solution are stored in -5 °C fridge in order to avoid the glucose diffusing out from the PHEMA specimen to be consumed by germs which may affect the accuracy of the experimental results. Thus, ICB SBA-90 laboratory glucose meter (± 0.01 g/L) is employed to measure the glucose concentration in the withdrawn solution samples. However in such step 4, the small amount of glucose exists in 3 ml solution which is extracted from the PBS buffer solution every time at t_x , but the 3 ml replaced PBS buffer solution does not contain any glucose. This process causes a glucose loss, thus underestimates the amount of glucose which is released from the PHEMA specimen. Aiming to eliminate such glucose loss, the amount of glucose released from PHEMA specimen has to be calculated:

$$M(t_x) = M_m(t_x) + \frac{3[\text{ml}]}{300[\text{ml}]} \times \sum_1^{x-1} M_m(t_x) \quad \text{Eqn.4-2}$$

where, $M(t_x)$ and $M_m(t_x)$ are the actual amount and measuring amount of glucose at the designated time interval points t_x respectively; x is the order number which indicates the withdraw time of the 3 ml PBS buffer solution. The equilibrium value of $M(t_x)$ equals to the value of M_∞ from Eqn.4-1.

Table 4-2. Process of the cumulative release experiment to determine the capacity of absorption of PHEMA hydrogel on glucose molecules.

Step 1	Step 2:	Step 3:	Step 4:
Glucose completely diffused in PHEMA	Diffuse glucose out in PBS buffer	Diffuse glucose out in fresh PBS buffer after 24 hours.	Diffuse glucose out in fresh PBS buffer until glucose reach 0 g/L
Conditions: <ul style="list-style-type: none"> • 200 g/L glucose solution • 37 °C, 100 r/min stirring • Swell for 72 hours 	Conditions: <ul style="list-style-type: none"> • 300 ml PBS buffer • 37 °C, 100 r/min stirring • Swell for 7 days • Extract 3 ml sample 		

The experimental set-ups, conditions and descriptions for the other type of cumulative release experiment (Purpose II) which aims to study the capacity of absorption of PHEMA hydrogel to glucose, are summarised in the Table 4-2. The step 1 in Table 4-2 is the same as the step 3 in Table 4-1, ensuring the glucose completely saturated inside the PHEMA specimen. The experimental steps of such cumulative release experiment (Purpose II) are described as follows: (1) Place the PHEMA specimen into PBS buffer solution to diffuse the glucose out from the specimen. (2) Keep the environment under 37 °C, 100 r/min stirring for 24 hours, which allows the releasing of the glucose reach the equilibrium. (3) Extract 3 ml of the PBS buffer, mark as sample number y and store in fridge to keep temperature of -5 °C, to avoid consumption of the glucose by germs. (4) Then place the PHEMA specimen into 300 ml fresh PBS buffer solution, and repeat the Step 2 and 3. This repeat process is terminated if the concentration of glucose in PBS buffer is zero (Step 4). To guarantee the zero concentration of glucose, many times of the repeat of Step 2 and 3 have to be implemented. In this study, seven times of repeat were carried out, which means the samples marked with y ($y=1, 2, 3...7.$) have been obtained. Therefore, the amount of glucose that is absorbed by the PHEMA specimen ($M_{glucose}$ [mol]) is given by:

$$M_{glucose}[\text{mol}] = \sum_{y=1}^7 M_y [\text{g}] \times \frac{1}{180} [\text{mol/g}] = 300[\text{ml}] \times \sum_{y=1}^7 C_y [\text{g/ml}] \times \frac{1}{180} [\text{mol/g}] \quad \text{Eqn.4-3}$$

where, M_y denotes the mass of glucose [g] that diffused out from PHEMA specimen at the time corresponding to the number y . C_y is the measured concentration of glucose [g/ml] from the withdrawn solution sample, which is marked as number y . As previously, the concentration of glucose was measured utilising the ICB SBA-90 laboratory glucose meter (± 0.01 g/L). Thus, the capacity of absorption of PHEMA hydrogel to glucose can be given by:

$$\text{Capacity of absorption } (\Gamma [\text{mol/kg}]) = \frac{\text{Amount of glucose absorbed by PHEMA } (M_{glucose} [\text{mol}])}{\text{Mass of PHEMA specimen } (M_{PHEMA} [\text{kg}])} \quad \text{Eqn.4-4}$$

4.2.3 Results and Discussion

4.2.3.1 Glucose Release Rate

According to the Eqn.4-1, the experimental results from the cumulative release experiment (Purpose I) are presented in Fig.4-1a in terms of the amount of glucose releasing from PHEMA hydrogel over time. It indicates that the diffusion speed of glucose from the PHEMA hydrogel decreases with time, and approaches the equilibrium after 24 hours. The high diffusion speed at the beginning is caused by the initial large difference of glucose concentration between inside and

outside environments of PHEMA specimen. With the increasing of time, glucose molecules diffuse out from PHEMA specimen and spread into the PBS buffer solution, thus reduce the difference of glucose concentration between inside PHEMA and the PBS buffer environment. To determine the value of the diffusion exponent n in Eqn.4-1, the linear equation of the positive correlation between $\ln(M_t/M_\infty)$ versus $\ln(t)$ is plotted in Fig.4-1b. According to the intercept and slope of the linear fit, the values of k and n are calculated by $k=0.273$, $n=0.456$. Based on the literature [157], the values of $n \sim 0.5/0.45/0.43$ for the specimen geometry of slab/cylinder/sphere respectively, indicate a diffusion-controlled drug release process, in other word, Fickian diffusion mechanism. Thus, the diffusion characteristics of PHEMA hydrogel to the water soluble molecules can be described by the Fick's law. This result offers an experimental validation for that the Fick's law is applicable to describe the behaviour of swelling, which is depicted in Section 3.2.3. Based on the Fickian diffusion for one-dimensional molecule transport, the equation for determining the diffusion coefficient D for initial stage is given by [158]:

$$\frac{M_t}{M_\infty} = 4 \sqrt{\frac{Dt}{\pi\delta^2}} \quad \text{Eqn.4-5}$$

where δ is the height of the PHEMA hydrogel cylinder, which is measured as 26 mm. Thus, the approximate value of the diffusion coefficient of PHEMA hydrogel for early time ($t=1$ s) is calculated as $D=0.099$ [cm²/s], by employing Eqn.4-5.

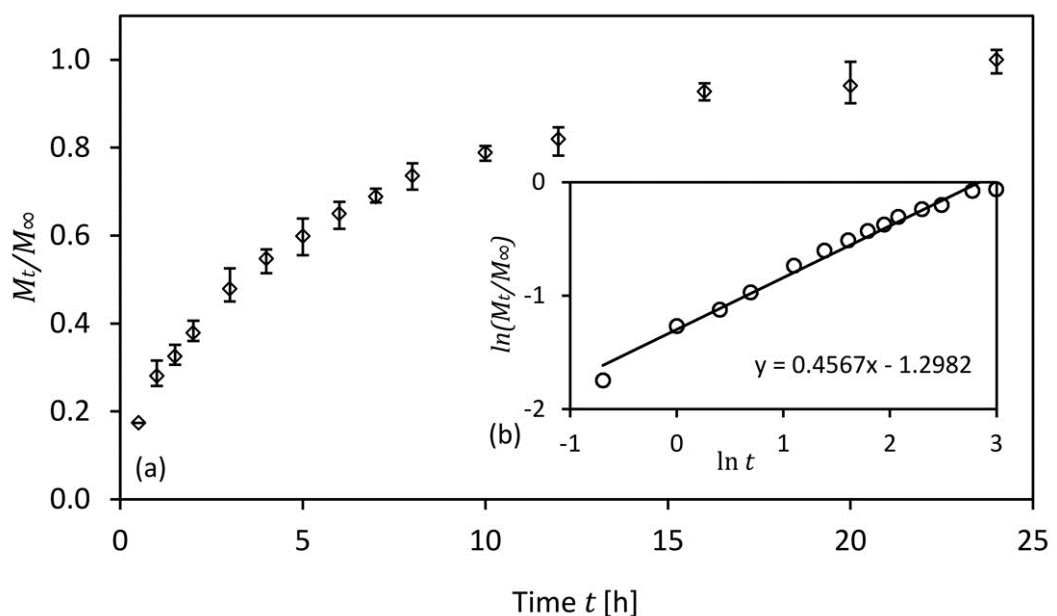


Fig.4-1. (a) Release profile of glucose from PHEMA hydrogel in PBS buffer solution at 37 Celsius degree for 24 hours. (b) linear plot of $\ln(M_t/M_\infty)$ versus $\ln(t)$, to determine the diffusion exponent. The equation of the linear fit of the data is shown. Each set of data was the value averaged from four parallel experiments.

4.2.3.2 Capacity of Absorption

The relationship between the mass of glucose that diffused out from PHEMA at the time corresponding to the number y is illustrated in the bar graph of Fig.4-2 with time. Two parallel experiments on the same PHEMA hydrogel specimens (Specimen 1 and Specimen 2) were conducted in this study. As is shown in the Fig.4-2, the PBS buffer solution from the first time refresh ($y=1$) contains most of glucose releasing from PHEMA specimen which is caused by large diffusion speed induced by the large difference of glucose concentration between the PHEMA inside and in the PBS buffer environment. After the wash by refreshing of PBS buffer ($y=2,3,4$), the glucose inside PHEMA is removed from PHEMA hydrogel, thereby causes less and less glucose molecules are detected from such PBS buffer samples. To ensure enough times of refreshing process have been conducted (step 2 and 3 in Table 4-2), the value of M_y ($y=7$) has to be identical to zero, thus guarantee all the glucose molecules have been removed from the PHEMA specimen, and the amount of such glucose molecules are all considered in the calculation of the capacity of absorption (Γ). Therefore, according to Eqn.4-3 and Eqn.4-4, the total amount of glucose $M_{glucose}$ [mol] and the capacity of absorption Γ [mol/kg] are calculated and listed in the Table 4-3.

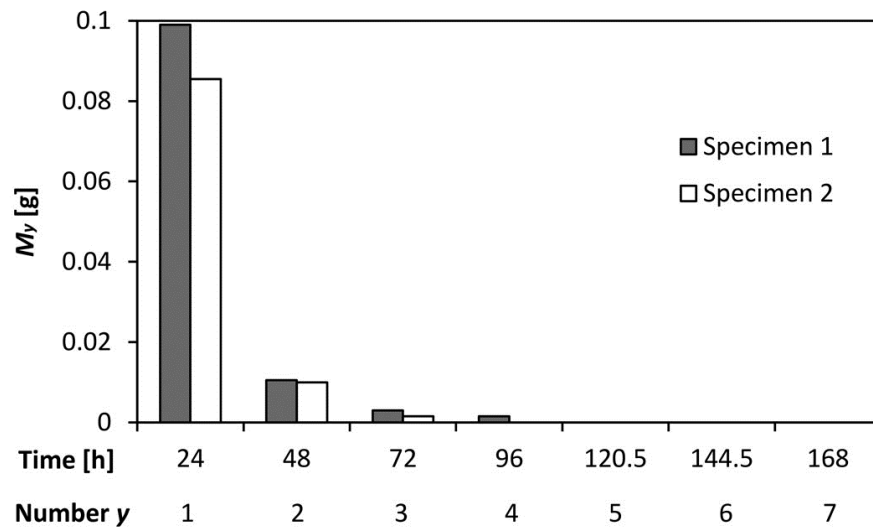


Fig.4-2. Bar graph of the amount of glucose detected from the PBS buffer solution versus the time. Sum the amount of glucose from all the refresh PBS buffer solutions, the amount of glucose absorbed by PHEMA hydrogel specimen can be obtained.

In summary, through the glucose release experiments, the diffusion characteristics of PHEMA hydrogel to glucose molecules can be described by Fickian diffusion, which is also known as the diffusion-controlled release process. The diffusion coefficient of glucose molecules in PHEMA hydrogel has been determined as $D=0.099$ [cm²/s]. Meanwhile, the capacity of absorption of

PHEMA hydrogel in terms of the amount of glucose absorbed by 1 kg swollen PHEMA hydrogel specimen that has been experimentally determined is 0.038 mol approximately. These two parameters, $D=0.099$ [cm²/s] and $\Gamma=0.038$ [mol/kg], will be retrieved and used in the simulation work in Chapter 7.

	Specimen 1	Specimen 2
$M_{glucose}$ [mol]	6.33x10 ⁻⁴	5.39x10 ⁻⁴
Dimensions [mm]	Ø29, h26	Ø29, h24
Volume [cm³]	17.16	15.84
Mass [kg]	0.016	0.015
Capacity of absorption [mol/kg]	0.039	0.037

Ø: Diameter. h: Height.

4.3 Cytotoxic effect of PHEMA on cells

4.3.1 Principle and Methods

The cytotoxicity of PHEMA has been examined by two methods: i) Live/Dead Cell Staining imaging, which is used to quantitatively determine the number of live cells or dead cells within a culturing well. ii) Cell viability measurement, which is a quantitative method to determine the viability of cells. Comparing the status of the cells which are cultured on PHEMA membrane and the status of those are cultured without PHEMA membrane, the effect of PHEMA membrane as a substrate to the proliferation or differentiation of cells can be obtained by utilising these two examining method, *i.e.* Live/Dead staining and cell viability measurement.

4.3.1.1 Live/Dead Cell Staining Imaging

Live/Dead cell staining imaging is a common staining technique to visualise the status of cells (*e.g.* live or dead) through highlighting specific chemicals or molecules in the biological tissues [159]. In this study, the staining assay which is named acetoxymethyl ester of calcein (Calcein AM) is incorporated to highlight the living cells. The Calcein AM is able to penetrate the cell membrane of living cells, and be hydrolysed by the cellular esterases inside living cells into green-fluorescent Calcein, which emits green light at the wavelength of 515 nm. As dead cells lack active esterases,

only live cells are able to be highlighted [160]. Thus, by adding the solution of Calcein AM into the cell culture plate, the number of live cells can be counted through detecting the green colour of the fluorescence reagents in cells using fluorescence microscope. Meanwhile, the total number of cells, including living cells and dead cells, can be obtained by observing the same visual range of the cell culture plate using normal optical microscope. Therefore, by calculating the percentage of living cells to the total number of cells which are observed within the same visual range, the toxicity of culture substrate (PHEMA hydrogel) to the cells can be quantitatively determined.

4.3.1.2 Cell Viability Measurement

The Cell Counting Kit-8 (CCK-8) assay (DOJINDO, Japan) is utilised in this study, to examine the viability of cells which are cultured on PHEMA hydrogel substrate for long period. Owing to the stability of CCK-8 solution, long time such as 24 to 48 hours incubation of cells becomes possible. CCK-8 allows sensitive colorimetric assays for the determination of cell viability in cell proliferation and cytotoxicity assays. The sensitivity of detection utilising CCK-8 assay is higher than that of experiments using other tetrazolium salts such as MTT, XTT or MTS [161].

CCK-8 assay primarily consists of a highly water-soluble tetrazolium salt with pink colour, WST-8 (2-(2-methoxy-4-nitrophenyl)-3-(4-nitrophenyl)-5-(2,4-disulfophenyl)-2H-tetrazolium), which can produce water-soluble formazan dye upon bioreduction in the presence of an electron carrier, 1-Methoxy PMS [162]. After the bioreduction of WST-8 performed by cellular dehydrogenases, an orange colour of formazan product is produced. Theoretically, the amount of formazan product is proportional to the number of living cells. Thus, the number of living cells can be obtained by detecting the amount of the formazan product by measuring its optical density value at the wavelength of 450 nm. In this study, the optical density values of the solutions were detected using the microplate reader, Tecan infinite F50.

To guarantee the experimental results are reliable, three experimental groups which were set up in this study to calculate the cell viability: (i) the experimental group (cells incubated upon PHEMA substrate), (ii) the control group (cells incubated normally, without PHEMA substrate) and (iii) the blank group (culturing media without any cells). As the colour of culturing media may affect the measurement of optical density, the measuring results (optical density ' A_{blank} ') of the blank group has to be excluded from the measuring results of both experimental group (A_{exper}) and control group

($A_{control}$). Thus, the cell viability of experimental group (V_{exper} [%]) is given by:

$$V_{exper} = \frac{A_{exper} - A_{blank}}{A_{control} - A_{blank}} \quad \text{Eqn.4-6}$$

According to the literatures [163,164], it can confidently draw the conclusion that the *in vitro* environment (e.g. PHEMA substrate in this study) does not affect the proliferation of cells, if the value of cell viability from experimental group (V_{exper}) is calculated larger than 80%. Otherwise, the *in vitro* environment is toxic to cells.

4.3.2 Preparation of PHEMA Substrates and Cells

The cells for both Live/Dead cell staining imaging and cell viability measuring are cultured on the PHEMA hydrogel membrane within a standard 96-well microplate from Corning corporation [165]. As is illustrated in Fig.4-3, cells are cultured on the top surface of the PHEMA substrate in the culture medium. In the present study, PHEMA hydrogel membrane has been synthesised and cut to fit the dimensions of the culture well, *i.e.* 6.8 mm diameter and 1mm thickness. Before placing the cells, the PHEMA membrane has to be firstly processed in ultrasonic cleaner for 10 mins to remove the dirt or other particles on the surface of membrane, then sterilised by autoclave for 20 mins under 121~125 °C, and finally dipped into the solutions of sterilised PBS (Hyclone, USA) for three days, and refreshed daily.

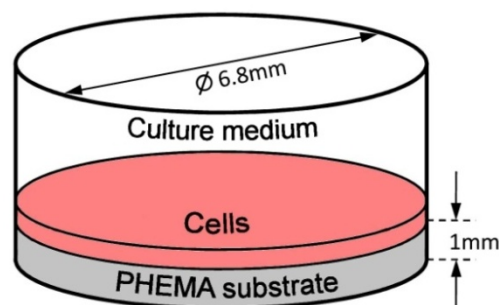


Fig.4-3. Schematic diagram of culturing cells on PHEMA hydrogel substrate in a 96-well plate. The thickness of PHEMA hydrogel membrane is 1 mm. Cells are incubated upon the surface of the PHEMA membrane. Culturing media is filled in the whole chamber.

For the Live/Dead cell staining imaging, primary human fibroblasts have been used as the cells which are cultured on PHEMA substrate, the shape of fibroblasts after differentiation is unique as they have branched cytoplasm surrounding its nucleus. It is easily to distinguish the living fibroblasts from dead ones by observing their characteristics of shapes. Living or active fibroblasts can be recognised by their abundant rough endoplasmic reticulum. Dead or inactive fibroblasts can

be found as a ball-like geometry (Fig.4-5a) which is far smaller than the active fibroblasts [166]. The primary human fibroblasts used in the present experiment were derived from human foreskins, from donors undergoing circumcision upon their informed consent, and were approved by the ethics committee of WUHAN Union Hospital (Wuhan, China). The cells were seeded on PHEMA hydrogel substrate in 96-well plates at a density of approximate 5000 cells/cm² and incubated in Dulbecco's Modified Eagle Medium (DMEM) (Hyclone, USA) with 10% fetal bovine serum (FBS) (Gibco, Invitrogen, USA) and 1% penicillin-streptomycin (MP Biomedicals, USA). The culturing of cells was maintained in an atmosphere of 37°C and 5.0% CO₂. After the incubation over 24 hours, the cells which are cultured on the PHEMA membrane are ready to be visualised using Live/Dead cell staining imaging.

Before staining cells using Calcein AM assay, 1 ml PBS (Hyclone, USA) has to be firstly added to the culture well enabling the washing of cells and removal of esterase from serum. Esterase may cause false positive results during the fluorescent measurement, for instance, esterase may be released from living cells and attached on the surface of dead cells, thereby causes the false positive results that dead cells can also emit green light and exhibits identical to living cells. After the washing process for cells, 200 µl Calcein AM assay was added to culture well under the conditions of 37°C and 5.0% CO₂. Such 1 mmol/L Calcein AM assay was obtained by mixing 1 mg Calcein AM (Dojindo, Japan) and 1 ml anhydrous DMSO (Dojindo, Japan). After the stirring and mixing over 20 minutes, the fluorescent reagents in the culture well were removed and replaced by 500 µl PBS prior to observing the results using fluorescence microscope (Olympus DP71, TH4-200).

For the experiment of cell viability measurement, human umbilical vein endothelial cells (HUVECs) derived from the endothelium of veins from the umbilical cord are used. HUVECs serve as a widely used model to study the functions of endothelial cells and the responses of such endothelial cells to stretch, shear forces or culturing environments *in vitro* [167,168]. In this study, HUVECs, which were collected by Peking Union Medical College Hospital (Beijing, China), were grown and differentiated under the same conditions that were used to culture fibroblast, 10% FBS and 1% penicillin-streptomycin within 37°C and 5.0% CO₂ atmosphere. After the incubation over 24 hours (group 1) and 48 hours (group 2), the values of the viability of the HUVECs cultured on PHEMA hydrogel substrate of each group are calculated using Eqn.4-6.

4.3.3 Results and Discussions

Based on the experiment of Live/Dead cell staining, Fig.4-4 illustrates the cells on PHEMA substrate in the same visual range under the same magnification, Fig.4-4a and Fig.4-4b were taken by optical microscope (Olympus IX71) and fluorescence microscope (Olympus DP71, TH4-200), respectively. According to Fig.4-4a, both the living and dead fibroblasts are clearly visualised: differentiated fibroblasts are exhibited as strips or branches; undifferentiated or differentiating fibroblasts are in the shape of bright spots. Fibroblasts of $N_{all}=55$ can be counted in this visual range of Fig.4-4a. Meanwhile, the number of live fibroblasts can be obtained from the image taken by fluorescence microscope (Fig.4-4b) at $N_{live}=46$, by counting the green illuminated points as the live cells. Owing to these two images are focused on the same area of the PHEMA substrate with same visual range, the cell viability which is defined as the percentage of live cells to all seeded cells can be given by:

$$Cell\ viability = \frac{N_{live}}{N_{all}} \times 100\% = 83.6\% \quad \text{Eqn.4-7}$$

According to the literatures [163,164], the testing environment is not cytotoxic to cells if the cell viability is higher than 80%. As a result of the current experiment, the cell viability which is calculated as 83.6% indicates that PHEMA membrane as a substrate for cell culture has no cytotoxic effect on the proliferation or differentiation of fibroblasts.

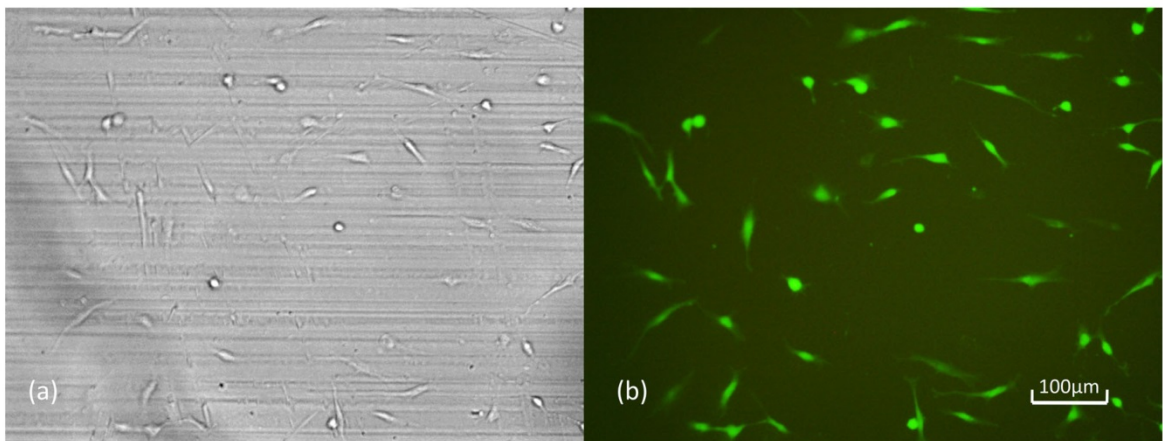


Fig.4-4. Image of fibroblasts cultured on PHEMA membrane over 24 hours, observed by optical microscope (Olympus IX71). (b) Image of fibroblasts cultured on PHEMA membrane over 24 hours, in same visual range and same scale of the image of (a), which is observed by fluorescence microscope (Olympus DP71, TH4-200). Colour reference: Green for live cell.

Another experiment for indicating that PHEMA hydrogel has no cytotoxicity to fibroblasts is through the observation on the individual shape of fibroblast using SEM photographs. Highly

differentiated fibroblasts are observed in Fig.4-5, in the shape of thin spindle (Fig.4-5a) and big flat plate with two branches (Fig.4-5b). A large number of fibroblasts on PHEMA substrate with such highly differentiated states can be found after 24 hours' incubation. Therefore, it is an individual and direct proof that fibroblast can be successfully cultured on PHEMA substrate, and PHEMA hydrogel has no cytotoxicity to fibroblast.

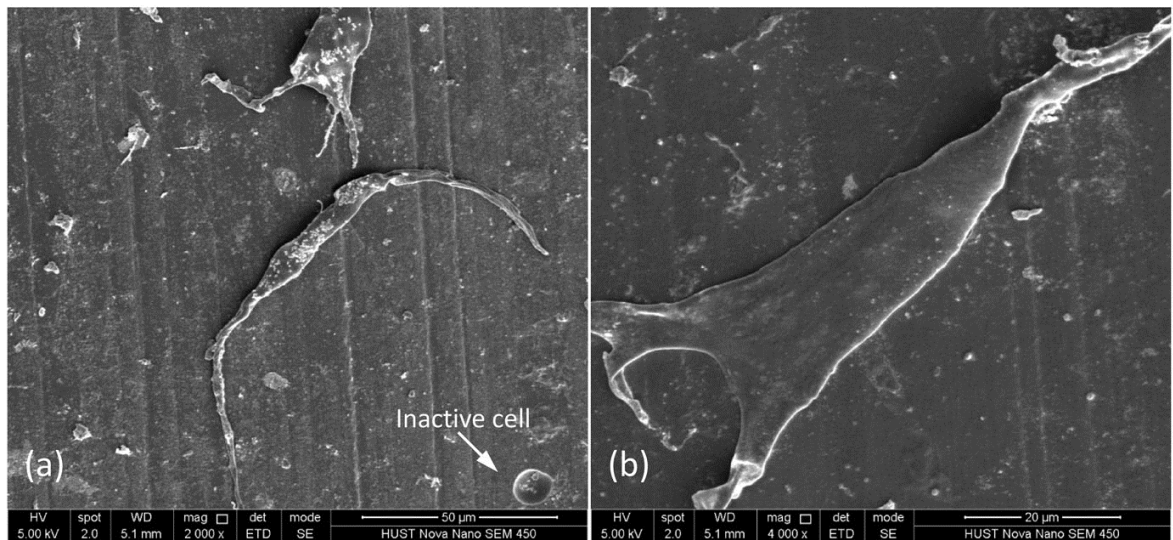


Fig.4-5. SEM photographs of fibroblasts which are cultured on PHEMA membrane. (a) Image of highly differentiated active fibroblast and an inactive fibroblast seed. The magnification is 2000x. (b) Image of an active fibroblast with two branched cytoplasm. The magnification is 4000x.

Moreover, quantitatively evaluation of the cell viability on PHEMA substrate was carried out based on the HUVECs cells. HUVECs were planted on the PHEMA membranes for two groups, one group for 24 hours' culture, and the other one for 48 hours' culture. When the incubation complete, CCK-8 assay was added to the culture medium and reacted with the living cells. After measuring of the optical density at the wavelength of 450 nm of the culture medium, the viability of HUVECs cells was quantitatively obtained utilising the equation of Eqn.4-6. The results of cell viability on each group are compared with that of their corresponding control group, and illustrated in the bar graph of Fig.4-6, thus 59.7% for the group of 24 hours' culture, while 80.6% for the group of 48 hours' culture. According to the literature [169,170], the degree of cytotoxicity may be underestimated if the incubation time is greater than 24 hours, because i) cytotoxicity (e.g. necrosis) normally occurs at the initial stage of culturing rapidly and ii) cells are able to adapt the severe environment through their differentiations. However, according to the aims & objectives in Chapter 1, the device which is developed in this study is designed to enable automatic perfusion cell culture for long term

incubation. Thus, the cell viability of longer culturing group (48 hours' culture) is more convincing to display the effect of PHEMA hydrogel to HUVECs than that of 24 hours' culturing group. Therefore, the viability at 80.6% concludes that PHEMA hydrogel membrane utilised as cell culture substrate is not toxic to HUVECs at long term incubation (48 hours).

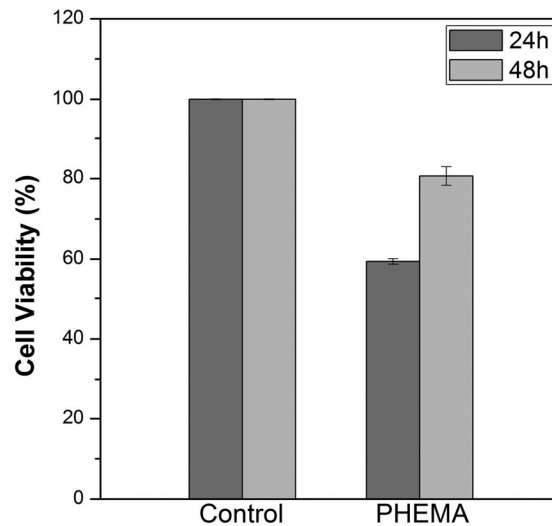


Fig.4-6. Cell viability test on HUVECs for 24 hours and 48 hours, was conducted using CCK-8 assay. Cells are incubated on PHEMA substrate in PHEMA group, and incubated normally (without PHEMA) in Control group. All incubation of cells was performed under 37°C and 5.0% CO₂ atmosphere. The error bar of each group consists of the results from three parallel tests.

To summarise the results from these experiments on the cytotoxicity of PHEMA as a substrate for cell culture, 83% fibroblasts with highly differentiated shapes are detected on PHEMA membrane; and approximate 80% cell viability are obtained by culturing HUVECs on PHEMA membrane over 48 hours. Accordingly, the conclusions that PHEMA hydrogel has no cytotoxic effect on both fibroblasts and HUVECs, and it can be used as culturing substrate for perfusion culturing devices based on the above results and the literatures [163,164,171].

4.4 Adhesion Strength of Cell-PHEMA

4.4.1 Principle and Method

When culturing cells using the PHEMA-based microfluidic device as designed (see Chapter 1), the cells are exposed under the dynamic fluid flow on the PHEMA membrane in the culture chamber during the culture process. If the fluid flow rate is high enough, cells may suffer a large fluidic shear stress induced by hydrodynamic shear force thereby make cells detach from their substrate. In this section, the minimum fluidic shear stress that makes cells (HUVECs) detach from their substrate

(PHEMA), which reflects the adhesion strength of HUVECs-PHEMA, has been experimentally measured based on the method reported by Rocha *et al.* [172].

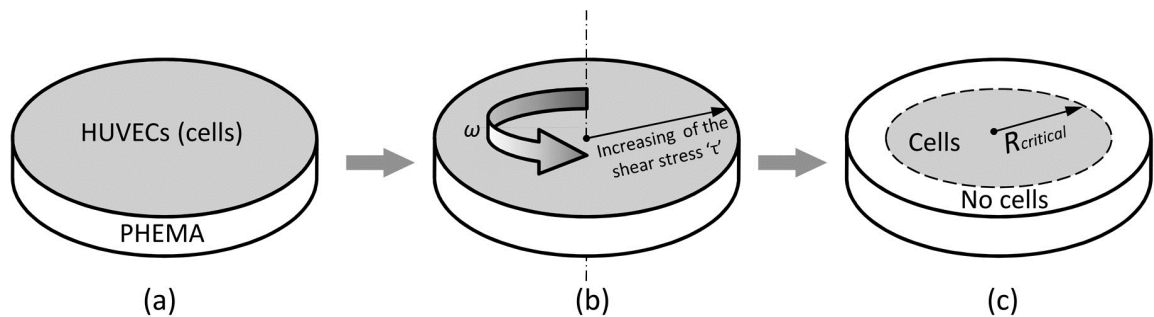


Fig.4-7. Schematic flow chart of the principle of the experiments to examine the cell-PHEMA adhesion strength. (a) HUVECs spread and occupy the surface of PHEMA membrane after at least 24 hours incubation. (b) Urging the culturing media flows rotationally at the speed of ω , shear stress with gradient (linear increasing) is formed and applied on cells. (c) Stop rotation and remove the culturing media with detached cells after 5 mins rotation, cells in a circle with radius of $R_{critical}$ will remain on the PHEMA surface.

Fig.4-7 schematically illustrates the process of the experiment that was carried out in this study. HUVECs are cultured on PHEMA membrane over 24 hours to ensure that the cells are fully occupied the surface of PHEMA substrate (Fig.4-7a). After the incubation, a rotated fluid flow at a certain angular velocity is applied on cell for at least 5 minutes. The fluidic shear stress is distributed linearly with the increase of the radius of the flow (Fig.4-7b). During the rotated fluid flow, cells are detached from substrate and suspended in the solution because of the high hydrodynamic shear stress towards the edge of substrate. Therefore, after refreshing of the culture medium in order to remove the suspended cells, a circular distribution of cells remains on the PHEMA substrate (see Fig.4-7c). During the rotation of fluid, the cells on the circular boundary (dashed line in Fig.4-7c) are under a critical constraint where adhesion strength to PHEMA substrate equals to the fluidic shear stress which applied on them. Hence, the radius of this critical circle $R_{critical}$ is correlated to the minimum shear stress that can make HUVECs detach from PHEMA substrate.

The assembly of a rotating system equipped with a cylindrical rotator and the cells cultured on PHEMA membrane is schematically illustrated in Fig.4-8a. The linear increasing fluidic shear stress along the radius is induced by a cylindrical rotator with a certain angular rotating velocity. If the angular velocity of the rotator is ω , the flat bottom of the rotator can offer that rotate velocity v is increasing with the radius r linearly (Fig.4-8b). As is shown in Fig.4-8c, the fluid in contact with the rotator is flowing together with the rotator in a same velocity distribution, and drag the fluid near cells following such velocity distribution, because of the hydrodynamic drag force.

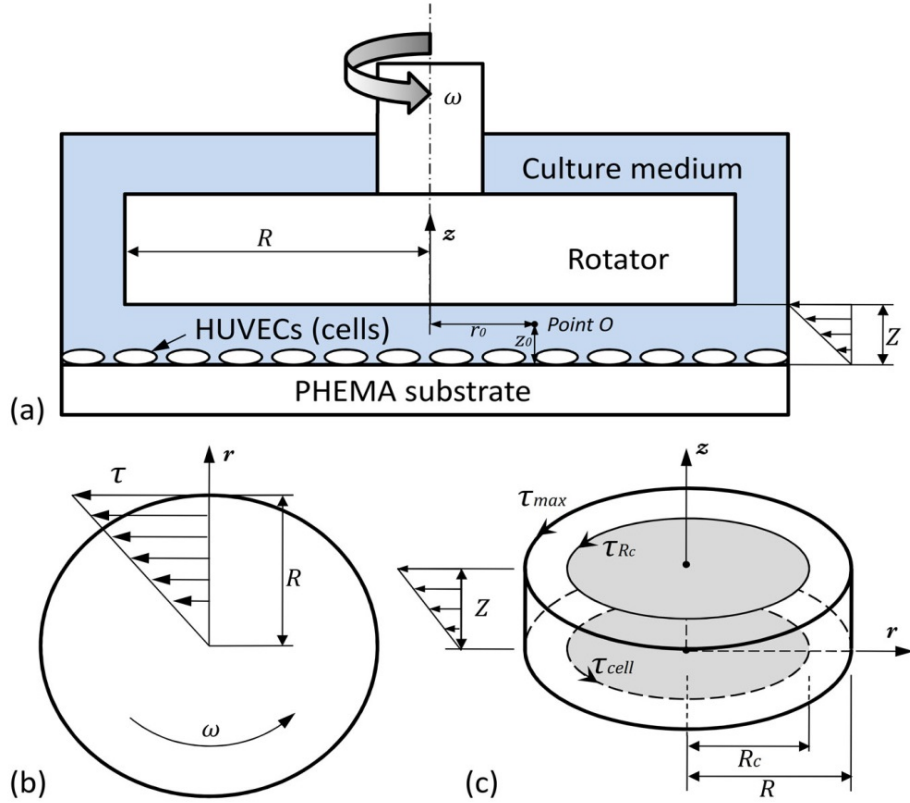


Fig.4-8. (a) Schematic diagram of the set-ups of rotated fluid flow. Agitator rotates at a certain speed of ω , it forces the culture medium rotate due to fluidic viscosity. Thus the fluidic shear stress τ will be applied on cells with linear gradient, which is depicted in (b), the top view of the PHEMA substrate with rotational flow. (c) Domain of fluid flow in the gap between the bottom of the agitator and the cells.

In a rotation flow with certain rotating angular velocity ω , the velocity (v_0) of any point (*Point O*, see Fig.4-8a) in the fluidic domain is given by:

$$v_0 = \omega r_0 z_0 / Z \quad \text{Eqn.4-8}$$

where, ω denotes the angular velocity of rotator moves, r_0 is the distance between *Point O* and the vertical axis (z axis), z_0 denotes the distance between *Point O* and the cells and Z is the gap (1 mm) between rotator and cells. For a Newtonian fluid, the fluidic shear stress (τ_0) at *Point O* is given by:

$$\tau_0 = \eta \cdot \left. \frac{\partial v}{\partial z} \right|_{v=v_0} \quad \text{Eqn.4-9}$$

where, η is the dynamic viscosity of the fluid. Combining Eqn.4-8 and Eqn.4-9 yields:

$$\tau_0 = \eta \cdot \left. \frac{\partial \omega r z / Z}{\partial z} \right|_{\substack{v=v_0 \\ z=z_0}} = \frac{\eta \omega r}{Z} \Big|_{v=v_0} = \eta \omega r_0 / Z \quad \text{Eqn.4-10}$$

Thus, on the basis of Eqn.4-10, the maximum shear stress (τ_{max}) in the fluidic domain, which is in contact with the edge of the rotator ($r_0=R$), can be transformed into:

$$\tau_{max} = \eta \omega R / Z \quad \text{Eqn.4-11}$$

where, R denotes the radius of rotator and equals to 16 mm.

By assuming the solution is Newtonian fluid without internal slip, the fluidic shear stress (τ) is considered to be linearly correlated to the distances away from the corresponding axes, e.g. the linear gradient of τ shown in Fig.4-8b&c. Thus, the fluidic shear stress on the critical circle near rotator (τ_{R_c}) can be determined according to Eqn.4-11, and the shear stress on the critical circle near cells (τ_{cell}) can be derived from the expressions of τ_{R_c} , which is shown in Eqn.4-13:

$$\tau_{R_c} = \frac{\tau_{max}R_{critical}}{R} = \frac{\eta\omega R_{critical}}{Z} \quad (0 < R_{critical} < R) \quad \text{Eqn.4-12}$$

$$\tau_{cell} = \frac{\tau_{R_c}Z_{cell}}{Z} = \frac{\eta\omega R_{critical}Z_{cell}}{Z^2} \quad (0 < R_{critical} < R) \quad \text{Eqn.4-13}$$

where, $R_{critical}$ is the radius of critical circle and Z_{cell} is the height of cells, which is 17 μm for HUVECs referenced to the information from source supplier [173].

τ_{cell} not only indicates the shear stress on the critical circles near cells, but also describes the minimum fluidic shear stress (critical shear stress) that can make HUVECs detach from PHEMA substrate. τ_{cell} is the parameter which reflects the adhesion strength of HUVECs-PHEMA. According to Eqn.4-13, the value of τ_{cell} can be obtained by measuring the radius of the critical circle $R_{critical}$ at a fixed rotational speed ω .

4.4.2 Details of the Agitator and Experimental Set-ups

If the rotational speed is low enough, $R_{critical}$ may be large enough to make the critical circle out of the range of culture chamber, as such the value of $R_{critical}$ cannot to be measured. If the rotational speed is high enough, $R_{critical}$ may be very small, thus hardly be captured. Therefore, an appropriate rotational speed that leads to a measurable value of the radius of critical circle ($R_{critical}$) is required. Referencing to works done by Rocha *et al.* [172], they determined that the radius of the critical circle $R_{critical}$ is approximate 10 mm when the rotational speed is 1000 r/min for the situation that HUVECs were cultured on PMMA substrate. Based on this, the rotational speed within the range of 100~150 r/min was chosen for the present experiment, to achieve an appropriate $R_{critical}$ of approximate 15 mm which is determined by the size of standard 6-well plate (radius at 17 mm) for cell culture. A self-built DC agitator is thus employed to achieve the steady rotational speed (± 0.1 r/min) within the speed range of 100~150 r/min. Using this agitator has some advantages over a commercial agitator which can hardly meet the requirements of continuously steady rotation with accurate control of rotation in our desired speed range. For examples, (1) the minimum spinning speed of normal

laboratory homogeniser or disperser is 300 r/min, which is out of the desirable speed range for this experiment; (2) for those homogenisers or dispersers that can meet the requirement of spinning speed, their rotational speed exhibit fluctuating at low speed range (~150 r/min) which may significantly affect the continuous of flow. Accordingly, a self-built DC agitator is built to acquire the steady and low speed rotating requirements which has been more satisfactory.

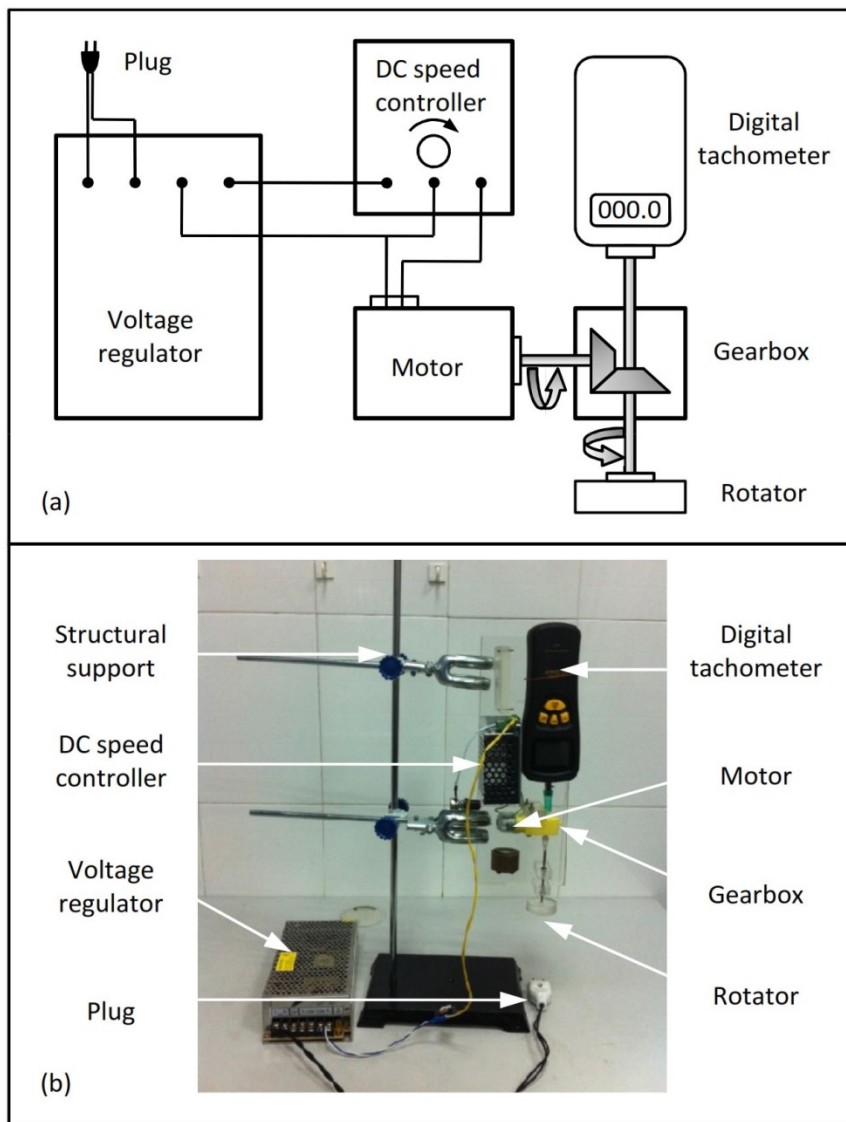


Fig.4-9. (a) Circuit diagrams of the agitator, aiming to achieve the rotation at a constant speed. (b) Photograph of the assembly of the agitator, on the basis of the electronic circuit diagram.

As illustrated in Fig.4-9a, the rotator and the digital tachometer are driven by a DC motor through a gearbox. Based on such mechanical transmission design, the spinning speed of the rotator can be directly displayed in the digital tachometer (Smart Sensor AR925, Shenzhen GRAIGAR Technology Co. Ltd, China). The DC speed controller is utilised to smoothly alter the

rotational speed through changing the input voltage of the motor. Thanking to the highly linear correlation between input voltage and output rotational speed of DC motor, the voltage regulator guarantees the steady voltage input for the whole circuit system including the input voltage of the DC motor, thereby ensures the steady rotational speed generated by the DC motor. The stability of the rotation is monitored by the digital tachometer which is capable of measuring the rotational speed range of 0.5 ~ 19999 r/min with the resolution of ± 0.1 r/min.

The rotator is made of poly(methyl methacrylate) (PMMA) on account of its transparency. A transparent rotator enables the opportunity to visualise whether the liquid fills the gap between cells and rotator before conducting the experiment, by observing the existence of bubbles directly through the rotator and liquid. In the present study, the rotator is manufactured by numerical turning lathe to minimise its geometrical run-out tolerance, which can therefore guarantee that the bottom surface of the rotator will not contact with the cells while rotating. According to the photograph of the assembled agitator in Fig.4-9b, the height of the rotator is fixed and can hardly be altered on the vertical direction (see z axis in Fig.4-8c). Thus, a laboratory lift platform (Manual Lifter SE1405, Sichuan Machinery Import and Export Corp.) has been utilised to alter the height of the 6-well plate in this experiment, in order to achieve the appropriate distance ' Z ' between rotator and cells.

The processes of such experiment to determine the adhesion strength of HUVECs to PHEMA substrate are described below:

- 1) Prepare HUVECs which are cultured on PHEMA membrane in 6-well plate, and replace culture medium by PBS buffer.
- 2) Clean the rotator using ultrasonic cleaner for 10 minutes.
- 3) Assemble the agitator, and test the function of the agitator, *e.g.* rotational speed, and make sure the cycle run-out (tolerance) of the rotator is hardly noticeable while the agitator is rotating.
- 4) Place the 6-well plate on the lab lift platform, and align the culture well with the rotator
- 5) Switch on the agitator, alter and hold the rotational speed at 110 r/min.
- 6) Raise the lift platform carefully to make the distance between rotator and cells around 1 mm, then start to count the rotating time using a stopwatch.
- 7) Switch off the agitator after 5 mins' rotating, lower down the lift platform gently, remove the

PBS buffer and suspended cells in the buffer solution, then replace the PBS buffer by formaldehyde solution to fix the location of remained cells.

- 8) Extract the PHEMA membrane out of the culture well, and find out the critical circle of remain cells on the PHEMA membrane using microscope.
- 9) Finally, mark the boundary of the critical circle on the plate, then measure the radius of the critical circle $R_{critical}$.
- 10) Calculate the adhesion strength of HUVECs to PHEMA using the equation shown in Eqn.4-13.

4.4.3 Results and Discussions

In Fig.4-10a~d, the dashed lines shown in the optical micrographs clearly illustrate the boundary of the critical circle. As is predicted, cells detach from the surface beyond the critical circle (Fig.4-10f), while the cells remain adherent within the critical circle (Fig.4-10e). Based on the boundary of the critical circle that is observed, the $R_{critical}$ for PHEMA is measured to be 12 ± 0.5 mm. After the measurement, this observed critical radius have to be translated into the critical shear stress (τ_{cell}) which is corresponding to the maximum allowed shear stress for cell culture.

In the steady-shear operation, the rotator rotates with a constant rotational speed at 110 r/min, which is $\omega = 11.51$ rad/s at angular velocity. Therefore, according to the parameters that media viscosity $\eta = 8.9 \times 10^{-4}$ Pa·s, height of cells $Z_{cell} = 17$ μ m, and the gap between rotator and cells $Z = 1$ mm, the value of the critical shear stress (τ_{cell}) can be calculated as 0.021 dyn/cm² based on the Eqn.4-13. This value of critical shear stress as the adhesion strength of HUVECs to PHEMA hydrogel is smaller than that of HUVECs to carbohydrate glass (1.0 dyn/cm²) determined by Miller *et al.* [174] and Jang *et al.* [175]; and is also much smaller than the adhesion strength of fibroblasts to PMMA (poly(methyl methacrylate)) at 21 dyn/cm² and to PC (polycarbonate) at 5.1 dyn/cm², which is reported by Rocha *et al.* [172]. Utilising the value of cell density (5000 cells/cm²), the critical shear stress (τ_{cell}) can be expressed as shear stress for individual cell at 4.18×10^{-6} dyn/cell. Such individual adhesion strength for HUVECs to PHEMA is also correspondingly smaller than that of fibroblast to Fibronectin (4×10^{-4} dyn/cell) and fibroblast to Tenascin (2×10^{-4} dyn/cell), by Lotz *et al.* [176].

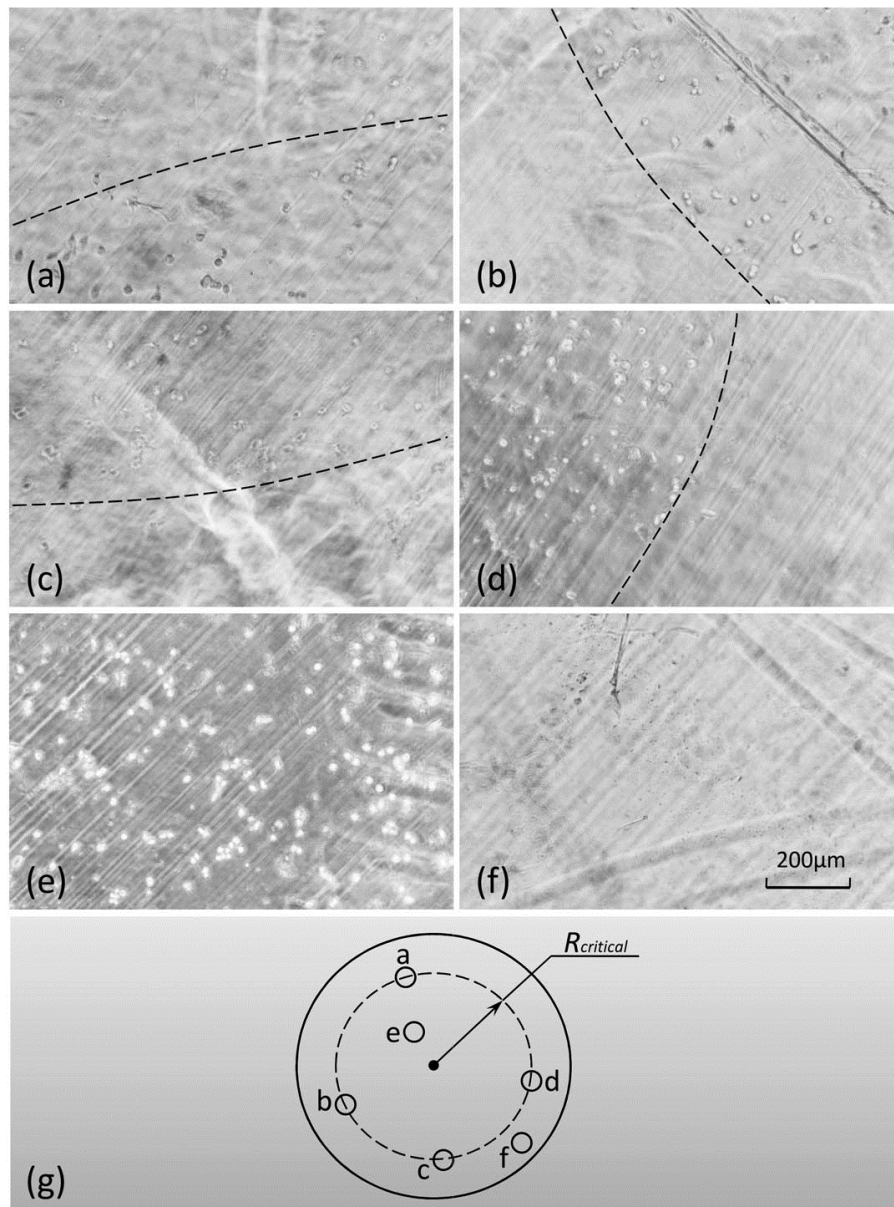


Fig.4-10. (a-f) images of PHEMA membrane after shear testing from optical microscope. This set of images was taken through the same magnification. (g) shows the location of the images (a-f) where they were taken.

Such results verified that the experimental approach introduced in this section is able to quantify the adhesion strength of HUVECs to PHEMA hydrogel. According to the comparison of literatures and the current experimental results, HUVECs present weaker adhesion strength to PHEMA hydrogel than that of fibroblast to carbohydrate glass, PMMA, PC, Fibronectin or Tenascin. From the aspects of physics, biology and biochemistry, three potential reasons can be proposed to give fundamental explanations for such results: i) Firstly, the adhesion strength between cells and substrate is dependent of the roughness of the substrate. High surface roughness of substrate can provide large area of contact interface for cells to attach, thus a strong adhesion between cells and

substrate. In the current experiment, the PHEMA substrate may be too smooth to offer a strong adhesion for cells. ii) Secondly, PHEMA hydrogel without any surface treatment is not a perfect substrate for culturing cells, though the value of cell viability (80.6%) on cells which are cultured on PHEMA substrate (demonstrated in Section 3.5) is larger than the criteria for judging the cytotoxicity of a material (80%). iii) Thirdly, it may be related to the molecular interaction at the cell-substrate interface. The molecular interaction between cells and substrate is primarily due to the chemical composition of proteins [172]. When culturing cells *in vitro*, the structural support and protection of cells are provided by polysaccharides (sugars) and collagen (proteins) which are from the extracellular matrix (ECM) [177]. These sugars and proteins are responsible for transporting necessary molecules through cells' wall, and controlling the elasticity, humidity and adhesion [178 , 179] of the environment around cells. This becomes the primary reason why Fibronectin/Tenascin (proteins) and carbohydrate glass (coated by polysaccharides) provide stronger adhesion than that by PHEMA hydrogel. Based on these three reasons, the adhesion strength of HUVECs to PHEMA hydrogel can be improved through: i) Increase the roughness of the surface by using a rough aluminium mould during the synthesis process (Fig.3-2), thus increase the surface roughness of the PHEMA specimen which is synthesised from such aluminium mould. Accordingly, the PHEMA hydrogel as a cell culture substrate can provide larger area of the contact interface for cells to attach. ii) Coat the PHEMA surface with a layer of protein or polysaccharides, or cover the PHEMA surface with other hydrogels which possess better biocompatibility, e.g. Gelatin. They are both useful to improve the biocompatibility of the cell culture substrate, thereby increase the adhesion strength between cells and PHEMA hydrogel substrate.

4.5 Summary

The characteristics of diffusion and biocompatibility of PHEMA hydrogel have been experimentally examined and discussed in this chapter. The diffusion characteristic of water swollen PHEMA hydrogel has been proved to obey the Fickian diffusion process for water soluble molecules, which refers to glucose in this study. The capacity of absorption for PHEMA hydrogel has also been examined by further studying of the characteristics of diffusion of glucose in PHEMA. It indicates that approximate 0.038 mol glucose can be absorbed by 1 kg swollen PHEMA specimen. Live/Dead cell stain imaging method and cell viability measurement have been used to evaluate the

cytotoxicity of PHEMA hydrogel to cells. The results demonstrate that PHEMA has no cytotoxicity to cells. To culture cells on PHEMA hydrogel directly, the PHEMA hydrogel may be lack of biocompatibility, because only 80% viability of cells which are cultured on the uncoated surface of PHEMA is observed. Therefore, the adhesion strength of HUVECs-PHEMA substrate is weaker than that of cells to protein substrate or substrates coated with polysaccharides. To cope with this issue, two methods utilised to improve the biocompatibility of PHEMA hydrogel are addressed: i) increase the roughness of the surface by using a rough aluminium mould during the synthesis process. ii) coat the surface with protein or polysaccharides or cover the surface with other hydrogel which has better biocompatibility, e.g. Gelatin.

To summarise, according to the results and conclusions from the current chapter (listed in Table 4-4), PHEMA hydrogel can be used as a biomaterial for the purposes of cell culture. Specifically in this study, PHEMA hydrogel is capable of being used as a sealing membrane for the microfluidic chips and a permeable substrate for cell culture, thanking to its non-cytotoxic property and diffusion property obeying Fickian diffusion process.

Table 4-4 Summary of results and conclusions in Chapter 4

Properties of PHEMA hydrogel	Description of Experiments	Results	Conclusion
Diffusion characteristics	Glucose release rate	$D=0.099$ [cm^2/s] $n=0.456$	PHEMA obeys Fickian diffusion process
	Capacity of absorption on glucose	$\Gamma=0.038$ [mol/kg]	
Cytotoxicity	Live/Dead cell staining imaging	83.6% (>80%)	PHEMA has no cytotoxicity to cells
	Cell viability measurement	80.6% (>80%)	
	Observation on fibroblasts incubated on PHEMA	Good shape	
Adhesion strength	Rotational fluidic flow on HUVECs cells incubated on PHEMA substrate	$\tau_{cell}=0.021$ [dyn/cm^2]	Relatively weak adhesion to cells, can be further improved.

Chapter 5. Mechanical Characteristics of PHEMA Hydrogel under the Compression

5.1 Introduction

Mooney-Rivlin theory and neo-Hookean theory which are used to analyse the nonlinear responses of hyperelastic materials to mechanical compression are elaborated in this chapter (Section 5.2). Numerical simulations have been built and investigated through these theoretical models, aiming to validate and predict the mechanical behaviour of PHEMA hydrogel. The mechanical properties of swollen PHEMA, including ultimate strength, ultimate strain and initial tangent modulus, are measured under the equivalent uniaxial compressive conditions, and the results are compared with the corresponding simulated results, thereby evaluate the quality that using such theoretical model to describe or predict the mechanical behaviour of PHEMA hydrogel (Section 5.3.1 and 5.3.2). According to the geometric design of the microfluidic device introduced in the Chapter 1, PHEMA hydrogel as an inserted membrane is utilised to seal the microfluidic system enabling assembly and dis-assembly routines in this case. In this chapter, the application of cycling compressive load on the PHEMA specimens has been considered to examine the resistant property of the PHEMA hydrogel to fatigue (Section 5.3.3), aiming to evaluate the repeatability of using PHEMA membrane as a sealing membrane for microfluidic device.

Moreover, PHEMA specimens in different degree of swelling have been prepared, and tested under uniaxial compression, to investigate the effect of degree of swelling to the mechanical behaviour of PHEMA hydrogel. Numerical simulations corresponded to various degrees of swelling under equivalent conditions are analysed and verified by the uniaxial compression experiments (see Section 5.4).

5.2 Theoretical Basis in Simulation

5.2.1 Mooney-Rivlin Model

The Mooney-Rivlin model [126] is a special case of the generalised Rivlin model [125] in which constitutive law can be expressed as:

$$W(I_1, I_2) = \sum_{i,j=0}^N C_{ij}(I_1 - 3)^i(I_2 - 3)^j + \sum_{m=1}^M D_m(J - 1)^{2m} \quad \text{Eqn. 5-1}$$

where W represents the strain energy density function, I_1 and I_2 are the first and second invariant of the unimodular component of the left Cauchy–Green deformation tensor, C_{ij} are the empirically determined material constants and D_m is material constants related to the volumetric response, in the case of compressible Mooney-Rivlin material, it is obtained from the polynomial form of the hyperelastic model by setting the polynomial parameter N to 1, i.e. the first order polynomial [125,180]. J is the elastic Jacobian, which equals to the determinant of deformation gradient (\mathbf{F}): $J = \det[\mathbf{F}]$ [181]. In the experiment of uniaxial compression, $C_{11}=0$ and $M=1$, thereby Mooney-Rivlin expressions can be written as

$$W(I_1, I_2) = C_{10}(I_1 - 3) + C_{01}(I_2 - 3) + D_1(J - 1)^2 \quad \text{Eqn. 5-2}$$

Thus, C_{10} , C_{01} and D_1 in the Eqn.5-2 are the related coefficients to be determined.

Determination of D_1 [182]

Only linear functions of the deviatoric strain invariants are used in the Mooney-Rivlin model due to the first polynomial form of the hyperelastic model. The relationship between shear modulus (μ), the bulk modulus (κ) and the Poisson's ratio (ν) are given by

$$\mu = 2(C_{10} + C_{01}) \quad \text{Eqn. 5-3}$$

$$\kappa = \frac{2}{D_1} \quad \text{Eqn. 5-4}$$

$$\nu = \frac{3\kappa/\mu - 2}{6\kappa/\mu + 2} \quad \text{Eqn. 5-5}$$

where C_{10} , C_{01} and D_1 are temperature-dependent material parameters, defined in Eqn.5-2.

According to the definition of D_m in Eqn.5-1, the parameter of D_1 is directly correlated to the compressibility of material. Combining Eqn.5-3 and Eqn.5-5, it gives the expression of κ :

$$\kappa = \frac{4(C_{10} + C_{01})(1 + \nu)}{3(1 - 2\nu)} \quad \text{Eqn. 5-6}$$

Mooney-Rivlin model is fundamentally established by considering the deformed specimen as ideal material (incompressible material), which means that the total volume of material is a constant during the deformation of the specimen, thereby the Poisson's ratio (ν) is 0.5 [125]. However, such value of Poisson's ratio leads to an infinite bulk modulus κ , because the denominator in Eqn.5-6 equals to zero ($1 - 2\nu = 0$). As a consequence, the value of D_1 is approximately zero based on the Eqn.5-4, if the bulk modulus κ is infinite. Therefore, by inserting $D_1=0$ into the Eqn.5-2, the expression of the Mooney-Rivlin strain energy density function for incompressible material can be

obtained that

$$W(I_1, I_2) = C_{10}(I_1 - 3) + C_{01}(I_2 - 3) \quad \text{Eqn. 5-7}$$

where, the explicit expressions for the coefficients of I_1 and I_2 are given in terms of the stretch ratio λ ,

$$I_1 = \lambda_1^2 + \lambda_2^2 + \lambda_3^2 \text{ and } I_2 = (\lambda_1\lambda_2)^2 + (\lambda_2\lambda_3)^2 + (\lambda_3\lambda_1)^2.$$

Determination of C_{10} , C_{01}

Due to the relationship between the Cauchy–Green strain tensor γ_{ij} and Kirchhoff stress tensor t_{ij} , it's possible to write

$$t_{ij} = \frac{\partial W}{\partial I_1} \frac{\partial I_1}{\partial \gamma_{ij}} + \frac{\partial W}{\partial I_2} \frac{\partial I_2}{\partial \gamma_{ij}} + \frac{\partial W}{\partial I_3} \frac{\partial I_3}{\partial \gamma_{ij}} \quad \text{Eqn. 5-8}$$

where, $I_3 = \lambda_1^2 \lambda_2^2 \lambda_3^2 = 1$ because of the assumption of incompressible material. Hence, the equation of material principle stress t_i and stretch ratio λ_i is given by

$$t_i = 2 \left(\lambda_i^2 \frac{\partial W}{\partial I_1} + \frac{1}{\lambda_i^2} \frac{\partial W}{\partial I_2} \right) + P \quad \text{Eqn. 5-9}$$

where P is the hydrostatic pressure. Then the differences between each principle stress for an incompressible hyperelastic material are given by

$$t_1 - t_2 = 2(\lambda_1^2 - \lambda_2^2) \left(\frac{\partial W}{\partial I_1} + \lambda_3^2 \frac{\partial W}{\partial I_2} \right) \quad \text{Eqn. 5-10}$$

$$t_2 - t_3 = 2(\lambda_2^2 - \lambda_3^2) \left(\frac{\partial W}{\partial I_1} + \lambda_1^2 \frac{\partial W}{\partial I_2} \right) \quad \text{Eqn. 5-11}$$

$$t_3 - t_1 = 2(\lambda_3^2 - \lambda_1^2) \left(\frac{\partial W}{\partial I_1} + \lambda_2^2 \frac{\partial W}{\partial I_2} \right) \quad \text{Eqn. 5-12}$$

where t is the true stress (in terms of current dimensions of material), which can be expressed by the engineering stress σ and the stretch ratio λ as $t = \sigma\lambda$. The stretch ratio is given by $\lambda_i = (L_i + \Delta L_i)/L_i = 1 + \varepsilon$, where L_i is the geometry length on the i direction and ε is the engineering strain (positive values for tension, negative values for compression). In this study, uniaxial compressive test is carried out on PHEMA specimen, which has only one direction of stress and gives $\lambda_1 = \lambda$ and $\lambda_2 = \lambda_3 = 1/\sqrt{\lambda}$. Thus, according to Eqn.5-7 and Eqn.5-10, the stress-strain equation under uniaxial compression or tension can be derived as:

$$\frac{\sigma}{2(\lambda - \lambda^{-2})} = C_{10} + \frac{C_{01}}{\lambda} \quad \text{Eqn. 5-13}$$

It is obvious to note that the relationship between $\sigma/2(\lambda - \lambda^{-2})$ and $1/\lambda$ is linear, with slope C_{01} and intercept C_{10} . The linear relationship between $\sigma/2(\lambda - \lambda^{-2})$ and $1/\lambda$ can be easily plotted as the experimental results from the uniaxial compressive test is obtained in terms of engineering stress σ and engineering strain ε . Consequently, the values of C_{01} and C_{10} can be determined.

5.2.2 Neo-Hookean Model

The neo-Hookean model offers a numerical solution for analysing the hyperelastic behaviour of materials, being similar to the Hooke's law [180]. Unlike Hooke's law, the curve described by the neo-Hookean model is not purely linear but presents an initial linear region for small deformation strain and then a nonlinear behaviour in the region of large deformation strain. It can predict the nonlinear deformation behaviour (stress-strain curve) for hyperelastic materials in the deformation range of 0~100%. This feature makes neo-Hookean model similar to the Mooney-Rivlin model. For a compressible hyperelastic material described using neo-Hookean model, the strain energy density function is given by [183]:

$$W = C_1 \left(J^{-\frac{2}{3}} I_1 - 3 \right) + D_1 (J - 1)^2; \quad J = \lambda_1 \lambda_2 \lambda_3 \quad \text{Eqn.5-14}$$

where C_1 is the constant for neo-Hookean model, which can be derived from the shear modulus μ that [183]:

$$C_1 = \mu/2 \quad \text{Eqn.5-15}$$

In the current study, PHEMA hydrogel are considered as an incompressible material. Thus, according to the descriptions in Page 65 with literatures [181,182], it leads to $J=1$ and $D_1=0$. Thus, for an incompressible neo-Hookean hyperelastic material, the strain energy density function can be derived by

$$W = C_1 (I_1 - 3) \quad \text{Eqn.5-16}$$

It is much simpler than the equation from the Mooney-Rivlin model, which is shown in Eqn.5-7. According to the characteristics of uniaxial compression that $\lambda_1 = \lambda$ and $\lambda_2 = \lambda_3 = 1/\sqrt{\lambda}$, the differences between each principle stress can be derived as

$$t_1 - t_2 = 2C_1 \left(\lambda^2 - \frac{1}{\lambda} \right); \quad t_2 - t_3 = 0 \quad \text{Eqn. 5-17}$$

According to the relationship between engineering stress (σ) and true stress (t), $t=\sigma\lambda$, the engineering stress on compressive direction can be derived in terms of shear modulus μ and stretch ratio λ :

$$\sigma = 2C_1 \left(\lambda - \frac{1}{\lambda^2} \right) = \mu \left(\lambda - \frac{1}{\lambda^2} \right) \quad \text{Eqn. 5-18}$$

Consequently, the mathematical model based on neo-Hookean theory for incompressive hyperelastic material can be established in simulation software (COMSOL Multiphysics) according to the values of shear modulus μ of PHEMA material.

5.3 Mechanical Behaviour of Fully Swollen PHEMA Hydrogel

5.3.1 Uniaxial Compressive Test to Determine the Coefficients for Simulation

5.3.1.1 Apparatus and Experimental Approach

Mechanical properties, such as ultimate strength, ultimate strain, shear modulus and Mooney-Rivlin coefficients are obtained in the uniaxial compressive experiment for PHEMA hydrogel. An Instron Series 3366 Model universal testing machine, equipped with 10 kN load cell, was utilised to measure the deformation response of PHEMA hydrogel specimens under compression. The accuracy of such deformation measurement is ensured by a screw-driven actuator with resolution at approximately $\pm 0.05\%$ of measured displacement, while loads can be precisely measured within $\pm 0.5\%$ of the indicated force at 25°C . This accuracy is acceptable for flexible hydrogel compressive tests [184].

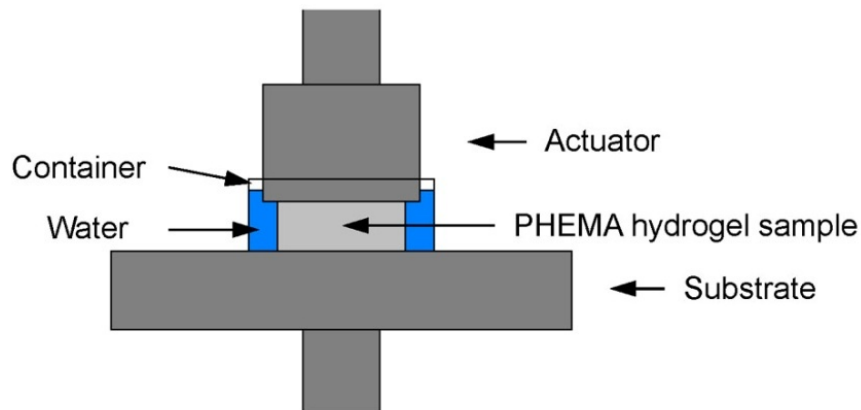


Fig.5-1. Schematics of experimental setup: Water in the container offered the proper aqueous environment for hosting the PHEMA hydrogel specimens during the whole testing process.

To preserve swelling and hydrated conditions of hydrogels, the compressive tests must be conducted in aqueous environment. The experimental set-up consists of the actuator (load cell), specimen (PHEMA cylinder), water container (polystyrene dish) and substrate (testing platform) has been schematically illustrated in Fig.5-1. Water in the container can offer a proper aqueous environment for housing the PHEMA hydrogel specimens during whole test. A compressive force is applied on PHEMA specimen to give a strain rate of 6 mm/min until the failure of specimen occurs, which is indicated by a singularity in the smooth curve in terms of compressive load *versus* compressive deformation.

The compressive tests were conducted based on two groups of cylindrical specimens with different diameters ($\text{Ø}18$ mm and $\text{Ø}32$ mm) but same height (12.5 mm). The goal of these experiments is to extract the stress-strain relationship up to 70% strain or find the ultimate strain. 70% strain is referring to compression of the PHEMA specimen by 8.75 mm, according to the specimen dimension/height. However, the distance of compression is determined on the basis of the maximum strain that can be reached prior to the material failure of the hydrogel. On the basis of the ideal compression theory [185], compressive stress has to be obtained in a slow-speed static testing condition in order to reduce the viscoelastic effect caused by the damping of the material. Therefore, the time to reach the maximum strain for specimen has been set to as 120 s, while the corresponding speed is calculated to be 100 $\mu\text{m/s}$. According to this loading speed, compressive loads [N] *versus* compressive extension [mm] are recorded by data acquisition system (50 sets of data per second). After normalising the stress and strain to make them dimensionless, the relationship between them in terms of compressive stress [MPa] *versus* compressive strain can be plotted, which is known as stress-strain curve. The shear modulus and Mooney-Rivlin coefficients can thereby be derived from the stress-strain curve.

5.3.1.2 Uniaxial Compressive Test Results

Repeatability of test

Evaluation of the repeatability of the current experimental method is essential. Five experiments were performed on group of PHEMA specimens of the same height but different diameters, $\text{Ø}18$ mm group and $\text{Ø}32$ mm group. Fig.5-2a illustrates the stress-strain curve for the specimens of $\text{Ø}32$ mm group. At small magnitudes of compressive strain, in both plots, the PHEMA specimens of each test exhibited identical behaviour except for the region after 45% compressive strain. This region corresponds to the hyperelastic deformation region it behaves as if the modulus of elasticity keeps increasing along this part. As compressive strain is further increased, the PHEMA specimens begin to reach the ultimate strain representing specimen failure. Fig.5-2b gives the error bar graph of failure strain for $\text{Ø}18$ mm and $\text{Ø}32$ mm group, showing the maximum, minimum and average values of strain when the specimen exhibits material failure. The values of strain at two diamond points are similar, indicating that geometry has no influence on the failure strain of PHEMA material in this particular experimental condition.

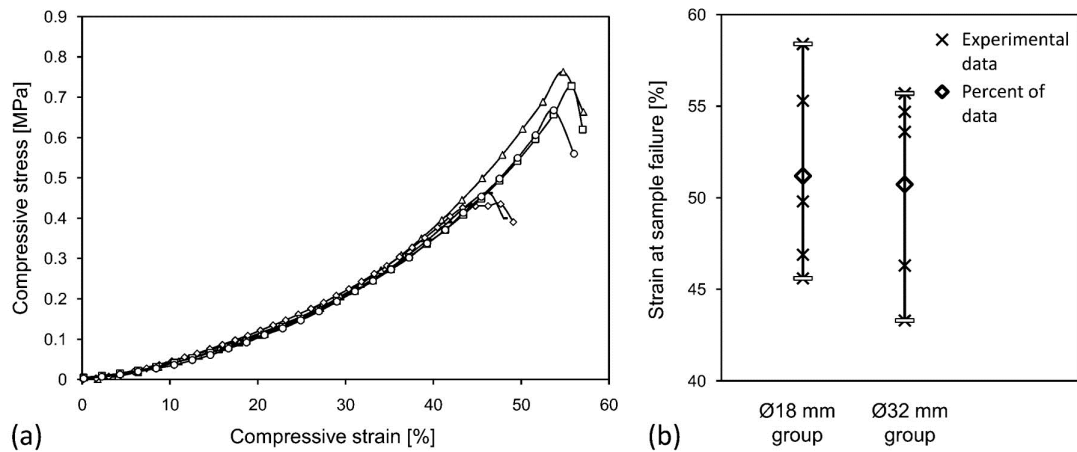


Fig.5-2 (a) Uniaxial compressive stress vs. compressive strain plots of five specimens in size of Ø32 mm testing group. (b) Error Bar Graph plot of ultimate strain of PHEMA specimens for both testing group including original specimen failure data points, marked as [X].

Thus, such strong agreement between the stress-strain curve and error bar analysis of the five PHEMA specimens of each group of different diameter indicates that it is repeatable and reliable to normalise the dimensions of cylindrical PHEMA specimen in the experimental compressive test. Therefore, the parameters (e.g. C_{10} and C_{01}) used in the numerical simulations can be determined based on these experimental data groups.

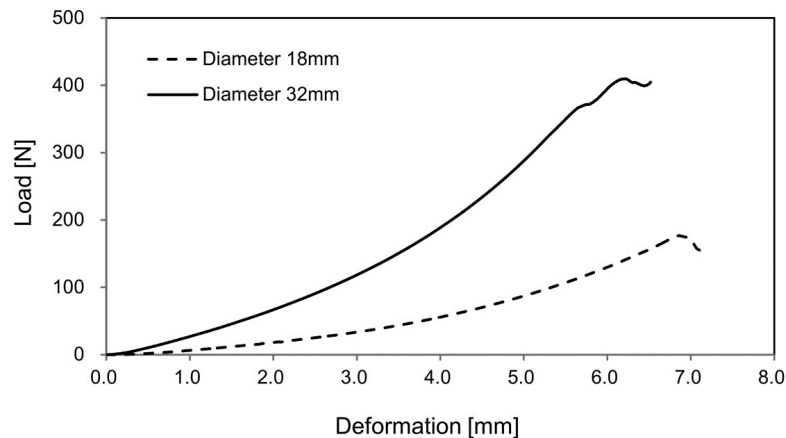


Fig.5-3. Difference in compression behaviour (compressive load versus compressive extension) between specimens with different dimensions: same height, different diameter.

Load versus extension

The data of load versus extension (compressive displacement) for the PHEMA specimen in various dimensions are recorded directly by the acquisition system in the compressive tests and are plotted in Fig.5-3. The solid line indicates the responses curve for the specimen with Ø32 mm and the dashed line for the specimen with Ø18 mm. According to the graph, both specimens failed at

extension of 5~7 mm. By comparing the curves shown in Fig.5-3, it is apparent that approximately two times larger compressive loads are required for the Ø32 mm specimen (in comparison with Ø18 mm specimen) to have same compressive strain.

Stress versus strain

The deformation characteristics of the PHEMA specimens under compression are illustrated in terms of engineering stress-strain (Fig.5-4a) and true stress-strain (Fig.5-4b). The graphs demonstrate that the ultimate true strains are higher than the ultimate engineering strains, e.g. 60% and 80% versus 45% and 55% for Ø18 and Ø32 mm specimen respectively. These data obtained from the stress-strain curves are analysed under both Mooney-Rivlin and neo-Hookean models.

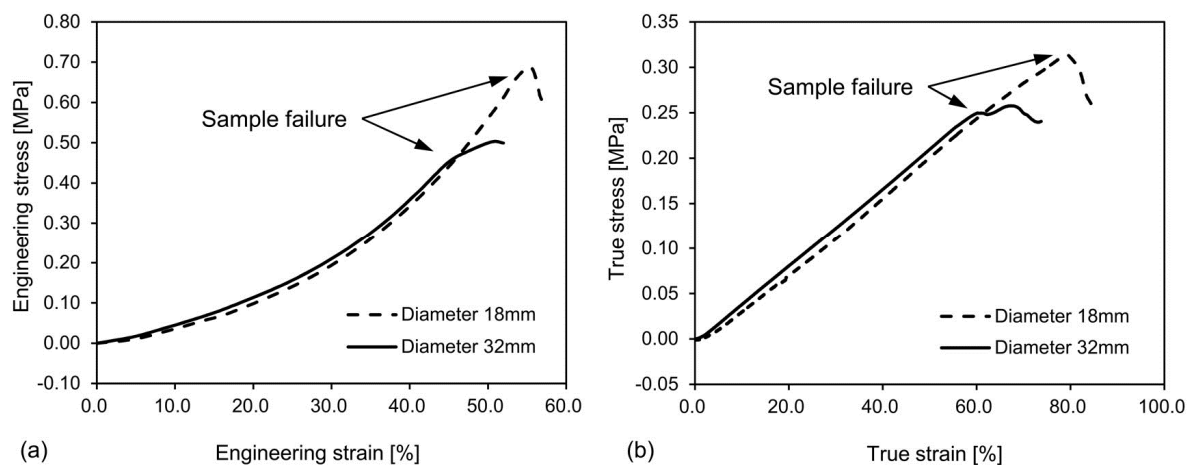


Fig.5-4. Difference in compression behaviour (stress versus strain) between specimens with different dimensions: same height, different diameter. (a) Engineering stress versus engineering strain. (b) True stress versus true strain.

As a summary of such experimental results, at room temperature, the ultimate engineering strain of water swollen hydrated PHEMA hydrogel under compression is in the range 45%~55%, corresponding to an ultimate yield strength in the range 0.45~0.7 MPa. The PHEMA hydrogel recovers its original geometry immediately if releasing the load applied on the specimen, unless the compressive stress is beyond the ultimate yield strength and causes the material failure.

Values of C_{01} and C_{10}

As is shown in Fig.5-4, an obvious difference between true stress vs. true strain and engineering stress vs. engineering strain can be observed. It results from the barrelling effect during the compressive experiments on specimens. The barrelling effect is a phenomenon that causes

specimen attains a barrel shape, due to the frictional force on the contact interface between specimen and actuator. Under compression, the specimen will tend to spread in the lateral direction and thereby increase the cross-sectional area according to Poisson's ratio of material. A frictional force on the contact interface between specimen and actuator/substrate will oppose the lateral spread. This frictional force consumes the energy which is induced by the compression equipment, and thereby slightly affects the value of engineering stress (σ) obtained from the experiment.

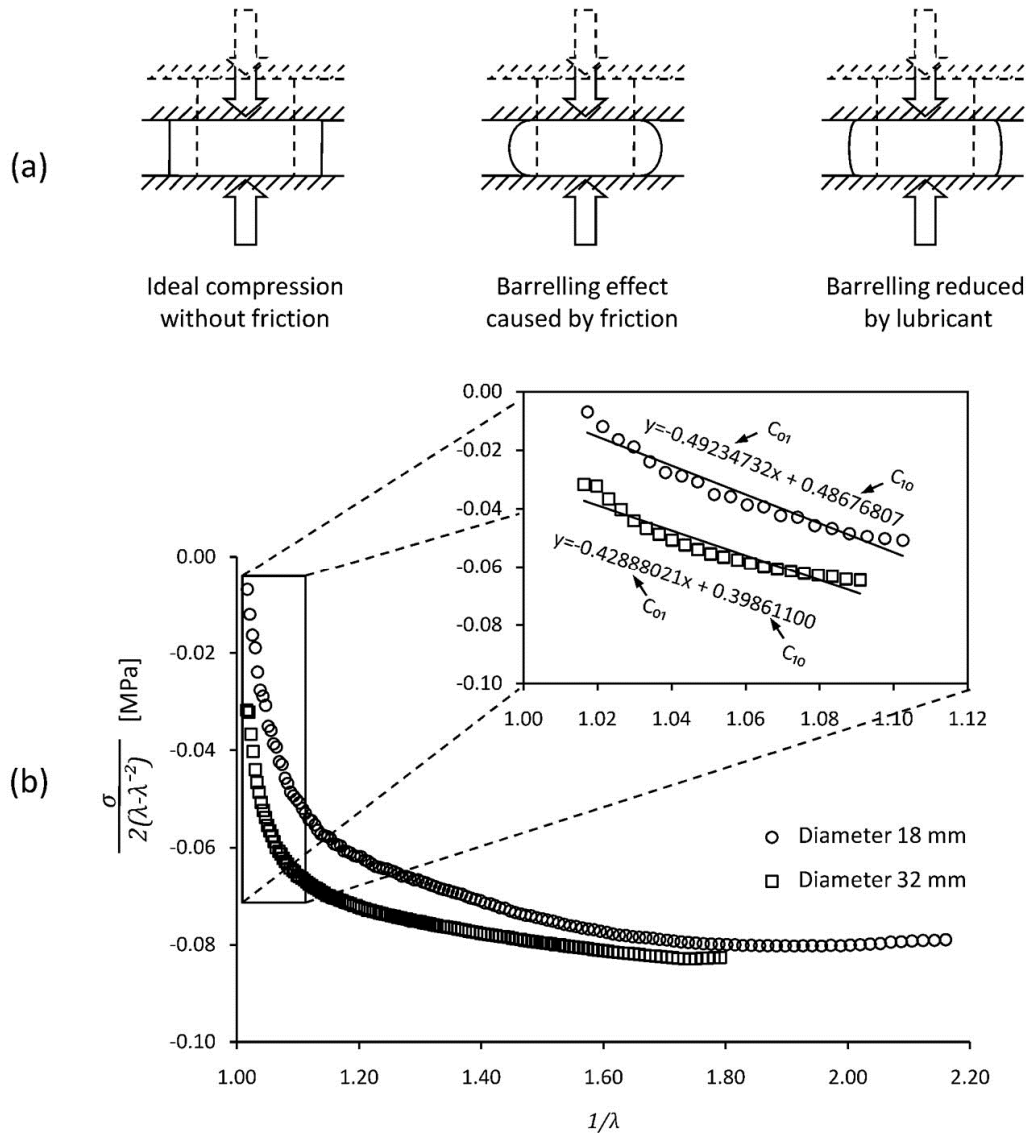


Fig.5-5. (a) Barrelling effect in the compressive tests. Lubricant was used in the test to reduce the barrelling effect on specimens. (b) Mooney-Rivlin analysis by operating a linear programming of $\sigma/2(\lambda-\lambda^{-2})$ and $1/\lambda$ on the initial stage of deformation in order to extract the Mooney-Rivlin coefficients. The data from initial stage of deformation has minimum effect by barrelling due to friction.

According to Fig.5-5a, the theoretical expressions to describe the mechanical behaviour of specimen under compression are based on the ideal compression without lateral friction. In reality,

the barrelling effect cannot be eliminated because frictions will always exist in experiment. In this study, lubricant (Dow Corning silicone compound) is coated at the contact interface between specimen and actuator/substrate to relieve the lateral friction, thereby to replicate the ideal compression as close as possible.

To calculate the values of C_{01} and C_{10} using the Eqn.5-13, the relationship between $\sigma/2(\lambda - \lambda^{-2})$ and $1/\lambda$ is plotted in Fig.5-5b based on the experimental results of engineering stress (σ) and engineering strain (ϵ). The relationship illustrated in Fig.5-5b is not a linear correlation as theoretical derived, due to the barrelling effect in experiments. To minimise the barrelling effect on the calculation of C_{01} and C_{10} , the initial stage of compression is chosen to implement the linear fitting, because the data from the initial stage represent the least effect of frictions. In the initial stage, the compressive force applied on specimen is small, which leads to small interfacial friction because the frictional force is proportional to the compressive force. Thus, the lubricant works more effectively due to the small compressive force, thereby makes the deformation of specimen closer to the ideal deformation induced by compression. Accordingly, the inclusion in Fig.5-5b, which is based on the extracted data from the initial stage of the compression, is used to carry out the linear fitting. From the equations derived from the linear fitting given in Fig.5-5b inclusion, the Mooney-Rivlin coefficients are derived. They are: $C_{01}=492347.3$ Pa, $C_{10}=486768.1$ Pa for the $\varnothing 18$ mm PHEMA specimen, and $C_{01}=428880.2$ Pa, $C_{10}=398611.0$ Pa for the $\varnothing 32$ mm PHEMA specimen.

5.3.2 Simulations of Mechanical Behaviour of Fully Swollen PHEMA Hydrogel

With the parameters extracted from experimental stress-strain relationships, Mooney-Rivlin and neo-Hookean models for PHEMA as incompressible materials are utilised to solve the corresponded constitutive equations, in order to obtain the deformation characteristics of PHEMA material under compression. Based on the assumption that there is no friction on the interface between cylindrical specimen and substrate (ideal compression in Fig.5-5a), the specimens are built as 2D-axisymmetric geometry domains in simulation. The schematic diagram such domain in simulation for the $\varnothing 32$ mm specimen is illustrated in Fig.5-6a. The boundary conditions for the PHEMA specimen in simulation are determined to achieve the ideal uniaxial compression without friction. Thus, focusing on the material slice in Fig.5-6a, the *base point* O is set to be fixed; the constraint of the bottom boundary of the domain is set to be partially free (fixed degree of freedom

on the central axis 'Z', and free on the radial axis 'R'). A force along the direction of central axis, increasing from 0 N to 400 N (step of 2 N) on the specimen with $\varnothing 32$ mm and from 0 N to 200 N (step of 2 N) on the specimen with $\varnothing 18$ mm, is set to be applied on the top boundary of the domain. The 2D material slice is meshed by rectangular elements with maximum size of 0.592 mm. Predefined Finer Quality and refining of the mesh space grid ensures that the solutions of the equation are independent of the spatial discretization. 2D-axisymmetric transform converts the material slice into a 3D cylindrical geometry, which deliberately replicate the exact dimensions of the specimens in experiments. In addition, the density of the PHEMA material is set as 1 g/ml due to the water swollen and hydrated status of the PHEMA specimen.

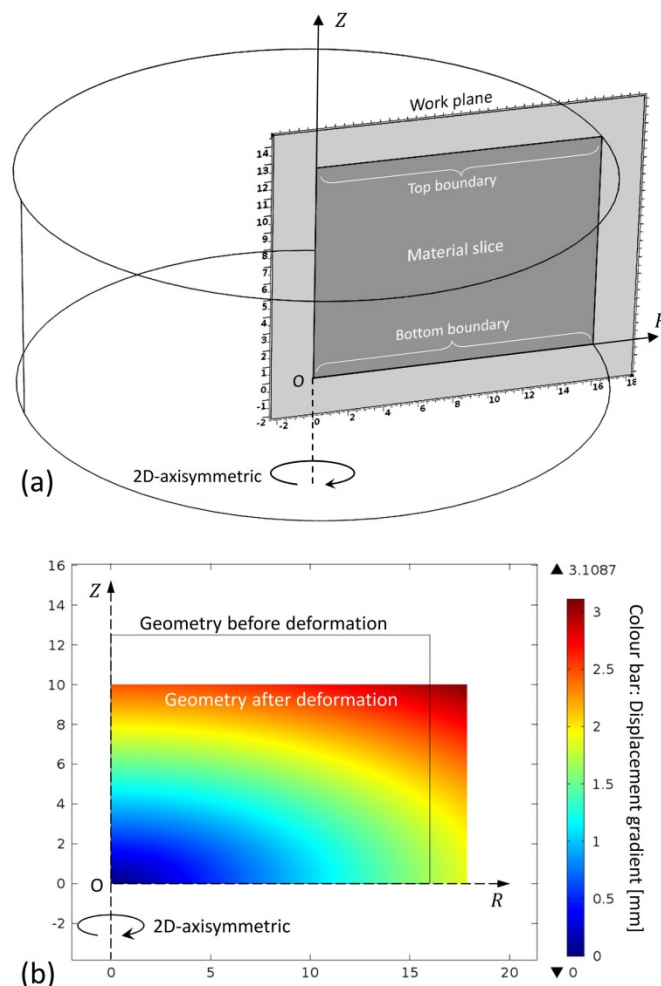


Fig.5-6. (a) Schematic diagram of the 2D-axisymmetric model for $\varnothing 32$ mm PHEMA specimens. (b) Simulation result in terms of displacement gradient for the $\varnothing 32$ mm PHEMA specimens based on Mooney-Rivlin theory, compressive strain is 20%

Simulation result in terms of displacement gradient has been illustrated in Fig.5-6b. By comparing the geometry of the material domain before and after deformation, it is obviously to see

that the deformation of the material domain follows the ideal deformation under uniaxial compression (see Fig.5-5a): the material domain spreads in the lateral direction 'R' because of Poisson's ratio effect, however, without barrelling effect. Thus, the simulation results in terms of stress-strain, which are able to be calculated from the correlation of force-displacement from the simulation, can be obtained and compared with experimental data.

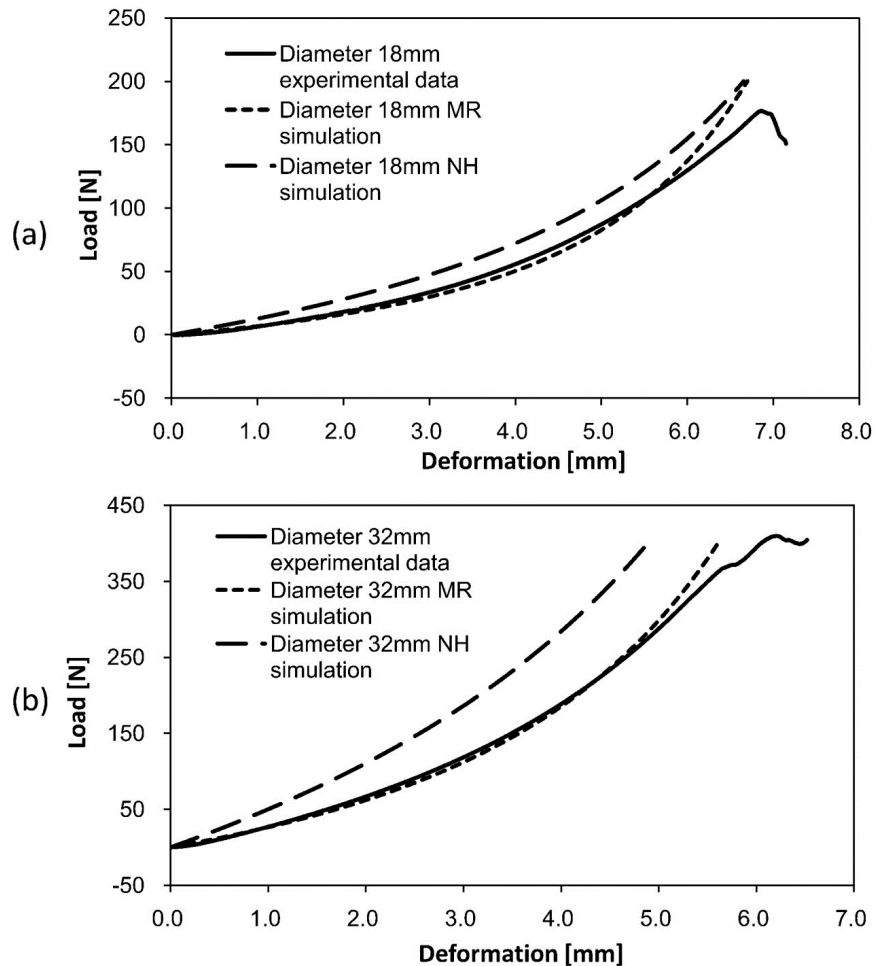


Fig.5-7. Comparison of experiment and simulation based on the Mooney-Rivlin (MR) model and the neo-Hookean (NH) model in (a) PHEMA specimens of $\varnothing 18$ mm and (b) PHEMA specimens of $\varnothing 32$ mm.

In Fig.5-7, the results from the simulations based on Mooney-Rivlin model and neo-Hookean model are plotted with the experimental results, for $\varnothing 18$ mm specimens (Fig.5-7a), and $\varnothing 32$ mm specimens (Fig.5-7b). To make such comparison quantitatively, the root mean square (RMS) analysis and coefficient of determination (COD) analysis are utilised in the calculation. The RMS analysis, similar to the mean squared error control, is a risk function corresponding to the expected value of the squared error loss or quadratic loss. In the current analysis, the comparison is induced between the simulations and the experimental results, thus the RMS method is used to address the

goodness-of-fit of simulated results to experimental results in the current study. The data selected from simulated results are marked as S_{ij} , where i ($= 1, 2$) indicate that i) S_1 stands for simulation data from Mooney-Rivlin model and ii) S_2 stands for simulation data from neo-Hookean model; where j stands for the index number. The data selected from experimental results corresponding to that from simulation are marked as E_j , where j is the corresponded index number.

Theoretically, $E_j - S_{ij}$ stands for the difference (error) between the experimental load [N] and the simulation load [N] under same deformation of specimen. Hence, the value of RMS (X_{rms}), which reflects the goodness-of-fit between the simulation and experiment, is given by

$$X_{rms} = \sqrt{\frac{1}{n} \sum (E_j - S_{ij})^2} \rightarrow 0 \quad \text{Eqn. 5-19}$$

where, n is the total number of the parameter j . According to its definition, the closer RMS value (X_{rms}) to zero, the higher goodness-of-fit between simulation and experiment.

Table 5-1. Summary of the RMS method applied to different sizes of PHEMA specimens based on Mooney-Rivlin and neo-Hookean model simulation analysis

	Mooney-Rivlin (S_1)	Neo-Hookean (S_2)
Expression	$\sqrt{\frac{1}{n} \sum (E_j - S_{1j})^2}$	$\sqrt{\frac{1}{n} \sum (E_j - S_{2j})^2}$
RMS for the Ø18 mm group	0.18941012	0.51399658
RMS for the Ø32 mm group	0.09087986	0.84695340

Table 5-1 presents the RMS values for PHEMA specimens in different dimensions based on Mooney-Rivlin model and neo-Hookean model. It is clear to see that the ranges of RMS value from the Mooney-Rivlin model are much smaller than that of the neo-Hookean model in each dimensional group. It concludes that the Mooney-Rivlin model presents a much better quality (one third of the RMS error) than that of the neo-Hookean model for describing the compressive deformation of water swollen PHEMA hydrogel at room temperature.

To further examine the goodness-of-fit between the simulated results based on Mooney-Rivlin model and the original experimental results, the COD is calculated using the formula

$$COD = R^2 = 1 - \frac{SS_{err}}{SS_{tot}} = 1 - \frac{\sum (E_j - S_{1j})^2}{\sum (E_j - \frac{1}{n} \sum_j^n E_j)^2} \rightarrow 1 \quad \text{Eqn. 5-20}$$

Therefore, the highest goodness-of-fit between simulation and experimental results is indicated

by a value of R^2 which is very close to 1 and slightly smaller than 1. For the current results from Mooney-Rivlin simulation and compressive experiments, the error between the acquired experimental results and the simulated results is within 5%, and the value of COD is calculated to be 0.9921 for Ø18 mm PHEMA specimens and 0.9973 for Ø32 mm PHEMA specimen. These values of COD indicate that the simulations which based on the Mooney-Rivlin theory provide a good prediction of the mechanical response of the PHEMA hydrogel material under compression.

Combining the results from RMS analysis and the COD analysis, it can be demonstrated that the Mooney–Rivlin model gives best fit to the experimental data for describing the PHEMA hydrogel mechanical response to compression.

5.3.3 Fully Swollen PHEMA Hydrogels under the Cycling Compressive Loads

5.3.3.1 Experimental Approach

To investigate the fatigue/creep behaviour of PHEMA hydrogel under the compressive load, the cycling compressive tests are carried out. In the cycling compressive test, each cycle of compressive loading is applied and released repeatedly. The Instron Series 3366 Model universal testing machine, which equipped with 50 N load cell, has been setup to generate the cycling compressive load, the samples have dimensions of 9 mm diameter and 7 mm height. The flowchart for schematically showing the process and set-ups of the cycling compressive testing is illustrated in Fig.5-8.

According to the Fig.5-8, the parameters of the compressive testing machine including F_{high} , F_{low} and N have to be determined prior to the cycling compressive tests. F_{high} is the maximum load which is determined by the value of the maximum strain of PHEMA hydrogel. For instance, in this experiment, the designated ultimate strains are set as 20% and 30%, the maximum stresses applied are thus determined as 0.1 MPa and 0.2 MPa according to the stress-strain curve shown in Fig.5-4a. Based on the dimensions (Ø9, h7 [mm]) of the specimen used in the cycling compressive test, the value of F_{high} is determined to be 6.35 N for the group with 20% compressive strain, and 12.72 N for the group with 30% compressive strain. During the stage of screw reversing, negative values of load of actuator may be resulted from that the actuator detaches from the top surface of specimen. To avoid such negative reading of the variable F , the minimum load during the cycling compressive test F_{low} is determined as 0.01 N.

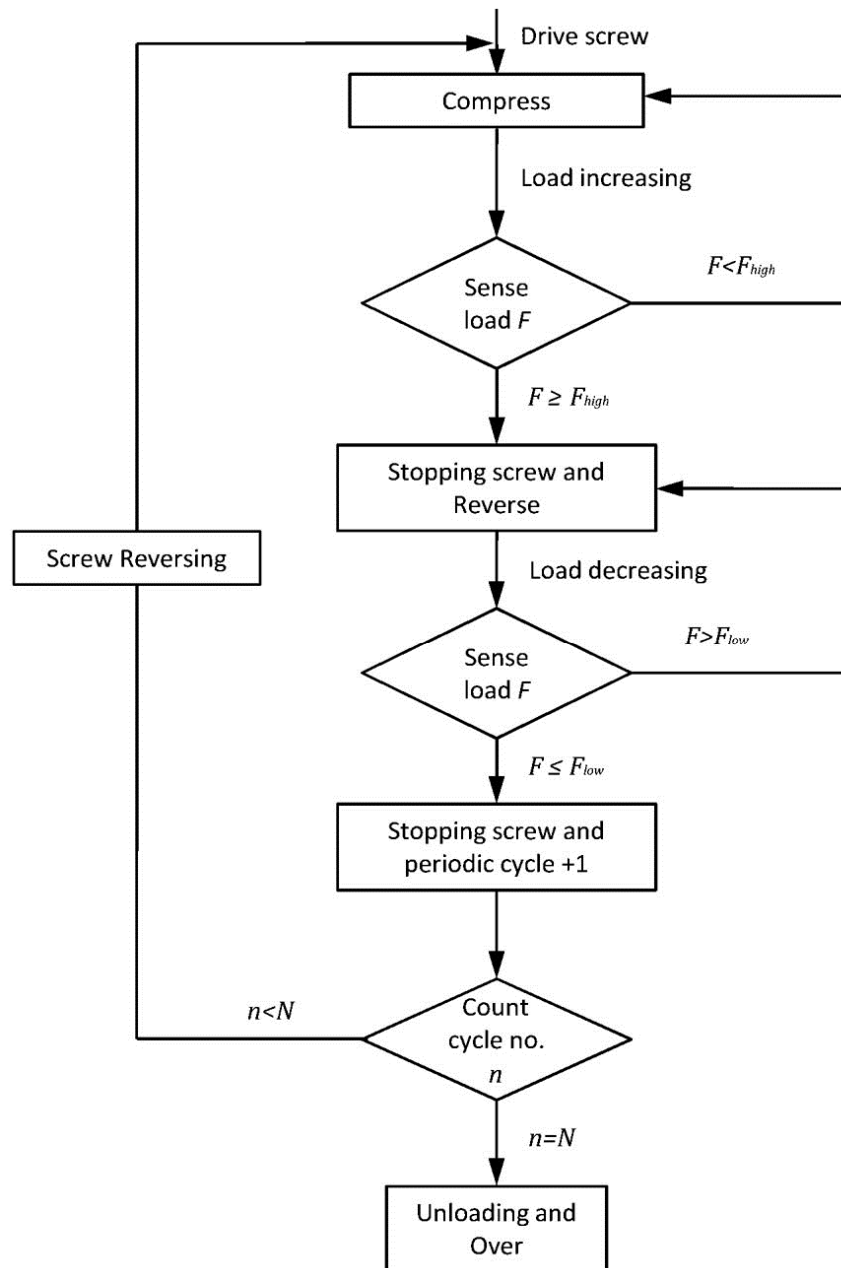


Fig.5-8. Flowchart of cycling compressive tests setup.

According to the flow chart shown in Fig.5-8, after the installation of specimen, the force sensor will measure the current load F at the moment while the screw-driven actuator begins to compress the specimen. The value of F increases along with the raising of compressive strain applied on the PHEMA specimen. When F equals to the value of F_{high} , screw for driving the actuator stops and reverses the direction, then start releasing the load respectively. During the releasing stage, the force sensor maintains the recording of the change of the current load F . When the value of F equals to F_{low} , the actuator stops and compresses again while the number of periodic cycle n is iterated by $n+1$ at the same time. Then, the processor of the system will compare the cycle number

n with the preset maximum cycle number N ($N=100$), if $n < N$, continue the experiment by applying another cycle of compressing/releasing; if $n = N$, terminate the experiment.

5.3.3.2 Test Results and Discussions

The cycling compressive test took 560 seconds to complete 100 cycles in total. Fig.5-9a and Fig.5-9b illustrates the displacement of the actuator plotted in terms of the time lapse (the initial 50 seconds), corresponding to the 20% and 30% compressive strain for PHEMA specimen, respectively. Similarly, the graphs of actuator's velocity versus time (initial 50 seconds) have been presented in Fig.5-9c and 5-8d for 20% and 30% compressive strain, respectively. It can be seen from Fig.5-9c&d that the actuator moves in a constant speed of 0.5 mm/s during the compression and release. The overshoots in these velocity graphs, which can be found before the actuator changed the moving directions every time, are caused by the motion delay of the servo motor. To be specific, it will take a short time for the driving screw to reach the same reversed rotating speed, including slow down, reverse the direction of turning and speed up again. Additionally, it can be found that there are 7 cycles appears in the Fig.5-9c, while nearly 5 cycles in the Fig.5-9d within the equivalent test time (50s). Due to the constant moving speed of the actuator, longer travel distance is needed to reach the 30% compressive strain than 20% compressive strain, thereby this requires longer cycle time for the group of 30% compressive strain. Furthermore, the *phase space portraits* in terms of velocity versus displacement are provided in Fig.5-9e and Fig.5-9f corresponding to 20% and 30% maximum compressive strain of PHEMA material respectively. *Phase space portrait* is one of the common used graphs to investigate the behaviour of periodic motion of resonator in vibration engineering, and it can give qualitative information on the stability of the periodic movements, which cannot be seen in other types of motion graph. The *phase space portrait* of a steady periodic motion consists of a series of closed lines with high consistency. According to the rectangular closed lines shown in Fig.5-9e&f, the highly consistent traces of actuator during 100 cycles of compressing/releasing indicate that PHEMA specimen under cycling compressive test behaves stable and reliable, and no material failure occurs during such cycling compressive test (up to 30% compressive strain). Similar conclusion was drawn in the literature [186] which is done by Bostan *et al.*, where they have experimentally examined that PHEMA specimen showing a good mechanical behaviour in dynamic conditions under even severer conditions, e.g. frequency at 1 Hz, over

100,000 cycles of test: one third of groups of specimen exhibit material failure after their flexion-extension cycling experiment.

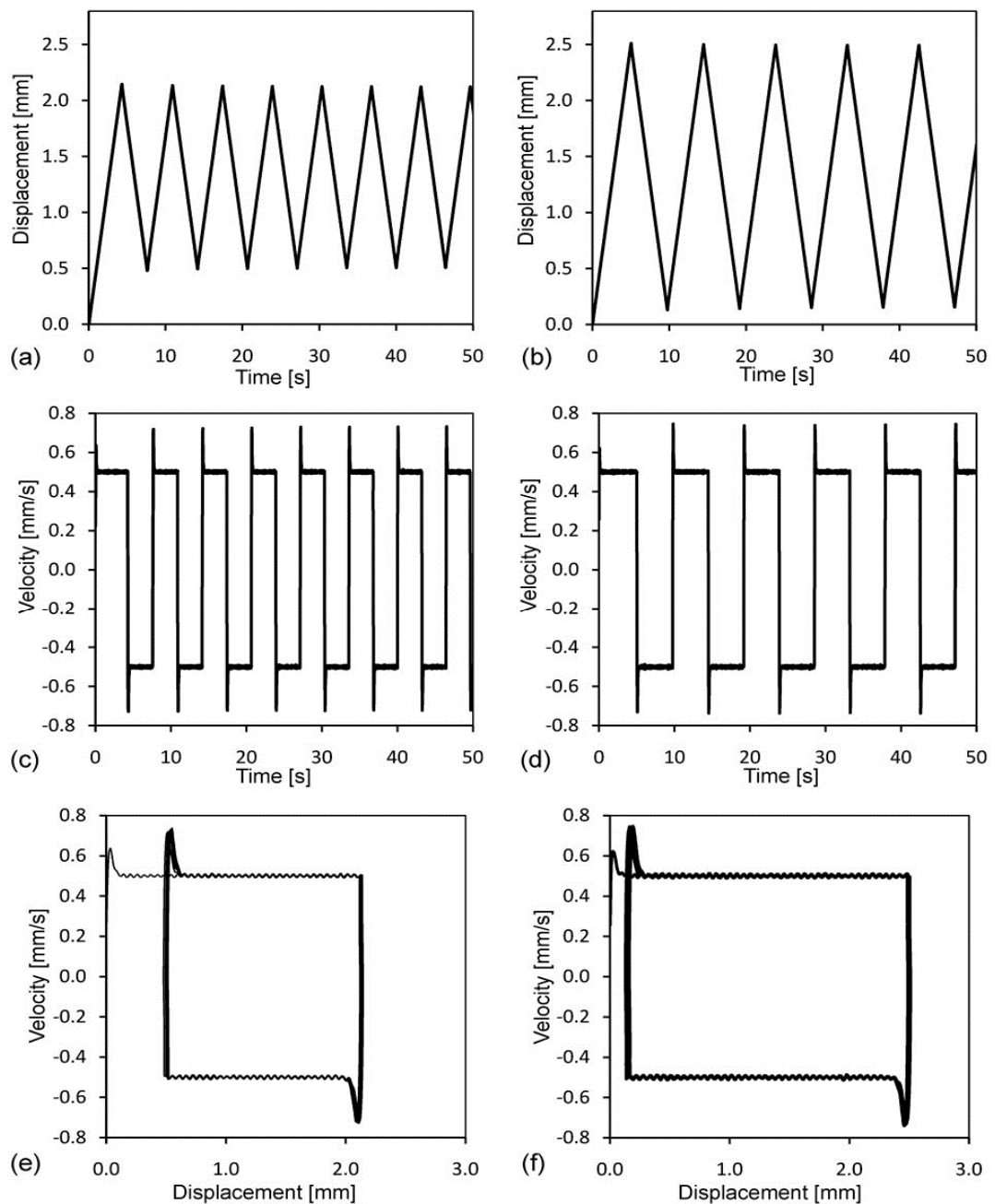


Fig.5-9. (a),(c),(e) corresponding to Displacement-Time graph, Velocity-Time graph and Phase space portrait, are the graphs for the actuator motion on PHEMA specimen up to 20% compressive strain. (b), (d) and (f) are the graphs for PHEMA specimen up to 30% compressive strain.

To further investigate the stability of PHEMA material under cycling compressive conditions, the stress response of PHEMA specimens are plotted in Fig.5-10, in terms of the stress-time curve for initial 50 seconds (Fig.5-10a) and the stress-strain curves for 100 cycles (Fig.5-10b). 100 times of

compressing and releasing have been applied on the PHEMA specimen, the maximum strain during the cycling loading is 30%, the strain rate is calculated as $0.5 \text{ [mm/s]} / 7 \text{ [mm]} = 0.071 \text{ [s}^{-1}\text{]}$. As is shown in Fig.5-10b, the stress-strain curve does not significantly vary with the cycle numbers, and illustrates similar behaviour between loading and unloading, without the obvious hysteresis loop (see Fig.3-1c). Thus, it qualitatively verifies that: i) the behaviour of PHEMA under compression can be categorised as hyperelastic responses; ii) no failure causing drastic change of stress-strain relationship is occurred during the cycling compressive test of PHEMA specimen, up to 30% compressive strain.

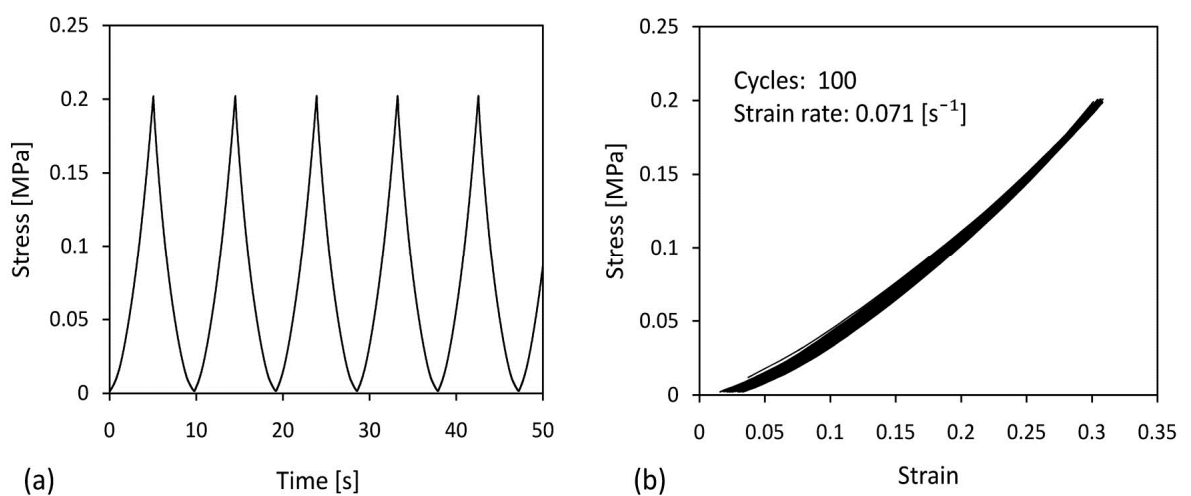


Fig.5-10. (a) Initial 50 seconds of stress response to the cycling compression for PHEMA specimen. (b) Stress-strain curves for PHEMA specimen. 100 cycles of compression under the strain rate of 0.071 s^{-1} .

To quantitatively evaluate the hysteresis loop for this cycling response of PHEMA material, the ratio of the unloading to loading area was calculated for selected cycle (each ten cycle). This ratio can reflect the degree of specimen resilience, and the size of hysteresis loop. A schematic diagram of stress-strain behaviour for material with significant hysteresis effect is illustrated in Fig.5-11a. It is obvious that the unloading area is smaller than (or equals to) the loading area, thus the ratio of the unloading to loading area is smaller than (or equals to) the value 1. Therefore, hyperelastic behaviour is indicated by the value of this ratio closer to 1 (or even equals to 1). As a result, the ratio of unloading to loading area with respect to cycle numbers has been illustrated in Fig.5-11b. The trendline of the data indicates that this area ratio maintains as a constant at the value of 0.971 for the PHEMA specimen under 100 cycles of compression. Therefore, two essential conclusions can be drawn. Firstly, the constant ratio indicates that no material failure of the specimen occurs

during the cycling compressive test, e.g. failure due to fatigue. It thereby verifies that PHEMA material behaves reliable and stable under cycling compressive load, at least for 100 cycles of loading. Secondly, the value of the constant ratio 0.971 means the small size of hysteresis loop (under 3% of loading area) for the PHEMA material under compression. The size of hysteresis loop is very small compared with typical viscoelastic materials. For instance, according to the work done by Anssari-Benam *et al.* [187], the size of hysteresis loop of aortic valve is determined at approximately 30%~50% of its loading area. This small size of the hysteresis loop obtained from PHEMA compressive behaviour suggests that PHEMA material possesses high resilience, and exhibit more hyperelastic response to compression than viscoelastic responses. Therefore, it validates that the feasibility of utilising hyperelastic theory (e.g. Mooney-Rivlin, neo-Hookean) to represent and simulate the mechanical characteristics of PHEMA material under compression.

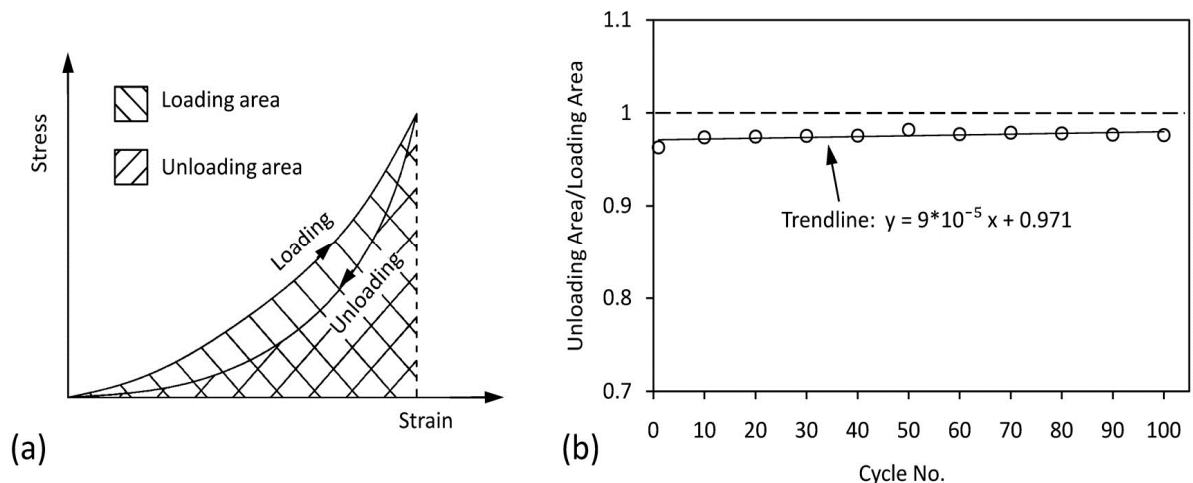


Fig.5-11. (a) Schematic diagram of stress-strain behaviour for material with significant hysteresis effect. Loading and Unloading area are indicated in the diagram. (b) Ratio between Unloading area and Loading area with respect to cycle numbers, for the PHEMA specimen under cycling compression.

As summary, based on the experimental results and discussions from cycling compressive tests on PHEMA specimen, PHEMA hydrogel material has been proven to be an excellent membrane candidate in its stable and recoverable mechanical responses to the cycling compressive loading, in terms of highly consistent stress-strain curves and constant size of hysteresis loop. No material failure of the specimen has been observed during the 100 cycles of compressing/releasing actions in the experiments. Therefore, the PHEMA hydrogel is a suitable and reliable hyperelastic material to be embedded in microfluidic device as a sealing membrane, enabling assembly and dis-assembly routines at least 100 times.

5.4 Mechanical Behaviour of Partially Swollen PHEMA Hydrogel

5.4.1 Uniaxial Compressive Test on Specimens with Different Degree of Swelling

5.4.1.1 Experimental Approach

Degree of Swelling (DOS), which is defined in Section 3.2.3 (Page 38), is commonly used to measure the degree of crosslinker of a network structural material, e.g. polymers. Different DOS may cause various mechanical properties of a polymer, because it significantly affects the consistence of polymer chains. Specifically, higher DOS indicates more solvent molecules inclusion in the polymer. At microscale, large number of solvent molecules inside the polymer makes the network junctions move away from each other, thereby leads to high stress of polymer chains because such polymer chains tend to return back to the relaxed state. Accordingly, parameters on mechanical properties of polymer will be affected, including Initial Tangent Modulus (Young's modulus) which represents the linear relationship at the beginning stage of deformation behaviour of nonlinear materials.

The compressive tests on PHEMA specimens with different DOS values were conducted. The apparatus and setups for the compressive test used in this study are similar to those introduced in Section 5.3.1, except the additional aqueous environment to immerse PHEMA specimen to facilitate the change of the DOS of the specimen during the test. The results such as stress-strain curves can then be obtained from the compressive tests under the equivalent conditions that were used for fully swollen hydrogels.

5.4.1.2 Test Results and Discussions

To examine the mechanical properties of PHEMA hydrogel under different degree of swelling, uniaxial compression has been applied on the cylindrical PHEMA specimens under the DOS of 1.1, 1.3, 1.35, and 1.45. Fig.5-12 depicts the relationship between the Initial Tangent Modulus of PHEMA and the DOS of PHEMA, which is ranging from the dry state (DOS=1) to the equilibrium swollen state (DOS around 1.5). The inverse proportion between the variables in Fig.5-12 illustrates that lower degree of swelling leads to a higher Initial Tangent Modulus. This has shown a strong agreement with the literature reported by Ganji *et al.* [155]. In other words, the PHEMA hydrogel

behaves much harder in its dried status than it is in the swollen status. In a dried polymer that has been cross-linked as a network, the polymer chains between the network junctions are entangled and relaxed at microscale. In the swollen status, however, the polymer chains are pushed apart by the solvent molecules, thus behave moveable because of the attached solvent molecules. Accordingly, PHEMA specimen exhibit larger Initial Tangent Modulus at a small value of DOS than that at large value of Degree of Swelling.

Fig.5-13 illustrates the relationship between stress and strain from PHEMA specimens in terms of various swelling status at 1.1, 1.3, 1.35 and 1.45. When the stress applied on PHEMA specimen is fixed, qualitatively, softer of specimen has been resulted from the higher value of degree of swelling.

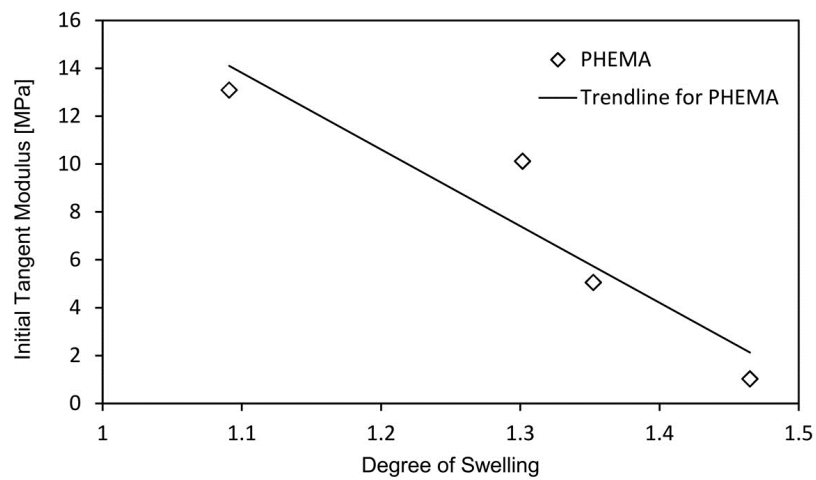


Fig.5-12. Initial Tangent Modulus for PHEMA specimen in variable degree of swelling ranging from 1 to 1.45. Trendline to indicate the general

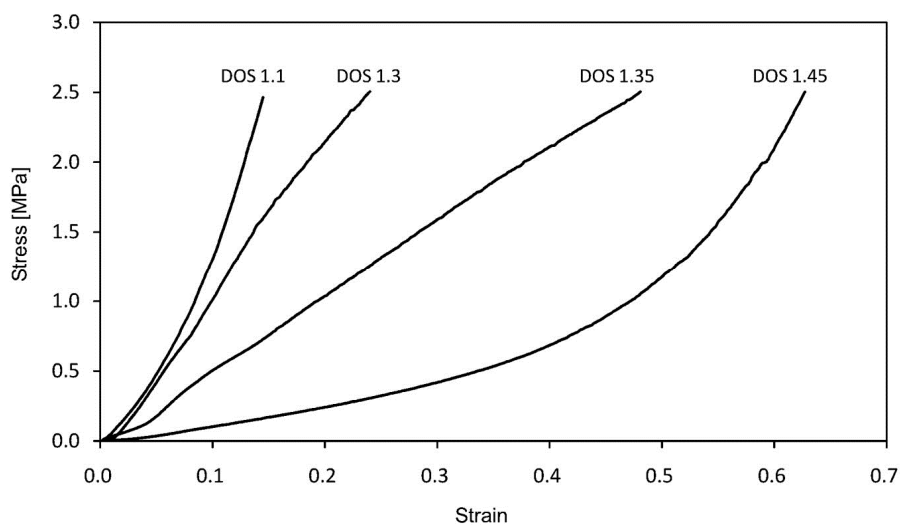


Fig.5-13. Compressive stress-strain curves of PHEMA specimen in different values of degree of swelling (DOS) at 1.1, 1.3, 1.35, 1.45, respectively. The compressive tests were performed perpendicular to the longitudinal direction of the cylindrical PHEMA specimen. The solvent for swelling is distilled water.

5.4.2 Simulations of Mechanical Behaviour of Partially Swollen PHEMA Hydrogel

According to Fig.5-13, PHEMA specimens remain the characteristics of hyperelastic material though they are in partially swollen status, *i.e.* with different degree of swelling values. Thus, the hyperelastic mechanical behaviour in terms of stress-strain curve from compressive test can be described and simulated based on Mooney-Rivlin theory. Following the same setup of simulation procedures introduced in Section 5.3.2, the Mooney-Rivlin coefficients (C_{01} and C_{10}) for determining material's mechanical property can be individually obtained from the compressive tests on the specimens in different DOS values. Table 5-2 lists the Mooney-Rivlin coefficients which are utilised to simulate the mechanical behaviour of PHEMA specimens with different DOS values. It can be seen that both the Mooney-Rivlin coefficients C_{01} and C_{10} are decreasing with the increase of the degree of swelling. This indicates that a variety of mechanical responses to compressive load is resulted from different degree of swelling of PHEMA specimen.

Degree of Swelling	C_{01} [Pa]	C_{10} [Pa]
1.1	1501395.92	2968133.75
1.3	913971.44	1990742.85
1.35	706625.60	879718.10
1.45	442090.57	554760.94

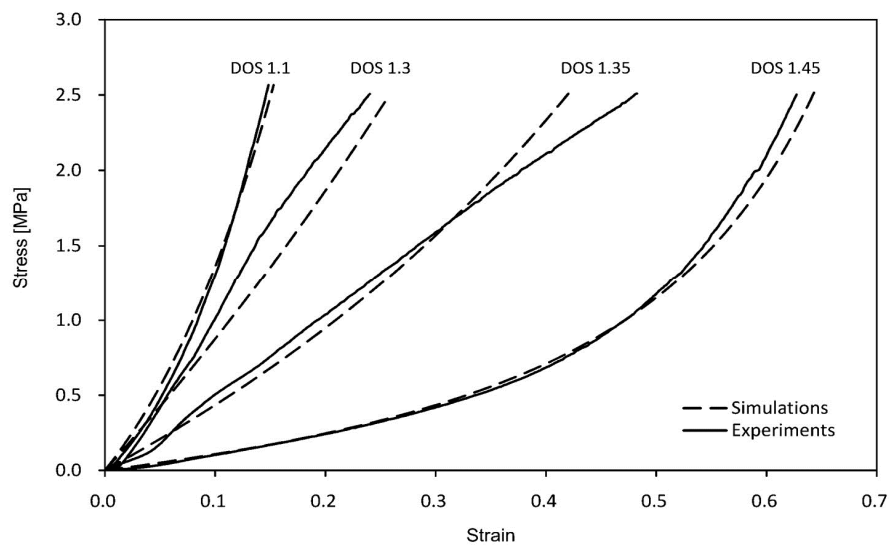


Fig.5-14. Compressive stress-strain curves of PHEMA specimen from experiments (solid curves) and simulations (dashed curves) versus degree of swelling (DOS) at 1.1, 1.3, 1.35, 1.45. The simulations established based on Mooney-Rivlin theory with coefficients C_{01} and C_{10} which are shown in Table 5-2.

In terms of stress-strain curves, the comparisons between the experimental results and Mooney-Rivlin simulated results are illustrated in Fig.5-14, based on the PHEMA specimens with various degree of swelling. According to this figure, the trends of all the stress-strain curves from simulation (dashed lines) generally match the trends of their corresponding curves from experiment, respectively. Quantitatively, for the PHEMA specimens with various degrees of swelling, the errors between experimental results and simulated results are all within 7%, based on the calculation of COD (Coefficient of Determination). Therefore, it concludes that the numerical simulation based on Mooney-Rivlin theory can predict the experimental mechanical responses of PHEMA hydrogel specimen to compressive stress, even with the hydrogel specimens are partially swollen.

5.5 Summary

Compressive tests have been conducted to investigate the mechanical properties of PHEMA hydrogel, which aims to provide the fundamental basis to the design of packaging of the hydrogel-based microfluidic device. The mechanical behaviours of PHEMA hydrogel (fully swollen or partially swollen) under static or dynamic cycling compression have been experimentally measured and simulated based on Mooney-Rivlin theory.

In general, both Mooney-Rivlin and neo-Hookean models, which are widely used for investigating rubber behaviour, can predict the mechanical behaviour of the hyperelastic material. In this chapter, the error analysis demonstrated that Mooney-Rivlin model can be better than neo-Hookean model in more accurately describing and predicting the mechanical response of PHEMA hydrogel to compression. Meanwhile, the feasibility and accuracy of using Mooney-Rivlin model to analyse and predict the hydrogel's mechanical behaviour have been quantitatively verified. To determine the reliability of using PHEMA material as an inserted membrane in the hydrogel-based microfluidic system, cycling compressive load has also been applied on PHEMA specimens. The results verified that the PHEMA is more suitable to be regarded as a hyperelastic material than a viscoelastic material and demonstrated that PHEMA specimen possesses good stability under cycling compression within 60% strain, unless the material failure will occur.

Furthermore, compressive tests on partially swollen PHEMA specimens conclude that the Initial Tangent Modulus decreases with the increasing of degree of swelling, and Mooney-Rivlin model is applicable to predict the general mechanical behaviour of such partially swollen PHEMA hydrogel.

Chapter 6. Assembly Process with PHEMA Membrane under Mechanical Fastening

6.1 Introduction

The assembly techniques for microfluidic devices such as thermal pressure bonding [46], solvent bonding [41] or surface pre-treated assisted bonding [44] are well established and have been applied in the fabrication of microfluidic device. However, these bonding procedures are not applicable when dealing with biocompatible soft materials integration (e.g. synthetic hydrogels) due to their thermo-sensitivity, which may cause damages potentially hindering their functionalities. Furthermore, these bonding methods are not particularly suitable for the construction of microfluidic device where the re-use through disassembly may be desirable. In coping with the manufacturing challenges of microfluidic devices that can work with hydrogel based platform implementation and be reusable through disassembly and re-assembly routines, suitable bonding methods are demanded to meet these requirements. Mechanical fastening using bolts and nuts is a conventional assembly technique, which has been extensively utilised in various industrial applications, in particular for large components construction (e.g. aircrafts). It has presented a number of advantages over other assembly/bonding methods, such as low processing (e.g. ambient) temperature, easy-to-repair or replacement, low costs and possibilities of multiple disassembly. For what concerns microfluidic devices packaging applications, the process is less prone to the potential contaminations of the components due to the relatively clean condition during the operation where no glue or adhesives are involved. However, various challenges arise when it comes to apply such assembly technique at small scales; in particular, providing an effective sealing (or isolation) through an optimum management of the layers packaging compression in respect to the flowing fluid pressure is critically important in order to prevent liquid leakage in any part of the system, which could lead to its malfunctioning or to unreliable measurements.

This chapter addresses fundamental aspects of mechanical fastening technique for hydrogel-based microfluidic devices realisation, when a PHEMA hydrogel thin film (in swollen statue) is integrated in the device as an inserted membrane. The mechanical responses (e.g. stress

distribution, geometric deformation) of PHEMA hydrogel in both microchannels and culture chamber due to the compression induced by the assembly process can be numerically visualised based on the Mooney-Rivlin theory. The reliabilities of such bonding technique have been examined through leakage tests at the hydrogel/thermoplastic interface on a custom designed PMMA-based prototype device.

Through this investigation, a guideline for optimization of the designs has been proposed through the selection of suitable parameters in terms of channel geometric parameter (e.g. depth, width, dip angle) and compressive pressure in assembly process.

6.2 Determination of Critical Leakage Pressure by Simulation

6.2.1 Principle Basis and Model Building

The investigation on the reliability of the mechanical fastening method for microfluidic device is inevitably to determine the possibility of leak of the microfluidic channels after the device is assembled. The aim is to ensure that the pressurised fluid will not leak when it is flowing within the microchannels of the device.

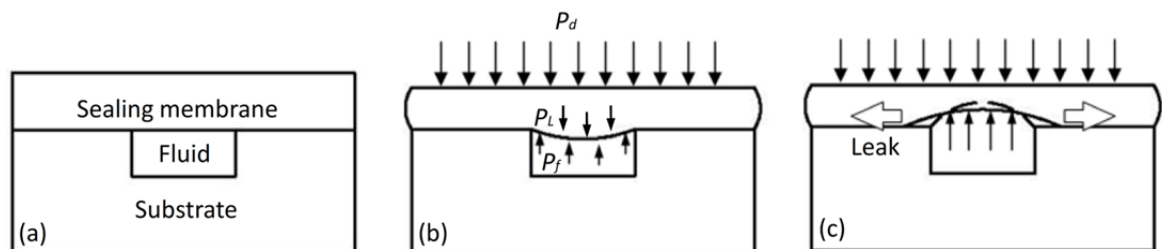


Fig.6-1. (a) Schematic diagram of device cross-sectional packaging structure. (b) Packaging pressures general distribution on the structure during operating condition. (c) Schematic diagram of liquid leakage situation due to high fluid pressure.

The leakage occurs along the crevice at the interface between microchannel and sealing membrane as a result of high pressure of liquid inside channel. According to the designed structure of the microfluidic device (see Chapter 1), Fig.6-1 shows a cross-sectional schematic diagram of the microfluidic device used in this study to determine the critical constraint parameters of leakage. The structure shown in Fig.6-1 consists of a cover (simplified as a distributed pressure P_d), sealing membrane, substrate with microchannel, and pressurised fluid. The sealing membrane is subject to the fastening pressure (P_d) when the device is assembled using mechanical fastening technique. Thus, a localised pressure (P_L) resulted from Poisson's effect forces the membrane to protrude into

the cavity of the microchannel (Fig.6-1b). However, the fluid in the channel applies a pressure (P_f) to resist the protrusion in the cavity of channel against the induced localised pressure (P_L). Therefore, the interaction between the localised pressure (P_L) and the fluid pressure (P_f) determines the criteria of the leakage of the system. When $P_L > P_f$, the membrane protrudes into the microchannel (see Fig.6-1b). Inversely when $P_L < P_f$, the membrane surface is inflated and indented, leaving a gap at the interface (see Fig.6-1c). This can ultimately lead to the liquid leakage in adjacent to the channel. Accordingly, the criteria to determine the leakage of the device can be addressed subject to the values of P_d and P_f , because P_L is induced by P_d .

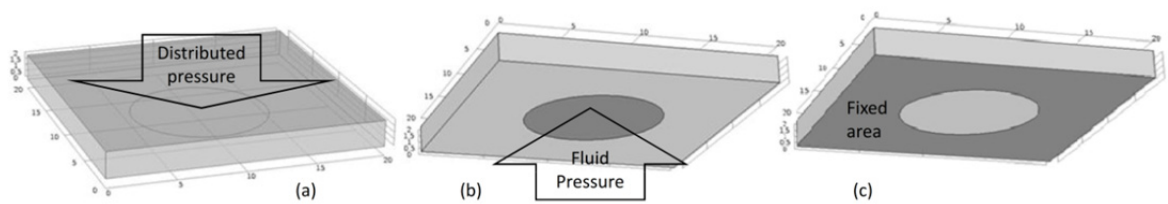


Fig.6-2. The dark areas are the force applied area, pressure direction is shown along the arrows. (a) Distribution pressure applied (Cover). (b) Fluid pressure applied (Fluid). (c) Fixed area (Substrate). All dimensions in mm.

Considering the criteria of leakage that is induced by the interaction between P_d and P_f , a three-dimensional modelling was established in the simulation using COMSOL Multiphysics software. Fig.6-2 illustrates the configurations of numerical constraints for the hydrogel membrane in simulation. The distributed pressure P_d applies on the top surface of membrane (Fig.6-2a), fluid pressure P_f applies on the circular area at the bottom (Fig.6-2b), and PMMA substrate engraved with microchannel are simplified as a fixed constraint (Fig.6-2c). Once a fixed value of P_d is applied on the hydrogel membrane (without P_f yet), PHEMA hydrogel membrane is deformed and protruded out of the circular area due to Poisson's effect. The displacement of the central point of the protrusion is recorded as s [μm], which indicates the maximum deformation of the membrane. When the fluid pressure P_f is applied, such displacement s [μm] will be decreased because P_f and P_d work against each other. Thus, by increasing the value of P_f , it is possible to determine the value of s and it will become zero when the localised pressure P_L equals to the fluid pressure P_f . Therefore, the maximum value of P_f that can cause any leakage may be derived.

6.2.2 Simulation Results and Discussions

In the simulation, PHEMA hydrogel is regarded as an incompressible hyperelastic material based on Mooney-Rivlin theory, which is elaborated in Chapter 3 and 5 of this thesis. Five groups of

simulations are carried out, in terms of the values of P_d at 5, 10, 20, 33.5, 99.1 [kPa] respectively. The values that 33.5 and 99.1 [kPa] are the engineering stress corresponded to 10% and 20% compressive strain, according to the stress-strain curve in Fig.5-4a. As an example, under a fixed value of the mechanical pressure P_d (=5 kPa), the reverse proportional relationship between the displacement of protrusion s and the fluid pressure P_f can be depicted in Fig.6-3. As is shown in this figure, $P_f = 9.92$ kPa when $s = 0$ mm, which means that the maximum allowed fluid pressure in channel is 9.92 kPa if the compressive pressure induced by mechanical fastening process is 5 kPa.

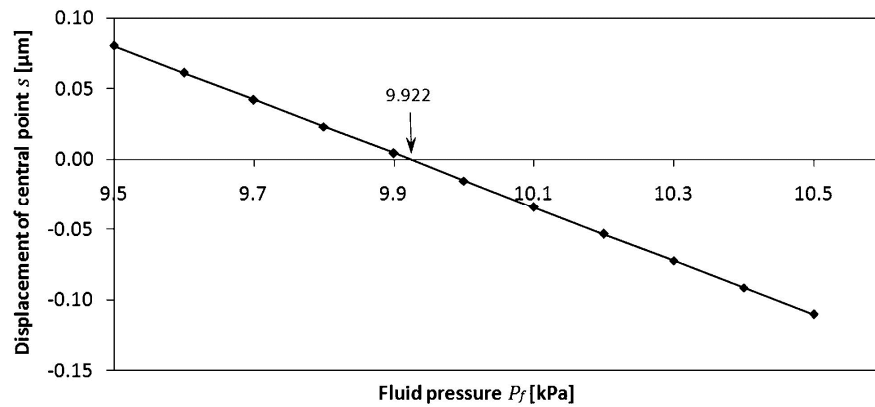


Fig.6-3. Displacement of central point s [μm] versus fluid pressure P_f [kPa]. Under mechanical compression of $P_d=5$ kPa, the displacement ' s ' reaches zero when the fluid pressure is 9.922 kPa.

Table 6-1 gives the values of the maximum allowed fluid pressure P_f corresponding to the various compressive pressure P_d from the five groups of simulations. The values of maximum allowed fluid pressure with respect to $P_d=33.5$ and 99.1 [kPa] (corresponding to 10% and 20% compressive strain) are read as 66.3 and 196.3 [kPa]. In literature, microfluidic valves that can achieve seal reliably against forward fluid pressure as high as 60 kPa is developed and reported by Zhang *et al.* [188,189]. Therefore, the ultimate fluid pressure of 60 kPa can be commonly applied for microfluidic systems, because valves are designed to resist high pressure and provide reliable blockage for a microfluidic device. Consequently in this case, the mechanical fastening process using hydrogel as an inserted sealing membrane is reliable as $P_f=66.3$ kPa (or 196.3 kPa) which are greater than 60 kPa.

	Test 1	Test 2	Test 3	Test 4 (10% strain)	Test 5 (20% strain)
P_d [kPa]	5	10	20	33.5	99.1
P_f [kPa]	9.9	19.8	39.6	66.3	196.3

6.3 Determination of Critical Leakage Pressure by Experiments

6.3.1 Design and Manufacturing of Testing Chip

A sandwich structure-based micro-device has been manufactured for leakage tests at the thermoplastic/hydrogel interface nearby the fluidic circuits which are machined on a thermoplastic plate. In this study, the material for manufacturing the test chip is PMMA (poly(methyl methacrylate)), which allows real time optical microscope observation as a transparent material. As schematically illustrated in Fig.6-4, the assembled 'sandwich' structure with an insertion of membrane made of PHEMA hydrogel was constructed embracing a single closed microchannel, sealed between cover and substrate through mechanical fastening assembly process. PMMA thermoplastic material, as the cover and substrate provides a rigid and conformed protection to the PHEMA hydrogel membrane. PHEMA, the inserted membrane, is utilised to seal the microfluidic channels owing to its flexibility and toughness as a hydrogel material. The microchannels with inflow and outflow ports are manufactured on the PMMA substrate by micro-milling machine. Then, the microchannels are covered by the PHEMA membrane thereby forming a closed fluidic environment.

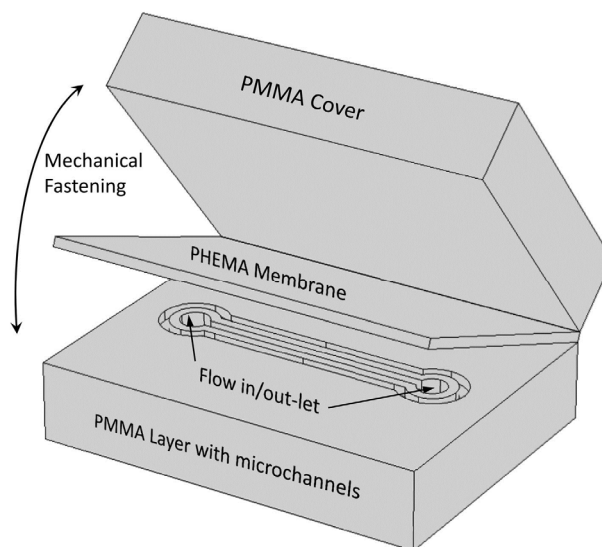


Fig.6-4. Schematic diagram of a microfluidic circuit in a stacked, PHEMA thin film sealed PMMA chip

Fig.6-5 shows the layout of the PMMA layer with microchannels which is machined on the surface of PMMA layer with an enlarged schematic diagram of its details. The microchannels can be divided into two groups: i) T-Channels for fluid flow, which stands for Test Channel; ii) L-Channels used to gather liquid flow at the interface between the hydrogel and the PMMA, indicating whether leakage is occurred. When carrying out the leakage testing experiment, pressurised fluid is injected

from inflow port into T-Channels at first, and come out from the outflow port. Owing to the gap (700 μm to 1000 μm) between T-Channel and L-Channel, they are not connected. Thus, under the situation of no leakage, L-Channel is dry and empty while the T-Channel which offers a perfect sealed pass route for fluid is full of flowing liquid. However, if the fluid pressure in T-Channel is high enough to raise the membrane protrusion towards the cavity of channel, it consequently makes the T-Channel and the L-Channel connected, thereby the leakage of the microfluidic system happens. Meanwhile, the L-Channel is able to seize the liquid which is leaked out from any direction of T-Channel or ports. Hence, the leakage can be determined by observing the existence of liquid in L-Channel.

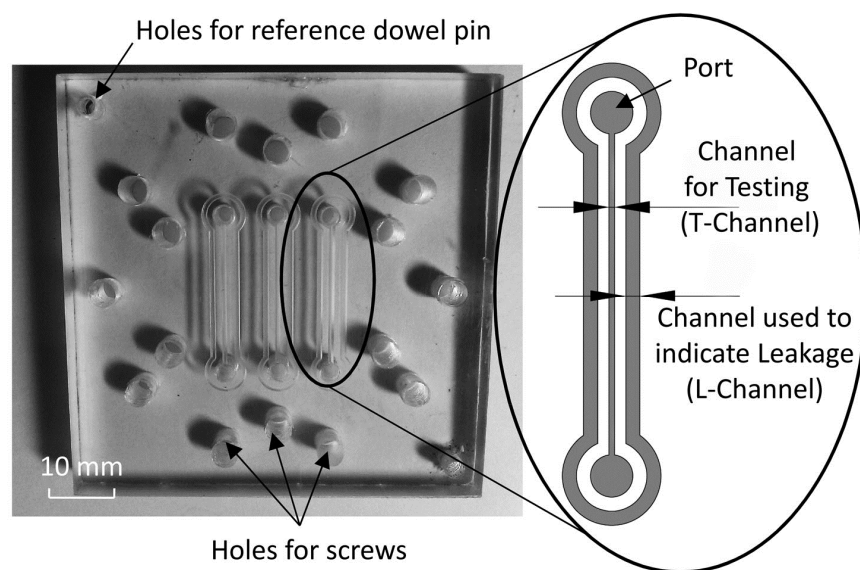


Fig.6-5. Overview of PMMA chip. Each independent channel consists of ports, T-Channel and L-Channel, used as in/outlet, testing channel and leakage indicative channel respectively.

Both T-Channel and L-Channel are micro-milled structure on the plate of PMMA. A circuit board engraving machine (Create-DCM3030) equipped with 30°/0.1 mm cutter (Fig.6-6b) is utilised to fabricate microchannels with trapezoidal cross-section on the thermoplastic PMMA substrate (Fig.6-6a). The dimensions of such microchannels are determined by the geometry of the cutter. The engraving machine ensures the accurate manufacturing at $\pm 5 \mu\text{m}$ for the depth of microchannel [190]. The speed of spindle during manufacturing is set to be 1500 rpm to avoid the melting of PMMA material due to the thermal effect induced by high spinning speed. T-channels with depths ranging from 200 μm to 1000 μm are manufactured allowing a comparative investigation on the mechanical responses of PHEMA hydrogel membrane to the different depths of microchannels.

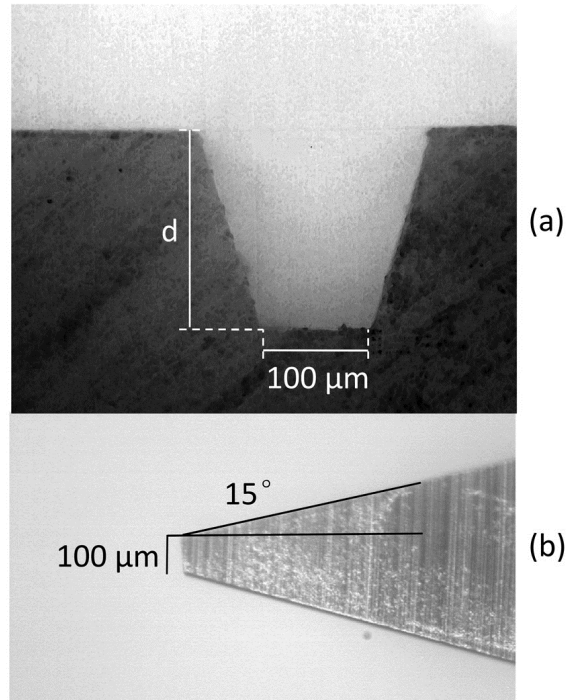


Fig.6-6. (a) Cross-sectional view of the channel in PMMA substrate; depth ranges from 200 μm to 1000 μm on each channel sets. (b) Cutter geometry of the micro-milling machine used in Testing Chip manufacturing.

6.3.2 Leakage Testing Device (LTD) Assembly and Installations

To achieve reliable sealing of the microchannels with hydrogel membrane, the control of compressive pressure induced by the mechanical fastening process is essential. Insufficient compression on hydrogel membrane may cause leakage of the microfluidic system. However, hydrogel membrane may be subject to material failure if the compression is so great that it makes the internal stress beyond the ultimate strain of material. According to the research on the mechanical properties of PHEMA hydrogel (Chapter 5), the compressive stress applied on the hydrogel membrane can be directly obtained from the stress-strain curve (see Fig.5-4a) if the compressive strain is known. Thus, the compressive pressure applied on the inserted sealing membrane in microfluidic device can be determined by controlling the compressive strain of the hydrogel membrane when it is assembled by mechanical fastening technique. Particularly, from Fig.5-4a, the engineering strain of PHEMA material in its water swollen state under compression can reach up to 55% without material failure at room temperature. Accordingly, the compressive strains varying from 10% to 50% are practically applied on the hydrogel membrane in current experiment to identify the optimum value which can establish reliable sealing for the hydrogel-based microfluidic device.

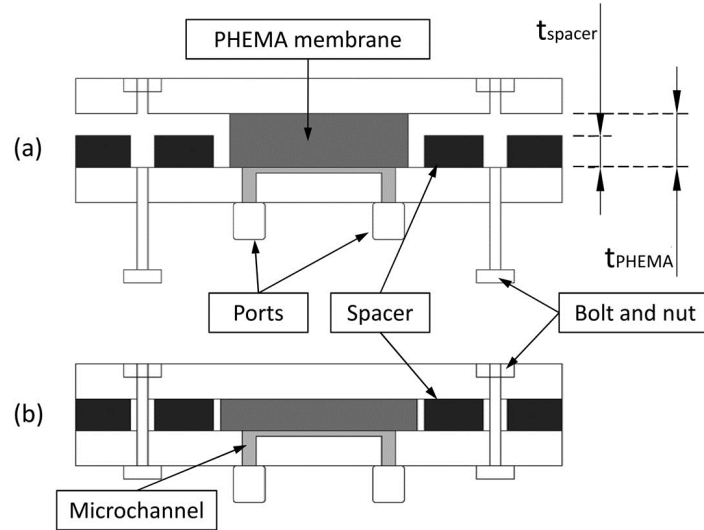


Fig.6-7. Two parameters have to be measured to calculate the compressive strain of the hydrogel membrane: t_{spacer} and t_{PHEMA} . (a) All components are assembled before the fastening process. PHEMA membrane covers all the channels and is inserted between the two PMMA jigs. (b) The multilayer microfluidic device is completely assembled by fastening the screws. The fluid inside the microchannels is sealed by membrane which has a protrusion into the cavity of the channels.

Fig.6-7 shows the cross-sectional view of the hydrogel-based microfluidic device before and after fastening. The original thickness of PHEMA membrane (t_{PHEMA}) was precisely prepared during the hydrogel synthesis process. The height of copper spacers (t_{spacer}) determined the final thickness of compressed hydrogel membrane after the microfluidic device is assembled. Hence, the compressive strain (ε) of PHEMA membrane under the compression can be obtained by:

$$\varepsilon = \frac{t_{PHEMA} - t_{spacer}}{t_{PHEMA}} \times 100\% \quad \text{Eqn. 6-1}$$

Table 6-2: Various values of compressive strains used in this study, in terms of combinations of spacers and PHEMA membrane with different thickness

t_{PHEMA} [mm]	t_{spacer} [mm]	Δt [mm]	ε Strain
1	0.5+0.2+0.2	0.1	10%
1	0.8	0.2	20%
1	0.5+0.2	0.3	30%
0.8	0.5	0.3	37.5%
1	0.5	0.5	50%

Due to the dimension of silicone moulds which were used for controlling the geometry of hydrogel, only the PHEMA membrane with thickness 0.8 mm or 1 mm can be fabricated, and the copper spacers were cut from commercial copper rolls, with standard thicknesses of 0.8 mm, 0.5 mm and 0.2 mm. By implementing specific combinations of copper spacers and PHEMA membranes, the designated compressive strains which are ranging from 10% to 50% can be obtained. They are listed in Table 6-2.

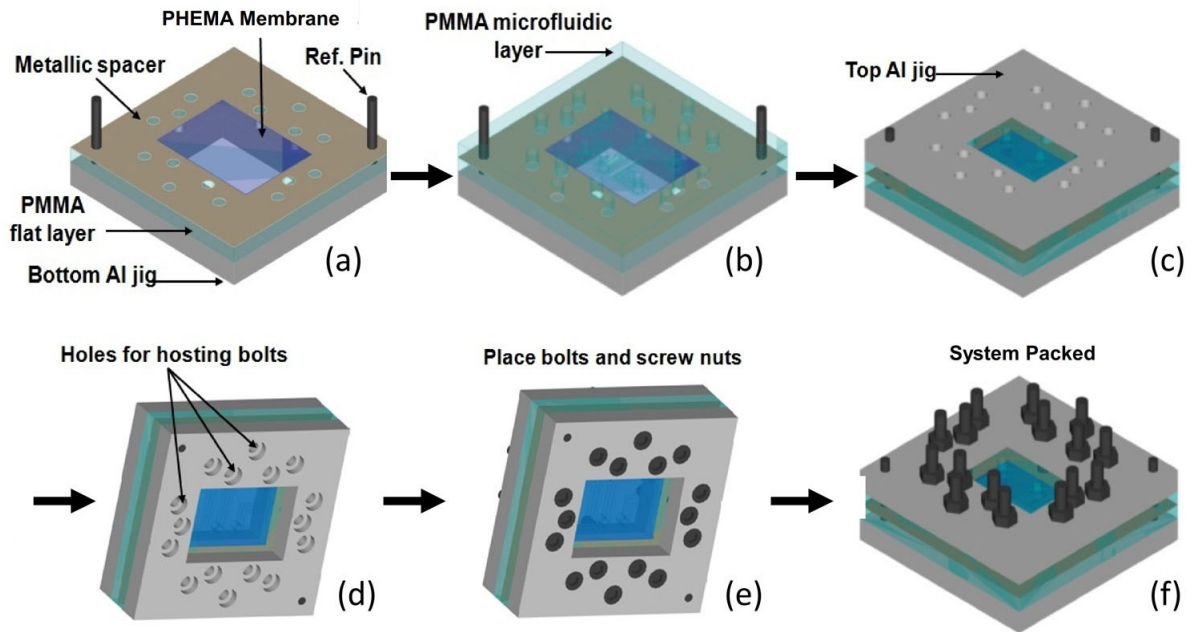


Fig.6-8. Assembly process of the leakage testing device. (a) PHEMA film is positioned over the flat PMMA surface in the region defined by the metallic spacer and (b) top PMMA layer is positioned; the micro-milled fluidic circuits cover the whole hydrogel membrane. [(c) and (d)] Top aluminium jig is positioned and then controlled compression is applied [(e) and (f)].

The assembly process of the actual leakage testing device (LTD) is schematically illustrated in Fig.6-8. PMMA slabs with thickness of 8 mm are used as the substrate for microchannels. All the fluidic circuits (*i.e.* microchannels and ports) are designed and fabricated within an area of 30x20 mm² in order to be entirely covered by the hydrogel membrane. The connectors which are used to host the tubes at the ports of inlet or outlet in the current study are selected as the model type of KJS02-M3 from Automation Distribution Incorporated [191]. The details about the dimensions of these connectors are listed in *Appendix 1*. Two aluminium jigs are fabricated and assembled to reinforce the multiple layers structure, avoiding the potential yield (*i.e.* bending) of the PMMA layer due to the stress induced by fastening. Hollow areas with the dimensions of 30x20 mm² are manufactured at the centre of both the aluminium jigs and the metallic spacers, to reserve an optical window to favour experimental observations through optical microscope. Meanwhile, the aluminium jigs, PMMA layers, metallic spacer, and the hydrogel membrane are aligned by two reference dowel pins and fastened by 16 screws with thread of 6 mm. The locations of these screws are designed to be evenly distributed around the fluidic circuits, in order to provide distributed compressive pressure for the PMMA layers, and to make sure the hydrogel membrane is under uniaxial compressive constraints.

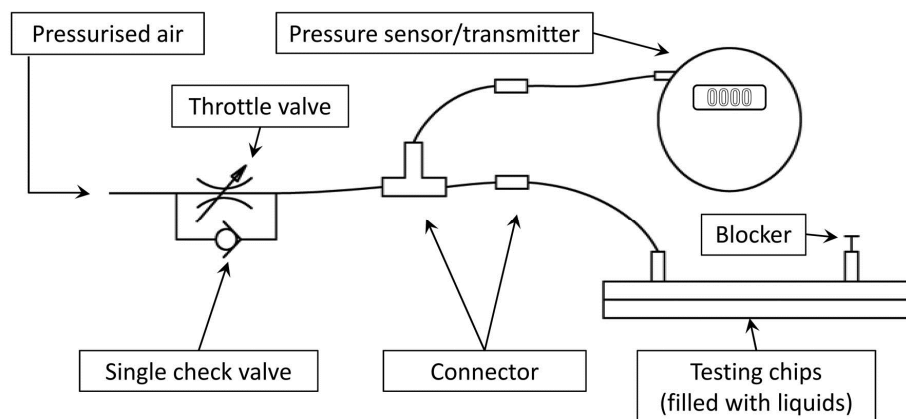


Fig.6-9. Schematic diagram of the flow measurement setup.

To demonstrate the feasibility and reliability of using mechanical fastening techniques to seal hydrogel-based microfluidic device, two conditions has to be satisfied: i) The fluid can pass through the microchannel. ii) There must not be any leakage anywhere in the fluidic system. Therefore, the examination of reliability can be examined by the determination of the critical leakage pressure, which is the maximum allowed fluid pressure in the fluidic circuit that will not cause leakage. A pressure generating system, consists of pressure sensor, testing chip, valves and connectors, has been built to measure the critical leakage pressure. As shown in Fig.6-9, the system ensures that the pressure is equal everywhere in the system. When pressurised air is injected into the device, air pressure gradually increases at the speed of approximately 500 Pa/s if the throttle valve is turned on. The air pressure is converted into the fluid pressure along the interface between air and fluid at the inlet port of the microchannel, because the testing chips is pre-filled with liquid prior to the air injection. Thus, the fluid pressure in the microchannels is equal to the air pressure which can be accurately measured from the pressure sensor/transmitter. In the current experiment, the real-time change of air pressure is recorded by the pressure sensor.

6.3.3 Experimental Results and Discussions

6.3.3.1 Material Failure Due to Fastening

As is described, the compressive strains of PHEMA membrane are controlled varying from 10% to 50% in the experiment. The experimental results demonstrate that 30% or higher strains can lead to potential failure of hydrogel membrane. A fractured PHEMA membrane due to application of 30% compressive strain is shown in Fig.6-10a. The indentations which sketch the contours of the

channels (both L-Channel and T-Channel) indicate that the mechanical failure of the hydrogel membrane is likely to take place at the edge of the microchannels. It has been found from Fig 5-4a that the ultimate compressive strain that hydrogel material can resist is approximately 55%, where the internal stress in hydrogel membrane is primarily concentrated at sharp corners in contact with the edge of channel (see Fig.6-6a). Before the leakage testing experiment is conducted, the PHEMA membranes under 30%, 37.5% and 50% compressive strains have already exhibited material failures due to the stress concentration. Thus, only 10% and 20% compressive strain was experimentally applied on PHEMA membrane to evaluate the maximum allowed pressure (P_f), without causing any cracks of PHEMA material.

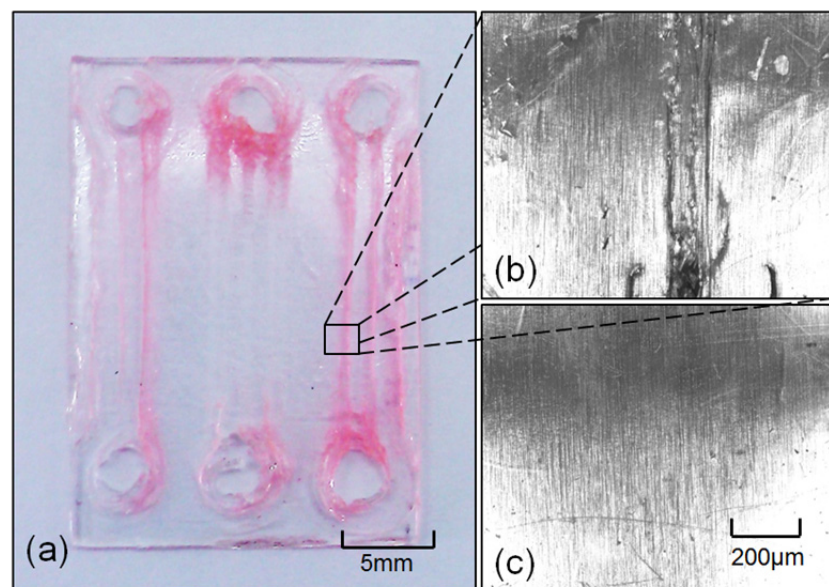


Fig.6-10. (a) Failed PHEMA hydrogel membrane, unstalled from 30% compressive strain. Cracks traced on microchannel edges, especially on the ports. (b) Optical microscope image of the membrane crack on the channel. (c) Normal PHEMA membrane surface image from optical microscope, act as reference when comparing with (b).

6.3.3.2 Determination of Maximum Allowed Fluid Pressure (P_f)

In order to make the optical observation of leaked liquid in L-Channel more distinctly, the flowing fluid in the microchannels is stained as red colour. Figure 6-11 indicates the microchannel and inlet port in the sealed state (Fig.6-11a&c) and in the leaked state (Fig.6-11b&d). Fig.6-11e schematically illustrates the change of pressure in the system with respect of time. Accordingly, at the early stage of the leakage test, the fluidic pressure was increasing rapidly with time from zero. The increase speed slowed down with the increase of time, because the difference between the pressure generator and internal pressure inside the microchannels became smaller and smaller. If

the pressure continually increases, a pressure collapse resulted from leakage can be observed. The criteria to judge whether the system leaks or not can be determined by such pressure collapse: no leaking before collapse; leaking after collapse. Therefore, according to the recorded pressure change by the transmitter/sensor, the critical leakage pressure which can be found at the pressure collapse equals to the maximum allowed fluid pressure in the microfluidic device that will not lead to leakage.

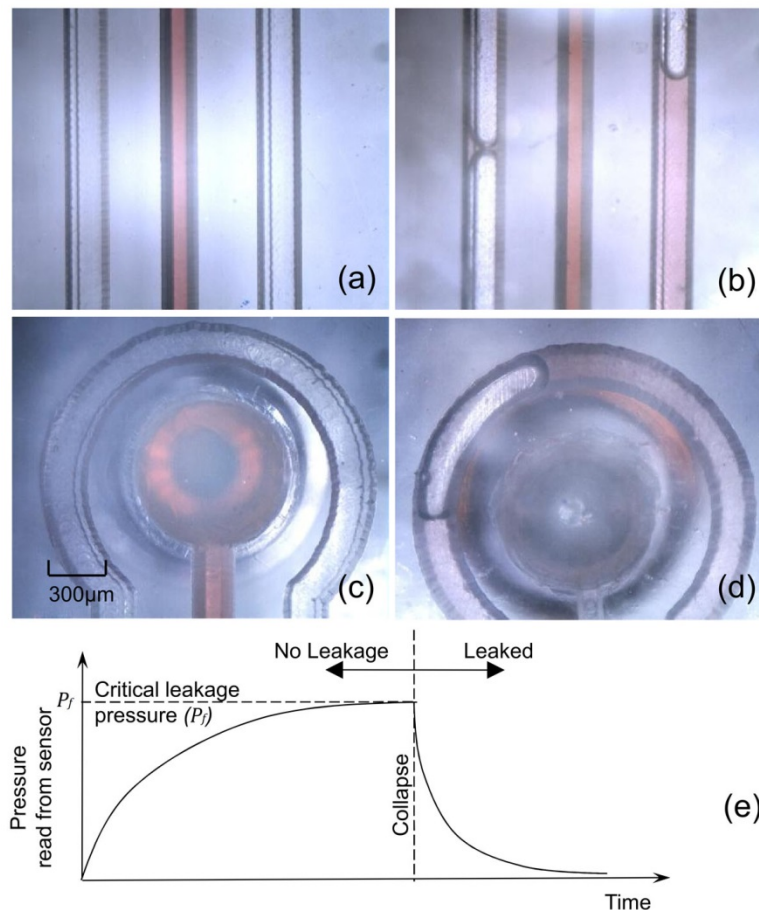


Fig.6-11. Images of the status (Sealed or leaked) of microchannel/port from optical microscope, taken under room temperature. (a) and (c) Microchannel/port operation without leakage, empty in L-Channel. (b) and (d) Microchannel/port operation with leakage, L-Channel filled with red liquids. (e) Schematic diagram for sensor pressure reading changes with time during leakage testing, the peak value of pressure donates the critical leakage pressure, which followed by a pressure collapse due to leakage.

The critical leakage pressure (P_f) with respect to the channel depths is provided in Fig.6-12, which is based on three groups of parallel experiments. According to Fig.6-12a, for 10% compressive strain, the critical leakage pressure P_f falls in the range of 200 kPa to 350 kPa on channel depths, which indicates a stable and reliable sealing of the microfluidic channels. Interestingly, under the constraint of 20% compressive strain, the channels with depth of 200 μm

and 300 μm are blocked by the hydrogel protrusions towards the cavity of microchannel. The fluid cannot pass these channels because of the blockage, and can potentially leak directly at the inlet port if the fluid pressure is high enough. Meanwhile, the rest of microchannels (e.g. depth of 400 to 1000 μm) under 20% compressive strain behaves normally as pressure increases following by a pressure collapse. By comparing the average pressure values between 10% and 20% strain, it is apparent that higher critical leakage pressure P_f is resulted due to 20% compressive strain in comparison with 10% compressive strain, excluding the blocked channels under 20% strain (e.g. depth of 200 and 300 μm). Therefore, the less pressure is applied, the smaller critical leakage pressure (P_f) is caused.

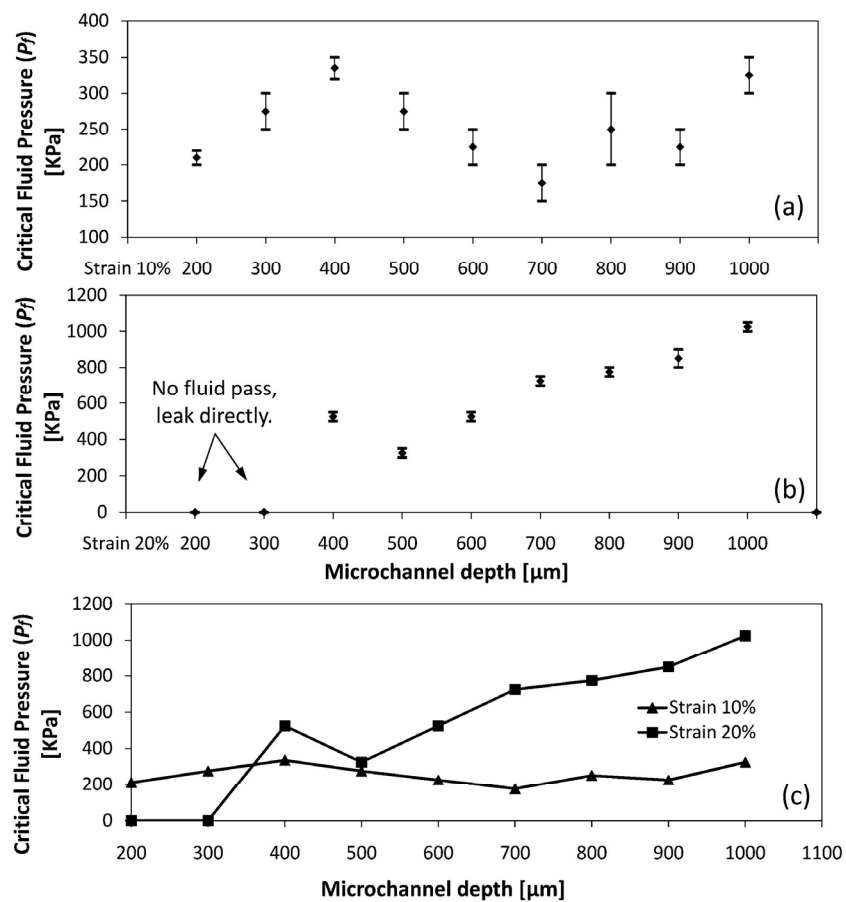


Fig.6-12. Critical leakage pressure under compressive strain of (a) 10%, (b) 20% with respect of the channel depth. (c) The median of critical leakage pressure data versus channel depth under both 10% and 20% compressive strain.

As a result of the experimental investigations on the fluid pressure in the fastening bonded hydrogel-based microfluidic device, the critical leakage pressure P_f shown in Fig.6-12c identifies that the maximum allowed fluid pressure enabling reliable seal of the microfluidic system lies in the range of 200 kPa to 350 kPa for 10% fastening strain, and 300 kPa to 1000 kPa for 20% fastening strain (if no blockage).

Table 6-3. Comparison of P_f values from simulation and experiment		
	10% fastening strain	20% fastening strain
Commonly LOC system pressure can reached	60 kPa	60 kPa
Maximum allowed pressure P_f (from simulation)	66.3 kPa	196.3 kPa
Maximum allowed pressure P_f (from experiment)	200~350 kPa	300~1000 kPa

Table 6-3 compares the results of maximum allowed fluid pressure which are derived from simulation (Section 6.2.2) and experiments (Section 6.3.3). As a result, both the maximum allowed fluid pressures (P_f) from simulation and experiments are larger than the maximum required fluid pressure for normal microfluidic system (60 kPa). Hence, it is numerically and experimentally proven that using mechanical fastening technique to assemble a hydrogel-based microfluidic device is an efficient and reliable packaging process.

Notably from the Table 6-3, the values of P_f from experiments are at least two times larger than that from the simulations, for both 10% and 20% compressive strains. Practically, when the situation shown in Fig.6-1c occurs, the fluid is hardly to break through the contact barrier between hydrogel sealing membrane and the microchannel, because the stress in the membrane induced by mechanical fastening process is concentrated at the edge of microchannels. This effect of stress concentration was not considered in the numerical model which is introduced in Section 6.2, thus led to the underestimation of the value of P_f from numerical simulation. Such effect of stress concentration is numerically investigated and discussed in the following Section 6.4.

6.4 Mechanical Behaviour of Hydrogel Membrane in Microchannel

The Section 6.3 has considered a number of challenges, such as the maximum allowed fluid pressure that the packaged microfluidic system may subdue. The results from that section can assist to improve the reliability of such assembled microfluidic system. However, the cause of the leakage has not yet been reported in detail. Concentrating on the interface of PHEMA hydrogel membrane and the microfluidic channels which is engraved on the PMMA substrate, two issues have to be coped with: i) the design or optimization of the geometry of the channel, ii) possibility to achieve higher compressive strain but cause neither failure of membrane material nor blockage of

channels.

In the present study, the responses in terms of materials deformation and stresses distribution of PHEMA hydrogel to the assembly compression and the geometries of microchannels are investigated to elaborate the hydrogel material characteristics as sealing membrane. In particular, the design parameters, including dip angle, depth and width of microchannels, and compression in terms of strain due to assembly process are theoretically examined through numerical simulations. The dip angle is used to define the slope of the channel walls with respect to the vertical axis. To validate the models which are obtained from the numerical simulations, experimental study has also been carried out by observing the deformation of PHEMA hydrogel membrane using 3D optical measuring system which is also known as confocal microscopy. It is anticipated that this study can assist the designer of such structural microfluidic device to understand the mechanical behaviour of PHEMA hydrogel membrane in the use in microfluidic device, thereby provide a guideline for optimization of the designs through the selection of suitable parameters in terms of channel geometric parameter and compressive pressure in assembly process.

6.4.1 Simulation of the Mechanical and Geometrical Response of Membrane

According to the geometric definition of the microchannels, the range of depth and width of microchannel (0.1 to 1.2 mm) is far smaller than the length of microchannel (30 mm). Hence, the deformation of membrane on the direction of length is far less than that on the direction of width. Thus, the principle stress on the direction of length can be neglected (assumed as zero in such a case), because the major issue that leads to failure of membrane is primarily caused by the principle stress on the direction of width. Thus, in this work, two-dimensional (2D) modelling was used in the simulations to establish a predictive model using COMSOL Multiphysics software. The details of relevant parameters of materials and the settings of modelling, including boundary conditions and meshing, are given in Table 6-4. It is pertinent to utilise a different mesh element types (e.g. rectangular for PHEMA, triangular for PMMA) thus the maximum mesh sizes according to the materials and their locations in the package. The ultra-fine mesh of PHEMA (0.02) versus PMMA (0.02) is used to allow the accurate mechanical deformation to be observed in PHEMA which is most concerned in this study. To avoid the obtaining of the false stress values which may be caused by numerical stress singularity at sharp corners (e.g. edge of microchannel in this case), all the

sharp corner which contact with PHEMA membrane have been filleted at radius of 0.1 mm, and the locations to obtain the value of stress have been selected away from the point of stress singularity (Fig.6-13a).

	PHEMA (sealing membrane)	PMMA (substrate)
Theoretical basis	Hyperelastic (Mooney-Rivlin)	Linear Elastic (Isotropic)
Material parameters	$C_{10}=385487$ [Pa]* $C_{01}=310401$ [Pa]*	$E=2940$ [MPa]** $\nu=0.38$ **
Boundary conditions	Rigid top boundary with prescribed displacement (compression)	Fixed constraint
Mesh element type	Rectangular	Triangular
Maximum mesh size	0.02 [mm]	0.02 [mm]

* data is obtained from reference [192].
** data is obtained from reference [193].

The parameters that can be used to describe the geometry of microchannels include the width, depth, and dip angle of channels as well as the compressive strain induced by fastening process in the assembled microfluidic device. They were assigned individually to investigate their effects on the deformation characteristics of the microchannels in the simulations. The selection of these parameters is based on the common uses of various design rules, and possible deformations that can be induced through assembly process of fastening. Table 6-5 provides these parameters that have been assigned in the modelling to enable a direct comparison of the changes of geometric parameters and compression and their effect on the mechanical behaviour of the PHEMA membranes. The displacement and Von Mises stress distribution across PHEMA hydrogel membrane, which reflects its deformation and internal stress distribution respectively, can therefore be obtained under various parameters in the simulations.

Compressive strain	10%, 20%
Dip angle of channel [mm]	0, 15°, 30°.
Width of channel [mm]	0.1~1.2 (step 0.05)
Depth of channel [mm]	0.1~1.0 (step 0.1)

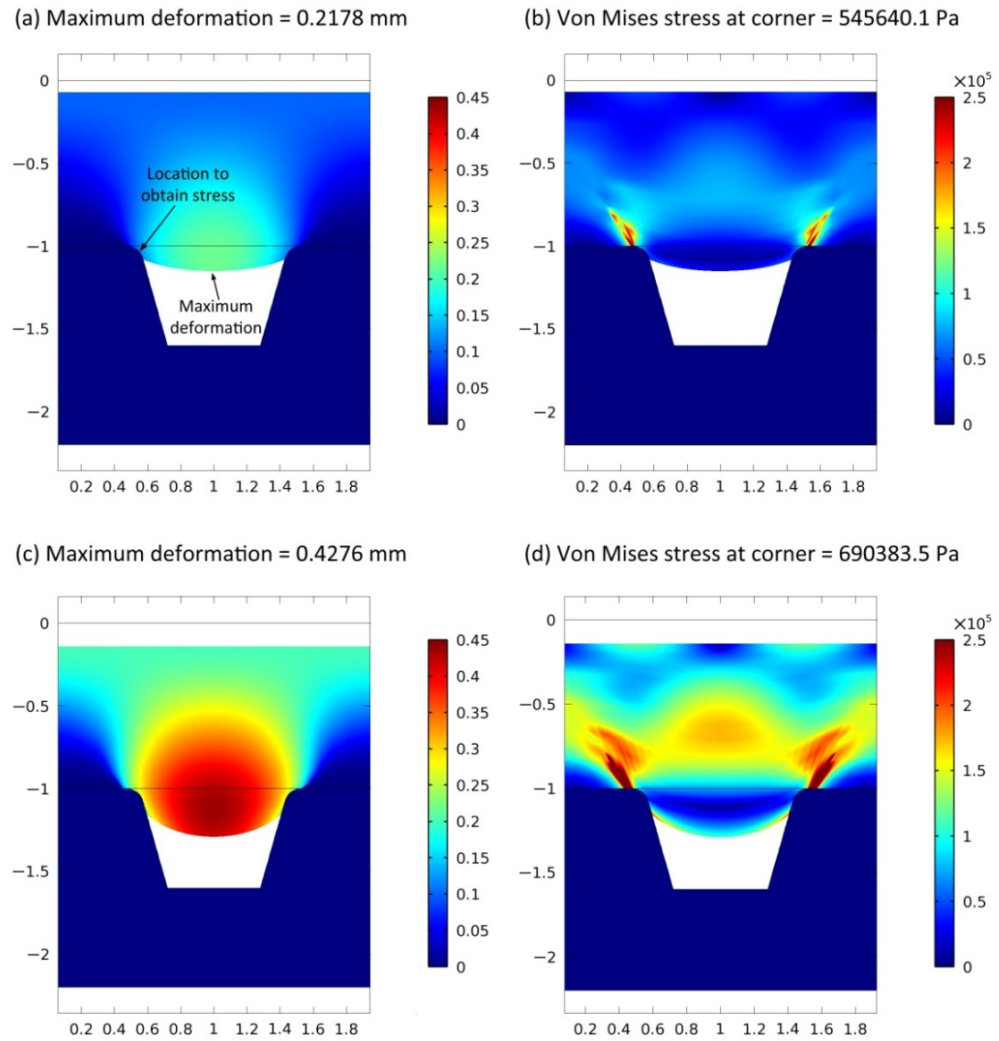


Fig.6-13. Distribution of membrane displacements (a) and (c) in millimetre, and Von Mises stress distributions (b) and (d) in Pascal, under the compressive strain of 10% for (a) and (b), and 20% for (c) and (d). The depth of channel is 0.6 mm, dip angle is 15°.

Displacement gradient and stress (Von Mises) concentration distributions of the hydrogel membrane in microchannel under compression induced by mechanical fastening technique, are shown as cross-sectional views in Fig.6-13. According to the displacement and Von Mises stress distribution shown in Fig.6-13, for both 10% and 20% applied compressive strain on the hydrogel membrane, similar displacement distribution and Von Mises distribution are observed. The displacement distribution indicates that the maximum deformation of hydrogel membrane is located at the centre of the protrusion (marked in Fig.6-13a). While the Von Mises stress in hydrogel is primarily concentrated near the corner in contact with the edge of microchannels (the bright regions in Fig.6-13b and Fig.6-13d), where a potential failure of hydrogel membrane is likely to occur if the stress level is high enough and beyond the ultimate tensile strength of PHEMA material. By

comparing the Fig.6-13a with Fig.6-13c, it is apparent that 2 times larger displacement from the compressive strain of 20% than that of 10% strain is observed. Similarly by observing Fig.6-13b and Fig.6-13d, it can be seen that the Von Mises stress at the corner induced by 20% compressive strain is nearly 1.4 times higher than that of 10% compressive strain. Therefore, it is important to take the compressive strain into account when applying compressive pressure in the assembly of the microfluidic device by fastening. The less pressure is applied, the smaller strain is induced thus less stress concentration is caused.

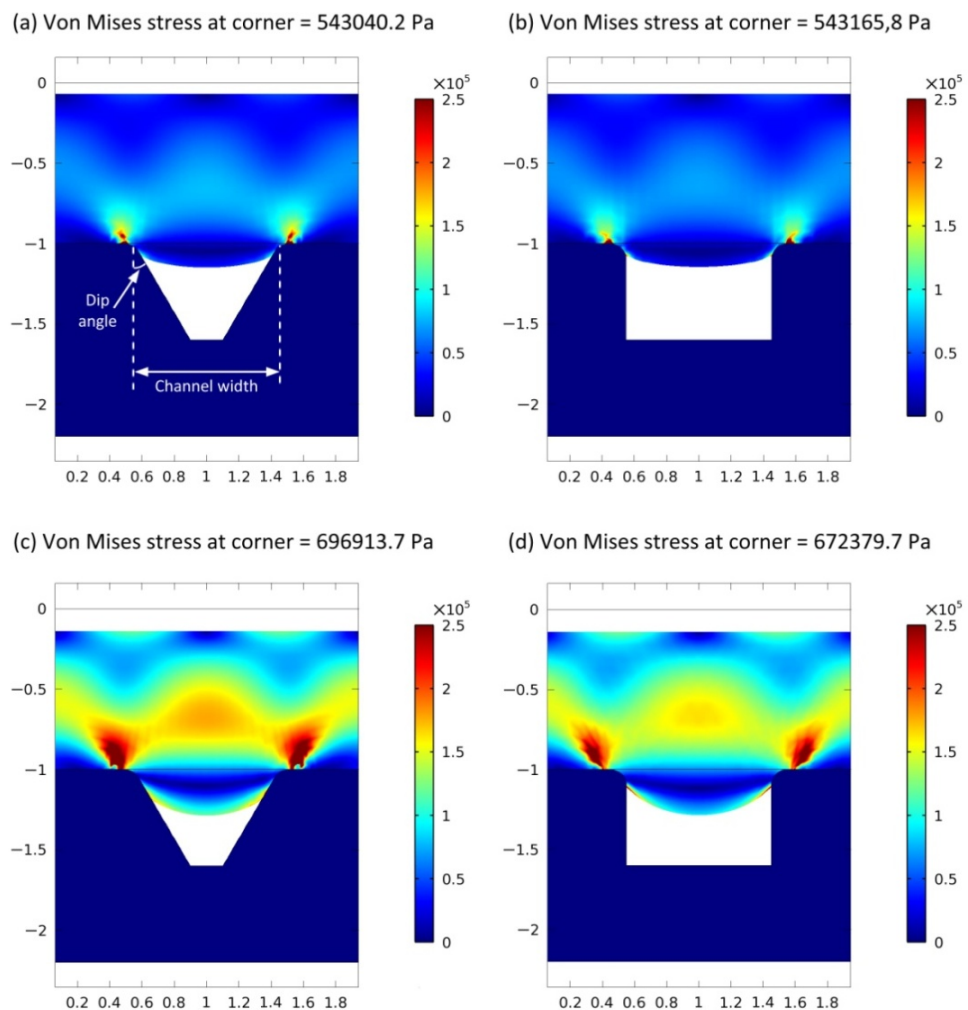


Fig.6-14. Von Mises stress distributions in Pascal due to different dip angle of channel at 0° (a,c) and 30° (b,c) under the compressive strain of 10%(a,b), 20%(c,d). The depth of channel is 0.6 mm, width of channel is 0.55 mm.

The mechanical responses of PHEMA hydrogel membrane to the different geometric parameters of microchannels, such as depth, width, and dip angle of channels, have also been investigated by modelling. In Fig.6-14 and Fig.6-15, the Von Mises stress distributions with respect to different dip angles and width of channel under the 10% and 20% compressive strains are

compared. In Fig.6-14a, the dip angle is defined. As it can be predicted, the maximum or peak values of Von Mises stress in PHEMA hydrogel membrane are all located near the corner in contact with the edge of microchannels. This indicates that the locations of the maximum Von Mises stress were not affected by the geometric parameters (*i.e.* dip angle, width of channel) of microchannels. Additionally, the stress distribution for 30° dip angle (Fig.6-14a) is almost identical to the one for 0° dip angle under the compressive strain of 10% (Fig.6-14b), which implies no effect of dip angle on the internal stress distribution under the given depth and width of the channels. This was also observed by comparing the stress distributions between Fig.6-14c and Fig.6-14d under the compressive strain of 20%. Therefore, in the design of a microfluidic channel, the dip angle of microchannel is not a prime geometric parameter which should be considered in terms of its effect on the internal stress distribution and concentration induced in PHEMA hydrogel membrane due to fastening.

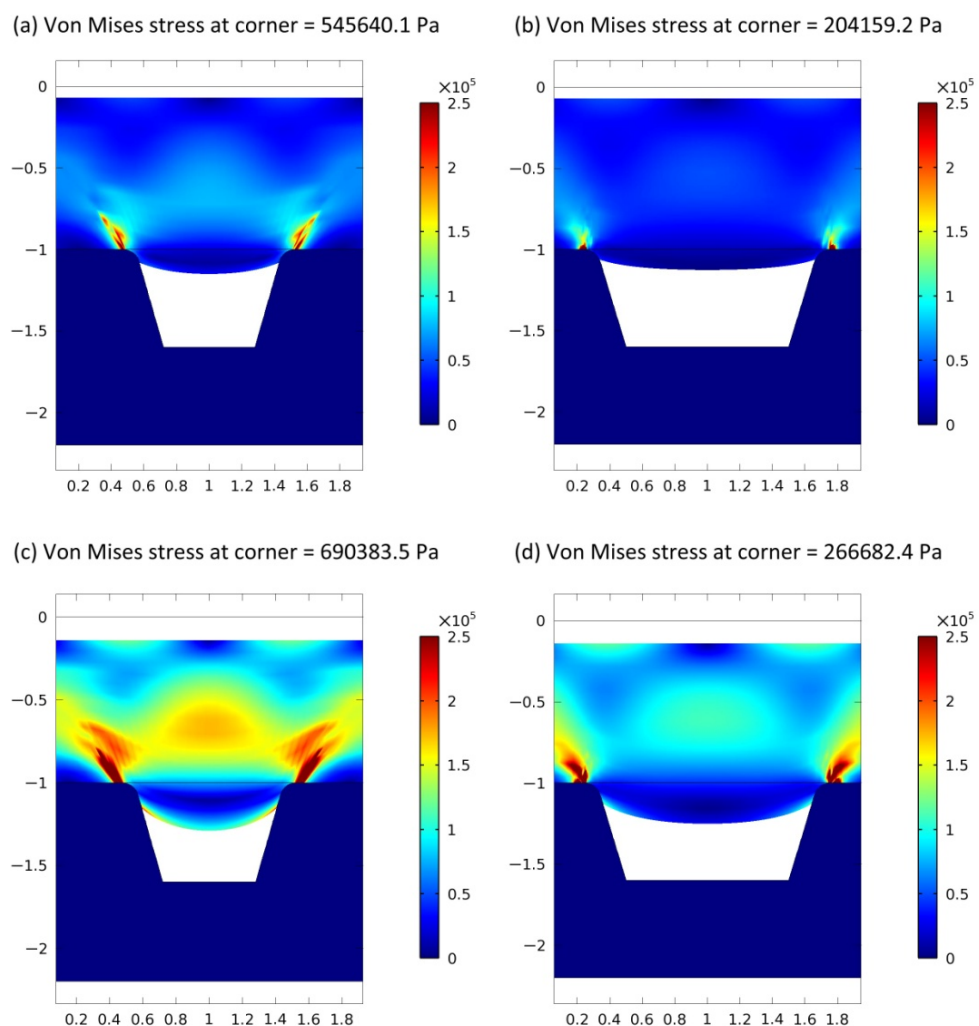


Fig.6-15. Von Mises stress distributions in Pascal with respect to different width of channel at 0.55 mm (a,c), and 1.20 mm (b,d) under the compressive strain of 10% (a,b), and 20% (c,d). The depth of channel is 0.6 mm, dip angle is 15°.

The width of microchannel is another geometric parameter to be considered which may significantly affect the internal stress distribution of hydrogel membrane under the compression. In Fig.6-15, under the 10% compressive strain, the microchannel width of 1.2 mm has caused a lower Von Mises stress value near the corner at 204159 Pa (Fig.6-15b), in comparison with the Von Mises value of 545640 Pa (Fig.6-15a) caused by 0.55 mm microchannel width. By examining the stress distributions between small and large channel width (Fig.6-15a versus Fig.6-15b, and Fig.6-15c versus Fig.6-15d), it is obvious that stress concentration induced in the membrane near the edge of microchannel for small width (Fig.6-15a and Fig.6-15c) is much severer than that for large width (Fig.6-15b and Fig.6-15d). The degree of the Von Mises stress in contact with the edge of channel has been exaggerated due to the increased compressive strain applied, for instance from 10% (Fig.6-15a, Fig.6-15b) to 20% (Fig.6-15c, Fig.6-15d).

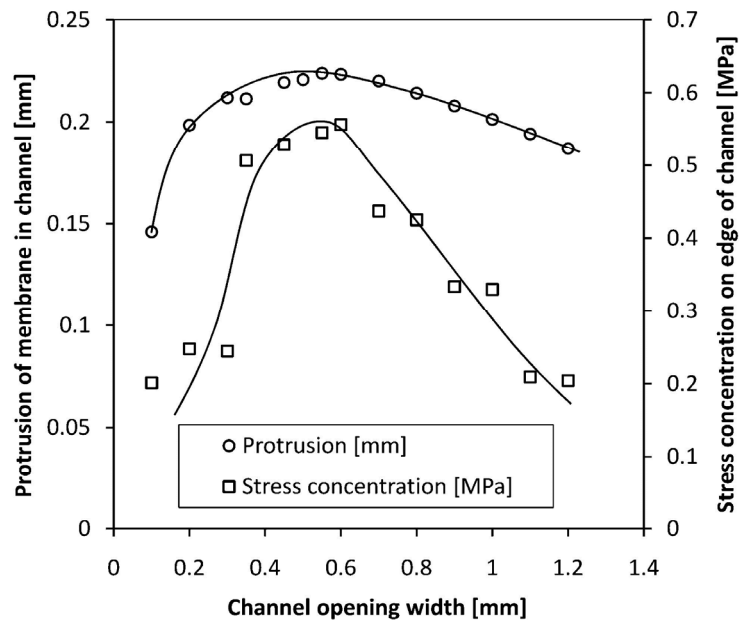


Fig.6-16. Membrane protrusion and Von Mises stress near the edge of channel as a function of width of channel under 10% compressive strain. The protrusion of membrane in channel refers to the value of ' r ' in Fig.6-18; The Von Mises stress on membrane is selected near the edge of the microchannel (without numerical stress singularity), based on the location shown in Fig.6-13.

To gain a better understanding about how the width of channel may affect the deformation and stress concentration of membranes, membrane protrusion r , which is defined as the maximum height of the hydrogel membrane that can be pressed in to the cavity of a channel due to compression (see Fig.6-13a), has to be investigated. Thus the values of Von Mises stress of the hydrogel membrane at the corner are plotted in Fig.6-16 versus the widths of microchannel ranging

from 0.1 mm to 1.2 mm. According to Fig.6-16, the details of the inter-relationship between the channel width and the membrane protrusion or the stress concentration can be found. As the width of channel increases, both membrane protrusion and the value of Von Mises stress at edge of microchannel increase drastically until the width of channel reaches approximately 0.6 mm, where the Von Mises stress exhibits its maximum value of 0.55 MPa. When the width is greater than 0.6 mm, the stress value starts to decline rapidly. Considering the dramatic increase of internal stress towards the channel width of 0.6 mm, where the highest stress concentration is expected to be induced in the membrane, this may ultimately cause mechanical failure of membrane under the compressive pressure as can be predicted. The design of such microfluidic channels should therefore take this into account, for instance, various approaches should be considered to use the channel width away from the range of 0.5~0.7 mm.

In terms of the membrane protrusion into the channel cavity due to the compression, it increases with the increase of the width of channel initially, until it reaches the peak value 0.22 mm near the channel width at 0.55 mm. During this increasing stage, the channel cavity is too small to fit the protrusion thereby the stretch force on the PHEMA membrane surface is on governing. Thus, the PHEMA material flows to its boundary rather than to the channel cavity, when it is under compression. Beyond the channel width at 0.55 mm, the protrusion remains relatively stable with a slight decrease. During this decreasing stage, the surface stretch does not play a primary role on the PHEMA membrane because it is reduced when PHEMA membrane is compressed on channel with large width. The height of protrusion r is reducing because the space of the channel cavity is getting larger. Therefore, such fluctuation of the membrane protrusion to the increasing of channel width has also been taken into account for the optimum design of the channels to ensure sufficient depth of channel to minimize the risk of channel blocking due to membrane protrusion.

The channel depth, H , which can have a significant effects on the displacement and the Von Mises stress distribution of membrane, is another important geometric parameter in the design of microfluidic channels. For the purpose of validation, the simulations were also carried out to determine the values of membrane protrusion under the different depths based on the design of microchannels with a dip angle of 15° . It should be noted that the channel width varies according to the depth in order to maintain the 15° dip angle, as such the effects of both channel width and depth have been incurred. The values of membrane protrusion from simulations are listed in Table 6-6.

Depth of channel [μm]	200	300	400	500	600	700	800	900	1000
Protrusion under 10% strain [μm]	111.8	151.8	171.1	183.2	192.0	200.8	209.1	217.1	220.6
Protrusion under 20% strain [μm]	200	248.2	274.4	300.5	318.6	331.4	340.1	334.0	323.6

6.4.2 Experimental Validation for the Simulation of Membrane

As the experimental validation for the numerical modelling, the behavioural characteristics of hydrogel membrane (e.g. protrusion) in the cavity of microchannels has to be experimentally examined, and compared with the protrusion data from numerical simulation which is displayed in Table 6-6. On the basis of the geometry of the testing device, multi-layered structural microfluidic chip assembled with a single microchannel was built and shown in Fig.6-17. It is difficult to observe the details of the membrane protrusion towards the cavity of microchannel when device is completely bonded by mechanical fastening process, though the material (PMMA) for cover and substrate is transparent. Thus, destructively making cross-section (the insert plane revealed in Fig.6-17) and observing through optical microscope is undertaken to visualise and measure the protrusion of membrane.

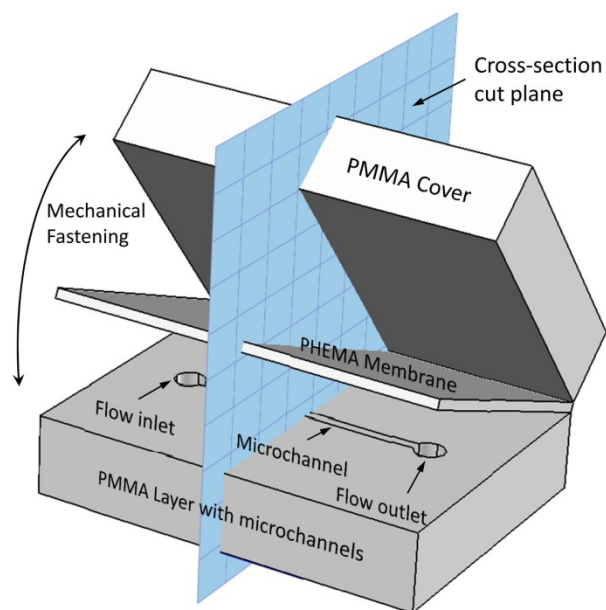


Fig.6-17. Schematic diagram of a microfluidic circuit in a stacked format, PHEMA thin film (membrane) is used to sealed PMMA chip. Cross-section inserted allows for a clear observation of the mechanical behaviour of PHEMA hydrogel membrane in microchannels.

In this experimental observation, 3D optical measuring system (also known as confocal microscopy) as an optical imaging technique was employed enabling the reconstruction of three-dimensional structures from the obtained images [194]. Keyence VHX1000 Series digital microscopy system equipped with 100X-1000X universal zoom lens has been used to visualise the membrane protrusion. Moreover, this 3D optical microscope enabling 0.1 μm accuracy of geometry measurements ensure a precise measurement of the height of the protrusion through observing the cross-section, which is shown in Fig.6-17.

As is described in Section 6.3.2, the microchannels with trapezoidal cross-section have been manufactured on the thermoplastic PMMA substrate. The trapezoidal cross-section of the microchannel is determined by the geometry of the cutter of the circuit board engraving machine. In the current experimental study, the cross-section of the microchannels sealed by compressed PHEMA hydrogel membrane through fastening process are examined using the same strain controlling method (10% and 20% compressive strain) as is described in Section 6.3.2 and illustrated in Fig.6-7.

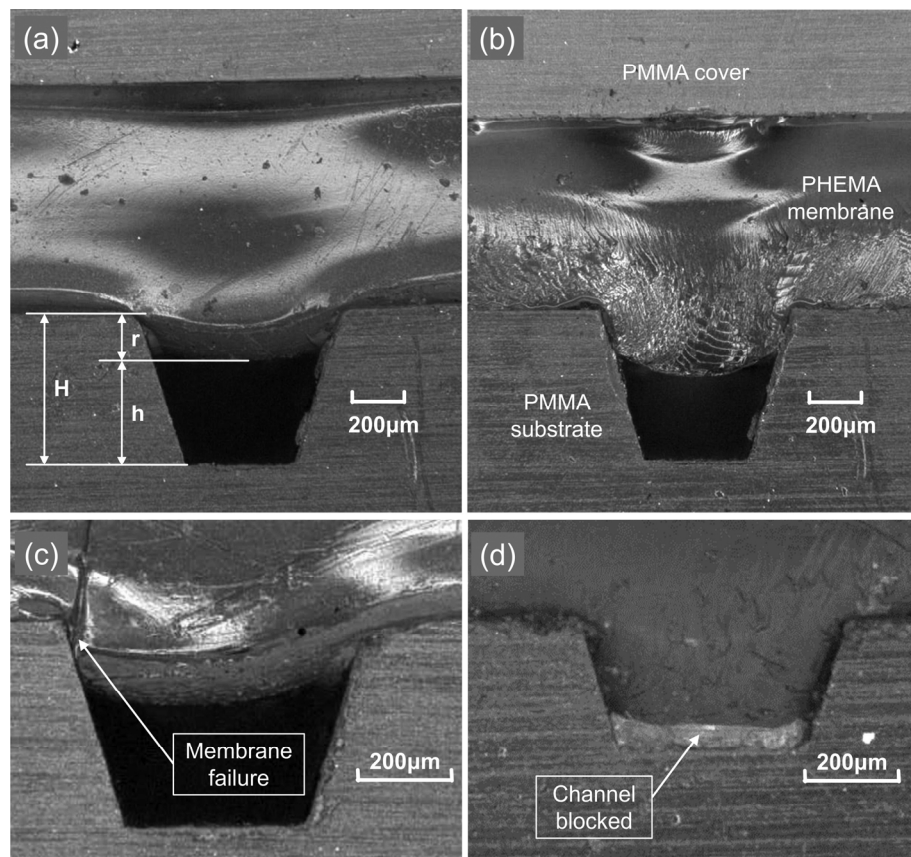


Fig.6-18. Cross-section's view of PHEMA hydrogel membrane packed in microfluidic device, (a) depth of channel 600 μm , compressive strain 10%; (b) depth of channel 600 μm , compressive strain 20%; (c) depth of channel 500 μm , compressive strain 10%, with membrane failure; (d) depth of channel 300 μm , compressive strain 20%, with microchannel blocked.

As can be seen from Fig.6-18, PHEMA hydrogel membrane was deformed and protruded into the cavities of microchannels under compressive strains in the fastening process, and membrane protrusion resulted from 20% compressive strain is overall much larger than that from 10% compressive strain (Fig.6-18a vs. Fig.6-18b). To validate the simulations that have been performed, the cross-section views in Fig.6-18a and Fig.6-18b deliberately replicated the exact parameters of the microchannels used in the simulation in Fig.6-13b and Fig.6-13d, *i.e.* with 600 μ m depth and 15° dip angle under 10% and 20% compressive strain, respectively. The protrusions of membrane were measured approximately in Fig.6-18a (196.1 μ m for 10% strain) and in Fig.6-18b (320.3 μ m for 20% strain), which are very close to the simulated results presented in Fig.6-13b (192.0 μ m for 10% strain) and in Fig.6-13d (318.6 μ m for 20% strain) respectively. This has indicated that the simulations are reliable in predicting the mechanical behaviour of membrane under the equivalent conditions.

On the basis of the results from modelling, the most risky points that may cause potential mechanical failure of membranes would be the contact regions near the edges of channels (see Fig.6-13b and Fig.6-13d) where the stress concentrations are of the highest in the hydrogel membrane due to fastening process, under 20% compressive strain (Fig.6-13d). This can ultimately result in the fracture of the membranes as it has been observed in Fig.6-18c. In such a case, the initiation and propagation of the cracks near the edge of the channel had occurred. This has strongly agreement with the simulation on the concentration of Von Mises stress (Fig.6-13b and Fig.6-13d). As has been predicted in the simulations, the blockage of microchannel with a depth of 200 μ m caused by the membrane protrusion under 20% compressive strain has also been experimentally observed in Fig.6-18d, which again demonstrated the validity of the modelling in the prediction of the protrusion of membranes that may become an issue in the design of microchannels.

To verify the simulation results, the experiments for the measurements of the membrane protrusion ranging from 200 to 1000 μ m both under 10% and 20% compressive strain have been carried out, and the results are plotted in Fig.6-19 in relation to the microchannel depth. From Fig.6-19, the scattered data indicates the variations of measurements on the protrusions, but the overall trend of these protrusion increases with the channel depth. However, the greater the compression strain, the larger the protrusion, for instance, the protrusion for the same channel depth under 20%

strain tends to be greater than that under the 10% strain. According to the experimental data shown in Fig.6-19, the protrusion under 10% compressive strain is all relatively small, e.g. below 200 μm .

The protrusion derived from experimental measurements in Fig.6-19 can be compared with the values of protrusion from the simulations listed in Table 6-6. Considering the deviations from the measurements indicated as the scattered data in Fig.6-19, the simulation results agree well with the experimental data, which indicates the confidence of modelling that has been performed on such an occasion.

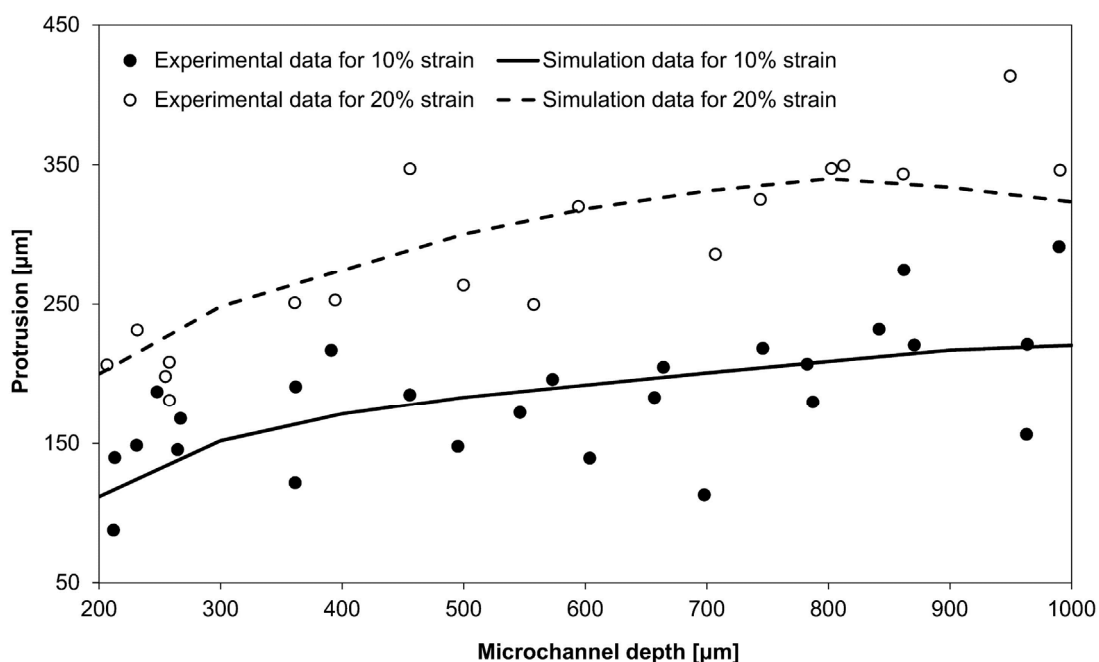


Fig.6-19. Membrane protrusion versus the microchannel depth under the compressive strain of 10% and 20%. The solid curve is based on the simulation under 10% compressive strain and the dashed curve is based on the simulation under 20% compressive strain.

6.4.3 Passable Rate and Optimum Design of Microfluidic Channels

The fluid flow capacity may be limited by the aspect ratio (*i.e.* the ratio of depth to width) of microchannel. According to the above experimental and simulation results, for a given channel which has a zero dip angle and fixed width, the protrusion of hydrogel membrane sealed under a certain compressive strain due to fastening is independent of the depth of channel. Therefore, for a small aspect ratio of microchannel, the channel depth has to be small with a fixed channel width. If the depth is smaller than the membrane protrusion (r), no fluid can pass through the channel causing ultimately a blockage, or fluid can hardly pass through requiring extremely high fluid pressure, which is under the risk of leakage. In the cases, the channel depth is greater than the

protrusion, then depending on the gaps remained in the channel cavity, the fluid may partially pass through the channel (see Fig.6-20 inclusion). Therefore, the term of passable rate can be defined by the ratio between the unblocked and entire channel cross-section areas. Therefore, the inter-relationship between passable rate and aspect ratio may be derived in Fig.6-20. Accordingly, passable rate increases with the aspect ratio of the channel under both compressive strains (10% and 20%). However, as have been noticed, the passable rates under the compressive strain of 10% are all greater than that under 20% strain for the same aspect ratio of channel.

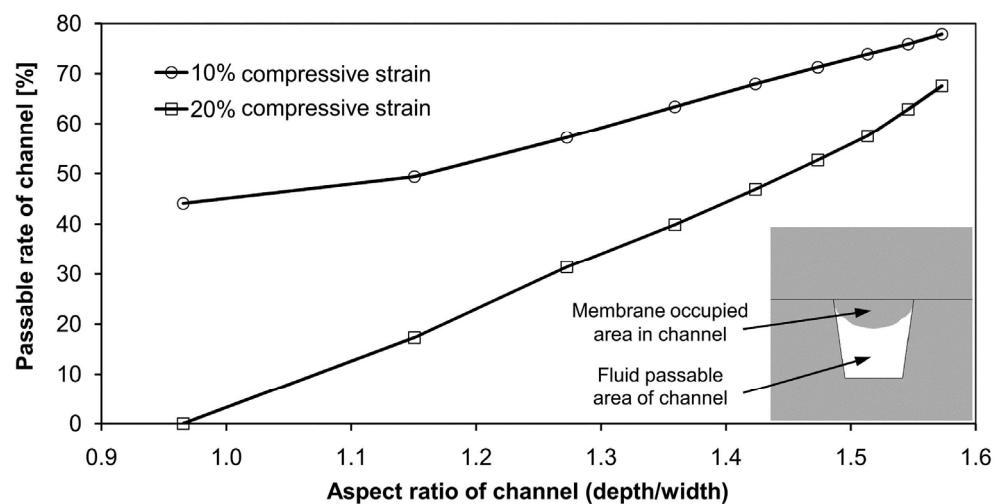


Fig.6-20. Passable rates as function of aspect ratio of microchannel obtained from simulation: inclusion is a schematic diagram of channel with protruded membrane to illustrate the passable rate.

In the design of microchannels for a microfluidic system, subject to the other requirements of such a system, the first step is to consider the required maximum fluidic pressure inside the channels. To ensure the reliable channel sealing, the parameters in the fastening process that is used to assemble the system can then be determined. These parameters including compressive strain and the thickness of hydrogel membrane are critical in the design of microchannels, as they can fundamentally affect the mechanical behaviour of membrane under the certain strains. The results presented in this paper are anticipated to assist such a process in the design of microfluidic channels, for instance, simulations that can be performed to evaluate the potential stress concentrations and protrusions of membranes under the pressure, thereby, recommendations on the correct selections of channel geometry and dimensions may be provided. It is also practical to estimate the passable rates that will be associated with the internal stresses and fluidic pressure inside the channels. On the basis of the required fluidic pressure, the fluidic passable rate and the

size of the membrane protrusion may be predicted using modelling technique, then the aspect ratio of microchannel can be determined according to the inter-relationship between the passable rate and aspect ratio, as is shown in Fig.6-20. However, the effects of the width of channel on the membrane protrusion (see Fig.6-16) have to be taken into account, in combinations with the other relevant factors. This can be implemented through the following procedures:

- (1) Channel width must be in the ranges of 0.1~0.5 mm, or larger than 0.7 mm.
- (2) The passable rate of fluidic in the channel should be ranging from 50% to 80%.
- (3) Aspect ratio of channels, depending on the compressive strains, should be in the range of 1.15~1.6 (under 10% strain) and 1.45~1.6 (under 20% strain).

This process in the design of microfluidic channels can be repeatedly applied to achieve optimum final parameters, which can then be used in the fastening assembly trials to validate the simulations.

6.5 Mechanical Behaviour of Hydrogel Membrane in Culture Chamber

According to structural design of the device which is shown in Fig.1-1, when such device is assembled, there can be potentially three types of constraints exerted on PHEMA membrane subject to their locations (see Fig.6-21): 1) 'two-sides constraint', two sides of PHEMA membrane contact with substrate (or cover), and the membrane is totally fixed by the compression which is induced by mechanical fastening. 2) 'one-side constraint', this can be found in the microchannel that only one side of PHEMA membrane contact with substrate, the other side of PHEMA membrane is deformed as protrusion towards the microchannel. 3) 'free-standing', this part of PHEMA membrane has no contact with substrate (or cover), and it can be found at the culture chamber. This part is designed to hold cells at culture chamber, and provide necessary molecular transportation between culture chamber and drug delivery reservoir. However, the internal stress may be severe at the boundaries between the 'free standing' part and the 'two-sides constraint' part, due to the drastic reduction of compression towards centre of culture chamber. Thus, the Von Mises stress inside the PHEMA membrane when it is inserted and fastened in the microfluidic device is investigated in this section.

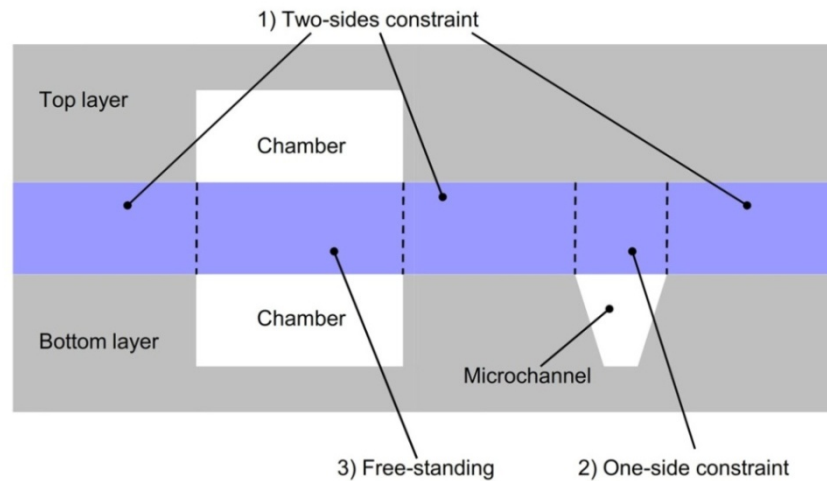


Fig.6-21. Schematic diagram to define the three types of constraint for PHEMA membrane (inserted blue rectangle): 1) Two-sides constraint; 2) One-side constraint; and 3) Free-standing.

6.5.1 Installation of PHEMA Membrane

As is revealed in the Fig.6-22, the microfluidic device consists of top layer, membrane and bottom layer as a 'sandwich' structure when it is assembled together (also see Fig.1-1). The PHEMA hydrogel membrane is experiencing compression between the top and the bottom layer (Fig.6-22a), due to the mechanical fastening. However, there is no pressure acting on the PHEMA membrane exposed in the culture chamber. Hence, the stress distribution from the compressed region (sealed region between layers) to the 'free standing' region (area of culture chamber) in the membrane is unclear and required further study. In the current study, internal stress distribution of PHEMA membrane in such regions is numerically simulated based on Mooney-Rivlin theory in terms of Von Mises stress versus the cross-sectional length of the membrane (revealed in Fig.6-22c).

To represent the conditions of PHEMA membrane experienced in situ, a 2D-axisymmetric model has been built according to the cross-sectional structure of the microfluidic device, which is schematically elaborated in Fig.6-22c. In Fig.6-22c, the substrate under the PHEMA membrane is set as fixed constraint, *i.e.* the grey block; and the cover is simplified as a distributed pressure which is applied on the top of the PHEMA membrane, *i.e.* the series of arrows. The PHEMA membrane is installed between the distributed pressure and the fixed block, which is illustrated as the blue block in Fig.6-22c. The axial symmetry of the constraints including the distributed pressure (the cover), the fixed block (the substrate) and the membrane is utilised to achieve the transformation from 2D geometry to 3D geometry, in order to minimise the computational power and calculation time.

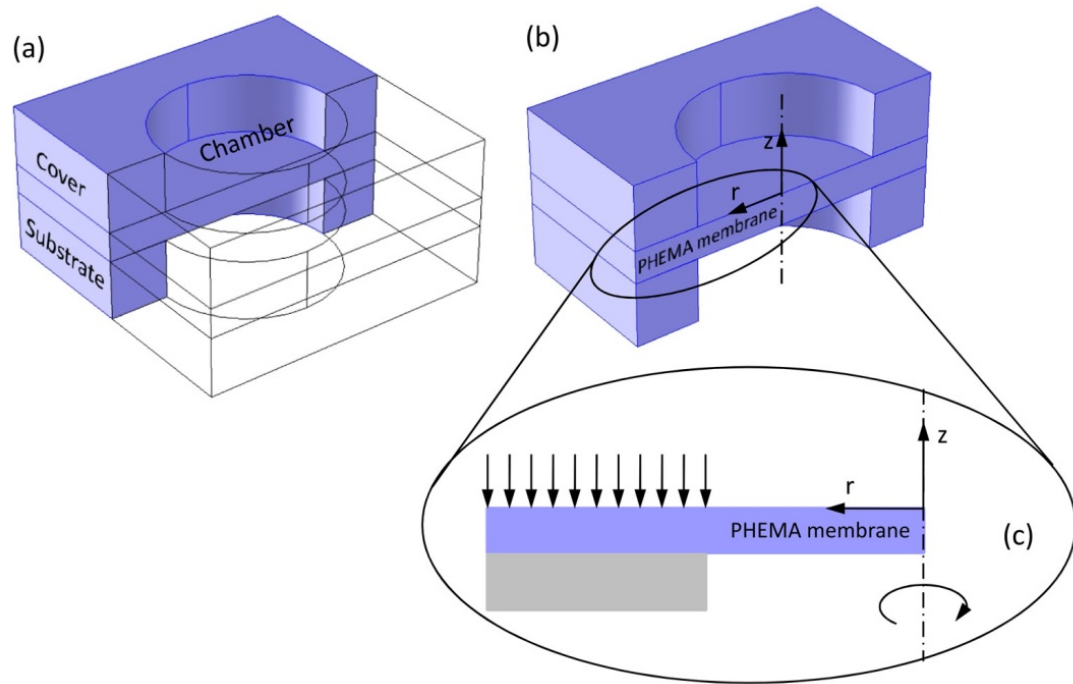


Fig.6-22. (a) The culturing chamber in multi-layered microfluidic device (half structure). Schematic diagram of modelling setups in 2D (c) which is extracted from 3D geometric modelling (b) to simulate the behaviour of PHEMA membrane under the mechanical fastening bonding.

6.5.2 Drastic Stress Distribution on PHEMA Membrane in Culture Chamber

Mooney-Rivlin theory has been applied on PHEMA material in the simulation, in order to predict the distribution of internal stress of the PHEMA membrane. The Mooney-Rivlin coefficients which are determined in Chapter 5 are used in the current modelling. Fig.6-23 depicts (a) the set-ups of the simulation model, (b) the two-dimensional stress distribution in PHEMA membrane under 10% strain, and (c) the distribution of Von Mises stress along the PHEMA membrane under the compressive strain of 10%, 20% and 30%. The results from this simulation are used to evaluate whether the concentration of Von Mises stress is high enough and beyond the ultimate tensile strength of PHEMA material thus causing a potential failure of hydrogel membrane.

According to the stress graph Fig.6-23c, the Von Mises stress remains almost unchanged at the beginning ($r=0\sim 2$ mm) and followed by a decrease in the region of $r=2\sim 2.5$ mm. A drastic increase (peaks) of the stress around the region of $r=2.5$ mm corresponding to the interface between the fixed part and the free standing part of PHEMA membrane. After this, the value of Von Mises stress declines rapidly at the region of $r=2.5\sim 3$ mm, and remains constant with a small stress near the symmetric axis, *i.e.* the location of $r=3.5\sim 5$ mm.

According to the Von Mises stress distribution shown in Fig.6-23c, for both 10%, 20% and 30% applied compressive strain on hydrogel membrane, the larger Von Mises stress in PHEMA membrane is resulted by the higher compression. By focusing on the location at $r=2.45$ mm, the maximum values of Von Mises stresses are measured 0.05, 0.08 and 0.16 MPa for 10%, 20% and 30% compressive strain respectively. Although these peak values may be caused by stress singularity in simulation, it can only illustrate that the PHEMA membrane has the risk of material failure at this region, because indentations or cracks were not found on the PHEMA membrane in experiments when the compressive strain is 10% or 20%.

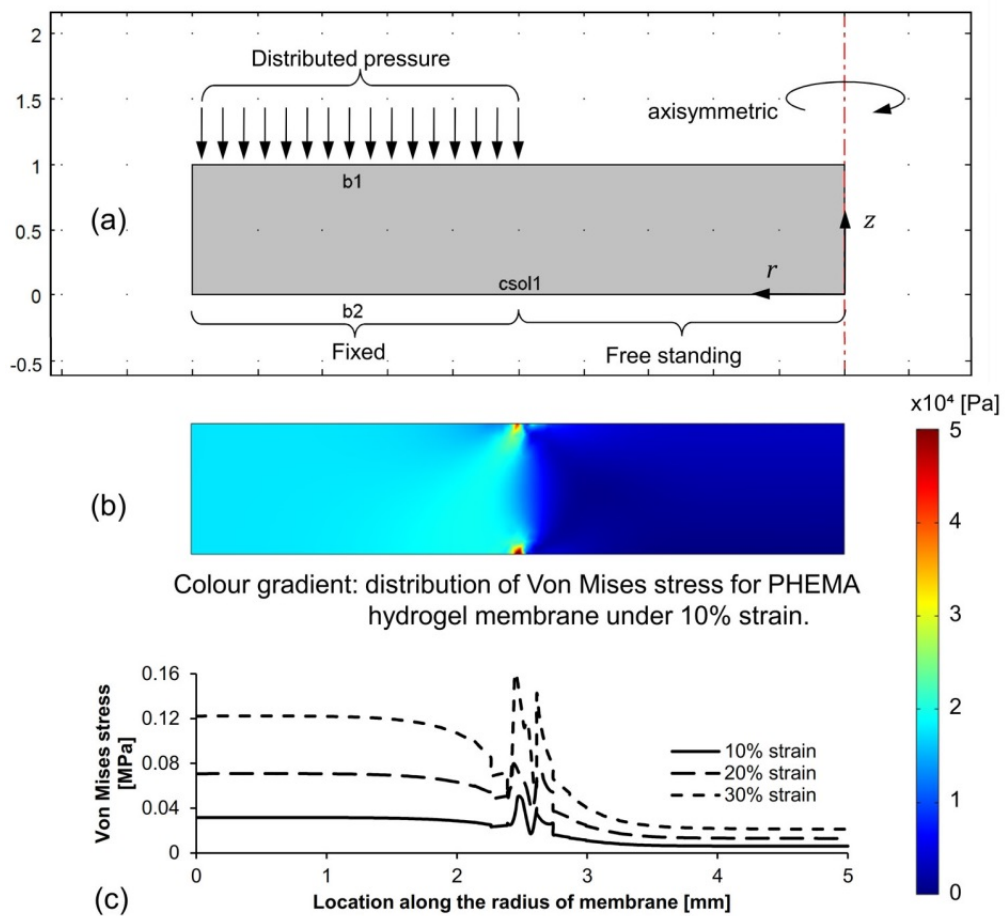


Fig.6-23. (a) Simulation setup on PHEMA membrane to analyse stress drop. (b) Two-dimensional plot with colour bar, in terms of distribution of Von Mises stress in PHEMA hydrogel membrane under 10% strain. (c) The line graphs shows the Von Mises stress versus top boundary of PHEMA membrane when membrane compressed by 10%, 20%, and 30% strain.

Moreover, Cauchy stress tensor, which can represent both the direction and the magnitude of the internal stresses, have been evaluated to elaborate the components on single direction of Von Mises stress [195]. In this study, the Cauchy stress tensors are defined on the longitudinal direction (z) and on the radial direction (r), because of the 2D-axisymmetric geometry of the simulation model.

The general correlation between Von Mises stress (σ_v) and the Cauchy stress tensors (σ_{ij}), is given by [196]:

$$\sigma_v = \sqrt{\frac{1}{2}[(\sigma_{11} - \sigma_{22})^2 + (\sigma_{22} - \sigma_{33})^2 + (\sigma_{33} - \sigma_{11})^2 + 6(\sigma_{12}^2 + \sigma_{23}^2 + \sigma_{31}^2)]} \quad \text{Eqn.6-2}$$

where $\sigma_{11}, \sigma_{22}, \sigma_{33}$ are the normal stresses and $\sigma_{12}, \sigma_{23}, \sigma_{31}$ are the shear stresses. In the current study, due to the uniaxial compression induced by mechanical fastening technique, all the shear stress are zero, and the stress vectors on longitudinal direction (σ_z) and radial direction (σ_r) are derived from the normal stresses $\sigma_{11}, \sigma_{22}, \sigma_{33}$.

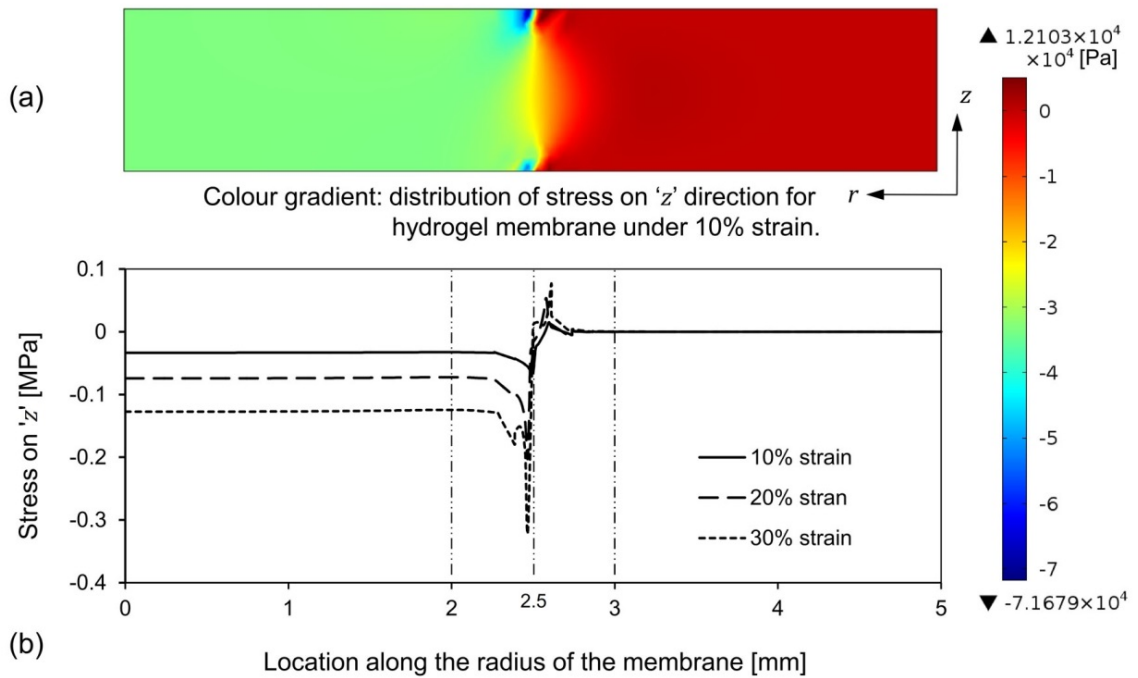


Fig.6-24. (a) Two-dimensional plot with colour range bar, indicating the distribution of stress on longitudinal direction 'z'. (b) Curves of stress vector on longitudinal direction 'z' versus distribution at the cross-sectional length of the PHEMA under 10%, 20%, 30% compressive strains. Approximate 1 mm length of 'stress buffer range' (2 mm-3 mm) can be determined by the stress distribution, which connects the compressed PHEMA and free standing PHEMA.

On the longitudinal direction 'z', the distribution of stress (σ_z) in the PHEMA hydrogel membrane under 10% compressive strain has been shown in Fig.6-24a. The corresponding stress (σ_z) along the top boundary of the material domain in Fig.6-24, under 10%, 20%, and 30% compressive strain, have been illustrated in Fig.6-24b respectively, because the top boundary of the material domain has the most severe change of stress. From Fig.6-24b, the stress at the locations from 0 to 2 mm, both the curves for 10%, 20% and 30% compressive strain exhibit constant values due to the distributed compression on PHEMA membrane. Higher compressive strain leads to larger value of the stress. According to the definition of positive force direction (see Coordinates in Fig.6-24a), the

negative values appear in Fig.6-24b indicate that the stress vector point downwards. The maximum value (absolute value) of the stress vector on 'z' direction can be found approximately $r=2.4$ mm at 0.065 MPa, 0.199 MPa and 0.316 MPa, corresponding to 10%, 20% and 30% applied compressive strain. For the locations ranging from 2 mm to 3 mm, the stresses exhibit fluctuation since the compression applied on PHEMA membrane is drastically released at the location of 2.5 mm. The stresses on the range of 3 mm to 5 mm under 10%, 20% and 30% compressive strains are all constants with the value of zero, because no longitudinal stress on the free-standing region of PHEMA membrane induced by mechanical fastening. In terms of the overall range (0~5 mm), the effects of compressive stress along the longitudinal direction can be completely reduced from stressed to free constrained within 1 mm long from 2 mm to 3 mm, which is named 'stress buffer range'.

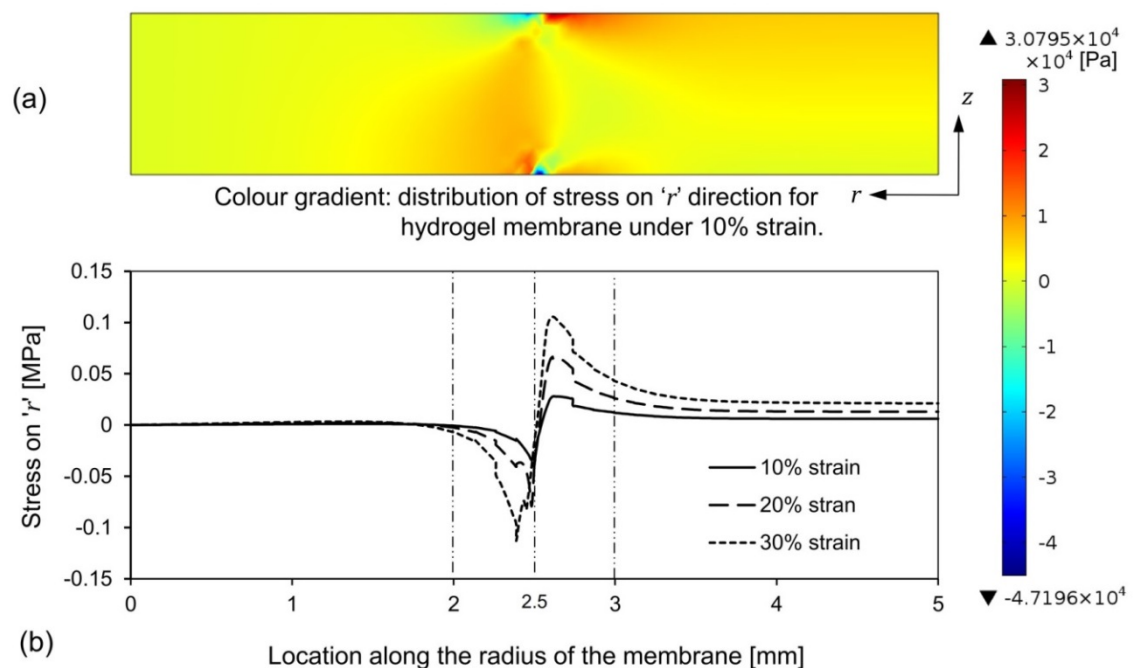


Fig.6-25. (a) Two-dimensional plot with colour range bar, indicating the distribution of stress on longitudinal direction 'r'. (b) Curves of stress vector on radial direction 'r' versus distribution at the cross-sectional length of the PHEMA under 10%, 20%, 30% compressive strains. Approximate 1 mm length of 'stress buffer range' (2 mm-3 mm) can be determined by the stress distribution, which connects the compressed PHEMA and free standing PHEMA.

Similar to the Fig.6-24, the distribution of stress on the radial direction 'r' (σ_r) in the PHEMA hydrogel membrane under 10% compressive strain has been shown in Fig.6-25a, and the corresponding stress (σ_r) along the top boundary of the material domain, under 10%, 20%, and 30% compressive strain, have been illustrated in Fig.6-25b, respectively. According to the line graphs of

Fig.6-25b, the stress values in the range from 0 mm to 2 mm are all zero, followed by a descending, a drastic direction reverse and another descending of the stresses on radial direction within the locations between 2 mm and 3 mm, which is the 'stress buffer range'. The drastic direction reverse of the stress occurs at the location of 2.5 mm, which is exactly at the boundaries between fixed part and free-standing part of PHEMA. In terms of the locations between 3 mm and 5 mm, the values of stresses in the membrane are slightly larger than zero away from the centre of the culture chamber. The stress at locations range of 0~2.5 mm induced by mechanical fastening can potentially move freely without constraints to the range of 2.5~5 mm, causing the stress on radial direction is partially applied on the free-standing region of the PHEMA membrane.

As a summary, the PHEMA membrane at the 'stress buffer range' is highly stressed with drastic stress direction change. It has risk to exhibit material's failure, but the risk is far less than that in 'one-side constraint' (see results of Section 6.4), because the values of such drastic stress in 'stress buffer range' are far below the ultimate stress that PHEMA material can resist.

6.6 Summary

Mechanical fastening packaging method has been investigated through simulation and experiment, which has been proved to be an efficient and reliable packaging method for assembling of microfluidic device with the embedded PHEMA hydrogel membrane. Fastening pressure which is applied on hydrogel membrane is determined in the mechanical fastening process by controlling the corresponding compressive strain. The compressive strain should not be larger than 20% in the present geometric configuration of the microchannels (*i.e.* sharp edges trapezoidal cross-section), in order to avoid the membrane material failure thus ensuring the stability of the fastening assembled device. The maximum allowed fluid pressure P_f that causes the microsystem to leak has been investigated. It is found that increasing the compressive strain applied on the membrane leads to a raise of the P_f for microchannel. The values of P_f have been experimentally determined to fall in the range of 200-350 kPa for 10% compressive strain, and 350-1000 kPa for 20% compressive strain, which is much higher than the maximum allowed pressure in normal microfluidic system (60 kPa).

Furthermore, the deformation (*e.g.* protrusion) and stress distribution of the PHEMA hydrogel membrane which is used to seal the microfluidic device have been specifically investigated.

Simulations using Mooney-Rivlin theory have been carried out to predict the mechanical behaviour of PHEMA hydrogel membrane in terms of displacement and the Von Mises stress. Von Mises stress distribution indicates the highly stress concentrated region is near the edge of channel, which is prone to the mechanical failure of the membrane under the compression. The geometric parameters of microchannels (*e.g.* width, depth or dip angle of the microchannels) can affect the Von Mises stress distribution in the hydrogel membrane, in particular, the width of channel. Additionally, these simulation results, including the deformation of membrane (*e.g.* protrusion into the cavity of microchannel), have been experimentally validated through the cross-sectional view of the deformed membrane under the compression. The results have been compared with the simulations that were undertaken under the same conditions and channel geometries, and it has been found the values of protrusion obtained from experimental measurements have agreed with the results from the simulations. Therefore, the simulation is reliable and has reflected the mechanical characteristics of membranes under the compression. Based on these simulated results, the generic design rules may be outlined for the optimum design of microchannels in terms of their geometry and dimensions. This will ultimately assist the process to enable rapid fixture of the related parameters in the fabrication of such microfluidic channels, in order to achieve reliable and efficient fluidic flow in the microfluidic device by minimising the internal stress concentration and enhancing the fluidic passable rate of the microchannels.

Finally, drastic internal stress distribution in the PHEMA membrane near the edge of culture chamber region is numerically visualised using the verified simulation model. The distributions of internal stress in terms of Von Mises stress and normal stresses elaborated that the stress in the membrane drastically changed within the 1 mm long 'stress buffer area', which is located at the boundary between the fixed constraint and free standing constraint of PHEMA membrane. For both 10% and 20% compressive strain induced by the mechanical fastening, such change of stress is yet able to cause the hydrogel material failure.

In conclusion, mechanical fastening technique has been demonstrated as a feasible and reliable packaging process for hydrogel-based microfluidic device fabrication.

Chapter 7. Dynamic Perfusion Process in Microfluidic Culture System

7.1 Introduction

In a perfusion culture device, inflow velocity, initial nutrient concentration, and the dimensions of culture chamber are the key parameters which are used to determine the performance of the device. The present chapter focuses on the determination of these parameters to develop a hydrogel-based cell culture microdevice with optimal performance. Inter-relationships between these functional parameters have also been investigated in order to develop a microdevice for culturing various types of cells.

In this chapter, the geometry and dimensions used in the simulation are closely associated with the structural design of the microfluidic device which is introduced in Chapter 1, and the optimal dimensions for microchannels which are identified in Chapter 6. The theoretical aspects of the simulations are based on the Navier-Stokes fluid dynamics and the Fickian diffusion property of hydrogel which was examined in Chapter 4. The results in terms of nutrient supply and fluidic shear stress are obtained from these simulations. Two optimum guidelines to restrict the range of such key parameters are proposed, which can potentially expand the range of inflow velocity thus facilitate different types of cells to be incubated using this microdevice.

7.2 Theoretical Basis

7.2.1 Fluid Dynamics

To determine the characteristics of fluidic flow in terms of laminar or turbulent forms, a preliminary calculation of the Reynolds constant (Re) which is correlated to the dimensions of the microchannel is made [197]. It indicates that the maximum Reynolds number is located at the smallest cross-section when fluid flows in a tube or closed channel. Comparing with the fluidic port and culture chamber, the smallest cross-section in fluid passage in this microfluidic device appears at the microchannel. Thus, the maximum Reynolds number occurs at the microchannel. According to the dimensions of the trapezoidal cross-section in the current study: widths $w_1=0.48$ mm, $w_2=0.1$ mm, height $h_c=0.7$ mm and dip angle $\theta=15^\circ$ (see Fig.6-14), the maximum Reynolds number (Re) of this microfluidic device can be calculated based on the equivalent dimensions of the microchannel:

$$Re = \frac{\rho v_{in} D_H}{\mu} = \frac{2\rho h_c(w_1+w_2)}{\mu(w_1-w_2)+\mu \sin\theta(w_1+w_2)} \cdot v_{in} \quad \text{Eqn.7-1}$$

where, μ is dynamic viscosity of fluid [Pa·s or kg/(m·s)], ρ is the density of fluid [kg/m³], and v_{in} is the mean velocity of the fluid in the channel [mm/s]. The hydraulic diameter of the trapezoidal duct D_H is given by $D_H = 4 \cdot \text{Cross-sectional Area [mm}^2] / \text{Wetted Perimeter [mm]}$. The wetted perimeter in this case is the total perimeter of cross-section of channel, because the channel is fully filled with fluid thus all channel walls are in contact with the fluid.

According to the initial flow rate (0.5 ml/hour) which is controlled by the micropump, and the area of the cross-section of microchannel ($w_1=0.48$ mm, $w_2=0.1$ mm, and $h_c=0.7$ mm), the value of v_{in} is calculated, which is 0.68 mm/s. Thus, with the parameters that are utilised in the simulation, i.e. $\mu=8.9 \cdot 10^{-4}$ Pa·s, $\rho=1000$ kg/m³ and $v_{in}=0.68$ mm/s, Eqn.7-1 yields a Reynolds number of 0.304. It indicates that the characteristics of fluidic flow in the microdevice is laminar flow, because the value of the maximum Reynolds number in the fluidic passage is much less than 1000 [198]. Accordingly, the theory on the momentum convection equation based on Navier-Stokes equations at steady state [199] can be implemented in the simulation which is used to represent the laminar fluid flow in the microdevice:

$$\left\{ \begin{array}{l} \rho \left(\frac{\partial \vec{u}}{\partial t} + \vec{u} \cdot \nabla \vec{u} \right) = -\nabla p + \mu \nabla^2 \vec{u} + f \\ \nabla \cdot \vec{u} = 0 \end{array} \right. \quad \begin{array}{l} \text{Eqn.7-2a} \\ \text{Eqn.7-2b} \end{array}$$

where, \vec{u} is the velocity field [m/s], p denotes the pressure [Pa], f denotes the volume force [N/m³], and ∇ is the standard del(nabla) operator, $\nabla = i \frac{\partial}{\partial x} + j \frac{\partial}{\partial y} + k \frac{\partial}{\partial z}$ [199]. The formula in Eqn.7-2a controls the momentum balance, and the other formula (Eqn.7-2b) defines the continuity for incompressible fluids.

7.2.2 Diffusion in Hydrogel

In terms of the diffusion property of PHEMA, it is represented based on Fick's law (demonstrated in Chapter 4) in the modelling. To make the model simple, the culture medium is assumed as a diluted solution of mixed glucose and water. Therefore, the equation to describe the diffusion behaviour of glucose in the culture medium is given by [153]:

$$-\nabla \cdot (-D \nabla c + c \vec{u}) = 0 \quad \text{Eqn.7-3}$$

where, \vec{u} is the velocity field [m/s], D denotes the diffusion coefficient [m²/s], and c is the current

concentration of glucose [mol/m³].

The PHEMA hydrogel membrane enabling the diffusion of molecules (e.g. glucose) through the material can be built in the modelling, the solute and solvent molecules pass through the hydrogel material obeying Fick's law. During the diffusion, the PHEMA hydrogel is saturated by glucose. The capacity that PHEMA hydrogel absorb glucose is another key parameter for the numerical simulation in this study. Therefore, the Langmuir adsorption equation [200] has been utilised to describe the capacity of absorption of PHEMA hydrogel to glucose molecules:

$$\Gamma = \Gamma_{max} \cdot \frac{kc}{1+kc} \quad \text{Eqn.7-4}$$

where Γ is the amount of glucose [mol] that absorbed by 1 kg PHEMA hydrogel in the solution of glucose concentration at c [mol/m³]. Γ_{max} is the maximum amount of glucose that PHEMA can absorb and independent to the value c . And k is the Langmuir equilibrium constant.

7.2.3 Diffusion and Reaction in Solution

In the perfusion culture, diffusion of molecules in the solution is assumed to follow the generic scalar transport equation in the format of conservation equation in terms of a substance c_i :

$$\frac{\partial \rho c_i}{\partial t} + \nabla(\rho \vec{u} c_i + \vec{j}) = R_i \quad \text{Eqn.7-5}$$

where \vec{j} stands for the diffusion transport of chemical solute of interest (e.g. glucose) [W/m²], c_i is the concentration of chemical solute caused by reaction [mol/m³] [201], and R_i denotes the rate of reaction [mol/m³·s]. Meanwhile, the reaction rate for glucose (i.e. consumption rate $R_{glucose}$) on the basis of Michaelis-Menten kinetics is given by [202]

$$R_{glucose} = R_{max,g} \frac{c_g}{c_g + C_{Hf,g}} \cdot \delta(c_g > c_t) \quad \text{Eqn.7-6}$$

where $R_{max,g}$ is the maximum reaction rate during the consumption of glucose [mol/m³·s], $C_{Hf,g}$ is the glucose concentration of half maximum response in the whole glucose consumption period [mol/m³]. c_t denotes the glucose concentration inside cell [mol/m³]. When the current concentration of glucose (c_g) is smaller than c_t , cells will die due to the lack of energy income. Smoothed Heaviside function (δ) guaranteeing convergence in iteration during computational calculation, is achieved by a built-in function which is named **flc1hs** [203] in COMSOL Multiphysics software version 4.1 (Burlington, MA, USA). This function was introduced and implemented by A.V. Hill [204,205] and Buchwald [206] in their works.

7.3 Simulation Details

7.3.1 Geometry Building

As is shown in Fig.1-1, the geometry of the numerical simulation in this chapter is built on the basis of the structural design: two individual perfusion sub-systems, including microchannel and culture chamber (or drug delivery reservoir). These two sub-systems are connected only through the diffusion of the hydrogel membrane which is located between them. Fig.7-1a schematically illustrates the fluid domains in simulation based on such structural design of the microdevice. To save the computational power and the time of calculation, the 3D model was half symmetrically transformed (Fig.7-1b) when carrying out the simulation. Due to the laminar flow determined by Reynolds number throughout the entire system (Section 7.2.1), the streams of fluid flow from each half of the geometry will not mix with each other. Thus, no convection existed between the two half symmetric parts. It therefore verified the feasibility that using half-symmetric geometry in the numerical modelling.

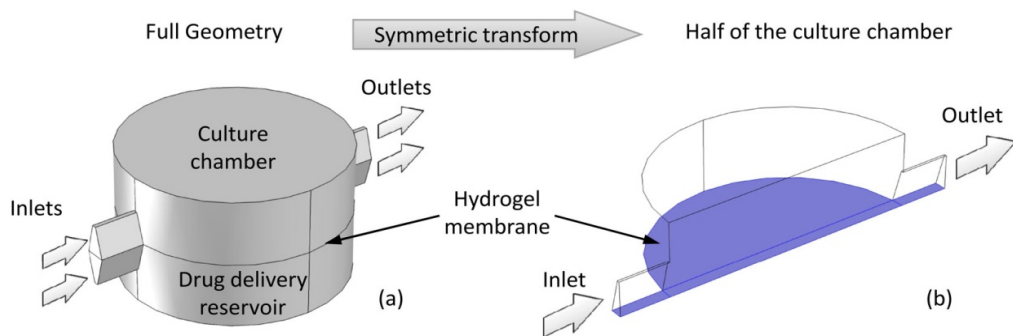


Fig.7-1. (a) Fluid domain in the microdevice, culture chamber and drug delivery reservoir, built in 3D in simulation. (b) Culture chamber after symmetric transform. The hydrogel membrane on the bottom of the culture chamber has been highlighted in blue.

The cylindrical culture chamber and drug delivery reservoir have the same dimension: diameter of 5 mm, height of 1.5 mm. The channels for fluid flow possesses trapezoidal cross-section, with the width of 0.48 mm and 0.1 mm, height of 0.7 mm which is selected from the optimum dimension range for the microchannels based on the investigations in Section 6.4. Overall, according to the dimensions and the geometries in this work, the model was built in COMSOL Multiphysics using laminar flow and transport of diluted species modules. The modelling was solved by the MUMPS direct solver on *hydra cluster* with 24GB of memory which is running by Bull Linux AS5. The *hydra cluster* consists of 161 compute nodes, and each node has two six-core Intel Westmere Xeon X5650 CPUs [207].

7.3.2 Determination of Input Parameters

Before the simulation for modelling, various parameters that define the physical environment for the simulation require to be determined. The basic parameters of the fluid and hydrogel, including dynamic viscosity, density of fluid and temperature of the perfusion solution, can be predefined as $\mu=8.9 \times 10^{-3}$ Pa·s, $\rho=1000$ kg/m³, $T=310.15$ K, respectively. The pressure of the fluid flow in the microchannels and culture chamber is determined based on the results from Section 6.3, which has to be smaller than the Critical Leakage Pressure (P_c) to guarantee the reliability of sealing of the channel-chamber system of the microdevice. The mean velocity of the fluid at inlet (inflow velocity) is indicated by a variable v_{in} [mm/s], which is dependent of the fluidic shear stress on the cells in culture chamber.

The culture medium used in this study is Dulbecco's Modified Eagle's Medium (DMEM) from Sigma-Aldrich. The concentration of glucose of this culture medium is 4500 mg/L (=25 mol/m³). Thus, the value of the glucose concentration at the inlet (c_{in}) is set to be 25 mol/m³. The glucose concentration from inlet of drug delivery reservoir is zero. The glucose concentration in cells c_t at 37°C is assumed as 8 mol/m³, according to the linear interpolation based on the experimental results (Table 7-1) developed by Foley *et al.* [208].

	Extracellular	Intracellular	
Literature from Foley <i>et al.</i> [208]	2 mol/m ³	Large cell	0.74~1.60 mol/m ³
		Small cell	0~1.36 mol/m ³
	5 mol/m ³	Large cell	2.03~3.67 mol/m ³
		Small cell	0.44~2.97 mol/m ³
	50 mol/m ³	Large cell	16.65~31.55 mol/m ³
		Small cell	5.13~11.52 mol/m ³
Assumption in this work	25 mol/m ³	Medium	8 mol/m ³

Moreover, diffusion coefficients of glucose in hydrogel are determined based on experimental results which were determined in Section 6.2.3. The experimental approaches demonstrated that the capacity of absorption of PHEMA hydrogel to glucose is $\Gamma=0.038$ mol/kg, in the solution with glucose concentration of 1111.1 mol/m³ (=200 g/L). The diffusion coefficient of glucose in PHEMA hydrogel was evaluated at 0.099 cm²/s. Combining such experimental results and the maximum capacity of absorption of PHEMA ($\Gamma_{max}=0.052$ mol/kg) from literature [209], the value of the

Langmuir equilibrium constant k can be determined as $0.0024 \text{ m}^3/\text{mol}$ according to Eqn.7-4. In literatures, the diffusion coefficient of glucose is $6.80 \times 10^{-10} \text{ m}^2/\text{s}$ at 20°C in water [153], and is measured as $9.59 \times 10^{-10} \text{ m}^2/\text{s}$ at 37°C in aqueous medium by Bashkatov *et al.* [210]. It is also evaluated by Li *et al.* [211] at $9.25 \times 10^{-10} \text{ m}^2/\text{s}$ in culture medium at 37°C . Thus, average diffusion coefficient $D_g=9.45 \times 10^{-10} \text{ m}^2/\text{s}$ of glucose in water under the temperature of 37°C is used in this study. Meanwhile, the diffusion coefficient of glucose in tissue (cells) is determined at $D_{g,t}=4.0 \times 10^{-11} \text{ m}^2/\text{s}$ in the current simulation, within the range from $2.3 \times 10^{-11} \text{ m}^2/\text{s}$ to $5.5 \times 10^{-11} \text{ m}^2/\text{s}$ reported by Casciari *et al.* [212]. The diffusion coefficient of glucose in ascites cells ($4.3 \times 10^{-11} \text{ m}^2/\text{s}$) determined by Busemeyer *et al.* [213], and inulin diffusivity in V79 Chinese hamster lung cell ($4.2 \times 10^{-11} \text{ m}^2/\text{s}$), which is detected by Freyer and Sutherland [214] have also been used in work.

According to the work done by Zhang *et al.* [215], the maximum glucose consumption rate for single cell is experimentally detected at the initial stage of cell culture with the value of $3.18 \times 10^{-19} \text{ mol/cell/s}$ ($=27.5 \text{ fmol/cell/day}$). After that, a decrease in the consumption takes place and followed by a constant consumption rate at $1.18 \times 10^{-19} \text{ mol/cell/s}$ ($=10.2 \text{ fmol/cell/day}$). Hence, the value of maximum glucose consumption rate for a single cell $R_{max, single}$ is assumed as $3.2 \times 10^{-19} \text{ mol/cell/s}$ in the current simulation. Moreover, as is described in Chapter 3 of this thesis, the size of single cell is approximate $\varnothing 17 \mu\text{m}$ for HUVECs, which gives the volume of cell at $V_{single}=2.57 \times 10^{-15} \text{ m}^3$. However, the cell is modelled as a semi-sphere attached to the bottom of culture chamber in the simulation, thus the volume of cell in the modelling is the half volume of sphere, $V_{half, single}=1.29 \times 10^{-15} \text{ m}^3$. Hence, the coefficient of glucose consumption rate in Eqn.7-6 is given by: $R_{max, g} = \frac{R_{max, single}}{V_{half, single}} = 2.42 \times 10^{-4} \text{ mol}/(\text{m}^3 \cdot \text{s})$. This value of the consumption rate reaches a very close agreement with $1.4 \text{ g}/(\text{L} \cdot \text{h})$ ($=2.16 \times 10^{-4} \text{ mol}/(\text{m}^3 \cdot \text{s})$) by Voulgaris *et al.* [216].

Additionally, during cell culture in vitro, the highest glucose concentration presents at inlet because the concentration of glucose keep decreasing because glucose is consumed by cells in the culture medium. According to the glucose concentration of the culture medium (DMEM) at 4500 mg/L ($=25 \text{ mol}/\text{m}^3$), the value of $C_{Hf, g}$ which is a constant in Eqn 7-6 can be determined to be $12.5 \text{ mol}/\text{m}^3$. This value has a good agreement with the value of $10.4 \text{ mol}/\text{m}^3$ from the literature reported by Zhang *et al.* [215]. As a summary, the parameters which can be used in the numerical simulation to investigate the dynamic perfusion behaviour of the hydrogel-based cell culture microdevice are determined and summarised in the Table 7-2.

Table 7-2. Summary of the parameters in simulation			
Category	Description	Name	Value
Geometrical dimensions	Radius of culture chamber	r	2.5 [mm]
	Height of culture chamber	h	1.5 [mm]
	Widths of channel	w_1, w_2	0.48, 0.1 [mm]
	Height of channel	h_c	0.7 [mm]
Properties of fluid	Dynamic viscosity	μ	8.9×10^{-4} [Pa·s]
	Density	ρ	1000 [kg/m ³]
Concentration of glucose	At inlet of culture chamber	c_{in}	25 [mol/m ³]
	At inlet of drug delivery reservoir	c_{in_res}	0 [mol/m ³]
	In cells under 37 °C	c_t	8 [mol/m ³]
	Half maximum response	$C_{Hf,g}$	12.5 [mol/m ³]
Diffusion coefficients	Glucose in culture medium	D_g	9.45×10^{-10} [m ² /s]
	Glucose in tissue (cell)	$D_{g,t}$	4.0×10^{-11} [m ² /s]
	Glucose in PHEMA hydrogel	D	9.9×10^{-6} [m ² /s]
Other	Langmuir equilibrium constant	k	0.0024 [m ³ /mol]
	Maximum glucose consumption rate	$R_{max,g}$	2.42×10^{-4} [mol/m ³ ·s]
Variables to be solved	Inflow velocity of culture medium	v_{in}	[mm/s]
	Glucose concentration around cells	c_g	[mol/m ³]
	Maximum shear stress around cells	τ_{max_cell}	[dyn/cm ²]

7.4 Results in Culture Chamber

7.4.1 Nutrient Supply to Cells

During the perfusion culture of cells using microfluidic device, the primary factor of extracellular matrix (ECM) which needs to be controlled is the nutrient supply for cells. According to Chapter 4, glucose is assumed as the only solute and only nutrient for cells in the culture medium in this study. Thus, the results of the modelling, in terms of the streamlines of both water molecules, isosurface of glucose concentration in the culture medium, and the equilibrium gradient of the glucose concentration in culture chamber, are illustrated in Fig.7-2. The glucose concentration is approximately uniform in culture chamber within the range of 24.98~25 mol/m³. It can be seen from the isosurface plot (Fig.7-2b) that the lowest concentration of glucose locates around cells near the bottom of the chamber with the value of 24.93 mol/m³. The homogeneous distribution of glucose molecules in the culture chamber is attributed to the flowing of the fluid which can only be achieved by perfusion culture. In traditional culture method, cells are seeded in a Petri dish which filled with

culture medium. The nutrient concentration in culture medium decreases during the growth of cells, with the nutrient consumption by cells. Inevitably, the culture medium has to be replaced periodically in the traditional cell culture. If compared with such kind of traditional culture using Petri dish, perfusion culture based on microfluidic system guarantees that the nutrients concentration in the extracellular matrix is a controllable constant, thus can automatically achieve culturing of cells.

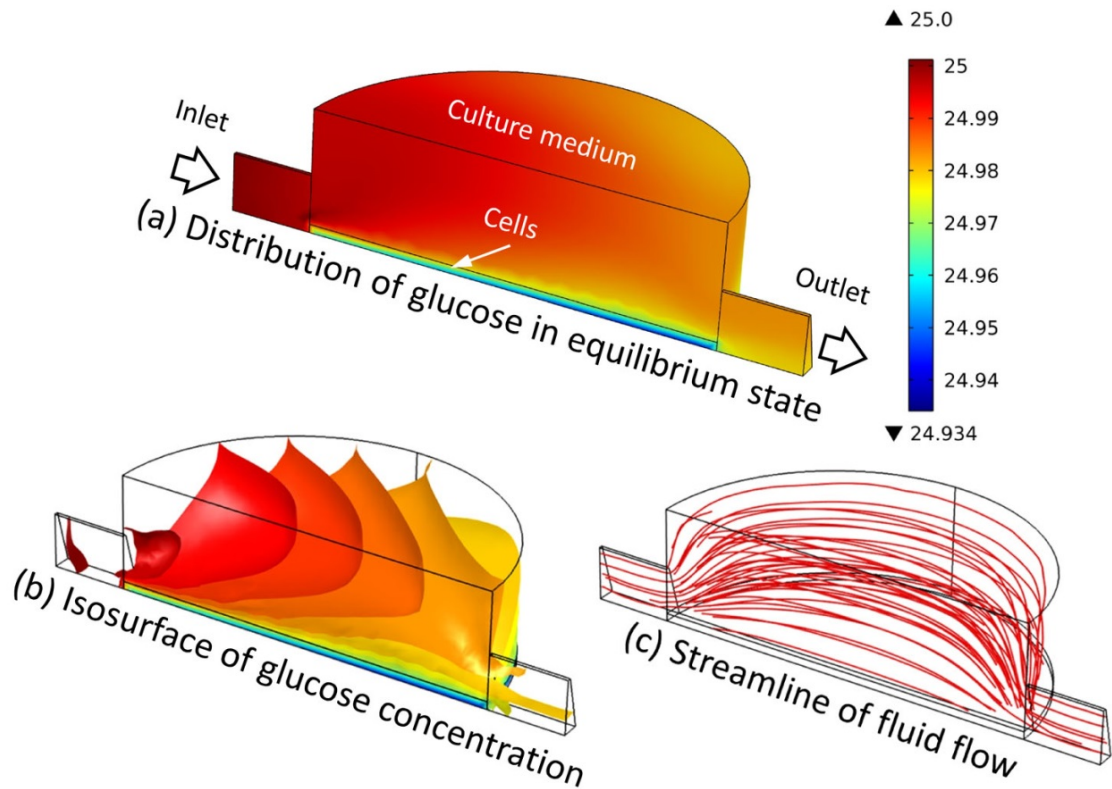


Fig.7-2. (a) Colour range: distribution of glucose in the equilibrium state under the conditions of $c_{in}=25 \text{ mol/m}^3$, $v_{in}=0.1 \text{ mm/s}$. (b) Isosurface of glucose concentration in the equilibrium state, maximum concentration at inlet then gradually decrease towards the bottom of the chamber, which is the location of cells. (c) Streamlines of fluid flow in the culture chamber.

In order for all the cells occupied on the bottom of the chamber to have sufficient glucose to consume, the minimum glucose concentration around cells (c_g) has been plotted in Fig.7-3a with respect to the inflow velocity (v_{in}) which is varying from 0 to 0.5 mm/s. In Fig.7-3a, when $v_{in}=0$, the corresponding c_g equals to 22.61 mol/m^3 . In this situation, the culture medium does not flow, but it connects to the inlet channel which provides fresh culture medium. Thus, the glucose molecules are transported from the inlet to cells only through the diffusion behaviour of culture in water, instead of transport through fluid flow. When $0 < v_{in} \leq 0.1$, it is apparent to see that the value of c_g have a drastic increase with the increasing of inflow velocity. Within this range of inflow velocity, efficiency of consuming glucose by cells is significantly increased, as such cells can have sufficient nutrients to

perform proliferation and differentiation. In the following range ($0.1 < v_{in} \leq 0.5$), the inflow velocity does not significantly affect the value of c_g . On account of the glucose concentration in culture medium c_{in} is fixed at 25 mol/m^3 , the value of c_g maintains approximately 24.51 mol/m^3 in this range of inflow velocity.

The relationship $v_{in} \sim c_g$ has been revealed at Fig.7-3a, and the relationship $c_g \sim R_{glucose}$ has been shown in Eqn.7-6. Thus, in order to determine the constraints of v_{in} , the correlation between v_{in} and $R_{glucose}$ can be seen in Fig.7-3b & c. Comparing with the maximum and minimum glucose concentration rate for single cells $R_{max,single}$ and $R_{min,single}$ from literature [215], the value of $R_{glucose}$ depicts as a constant (approximately $2.09 \cdot 10^{-19} \text{ mol/cell/s}$), which is in the middle of the range $R_{min,single} \sim R_{max,single}$. Accordingly, no matter what the value of v_{in} is, it gives that $R_{min,single} < R_{glucose} < R_{max,single}$. Thus, it can conclude that cells can be well cultured in all range of inflow velocity (v_{in}), because the culturing microdevice provides sufficient nutrients even $v_{in}=0$.

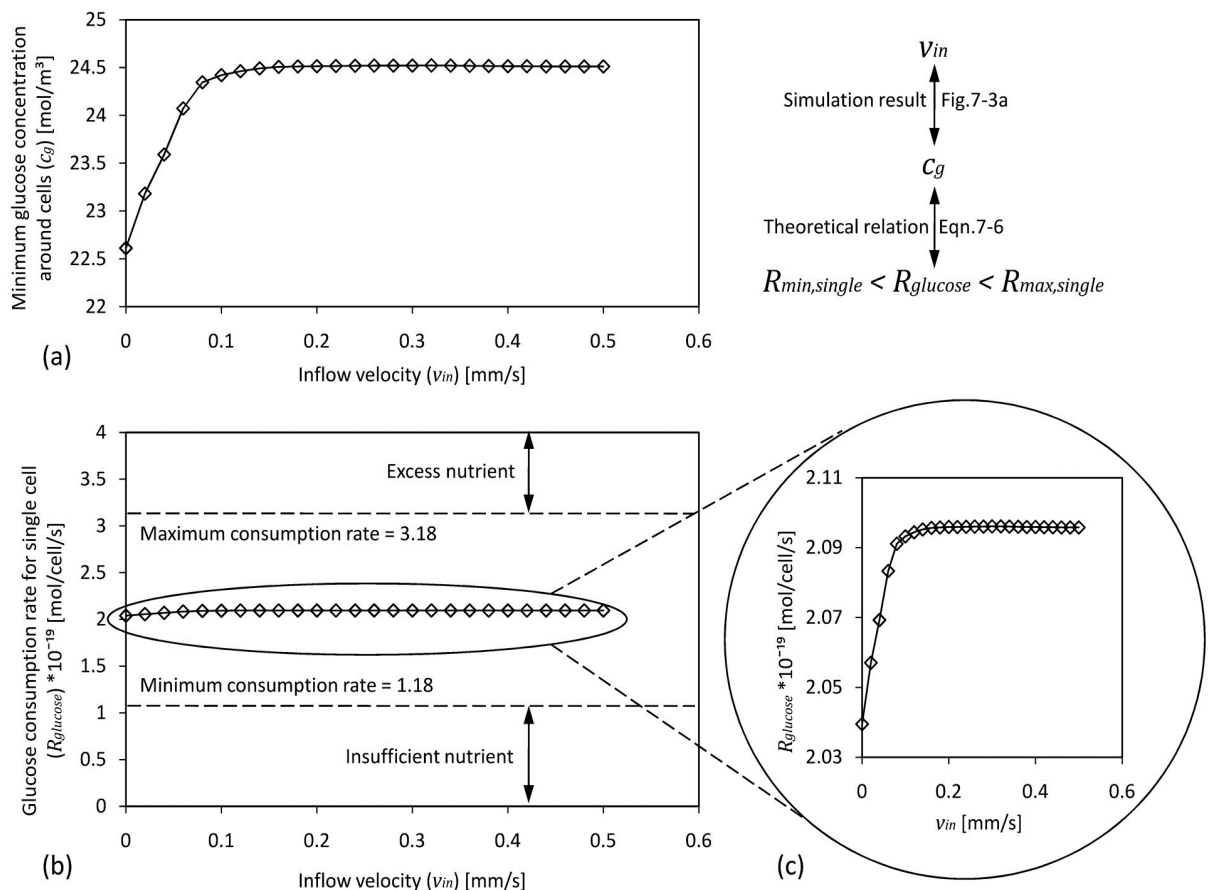


Fig.7-3. (a) Correlation between minimum glucose concentration around cells (c_g) and inflow velocity (v_{in}), from simulation. (b) Correlation between glucose consumption rate for single cell ($R_{glucose}$) and inflow velocity (v_{in}), based on Eqn.7-6. (c) Enlarged plotted data from (b)

7.4.2 Fluidic Shear Stress on Cells

Apart from the nutrient supply, another essential factor affecting the physical environment in perfusion culture in microfluidic system which is different from traditional culture is the flow of the culture medium during the incubation of cells. Theoretically, if there is fluid flow, then there is hydrodynamic shear. For the perfusion culture microdevice in this study, cells are incubated in an environment with a dynamic fluid flow and exposed in the field of hydrodynamic shear. If the shear stress which is applied on cells is high enough, it can potentially cause the decrease of proliferation rate of cells, or even cells to be detached from their substrate and flew away. To avoid this, the shear stress in terms of fluidic viscous force which is applied on cells has to be constrained smaller than the maximum adhesion strength of cells to substrate. The fluidic shear stress (τ [dyn/cm²]) at the bottom of the culture chamber where the cells are located is the parameter of interest for simulation study. Thus, numerical modelling has been established for dual purposes: i) to visualise the gradient of fluid flow velocity and the gradient of shear stress in the culture chamber during the perfusion culture, and ii) to examine the relationship between fluidic shear stress at the bottom of chamber (τ) and the fluid velocity at inlet (inflow velocity v_{in}).

The characteristics of fluid flow in the culture chamber in terms of the gradient of velocity and shear stress are numerically studied. Fig.7-4 illustrates the simulation results when the inflow velocity (v_{in}) is fixed as 0.5 mm/s. It can be observed that the maximum fluid flowing velocity occurs at the inlet and outlet from Fig.7-4a, corresponding to the locations with high fluidic shear stress (shown in Fig.7-4b). The distribution of fluid velocity and the fluidic shear stress are relatively uniform in the culture chamber as shown blue in Fig.7-4a&b. The drastic changes of the velocity gradient and shear stress gradient near inlet and outlet are induced by the sudden change of the cross-sectional areas at the interface between microchannels and culture chamber. Meanwhile, focusing on the bottom plane of the culture chamber where the cells located, the distribution of the shear stress on the plane and the streamline of the fluid flow are shown in Fig.7-4c. The scattered plot in Fig.7-4c shows the magnitude of shear stress along the central line from the fluid entrance to the fluid exit on the bottom of chamber. This scattered plot indicates that the maximum shear stress around cells (τ_{max_cell}) is 0.0215 [dyn/cm²] at the location near the entrance of chamber, but the average shear stress around cells is calculated at 0.0044 dyn/cm². It implies that the maximum shear stress (τ_{max_cell}) is nearly 5 times larger than the average shear stress. Therefore, if the

maximum shear stress at the bottom plane of chamber (τ_{max_cell}) is smaller than the maximum adhesion strength of cells to PHEMA substrate ($\tau_{cell}=0.021 \text{ dyn/cm}^2$) which is experimentally examined and described in Chapter 4 of this thesis, it can guarantee that shear stress anywhere else in the bottom of chamber is much smaller than τ_{cell} , thereby the cells are well cultured.

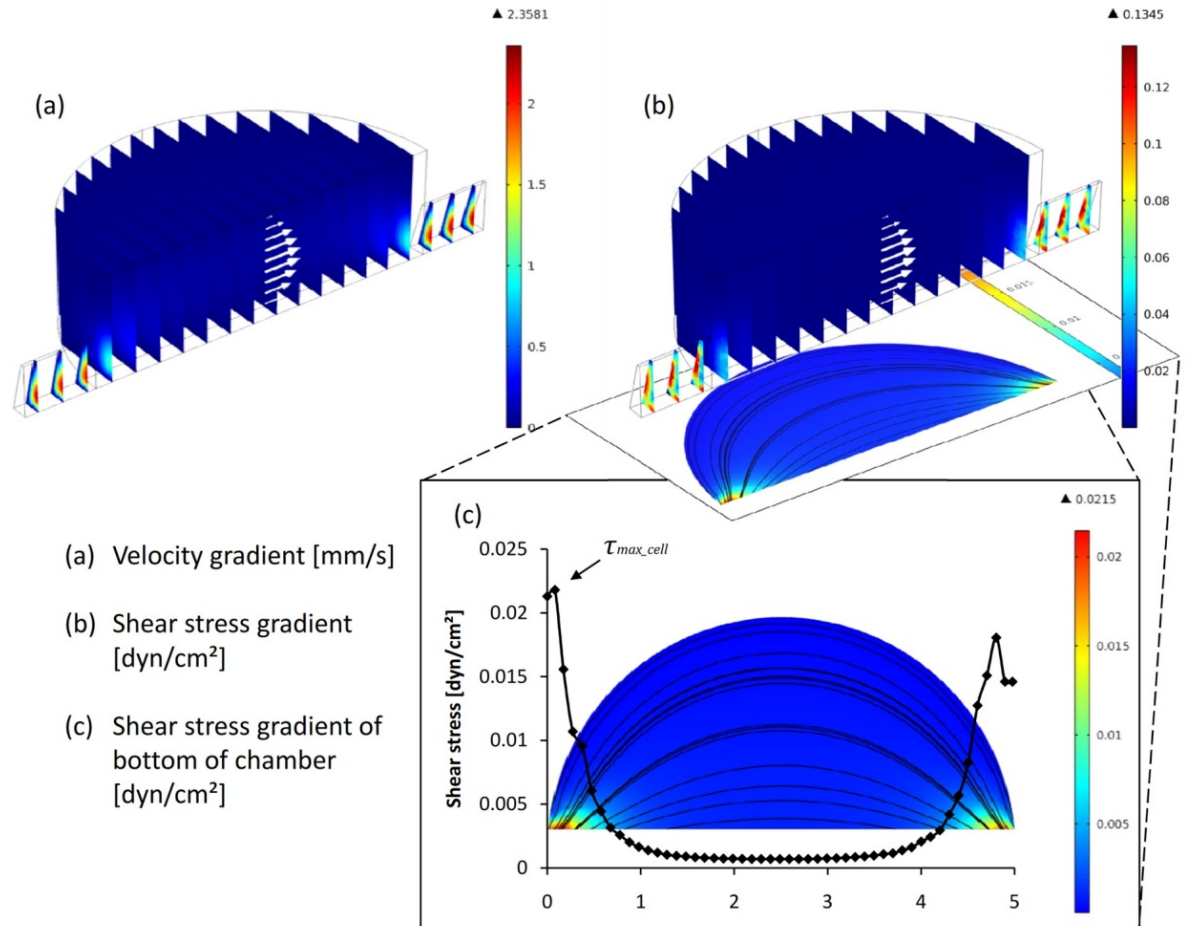


Fig.7-4. (a) Velocity gradient of the fluid in culture chamber, when inflow velocity is 0.5 mm/s. (b) Field of hydrodynamic shear stress in culture chamber, when inflow velocity is 0.5 mm/s. The white arrows in (a) and (b) indicates the velocity field of fluid in chamber. (c) Enlarged graph of fluidic shear stress gradient and the velocity streamline at the bottom of chamber. The plot is the shear stress along the central line of the bottom of chamber, maximum stress at inlet, minimum stress at centre.

The simulation results in terms of the relationship between the maximum shear stress at the bottom of culture chamber (τ_{max_cell}) and the inflow velocity (v_{in}) are presented in Fig.7-5, as a proportional correlation between them. The horizontal dashed line in the figure indicates the value of the maximum adhesion strength $\tau_{cell}=0.021 \text{ dyn/cm}^2$. This dashed line constrains the maximum allowed inflow velocity v_{in} , corresponding to the value of 0.49 mm/s. Therefore, using any value smaller than 0.49 mm/s for inflow velocity, it can thus satisfy the requirements that cells will not be detached from their substrate during perfusion culture. Thus, the vertical dashed line ($v_{in}=0.49 \text{ mm/s}$)

constrains the maximum allowed fluid velocity for the perfusion culture microdevice when HUVECs cells are cultured on PHEMA substrate.

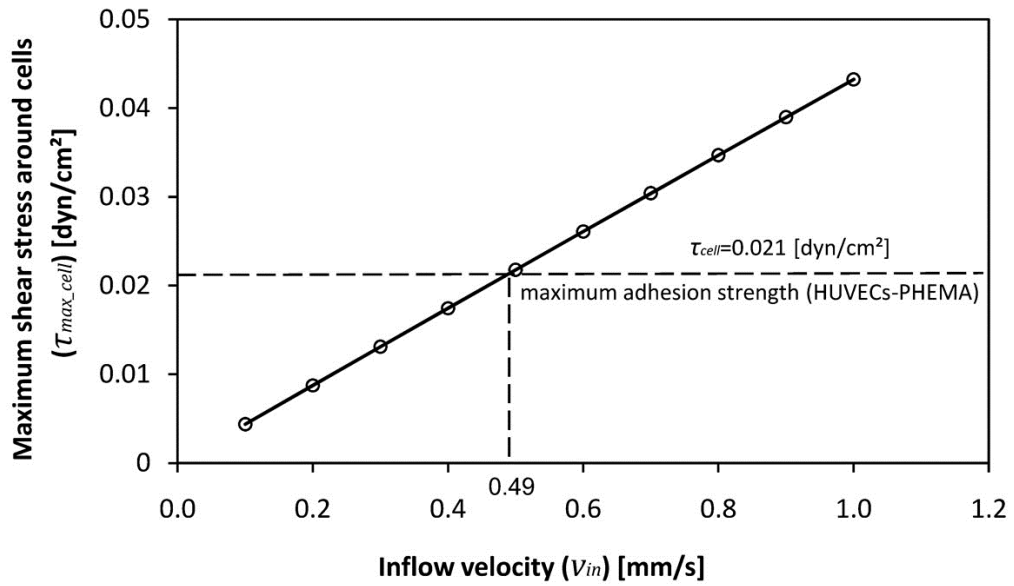


Fig.7-5. The correlation between maximum shear stress around cells (τ_{max_cell}) and inflow velocity (v_{in}), obtained from modelling. The maximum adhesion strength is tested in Section 4.6 of this thesis. Cell type: HUVECs. Substrate: PHEMA hydrogel.

7.4.3 Determination of Inflow Velocity for Perfusion Culture

Two primary variables, *i.e.* fluidic shear stress (τ) and glucose concentration around cells (c_g), were investigated, since both can affect the viability of cells during culture in the perfusion cell culture microdevice. Based on these two variables, the suitable range for choosing the value of inflow velocity can be proposed. The minimum allowed inflow velocity (v_{low}) is determined from the investigation of nutrient concentration, because low enough fluid flow may potentially cause insufficient nutrient supply, thus cause cells shrink or die. From the work carried out in Section 7.4.1, $v_{low}=0$ is determined in this study, based on the assumption that the glucose is the only nutrient. Meanwhile, from Fig.7-5 in Section 7.4.2, the value of maximum adhesion strength for cells ($\tau_{cell}=0.021 \text{ dyn/cm}^2$) and the relationship between shear stress versus inflow velocity has led to the maximum allowed inflow velocity (v_{high}) of 0.49 mm/s. Thus, by combining these two results, the applicable range of the inflow velocity ($v_{low}\sim v_{high}$) for the perfusion culture microdevice can be 0~0.49 [mm/s]. Apparently, any value within this range is chosen for the inflow velocity to perfuse culture medium into the culture chamber, it can guarantee that cells are well incubated in the perfusion culture microdevice.

Accordingly, an economic issue can emerge: culture medium may be wasted if the correct inflow velocity (v_{in}) is not selected, even within the applicable range (0~0.49 mm/s). For example, there are two groups (e.g. group A and group B) of culturing system with same configurations of chamber geometry, cells type and substrate material, but different inflow velocity (v_{in}). Group A uses a small value v_{in} in the applicable range of velocity, e.g. $v_{in,A}=1*10^{-5}$ mm/s, and Group B uses a large value in contrast, e.g. $v_{in,B}=v_{high}=0.49$ mm/s. After a certain period of time, both their configurations can keep that cells are well cultured and even potentially achieve the similar results (e.g. viability or density of cells), because of the friendly environments for cells are provided during culturing, with sufficient nutrient supply and acceptable hydrodynamic shear. The only difference between these two groups is that the consumption of the culture medium of Group B is far larger than that of Group A during the same period of culture, for $v_{in,A} \gg v_{in,B}$. Therefore, to avoid the high consumption of culture medium but keep the friendly culturing environment for cells, two alternative practical approaches may be proposed: i) choosing relatively low inflow velocity in the applicable range for the perfusion microdevice, e.g. $v_{in} = 0.1$ mm/s, to optimize the consumption of culture medium. ii) performing the periodic “flow-stop” perfusion using CNC (Computer Numerical Control) technique, to enable automatic refreshment of culture medium. Such “flow-stop” method of perfusion culture, which mixes perfusion culture and traditional culture, has been reported by Korin *et al.* [217] in literature.

7.4.4 Dimensional Effects on Nutrient Supply

A number of problems can be solved if the culture chamber is well designed. For instance, sufficient nutrient supply can be guaranteed by proper distance of inlet to cell; hydrodynamic shear can be reduced by choosing appropriate height and/or radius of chamber. Investigations on these influences for the perfusion culture microdevice are rarely found in the literature.

In this section, the effects of dimensions of cylindrical culture chamber on the glucose concentration around cells are discussed, in order to achieve an optimal dimensional design for the culture chamber. Based on the geometry of the culture chamber which is shown in Fig.7-1b, the correlations between the glucose concentration around cells (c_g) and the radius and height of the culture chamber are obtained in Fig.7-6 as a 3D surface profile. Accordingly, for a fixed radius of chamber (r), the linear relation between glucose concentration around cells (c_g) and height of

chamber (h) is found, but the glucose concentration does not vary significantly with the height of chamber. The estimated variability of c_g is less than 0.2 mol/m^3 over the range of the height of chamber h from 1 mm to 4 mm. However, the value of c_g varies from 22.8 to 24.3 mol/m^3 when the radius (r) in the range of 1~3 mm. For a given height of chamber (h), c_g decreases with the increase of r initially, until it reaches the minimum value of 22.8 mol/m^3 at $r=2.5$ mm, and followed by a gradual increase. The maximum value of the glucose concentration is corresponding to the smallest radius $r=1$ mm, because smaller the chamber is, the less cells that can survive due to the limited spaces in the chamber, which can result in less consumption of glucose. Considering the requirements on the cells density, the radius of culture chamber cannot be too small in order to reserve enough space for cells to proliferate.

In summary, in terms of the glucose concentration around cells (c_g), it does not vary significantly with the height of chamber h , the change of radius of chamber r can cause 6% variation of c_g . With such insignificant effects of h and r on the value of c_g , the dimensions of culture chamber is primarily depending on the requirements on the cells density in culture chamber.

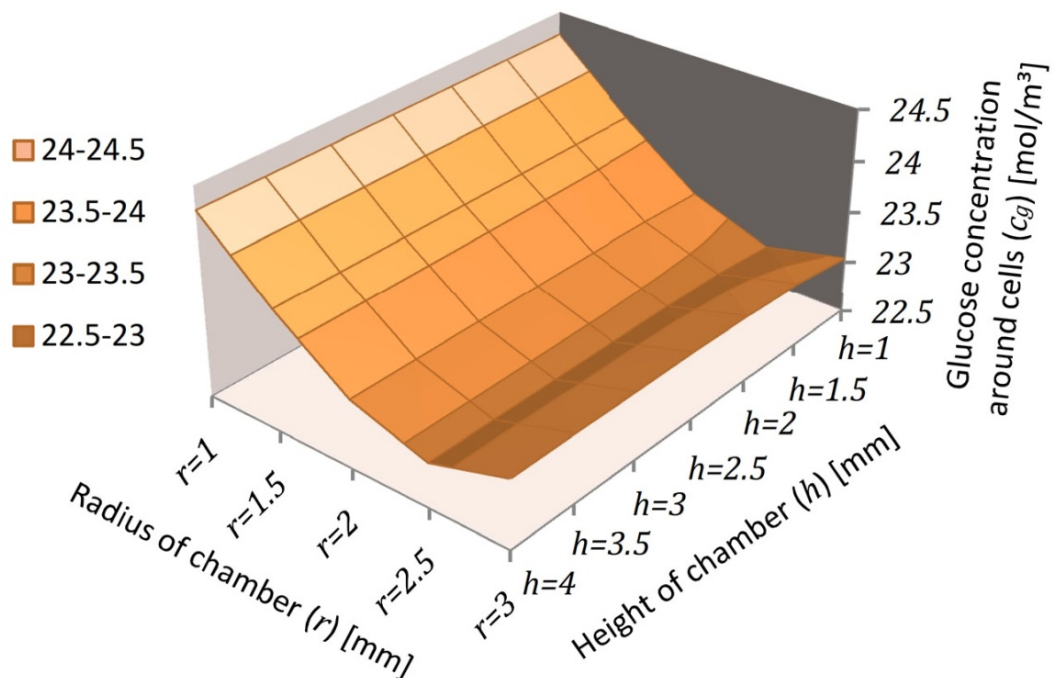


Fig.7-6. The dimensional effects of culture chamber (radius and height) on the glucose concentration around cells, based on the configuration of culture chamber which is shown in Fig.7-1b. The inflow glucose concentration is 25 mol/m^3 due to the properties of culture medium. The inflow velocity is assigned as 0, because it gives minimum glucose concentration around cells according to Fig.7-3a.

7.4.5 Dimensional Effects on Fluidic Shear Stress

When the dimensions (*i.e.* radius or height) of the culture chamber are changed, the flowing streamlines of the fluid in the perfusion culture device will be completely re-distributed. Consequently, the fluidic shear stress which is applied on cells will be totally different. In this section, the radius (r) and height (h) of the culture chamber are varied independently to numerically investigate the effect of these dimensions on the maximum shear stress around cells (τ_{max_cell}). The simulation results are illustrated in Fig.7-7.

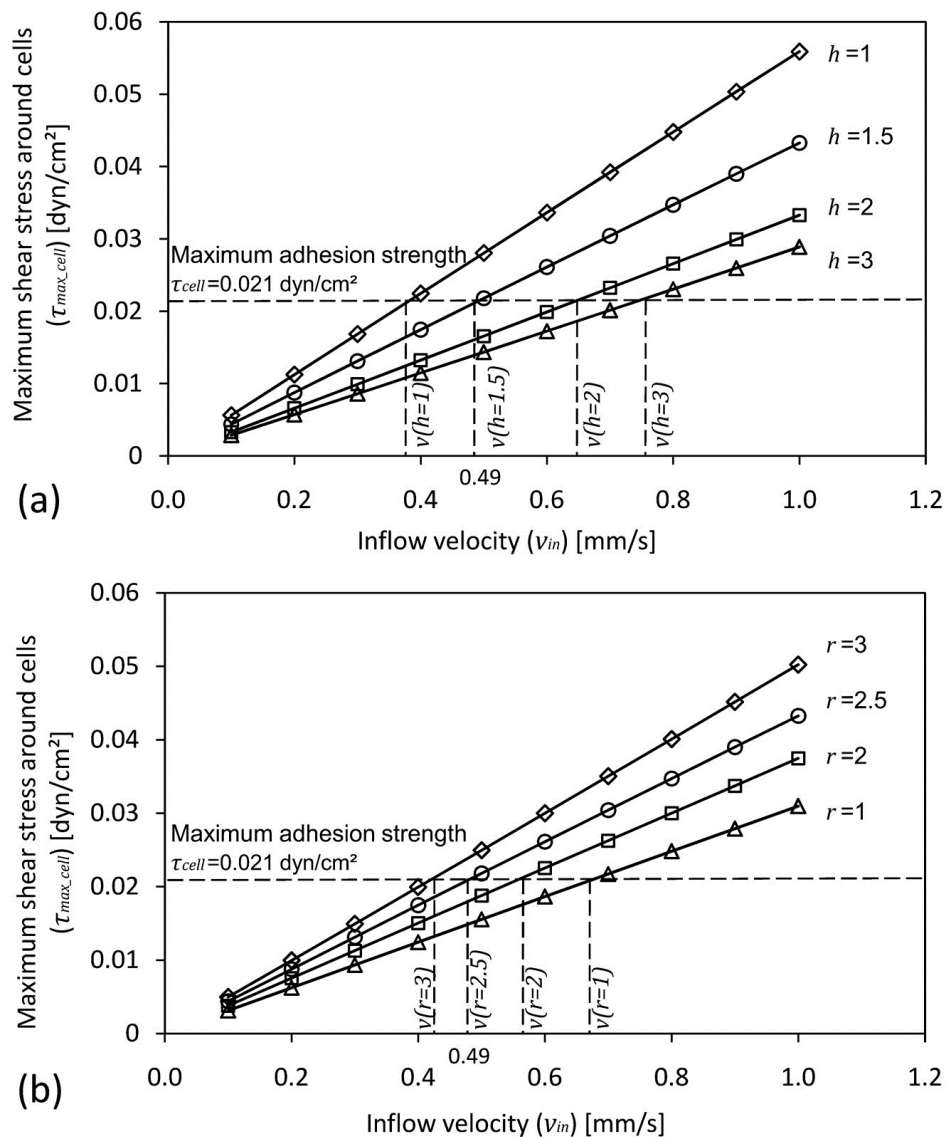


Fig.7-7. The relationship of maximum shear stress around cells (τ_{max_cell}) and inflow velocity (v_{in}), with respect to (a) the height of chamber h , when $r=2.5 \text{ mm}$; and (b) the radius of chamber r , when $h=1.5 \text{ mm}$. Increase of h , or decrease of r , can result in larger maximum allowed inflow velocity (v_{high}).

Firstly, fixing the value of radius of the culture chamber as 2.5mm, the height of the culture chamber h , the only variable varies from 1 to 3 [mm]. Fig.7-7a shows the correlation between

maximum shear stress around cells (τ_{max_cell}) and the inflow velocity (v_{in}), with respect to the height of culture chamber (h). As seen in the Fig.7-5, the maximum allowed inflow velocity is depending on the maximum adhesion strength of cell to PHEMA substrate. In the Fig.7-7a, we have $v(h=3)>v(h=2)>0.49>v(h=1)$, which means if the height of culture chamber increases, the range of applicable inflow velocity will be increased by changing the upper limit (v_{high} in Fig.7-6). Specifically, the inflow velocity range has been expanded by 80%, when h increases from 1 mm to 2 mm, because the upper limit v_{high} has been increased from $v(h=1)=0.36$ mm/s to $v(h=2)=0.65$ mm/s. Similarly, inflow velocity range is expanded by over two times when h increases from 1 mm to 3 mm. Thus, the height of culture chamber can significantly affect the applicable range of the fluid velocity at inlet. Meanwhile, for a fixed v_{in} , it can also be seen from the Fig.7-7a that τ_{max_cell} is decreasing with the increase of h . Therefore, a guideline can be proposed when selecting a proper value of height for culture chamber: the height of culture chamber h should be as large as possible to reduce the shear stress on cells and expand the applicable range of inflow velocity.

Secondly, the relationships between τ_{max_cell} and v_{in} , with respect to the radius of the culture chamber r , are numerically studied and shown in Fig.7-7b, and we can have $v(r=1)>v(r=2)>v(r=3)$, which means the applicable range of inflow velocity is expanded by reducing the radius of culture chamber. When the radius of culture chamber is reduced from 3 to 2 or 1 [mm], the applicable range of inflow velocity is expanded from 0~0.42 [mm/s] to approximate 0~0.56 [mm/s] or 0~0.67 [mm/s] respectively, increasing up to 60%. Thus, the radius of culture chamber r can significantly affect the applicable range of the inflow velocity (v_{in}) with a inverse correlation.

Consequently, brief suggestions for designing the dimensions of culture chamber, in terms of the height of chamber h and the radius of chamber r , can be proposed: i) For the height of culture chamber, it has to be designed as large as possible within the requirements of the dimensions. ii) For the radius of culture chamber, it has to be determined as small as possible to reduce the fluidic shear stress which is applied on cells. These design guidelines can be utilised to optimize the dimensions of culture chamber, in order to achieve a reliable cell culture microdevice.

7.4.6 Effect of Location of the Microchannel on Shear Stress

Beyond the original design of the culture chamber in Fig.1-1, the fluid stress on cells (τ) is also dependent on the location of microchannels (*i.e.* inlet and outlet), because different location of

microchannels leads to various streamlines of the fluid flow, and results in a re-distribution of hydrodynamic shear. In this section, the effect of distance between channel (d) and cells on the fluidic shear stress on cells (τ) is numerically investigated. The distance between channel and cells d is defined in Fig.7-8b.

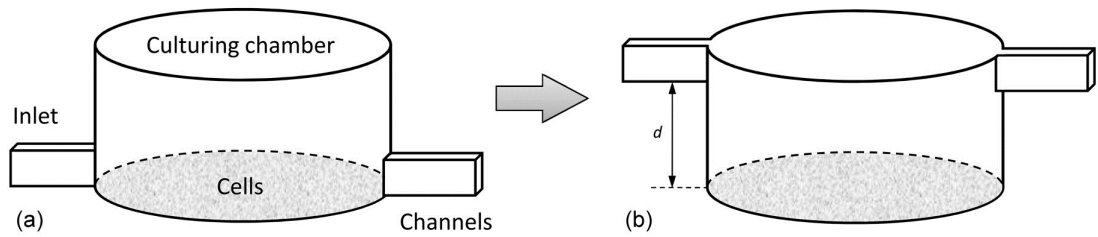


Fig.7-8. (a) Original design of the culture chamber with channels. (b) Definition of ' d ', the distance of channel to the surface of cells.

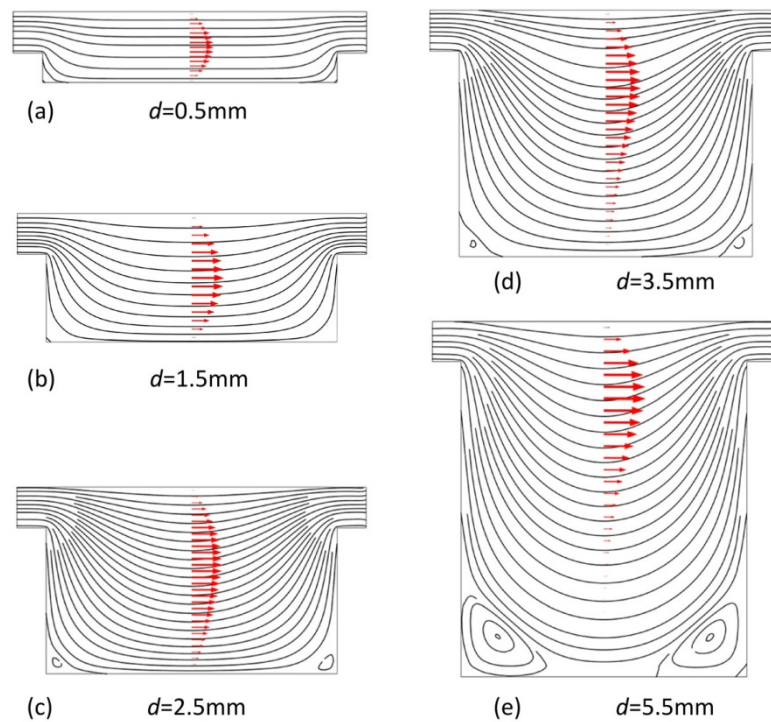


Fig.7-9. The fluid velocity (arrows) and velocity streamlines (black curves) in vary value of ' d ', which is ranging from 0.5 to 5.5 mm. Vortex flow can be found in (c), (d), and (e) at the corner of the chamber.

The variable d is assigned ranging from 0.5 to 5.5 mm in the modelling, by fixing the radius of chamber r at 2.5 mm, and the inflow velocity at 0.1 mm/s. Fig.7-9 presents the simulation results in terms of the fluid flow velocity distribution, and the streamline in the central cross-section of the culture chamber. By increasing the variable d from 0.5 mm to 2.5 mm, the streamlines of fluid flow behave continuously from the inlet to outlet. Beyond the distance d at 2.5mm, it can be apparently observed that there is vortex flow at the corners of the chamber, *i.e.* both lower corners for Fig.7-9c,

Fig.7-9d and Fig.7-9e. If cells are incubated in such configurations of chamber, the vortex flow will not carry the fresh nutrients from inflow but will remain at the corner all the time, thereby deteriorate the extracellular environment. Thus, large distance between inlet channel and cells has to be avoided when designing the culture chamber.

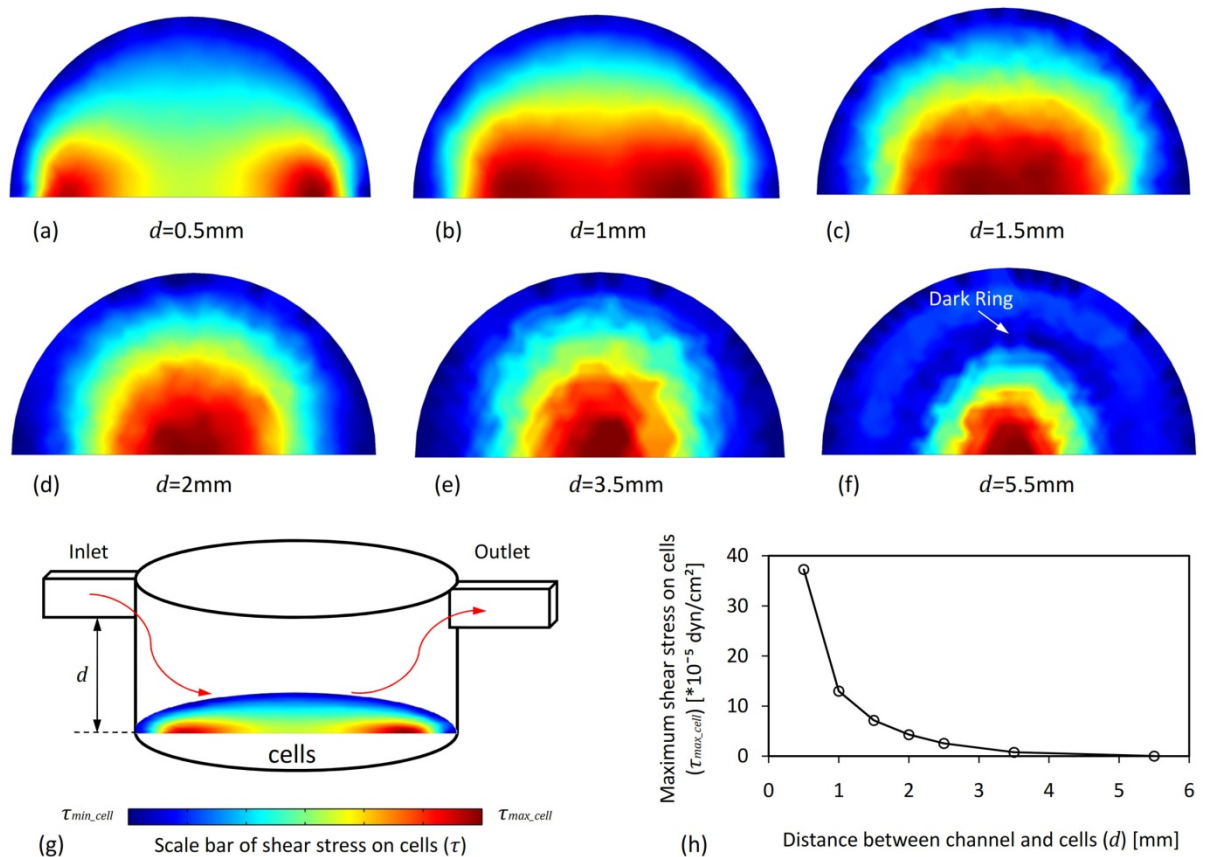


Fig.7-10. (a)~(f) Spatial distribution of shear stress on the bottom of the culture chamber. (g) The schematic diagram of the settings of the simulation. Scale bar of the distributions is given, red for maximum shear stress, blue for minimum shear stress. (h) The relationship between the maximum shear stress around cells (τ_{max_cell}) and the distance between channel and cells d .

Furthermore, the distributions of the fluidic shear stress induced at the bottom of the culture chamber with respect to the value of d are shown in Fig.7-10 in colour map. At small magnitude of d , e.g. 0~1 mm, two regions with high value of shear stress are caused (red parts in Fig.7-10a&b), which located near inlet and outlet regions respectively. With the further increase of d , these two regions move towards the centre of the bottom surface, and form one large high stress (red) region. This movement can be observed through Fig.7-10c&d. By continually increasing the value of d , the region with maximum fluidic shear stress becomes more concentrated (see Fig.7-10d,e&f). According to Fig.7-10f, a 'dark ring' is clearly observed, which corresponds to the interface of fluid streamline and the vortex streamline (see Fig.7-9e). The data that maximum shear stress (τ_{max_cell})

with respect to the distance of inlet and cells (d) are collected and plotted in Fig.7-10h. As the value of d increases, τ_{max_cell} declines rapidly at the initial stage, *i.e.* $d=0\sim 2.5$ mm. Beyond 2.5 mm, the decrease rate of τ_{max_cell} is reduced. Accordingly, at small magnitude (*i.e.* 0~2.5 mm), increasing the value of d can significantly reduce the maximum shear stress applied on the cells. At large magnitude (*i.e.* 2.5~5.5 mm), the maximum shear stress on cells does not vary significantly with the variable d .

As a summary, the location of inlet and outlet will significantly affect the fluidic shear stress on cells which located on the bottom of the culture chamber, in terms of the maximum shear stress (τ_{max_cell}) and the distribution of shear stress on the bottom of chamber. Two guidelines used to determine the location of microchannels for the culture chamber are proposed:

- 1) The distance between the inlet channel and the bottom of culture chamber (d) is recommended to be $\leq r$ ($=2.5$ mm), which is the radius of culture chamber.
- 2) The distance between the inlet channel and the bottom of culture chamber (d) can be zero.

But high hydrodynamic shear may potentially applied on cells during the perfusion culture in this configuration.

7.5 Results in Whole System

When the hydrogel-based cell culture microdevice is assembled, it consists of culture chamber, hydrogel membrane, and the drug delivery reservoir. The glucose molecules exist not only in the culture chamber, but also in the drug delivery reservoir due to diffusion through hydrogel membrane. Likewise, due to diffusion property of hydrogel membrane, the testing drug which is stored in the drug delivery reservoir can be transported to the culture chamber through hydrogel membrane to react with cells. Distribution of glucose in drug delivery reservoir and distribution of testing drug in culture chamber can be investigated and visualised using numerical modelling. Overall, the modelling in this study verified the feasibility of using hydrogel membrane as an interlayer for transportation of molecules, to connect culture chamber and drug delivery reservoir.

7.5.1 Glucose from Culture Chamber to Drug Delivery Reservoir

To investigate the characteristics of the transport behaviour of glucose molecules, the numerical simulation which consists of two chambers embracing a semi-permeable membrane has

been established. According to the determination of input parameters in Section 7.3.2, the glucose concentration at inflow entrance (*Inlet 1* in Fig.7-11a) is assigned to be 25 mol/m^3 . The glucose concentration at *Inlet 2* is assigned as 0, because the reservoir chamber is only designed to diffuse testing drug through hydrogel membrane to the culture chamber. The fluid flow velocity (v_1) of the culture medium is assumed to be 0.1 mm/s . Meanwhile, the fluid velocity of *Inlet 2* (v_2) is assigned as 0. The cells are built as a film occupies the area of the culture chamber to replicate the cell groups. The diffusion of glucose in the hydrogel membrane between two chambers is simulated based on Langmuir adsorption equation for absorption of glucose molecules and the Fickian diffusion equation for molecule transportation.

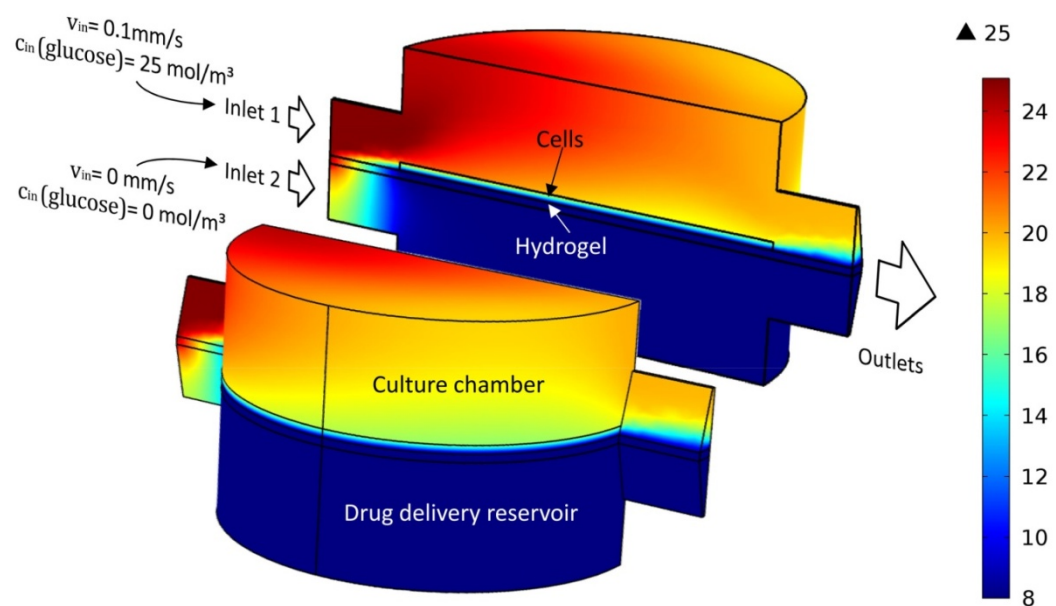


Fig.7-11. Sectional view of all the fluidic domains including culture chamber, membrane and drug delivery reservoir. The colour illustrates the distribution of glucose concentration in the whole system under the equilibrium. The initial constraints at inlets are indicated at the corresponding places. The glucose concentration in cells is 8 mol/m^3 . Glucose transport from culture chamber to drug delivery reservoir through diffusion by PHEMA hydrogel membrane.

The simulation results in terms of the glucose distribution and glucose concentration in the device, including the culture chamber, hydrogel membrane and drug deliver reservoir, are illustrated in Fig.7-11. The distribution of glucose concentration in the culture chamber exhibit the same characteristics as shown in Fig.7-2 based on the same input parameters and setups. According to the colour map in Fig.7-11, the maximum glucose concentration in the drug delivery reservoir is located at the entrance of *Inlet 2* (see Fig.7-11). Due to the difference of glucose concentration between *Inlet 1* (25 mol/m^3) and *Inlet 2* (0 mol/m^3), glucose concentration is gradually decreased from the *Inlet 1* to *Inlet 2* through the hydrogel membrane. As a glucose consumer, cells occupying

the bottom of the culture chamber, maintain the intracellular glucose concentration (c_i) at 8 mol/m^3 , and consume the glucose around them, including the glucose molecules flowing in culture chamber and the glucose molecules diffuse up from delivery reservoir through hydrogel membrane. Thus, the consumption has resulted in i) a homogeneous distribution of glucose at approximate 8 mol/m^3 in the drug delivery reservoir; and ii) the difference of glucose concentration between *Inlet 1* (25 mol/m^3) and outlet of culture chamber (approximately 18 mol/m^3).

According to the glucose concentration gradient of Fig.7-11, the glucose molecules which are originated from the *Inlet 1* with highest glucose concentration are transported through the culture chamber toward the cells, and contact with the cells for reaction. Some glucose molecules which are not consumed by cells may i) directly flow away above the cells to the outlets due to fluid flowing in culture chamber; ii) further travel through the hydrogel membrane to the drug delivery reservoir due to diffusion. Such results from numerical simulation demonstrated that glucose from the culture medium can be found in the drug delivery reservoir, and the concentration of such glucose in drug delivery reservoir is approximately 8 mol/m^3 under the conditions in this study.

7.5.2 Testing Drug from Delivery Reservoir to Culture Chamber

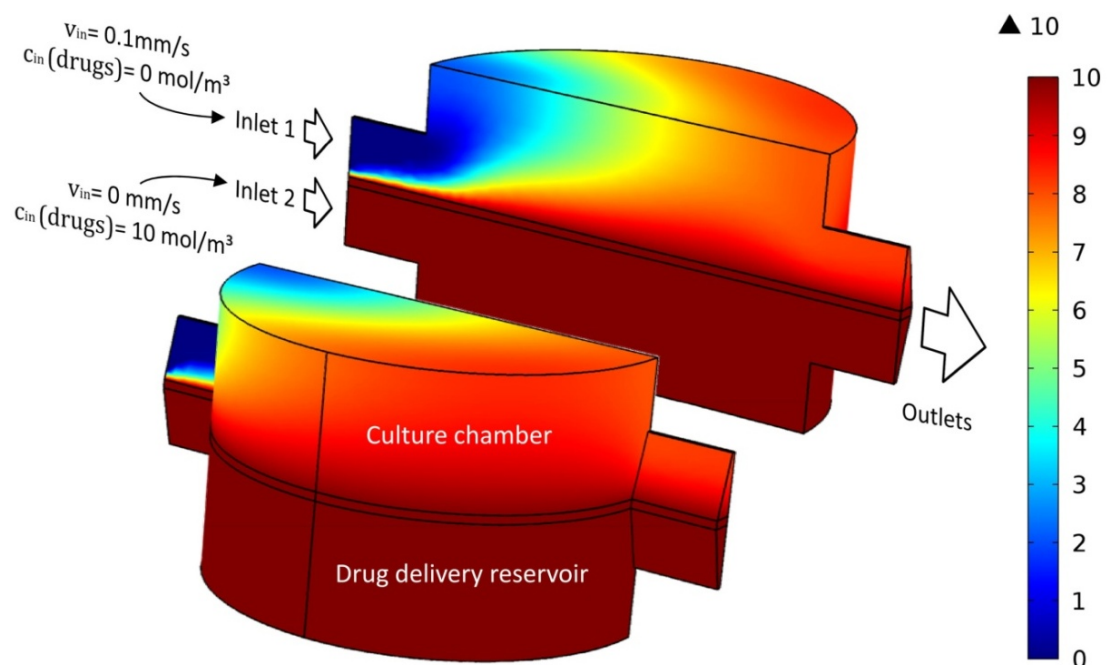


Fig.7-12. Sectional view of all the fluidic domains including culture chamber, membrane and drug delivery reservoir. The colour illustrates the distribution of testing drug concentration in the whole system under the equilibrium. The initial constraints at inlets are indicated at the corresponding places. Drug molecules are transported from drug delivery reservoir to culture chamber through diffusion by PHEMA hydrogel membrane.

The transport characteristics of the drug molecules in the extracellular environment including culture chamber, drug delivery reservoir and hydrogel membrane are also numerically investigated. As designated, testing drug are supplied from the drug delivery reservoir and transported through diffusion to the culture chamber for reaction with cells. The distribution of the drug concentration can be visualised in Fig.7-12 based on simulation results. The lowest drug concentration is located at the *Inlet 1*, as only nutrients are perfused into the culture chamber without testing drug. Accordingly, the drug molecules will be transported through hydrogel membrane to reach the cells and reacted with cells, due to the difference of the testing drug concentration between culture chamber and delivery reservoir. This has qualitatively demonstrates that the drug molecules from the drug delivery reservoir are able to reach the culture chamber and react with cells through diffusion.

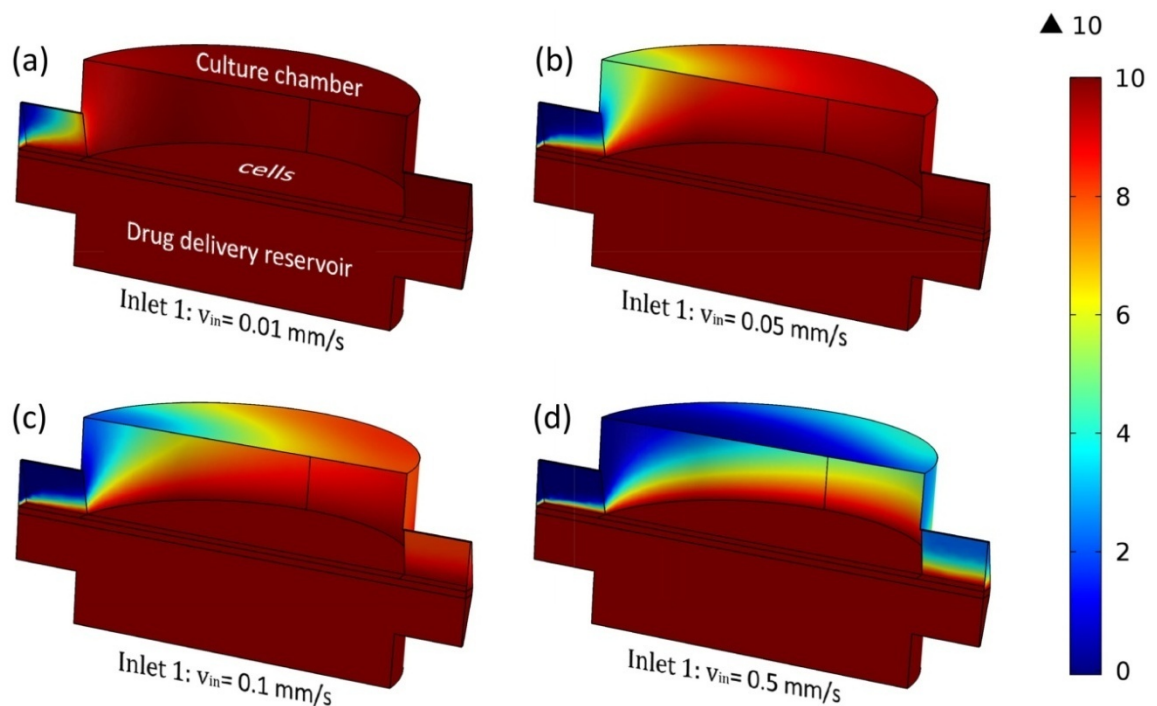


Fig.7-13. Sectional-inside view of the fluidic domains. Colour map shows the distribution of testing drug concentration with respect to the various inflow velocities at *Inlet 1*.

To understand the interaction of testing drug and cells at the bottom of culture chamber, quantitative evaluation of the testing drug concentration around cells has been carried out by simulation. Fig.7-13 is the colour map in terms of the distribution of testing drug concentration with respect to the inflow velocity (v_{in}) at *Inlet 1*. As is shown in this figure, different inflow velocity causes various distributions of drug concentration in the culture chamber, larger inflow velocity (e.g. Fig.7-13d) leads to inhomogeneous drug concentration in culture chamber. However, the drug concentration at the bottom of culture chamber, where the cells located, does not change

significantly with the inflow velocity (v_{in}) at *Inlet 1*. The averaged values of the concentration of testing drug (C_{drug_avg}) at the bottom of culture chamber are given in Table 7-3 with respect to the inflow velocity (v_{in}) at *Inlet 1*. As is shown in the table, though the inflow velocity increases from minimum ($v_{in}=0$) to its maximum limit ($v_{in}\sim 0.5$, see Section 7.4.3), the value of C_{drug_avg} is changed from 10 to 9.99781 [mol/m³]. The variation of C_{drug_avg} is less than 0.3%. Similar results can also be found according to the work done by Shah *et al.* [218]. Thus, it is evident that the supply of testing drug from the drug delivery reservoir for cells through diffusion in hydrogel is stable, and can provide homogeneous concentration of drug to react with cells.

v_{in} at <i>Inlet 1</i> [mm/s]	0	0.01	0.05	0.1	0.5
Averaged concentration of testing drug (C_{drug_avg}) [mol/m ³]	10	9.99934	9.99867	9.99803	9.99781

7.6 Discussions

7.6.1 Optimum Design of the Culture Chamber

According to the simulation results in Section 7.4, the increase of the distance between channel and cells (d) can be beneficial, and the optimal value d was determined as 2.5 mm. To consider this into the design of culture chamber for improvement, it can be difficult to make the top layer of the microfluidic chip as one piece (see Fig.1-1). This demands a new design of the structure of the top layer to identify the geometric parameters of culture chamber or channels, e.g. height of chamber (h), radius of chamber (r) and distance of inlet to cells (d).

Fig.7-14b shows a possible solution through separating the top part into two layers (channel layer and chamber layer) and manufacturing them individually. After the fabrication process, these two layers have to be bonded together permanently, e.g. by hot-embossing or adhesives. Utilising this structural design, the culture chamber is still sealed by the hydrogel membrane using mechanical fastening technique, and the multi-layers device can still be dismantling without affect the cells or membrane.

By collecting the results and conclusions from the Section 7.4.4, 7.4.5 and 7.4.6 above, dimensional optimization for the culture chamber design can be proposed as: i) optimum radius of the culture chamber (r) should provide enough space for cells to proliferation, in the range of 1~2

mm. ii) The height of the culture chamber h is dependent on sum of the value of d and the height of channel h_c (see Fig.7-14b). iii) The distance between the inlet and the cells d is recommended to be 1~2.5 mm given the range of $r=1\sim 2$ mm. Using the parameters that have been assigned in such optimum guidelines to design the culture chamber, the perfusion culture device should provide reliable and efficient incubation of the cells.

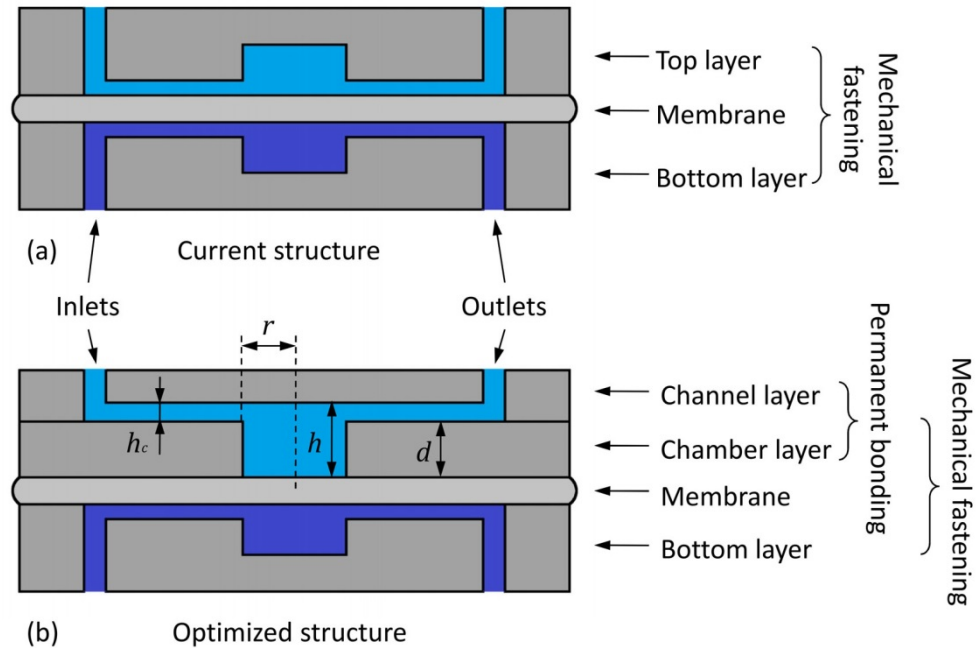


Fig.7-14. (a) The original structural design of the multi-layers microfluidic device, which is illustrated in the Chapter 1. (b) the optimized structure of the device which satisfies the required values of the distance (d) between channels and cells. r is the radius of the culture chamber, h is the height of the culture chamber, h_c is the height of microchannel.

7.6.2 Experimental Validation of Simulations

In order to validate the function of the cell culture device which is developed based on simulation, a prototype of the hydrogel-based microfluidic culture system was fabricated. The schematic diagram of the system is shown in Fig.7-15. Micropump provides the pressure and power to generate fluid flowing within the system, achieving perfusion culture. Culture medium is stored and recycled in a reservoir. The prototype chip which is assembled using mechanical fastening technique consists of PMMA cover, PHEMA membrane and PMMA microfluidic chip. Three parallel culture chambers and corresponding microchannels were engraved on the PMMA microfluidic chip, to be compared with each other as control groups. To replicate the extracellular environment for cells which is shown in Fig.7-14b, a piece of PHEMA hydrogel is placed at the bottom of each culture chamber as culturing substrate where cells were seeded. Accordingly, two goals are

expected from this experimental test on this prototype system: i) to validate the perfusion culture of cells on PHEMA substrate using the structural design shown in Fig.7-14b; ii) to further verify the reliability of mechanical fastening bonding method.

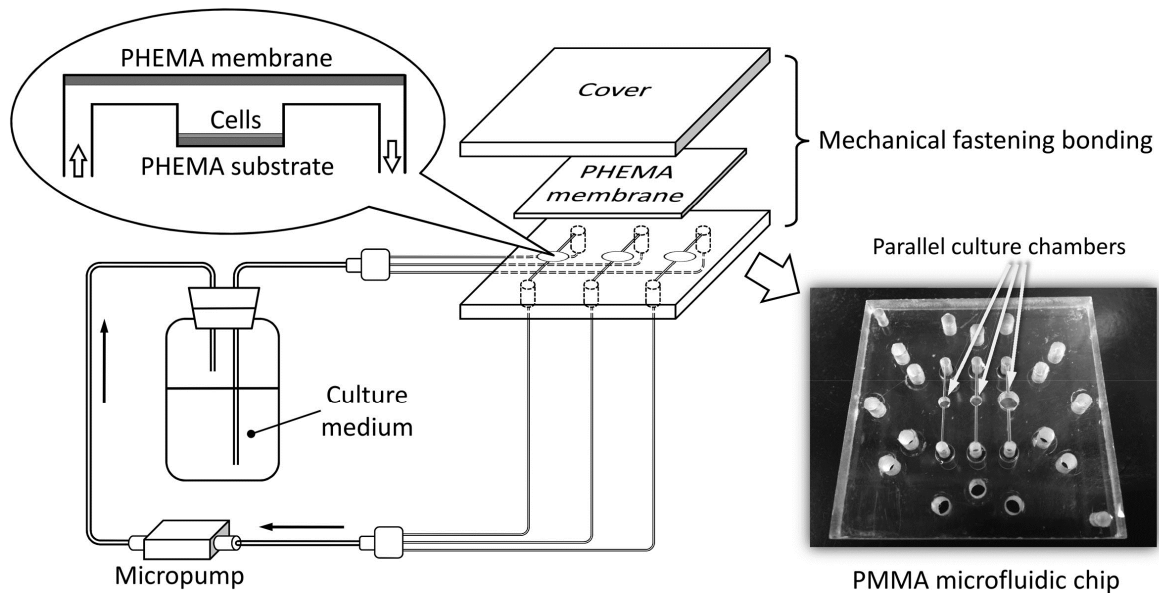


Fig.7-15. Schematic diagram of the prototype system to verify the function of culture chamber. PHEMA membrane is used to seal the microchannel system, and PHEMA substrate is used to replicate the environment for cells which is shown in Fig.7-14b. Fluid flow rate in the whole system is controlled by the micropump.

Within the limited time left for this project, the experimental test on the prototype was not successfully completed because HUVECs cells were mostly dead during the preparation period before transfer to the hydrogel-based prototype. Further trials of such experimental test on the prototype were confronted with three obstructions: i) *Cells dead due to contamination*. Side reactions during the synthesis process of PHEMA hydrogel were kept as minimum by maintain the constant environmental temperature, and most of contaminants were removed during the washing process. However, few contaminants (e.g. incomplete reacted chemicals) may be still attached on the polymer chains after the washing process of specimens. According to literatures [219,220], such contaminants can be potentially released from PHEMA hydrogel after a long time since the hydrogel is synthesised, and contact with cells which are seeded on PHEMA substrate, causing the deactivation or even death of cells. ii) *Inactive generation of cells*. Activity of cells in terms of the metabolism is highly dependent on the incubation environment during the preparation stage of cells. The degree of activity of cells between their generations may be various due to unequal incubation conditions. If the generation of cells with low degree of activity was used in experiment, it

is highly possible to obtain unsatisfied results, such as non-proliferative cells or even dead cells. This should be avoided only by conducting several times of experiments using different generations of cells, and draw the conclusions by summarising all the obtained results. iii) *Project funding expired*. The experimental test on this prototype was carried out at CIMAINA in the University of Milan, Italy. It was supported by the Fondazione CARIPLO for the project Hybrid Multifunctional Microdevices to Probe Cell Biology, under the programme *Promuovere progetti internazionali finalizzati al reclutamento di giovani ricercatori*. The experiment was scheduled on June/July 2013, but the funding was expired by the end of July 2013. Therefore, there is no sufficient time to repeat experiments, because preparing cells in different generations is a time-consuming process.

To consider various issues in the experimental tests of the prototype, based on the current research findings, this investigation has proposed the future work which is included in Chapter 8.

7.7 Summary

The dynamic perfusion behaviour of the hydrogel-based cell culture microdevice has been simulated and analysed. The following three primary physical mechanisms have been incorporated in the modelling: i) the dynamic characteristics of fluid in culture chamber; ii) diffusion of glucose and drug molecules in extracellular environment including the culturing solution and the semi-permeable hydrogel; and iii) consumption of energy molecules (e.g. glucose) by cells.

For the culture chamber, the glucose concentration around cells and the fluidic shear stress which is applied on cells are numerically analysed through simulations. The results show that the inflow velocity range is dependent to the glucose supply and maximum adhesion strength of cells to substrate. The glucose concentration at inlet determines the lower limit of the range of allowed fluid velocity (v_{low}) at the value of 0 in this case. However, the fluidic shear stress which is applied on cells determines the upper limit of that range (v_{high}) with the value of 0.49 mm/s. By further investigating the influences of dimension of culture chamber on the nutrient supply and fluid shear stress, guidelines which aim to achieve optimal design of the culture chamber are proposed. The applicable range of geometric parameters has been determined: the radius of culture chamber $r=1\sim 2$ mm; the distance between inlet and cells $d=1\sim 2.5$ mm; the height of chamber $h=d+h_c$, where h_c is the height of channel (determined in Chapter 6).

For the whole device including culture chamber, hydrogel membrane and the drug delivery

reservoir, a structural optimization has been developed to realise the manufacturing approach of the microdevice with optimized structure. Additionally, the simulations to visualise the transport of testing drug from delivery reservoir to culture chamber, and the transport of glucose from culture chamber to delivery reservoir, are established. It demonstrated that the molecules of testing drug are able to reach cells by crossing the hydrogel membrane through diffusion, and forming a homogeneous distribution on the bottom of culture chamber to react with cells. This result validates the original concept that maintaining drug and culture medium in their individual chamber, providing reliable incubation of cells in culture chamber and offering stable testing of drug by exchanging assigned molecules through diffusion in PHEMA hydrogel membrane.

Chapter 8. Conclusions, Recommendations and Future Works

8.1 Main Conclusions

The conclusions from the research work presented in this thesis are summarised in this section and categorized into three main components: i) experimental work on the properties of hydrogel material, ii) experimental and simulation work on the packaging of the hydrogel-based microfluidic device, and iii) simulation work on the perfusion culturing of cells using the hydrogel-based microfluidic device.

8.1.1 Properties of PHEMA Hydrogel Material

Diffusion characteristics: Two parameters, *i.e.* glucose release rate and capacity of absorption, which are related to the diffusion characteristics of PHEMA hydrogel material, have been experimentally examined. The glucose is chosen to be the only type of molecules for investigating the diffusion characteristics of PHEMA, because it is the prime energy source for cells during incubation of cells. The diffusivity of glucose molecules in PHEMA hydrogel has been experimentally proven obeying the Fickian diffusion behaviour in this study. Accordingly, the diffusion coefficient which indicates the transport speed of glucose in PHEMA hydrogel is calculated as $D=0.099 \text{ cm}^2/\text{s}$, based on the formula of Fickian diffusion for one-dimensional molecule transport. Meanwhile, the capacity of absorption (Γ) has also been determined from the experiment, with the value of $\Gamma=0.038 \text{ mol/kg}$.

Cytotoxicity: The effect of PHEMA hydrogel to cells, including HUVECs and fibroblast, has been investigated through three experiments with different focuses on the cells: i) When cells (HUVECs and fibroblast) cultured on the PHEMA substrate, 83.6% of fibroblasts are observed alive and emits bright green light from the experiment of Live/Dead staining; ii) Great shapes of these living fibroblasts, which reflect a good differentiation and proliferation environment, are observed through SEM photographs. iii) Over 80% cell viability for HUVECs cells has been obtained from the cell viability test through staining cells by CCK-8 assay. These three experimental results demonstrate that PHEMA can be used as culturing substrate for perfusion culturing devices.

Adhesion strength: An agitator has been built in the experimental determination of the maximum adhesion strength of HUVECs cells to the PHEMA hydrogel membrane. The value of maximum adhesion strength for HUVECs to PHEMA hydrogel substrate has been experimentally determined as 0.021 dyn/cm^2 , through measuring the critical radius. It is demonstrated that the adhesion strength of HUVEC cells to PHEMA hydrogel is relatively weak if comparing with the adhesion strength of HUVEC cells to other materials (e.g. PMMA or Fibronectin) from literature. This is attributed to the molecular interaction at the cell-substrate interface of PHEMA hydrogel though PHEMA has no cytotoxicity.

Mechanical deformation: Standard tests under constant load and cycling compressive load with PHEMA hydrogel specimens have been conducted. These experimental results verified the hyperelastic response of PHEMA hydrogel to mechanical compression (fracture occurs over 55% compressive strain), and demonstrated the reliability of using PHEMA hydrogel membrane as a sealing membrane under compression (allowing the assembly and re-assembly of microdevice at least 100 times). Meanwhile, numerical simulations to investigate the mechanical responses of PHEMA to compression have also been established. The simulation results indicate that the Mooney-Rivlin theory can be employed to describe the hyperelastic behaviour of PHEMA hydrogel.

8.1.2 Packaging for PHEMA-Based Microfluidic Device

A novel packaging process for bonding of the multilayer hydrogel-based microfluidic device has been developed and tested in this research. A number of significant findings have resulted from these experiments and simulations. The technique could be used to bond any kind of microfluidic system with embedded hydrogel membrane or any other kind of soft membrane.

Feasibility of mechanical fastening packaging process (simulation): The fundamental definitions of leakage in the microfluidic channels has been introduced and assumed in the modelling. The simulation using the Moony-Rivlin theory to predict the hyperelastic properties of PHEMA hydrogel has been established. It has been found that the maximum internal fluid pressures are 66.3 kPa and 196.3 kPa, when the hydrogel membrane is compressed by 10% and 20%, respectively, through mechanical fastening process. These values are larger than the ultimate fluid pressure for normal commercial microfluidic system (60 kPa), thereby guarantees that the

mechanical fastening packaging process is feasible for the bonding of hydrogel-based microfluidic system.

Reliability of mechanical fastening packaging process (experiment): Microchannels with various depths are bonded with PHEMA hydrogel membrane through mechanical fastening packaging process to construct a multilayer microfluidic device. The reliability of mechanical fastening packaging process is experimentally tested by obtaining the critical leakage pressure under the given pressurised fluid flowing in the microdevice. Conclusions from this experiment are summarised as: i) the compressive strain which applied on the PHEMA membrane should be $\leq 20\%$ due to the high potential risk of material failure; ii) the maximum allowed fluid pressure is determined as 200~350 kPa for 10% compressive strain, and 350-1000 kPa for 20% compressive strain, which are much higher than the ultimate fluid pressure for normal commercial microfluidic system (60 kPa); iii) it has proven that a good packaging reliability for hydrogel-based microfluidic device using the mechanical fastening process can be achieved.

Behaviour of PHEMA hydrogel in the packaging process (simulation&experiment): The deformation (e.g. protrusion) and internal stress distribution of the PHEMA hydrogel membrane were estimated and analysed through both experimental measurements and the simulation. The results has shown: i) higher compressive strain applied on the PHEMA membrane causes larger protrusion of the PHEMA membrane into the microchannel, ii) severer internal stress concentration occurs at the contact edge of microchannels. Internal stress concentration at the contact edge of the microchannels resulted in a high potential risk of material failure, indicating that compressive strain applied on PHEMA membrane should be $\leq 20\%$. Additionally, the consistency between simulation and experiment was confirmed, thereby the validity of using Mooney-Rivlin theory to predict behaviour of PHEMA hydrogel material was experimentally verified.

8.1.3 Cell Culture in PHEMA-Based Microfluidic Device

The dynamic interactions between cells and extracellular matrix which can be provided by the hydrogel-based microfluidic device were simulated and analysed to elaborate the dynamic characteristics of fluid in culture chamber, diffusion of glucose and drug molecules in extracellular matrix and in hydrogels, and consumption of energy molecules (e.g. glucose) by cells. Based on

two key factors, *i.e.* nutrient supply and fluidic shear stress, a methodology which can be used to quickly evaluate the functional capacity of the perfusion cell culture devices has been developed.

Nutrient supply in the cell culture: The nutrient supply (glucose) for cells was proved to be slightly dependent to the fluid flow rate during perfusion culture. To maintain sufficient nutrient supply for cells, the lower limit of the range of allowed fluid velocity (v_{low}) can be determined. The simulation results showed that being independent of the inflow velocity (v_{in}), the glucose concentration around cells (c_g) varies in the range of 22.5~24.51 mol/m³, which induces the glucose consumption rate of cells larger than the minimum allowed glucose consumption rate ($R_{min,single}$). This can ensure sufficient glucose for cells to perform their proliferation and differentiation during the perfusion culture. Therefore, the lower limit of the range of allowed fluid velocity (v_{low}) is calculated as 0 mm/s in this study.

Fluidic shear stress on cells: Based on the adhesion strength of HUVEC cells to PHEMA membrane which was detected at 0.021 dyn/cm², the maximum inflow velocity was thereby determined at $v_{high}=0.49$ mm/s, in order to avoid detaching of cells from their substrate due to high level of hydrodynamic shear. Combining the value of v_{low} which is evaluated by nutrient supply, the range of allowed inflow velocity which reflects the cell culture capacity of the hydrogel-based microfluidic device is therefore identified as 0~0.49 mm/s. Utilising this method, the controlling variables of the hydrogel-based microfluidic device (*e.g.* inflow rate, type of culture medium, time of perfusion culture) can be directly derived for a given type of cell.

8.2 Recommendations for Optimum Design of Microfluidic Device

A number of recommendations for design and optimization of hydrogel-based microfluidic device were made to enable such microfluidic device efficient and reliable. They are summarised as follows:

Design of microchannels: To ensure enough space for fluid flow inside the microchannels sealed by hydrogel membrane, the channel width must be in the ranges of 0.1~0.5 mm, or greater than 0.7 mm, and the passable rate of the channel should be from 50% to 80%. To avoid the failure

of hydrogel membrane due to the compressive strain induced by mechanical fastening bonding in the device, the aspect ratio of microchannels should be in the range of 1.15~1.6 (under 10% strain) and 1.45~1.6 (under 20% strain).

Optimization of culture chamber: During the perfusion cell culture using the hydrogel-based microfluidic device, cells are suffering fluidic viscous stress at the bottom of culture chamber. Optimization of the dimensions of the culture chamber can help reduce such fluidic viscous stress: i) Optimum radius of the culture chamber (r) can provide enough space for cells to proliferation, which has been determined as 1~2 mm in this case. ii) The distance between inlet and cells (d) is recommended to be 1~2.5 mm. iii) The height of the culture chamber (h) is subject to the sum of the value of d and the height of channel h_c . Based on these optimal guidelines, the culture chamber can provide reliable and efficient culturing of cells if using a suitable inflow velocity v_{in} , *i.e.* 0~0.49 mm/s. To fabricate the microfluidic chip with such optimal dimensions, the PMMA plate with culture chamber has to be fabricated separately as two chips due to the requirement of manufacturing, and then be assembled by permanent bonding.

8.3 Future Works

Due to the constraints of research facilities and limited time for this research, a number of areas have not been fully investigated. Therefore, future work on hydrogel-based microfluidic cell culture device can be outlined:

PHEMA coating: The weak adhesion strength of cells to PHEMA indicated the constraint of using PHEMA hydrogel material in bio-purpose application. To provide a strong adhesion between cells and the hydrogel substrate in the cell culture device, coating of the substrate by polysaccharides or protein particles is considered to enhance the interfacial adhesion. The improvement of the adhesion strength between cells and substrate can increase the resistance of cells to the fluidic viscous stress, consequently this can expand the range of inflow rate in the device.

Experimental validation based on prototype: The feasibility of the hydrogel-based microfluidic device has been numerically examined through determining the parameters (*e.g.* inflow velocity) of such device. However, it would be more credible to conduct the perfusion culture

experiment of cells using the prototype of the hydrogel-based microfluidic device which has been introduced in the Chapter 7 in this thesis, to validate its performance and capability as a perfusion culture microfluidic device in practice. Two suggestions which are summarised from the previous issue (e.g. cells died before conducting the experiment) may be considerable for further experiments: i) Use freshly synthesised PHEMA hydrogel to avoid any contaminants released from the PHEMA hydrogel; ii) Conduct repeated groups of validate experiments based on different generations of cells, to avoid poor results caused by various bioactivity of testing cells.

Multiple variables in nutrient supply: Only the effect of glucose to cells has been taken into account in the current investigation of the extracellular matrix around cells in the culture chamber. In reality, numbers of variables, including the concentration of oxygen, carbon dioxide, fetal bovine serum or other growing factors can affect the differentiation and proliferation of cells during incubation in the culture chamber. Based on the numerical simulations introduced in this thesis, there is a potential need to establish the FEA modelling to include multiple variables for the study of the effect of nutrient supply on cells. It is expected that the model established may be employed to accurately predict the response of cells to the ECM involved with multiple variables. This can be a potential future research topic to allow numerical study for identifying optimum constraints of culturing cells under multi-parametric environment.

Reference

- [1] Haycock JW (eds), 3D Cell Culture: A Review of Current Approaches and Techniques. In *3D Cell Culture: Methods and Protocols*. Methods in Molecular Biology Vol.695. Springer, London, **2011**, Chapter 1, pp.1-15. DOI: 10.1007/978-1-60761-984-0
- [2] El-Ali J, Sorger PK, Jensen K. Cells on chips. *Nature*, **2006**, 442, 403-411.
- [3] Whitesides GM. The origins and the future of microfluidics. *Nature*, **2006**, 442, 368-373.
- [4] Franchini J, Ranucci E, Ferruti P, Rossi M, Cavalli R. Synthesis, Physicochemical Properties, and Preliminary Biological Characterizations of a Novel Amphoteric Arginine-Based Poly(amidoamine) with RGD-Like Repeating Units. *Biomacromolecules*, **2006**, 7(4), 1215-1222.
- [5] Jacchetti E, Emilietti E, Rodighiero S, Indrieri M, Giannelis A, Lenardi C, Podesta A, Ranucci E, Ferruti P, Milani P. Biomimetic poly(amidoamine) hydrogels as synthetic materials for cell culture. *J Nanobiotechn*, **2008**, 6, 1-15. doi:10.1186/1477-3155-6-14.
- [6] Whitesides GM. The origins and the future of microfluidics. *Nature*, **2006**, 442, 368-373.
- [7] Zheng B, Tice JD, Roadch LS, Ismagilov RF. A droplet-based, composite PDMS/glass capillary microfluidic system for evaluating protein crystallization conditions by microbatch and vapour-diffusion methods with on-chip X-ray diffraction. *Angew Chem Int Ed Engl*, **2004**, 43(19), 2508-2511.
- [8] Shim JU, Cristobal G, Link DR, Thorsen T, Fraden S. Using microfluidics to decouple nucleation and growth of protein crystals. *Cryst Growth Des*, **2007**, 7(11), 2192-2194.
- [9] Hansen CL, Skordalakes E, Berger JM, Quake SR. A robust and scalable microfluidic metering method that allows protein crystal growth by free interface diffusion. *Proc Natl Acad Sci*, **2002**, 99, 16531-16536.
- [10] Dittrich PS, Manz, A. Lab-on-a-chip: microfluidics in drug discovery. *Nature Rev Drug Discov*, **2006**, 5, 210-218.
- [11] Pihl J, Karlsson M, Chui DT. Microfluidic technologies in drug discovery. *Drug Discov. Today*, **2005**, 10, 1377-1383.
- [12] Garstecki P, Gitlin I, DiLuzio W, Whitesides GM. Formation of monodisperse bubbles in a microfluidic flow-focusing device. *Appl Phys Lett*, **2004**, 85, 2649-2651.
- [13] Ganan-Calvo AM, Gordillo, JM. Perfectly monodisperse microbubbling by capillary flow focusing. *Phys Rev Lett*, **2001**, 87(27), 274501.
- [14] Thorsen T, Roberts RW, Arnold FH, Quake SR. Dynamic pattern formation in a vesicle-generating microfluidic device. *Phys Rev Lett*, **2001**, 86, 4163-4166.
- [15] Link DR, Anna SL, Weitz DA, Stone HA. Geometrically mediated breakup of drops in microfluidic devices. *Phys Rev Lett*, **2004**, 92, 054503.
- [16] Tan YC, Fisher JS, Lee AI, Cristini V, Lee AP. Design of microfluidic channel geometries for the

- control of droplet volume, chemical concentration, and sorting. *Lab Chip*, **2004**, 4, 292–298.
- [17] Breslauer DN, Lee PJ, Lee LP, Microfluidics-based systems biology. *Mol Biosys*, **2006**, 2, 97–112.
- [18] Auroux PA, Koc Y, deMello A, Manz A, Day PJ. Miniaturised nucleic acid analysis. *Lab Chip*, **2004**, 4(6), 534–546.
- [19] Huh D, Gu W, Kamotani Y, Grotberg JB, Takayama S. Microfluidics for flow cytometric analysis of cells and particles. *Physiol Meas*, **2005**, 26, R73–R98.
- [20] Hupert ML, Witek MA, Wang Y, Mitchell MW, Liu Y, Bejat Y, Nikitopoulos DE, Goettert J, Murphy MC, Soper SA. Polymer-based microfluidic devices for biomedical applications. *Proc SPIE*, **2003**, 4982, 52-64.
- [21] Ueda M, Nakanishi H, Tabata O, Bada Y. Imaging of a band for DNA fragment migrating in microchannel on integrated microchip. *Mater Sci Eng C Biomim Mater Sens Syst*. **2000**, 12, 33-36.
- [22] Mukhopadhyay. R. When PDMS isn't the best: What are its weaknesses and which other polymers can researchers add to their toolboxes? *Anal Chem*, **2007**, 79, 3248–3253.
- [23] Yu X, Zhang D, Li T, Hao L, Li X. 3D microarrays biochip for DNA amplification in polydimethylsiloxane (PDMS) elastomer. *Sens Actuators A Phys*, **2003**, 108, 103-107.
- [24] Fukuba T, Naganuma T, Fujii T. Microfabricated flow-through PCR device for underwater microbiological study. *Underwater Technology 2002. Proceedings of the 2002 international Symposium*. **2002**, 101-105. doi: 10.1109/UT.2002.1002401
- [25] Michael W, Toepke MW, Beebe DJ. PDMS absorption of small molecules and consequences in microfluidic applications. *Lab Chip*, **2006**, 6, 1484-1486.
- [26] Miao JC, Chen GL, Lai XM, Li HT, Li CF. Review of dynamic issues in micro-end-milling. *Int J Adv Manuf Technol*, **2007**, 31, 897-904.
- [27] Juang YJ, Lee LJ, Koelling KW. Hot embossing in microfabrication. Part I: Experimental, *Polym Eng Sci*, **2002**, 42(3), 539–550.
- [28] Juang YJ, Lee LJ, Koelling KW, Hot embossing in microfabrication. Part II: Rheological characterization and process analysis. *Polym Eng Sci*, **2002**, 42, 551–566.
- [29] Schulz H, Wissen M, Scheer HC, Local mass transport and its effect on global pattern replication during hot embossing. *Microelectron Eng*, **2003**, 67–68, 657–663.
- [30] Hecke M, Bacher W, Mueller KD. Hot embossing-the moulding technique for plastic microstructures. *Microsyst Technol*, **1998**, 4(3), 122–124.
- [31] Becker H, Gartner C. Polymer microfabrication technologies for microfluidic systems. *Anal Bioanal Chem*, **2008**, 390, 89-111.
- [32] Cao H, Yu Z, Wang J, Tegenfeldt J, Austin R, Chen E, Wu W, Chou S. Fabrication of 10 nm

- enclosed nanofluidic channels. *Appl Phys Lett*, **2002**, 81, 174–176.
- [33] Mills CA, Martínez E, Errachid A, Gomila G, Samsó A, Samitier J. Small scale structures: the fabrication of polymeric nanostructures for biomedical applications using pattern replication techniques. *Contrib Sci*, **2005**, 3(1), 47–56.
- [34] Becker EW, Ehrfeld W, Hagmann P, Maner A, Munchmeyer D. Fabrication of microstructures with high aspect ratios and great structural heights by synchrotron radiation lithography, galvano forming and plastic moulding (LIGA process), *Micro Eng*. **1986**, 4, 35-56.
- [35] Metz S, Holzer R, Renaud P. Polyimide-based microfluidic devices. *Lab Chip*, **2001**, 1, 29–34.
- [36] Metz S, Bertsch A, Bertand D, Renaud P. Flexible polyimide probes with microelectrodes and embedded microfluidic channels for simultaneous drug delivery and multi-channel monitoring of bioelectric activity. *Biosens Bioelectron*, **2004**, 19, 1309–1318.
- [37] Bianchi F, Chevelot Y, Mathieu HJ, Girault HH. Photomodification of Polymer Microchannels Induced by Static and Dynamic Excimer Ablation: Effect on the Electroosmotic Flow. *Anal Chem*. **2001**, 73, 3845–3853.
- [38] Johnson TJ, Ross D, Gaitan M, Locascio LE. Laser Modification of Preformed Polymer Microchannels: Application To Reduce Band Broadening around Turns Subject to Electrokinetic Flow. *Anal Chem*, **2001**, 73(15), 3656–3661.
- [39] Niklaus F, Enoksson P, Kälvesten E, Stemme G. Low-temperature full wafer adhesive bonding. *J Micromech Microeng*, **2001**, 11, 100–107.
- [40] Jackman R, Floyd T, Ghodssi R, Schmidt M, Jensen K. Microfluidic systems with on-line UV detection fabricated in photodefinable epoxy. *Micromech Microeng*, **2001**, 11, 263–269.
- [41] Hiratsuka A, Muguruma H, Lee KH, Karube I. Organic plasma process for simple and substrate-independent surface modification of polymeric BioMEMS devices. *Biosens Bioelectron*, **2004**, 19, 1667–1672.
- [42] Klank H, Kutter JP, Geschke O. CO₂-laser micromachining and back-end processing for rapid production of PMMA-based microfluidic systems. *Lab Chip*, **2002**, 2(4), 242–247.
- [43] Hong SM, Kim SH, Kim JH, Hwang HI. Hydrophilic Surface Modification of PDMS Using Atmospheric RF Plasma. *J Phys Conf Ser*, **2006**, 34, 656–661.
- [44] Locascio LE, Henry AC, Johnson TJ, Ross D. Surface chemistry in polymer microfluidic systems. In *Lab-on-a-Chip*; Oosterbroeck RE, van den Berg A, Eds. Elsevier, Amsterdam, **2003**, pp 65–82.
- [45] Soper SA, Henry AC, Vaidya B, Galloway M, Wabuyele M, McCarley RL. Surface Modification of Polymer-Based Microfluidic Devices. *Anal Chim Acta*, **2002**, 470, 87–99.
- [46] Klintberg L, Svedberg M, Nikolaejeff F, Thornell G. Fabrication of a paraffin actuator using hot embossing of polycarbonate. *Sens Actuators A*, **2003**, 103, 307–316.
- [47] Yao L, Liu B, Chen T, Liu S, Zuo T. Micro flow-through PCR in a PMMA chip fabricated by KrF

- excimer laser. *Biomed Microdevices*, **2005**, 7(3), 253–257.
- [48] Pan CT, Yang H, Shen SC, Chou MC, Chou HP. A low-temperature wafer bonding technique using patternable materials. *J Micromech Microeng*, **2002**, 12(5), 611–615.
- [49] Li J, Chen D, Chen G. Low-Temperature Thermal Bonding of PMMA Microfluidic Chips. *Anal Lett*, **2005**, 38, 1127–1136.
- [50] Truckenmüller R, Ahrens R, Cheng Y, Fischer G, Saile V. An ultrasonic welding based process for building up a new class of inert fluidic microsensors and actuators from polymers. *Sensor Actuat A*, **2006**, 132, 385–392.
- [51] Truckenmüller R, Cheng Y, Ahrens R, Bahrs H, Fischer G, Lehmann J. Micro ultrasonic welding: joining of chemically inert polymer microparts for single material fluidic components and systems. *Microsyst Technol*, **2006**, 12(10-11), 1027–1029
- [52] Pfleging W, Baldus O, Bruns M, Baldini A, Bemporad E. Laser assisted welding of transparent polymers for micro chemical engineering and life science. *Proc SPIE*, **2005**, 5713, 479-488.
- [53] Chen JW, Zybko JM, Clements J. Diode laser bonding of planar MEMS, MOEMS, and microfluidic devices. *Proc Mat Res Soc Symp*. **2005**, 872, J15.6.1-J15.6.6.
- [54] Griebel A, Rund S, Schönfeld F, Dörner W, Konrad R, Hardt S. Integrated polymer chip for two-dimensional capillary gel electrophoresis. *Lab Chip*, **2004**, 4(1), 18–23.
- [55] Kim J, Xu X. Excimer laser fabrication of polymer microfluidic devices. *J Laser Appl*, **2003**, 15, 255-260.
- [56] Tan R, She Z, Wang M, Fang Z, Liu Y, Feng Q. Thermo-sensitive alginate-based injectable hydrogel for tissue engineering. *Carbohydr Polym*, **2012**, 87(2), 1515-1521.
- [57] Huang Y, Zeng M, Ren J, Wang J, Fan L, Xu Q. Preparation and swelling properties of grapheme oxide/poly(acrylic acid-co-acrylamide) super-absorbent hydrogel nanocomposites. *Colloid Surf A*, **2012**, 401, 97-106.
- [58] Liu J, Li Q, Su Y, Yue Q, Gao B. Characterization and swelling-deswelling properties of wheat straw cellulose based semi-IPNs hydrogel. *Carbohydr Polym*. **2014**, 107, 232-240.
- [59] Clayden J, Greeves N, Warren S. Organic Chemistry (2nd ed.). Oxford University Press. New York. **2012**. p.27.
- [60] Verhulsel M, Vignes M, Descroix S, Malaquin L, Vignjevic DM, Viovy JL. A review of microfabrication and hydrogel engineering for micro-organs on chips. *Biomaterials*, **2014**, 35(6), 1816-1832.
- [61] Michel G, Tonon T, Scornet D, Cock JM, Kloareg B. The cell wall polysaccharide metabolism of the brown alga *Ectocarpus siliculosus*. Insights into the evolution of extracellular matrix polysaccharides in Eukaryotes. *New Phytologist*, **2010**, 188(1), 82-97.
- [62] Butcher JT, Nerem RM. Porcine aortic valve interstitial cells in 3D culture: Comparison of phenotype with aortic smooth muscle cells. *J Heart Valve Dis*, **2004**, 13, 478-485.

- [63] Eyrich D, Brandl F, Appel B, Wiese H, Maier G, Wenzel M, Staudenmaier R, Goepferich A, Blunk T. Long-term stable fibrin gels for cartilage engineering. *Biomaterials*, **2007**, 28(1), 55-65.
- [64] Masters KS, Shah DN, Walker G, Leinwand LA, Anseth KS. Designing scaffolds for valvular interstitial cells: cell adhesion and function on naturally derived materials. *J Biomed Mater Res*, **2004**, A 71(1), 172-180.
- [65] Azab AK, Orkin B, Doviner V, Nissan A, Klein M, Srebnik M, Rubinstein A. Crosslinked chitosan implants as potential degradable devices for brachytherapy: In vitro and in vivo analysis. *J Control Release*, **2006**, 111(3), 281-289.
- [66] Barralet JE, Wang L, Lawson M, Triffitt JT, Cooper PR, Shelton RM. Comparison of bone marrow cell growth on 2D and 3D alginate hydrogels. *J Mater Sci Mater Med*, **2005**, 16, 515-519.
- [67] Lee KY, Mooney DJ. Hydrogels for tissue engineering. *Chem Rev*, **2001**, 101(7), 1869-1879.
- [68] Malafaya PB, Silva GA, Reis RL. Natural-origin polymers as carriers and scaffolds for biomolecules and cell delivery in tissue engineering applications. *Adv Drug Deliv Rev*, **2007**, 59(4-5), 207-233.
- [69] Dawson E, Mapili G, Erickson K, Taqvi S, Roy K. Biomaterials for stem cell differentiation. *Adv Drug Deliv Rev*, **2008**, 60(2), 215-228.
- [70] Cushing MC, Anseth KS. Hydrogel cell cultures. *Science*, **2007**, 316(5828), 1133-1134.
- [71] Sawhney AS, Pathak CP, Hubbell JA. Bioerodible hydrogels based on photopolymerized poly(ethylene glycol)-co-poly(α -hydroxy acid) diacrylate macromers. *Macromolecules*, **1993**, 26(4), 581-587.
- [72] Matters AT, Anseth KS, Bowman CN. Fundamental studies of a novel, biodegradable PEG-b-PLA hydrogel. *Polymer*, **2000**, 41(11), 3993-4004.
- [73] Chirila TV, Constable IJ, Crawford GJ, Vijayasekaran S, Thompson DE, Chen YC, Fletcher WA, Griffin BJ. Poly(2-hydroxyethyl methacrylate) sponges as implant materials: In vivo and in vitro evaluation of cellular invasion. *Biomaterials*, **1993**, 14(1), 26-38.
- [74] Bryant SJ, Anseth KS. Hydrogel properties influence ECM production by chondrocytes photoencapsulated in poly(ethylene glycol) hydrogels. *J Biomed Mater Res*, **2002**, 59(1), 63-72.
- [75] Micic M, Zheng YJ, Moyb V, Zhang XH, Andreopoulos FM, Leblan RM. Comparative studies of surface topography and mechanical properties of a new, photo-switchable PEG-based hydrogel. *Biointerfaces*, **2002**, 27, 147-158.
- [76] Irani M, Ismail H, Ahmad Z. Preparation and properties of linear low-density polyethylene-g-poly(acrylic acid)/organo-montmorillonite superabsorbent hydrogel composites. *Polymer Testing*, **2013**, 32(3), 502-512.
- [77] Nafea EH, Marson A, Poole-Warren LA, Martens PJ. Immunoisolating semi-permeable membranes for cell encapsulation: Focus on hydrogels. *J Control Release*, **2011**, 154(2), 110-

- [78] Pozuelo J, Compan V, Gonzalez-Meijome JM, Gonzalez M, Molla S. Oxygen and ionic transport in hydrogel and silicone-hydrogel contact lens materials: An experimental and theoretical study. *J Membrane Sci*, **2014**, 452, 62-72.
- [79] Chen R, Chen Q, Huo D, Ding Y, HU Y, Jiang X. In situ formation of chitosan-gold hybrid hydrogel and its application for drug delivery. *Colloid Surface B*, **2012**, 97, 132-137.
- [80] Amsden B. Solute Diffusion within Hydrogels, Mechanisms and Models. *Macromolecules*, **1998**, 31, 8382-8395.
- [81] Dinarvand R, D'Emanuele A, The use of thermoresponsive hydrogels for on-off release of molecules, *J Control Release*, **1995**, 36, 221-227.
- [82] Gant RM, Hou Y, Cummins BM, Grunlan MA, Coté GL. Development of a self-cleaning sensor membrane for implantable biosensors. *J Biomed Mater Res A*, **2008**, 90(3), 695-701.
- [83] Gant RM, Abraham AA, Hou Y, Cummins BM, Grunlan MA, Coté GL. Design of a self-cleaning thermoresponsive nanocomposite hydrogel membrane for implantable biosensors. *Acta Biomaterialia*, **2010**, 6, 2903-2910.
- [84] Ratner BD, Hoffman AS. Synthesis hydrogels for biomedical applications, In Hydrogels for medical and related applications, JD Andrade, Eds, *ACS Symp. Ser.* **1976**, 31, 1-36.
- [85] Tranoudis I, Efron N. Tensile properties of soft contact lens materials. *Contact Lens & Anterior Eye*, **2004**, 27, 177-191.
- [86] Compan V, Andrio A, Lopez-Alemany A, Riande E, Refojo, MF. Oxygen permeability of hydrogel contact lenses with organosilicon moieties. *Biomaterials*, **2002**, 23, 2767-2772.
- [87] Azad AK, Sermsintham N, Chandkrachang S, Stevens WF. Chitosan membrane as a wound-healing dressing: Characterization and clinical application. *J Biomed Mater Res B*, **2004**, 69B, 216-222.
- [88] Wang T, Zhu XK, Xue XT, Wu DY. Hydrogel sheets of chitosan, honey and gelatin as burn wound dressings. *Carbohydr Polym*, **2012**, 88(1), 75-83.
- [89] Lionetto F, Sannino A, Mensitieri G, Maffezzoli A. Evaluation of the degree of crosslinking of cellulose-based hydrogels: a comparison between different techniques. *Macromol Symp*, **2003**, 200, 199-207.
- [90] Farkish A, Fall M. Rapid dewatering of oil sand mature fine tailings using super absorbent polymer (SAP). *Miner Eng*, **2013**, 50, 38-47.
- [91] Korpe S, Erdogan B, Bayram G, Ozgen S, Uludag Y, Bicak N. Crosslinked DADMAC polymers as cationic super absorbents. *React Funct Polym*, **2009**, 69(9), 660-665.
- [92] Perale G, Rossi F, Santoro M, Peviani M, Papa S, Llupi D, Torriani P, Micotti E, Previdi S, Cervo L, Sundstrom E, Boccaccini AR, Masi M, Forloni G, Veglianesse P. Multiple drug delivery hydrogel system for spinal cord injury repair strategies. *J Control Release*, **2012**, 159(2), 271-

- [93] Wilson AN, Guiseppi-Elie A. Targeting homeostasis in drug delivery using bioresponsive hydrogel microforms. *Int J Pharm*, **2014**, 461(1-2), 214-222.
- [94] Kimelaman-Bleich N, Pelled G, Sheyn D, Kallai I, Zilberman Y, Mizrahi O, Tal Y, Tawackoli W, Gazit Z, Gazit D. The use of a synthetic oxygen carrier-enriched hydrogel to enhance mesenchymal stem cell-based bone formation in vivo. *Biomaterials*, **2009**, 30(27), 4639-4648.
- [95] Lysaght MJ, Aebischer P. Encapsulated cells as therapy. *Sci Am*, **1999**, 280(4), 76-82.
- [96] Visser J, Peters B, Burger TJ, Boomstra J, Dhert WJA, Melchels FPW, Malda J. Biofabrication of multimaterial anatomically shaped tissue constructs. *Biofabrication*, **2013**, 5, 035007, 1-9.
- [97] Comez-Guillen MC, Gimenez B, Lopez-Caballero ME, Montero MP. Functional and bioactive properties of collagen and gelatin from alternative sources: A review. *Food Hydrocolloid*, **2011**, 25(8), 1813-1827.
- [98] Bertagnoli R, Sabatino CT, Edwards JT, Gontarz GA, Prewett A, Parsons JR. Mechanical testing of a novel hydrogel nucleus replacement implant. *Spine J*, **2005**, 5, 672-681.
- [99] Leclerc E, Sakai Y, Fujii T. Microfluidic PDMS (polydimethylsiloxane) bioreactor for large-scale culture of hepatocytes. *Biotechnol Progr*, **2004**, 20(3), 750-755.
- [100] Baudoin R, Griscom L, Monge M, Legallais C, Leclerc E, Development of a renal microchip for in vitro distal tubule models. *Biotechnol Progr*, **2007**, 23, 1245-1253.
- [101] Di Carlo D, Wu LY, Lee LP. Dynamic Single Cell Culture Array. *Lab Chip*, **2006**, 6, 1445-1449.
- [102] Hung PL, Lee PJ, Sabounchi P, Aghdam N, Lin R, Lee LP. A novel high aspect ratio microfluidic design to provide a stable and uniform microenvironment for cell growth in a high throughput mammalian cell culture array. *Lab Chip*, **2005**, 5, 44-48.
- [103] Liu K, Pitchimani R, Dang D, Bayer K, Harrington T, Pappas D. Cell Culture Chip with Low-Shear Mass Transport. *Langmuir*, **2008**, 24, 5955-5960.
- [104] Gomez-Sjoeberg R, Leyrat AA, Pirone DM, Chen CS, Quake SR. Versatile, fully automated, microfluidic cell culture system. *Anal Chem*, **2007**, 79(22), 8557-8563.
- [105] Leclerc E, David B, Griscom L, Lepioufle B, Fujii T, Layrolle P, Legallais C. Study of osteoblastic cells in a microfluidic environment. *Biomaterials*, **2006**, 27(4), 586-595.
- [106] Gottwald E, Giselbrecht S, Augspurger C, Lahni B, Dambrowsky N, Truckenmueller R, Piotter V, Gietzelt T, Wendt O, Pfleging W, Welle A, Rolletschek A, Wobus AM, Weibezahn KF. A chip-based platform for the in vitro generation of tissues in three-dimensional organization. *Lab Chip*, **2007**, 7(6), 777-785.
- [107] Engler AJ, Sen S, Sweeney HL, Discher DE. Matrix elasticity directs stem cell lineage specification. *Cell*, **2006**, 126(4), 677-689.
- [108] Engler AJ, Rehfeldt F, Sen S, Discher DE. Microtissue elasticity: Measurements by atomic

- force microscopy and its influence on cell differentiation. In *Methods in cell biology: Cell mechanics*. Wang Y-L, Discher DE, Eds. Elsevier, Amsterdam, **2007**. pp 521–545.
- [109] Ashe HL, Briscoe J. The interpretation of morphogen gradients. *Development*, **2006**, 133(3), 385–394.
- [110] Mahoney MJ, Anseth KS. Three-dimensional growth and function of neural tissue in degradable polyethylene glycol hydrogels. *Biomaterials*, **2006**, 27(10), 2265-2274.
- [111] Liu TV, Chen AA, Cho LM, Jadin KD, Sah RL, DeLong S, West JL, Bhatia SN. Fabrication of 3D hepatic tissues by additive photopatterning of cellular hydrogels. *Fasen J*, **2007**, 21(3), 790-801.
- [112] Tourovskaja A, Figueroa-Masot X, Folch A. Differentiation-on-a-chip: a microfluidic platform for long-term cell culture studies. *Lab chip*, **2005**, 5, 14-19.
- [113] Korin N, Bransky Avishay, Dinnar U, Levenberg S. Periodic “flow-stop” perfusion microchannel bioreactors for mammalian and human embryonic stem cell long-term culture. *Biomed Microdevices*, **2009**, 11, 87-94.
- [114] Yun KS, Yoon E. Micro/nanofluidic device for single-cell-based assay. *Biomedical Microdevices*, **2005**, 7, 35–40.
- [115] Tortora GJ, Derrickson B. The cardiovascular system: Blood vessels and hemodynamics. In *Principles of Anatomy & Physiology*, 13th, John Wiley & Sons, Inc. **2012**, p. 816.
- [116] Griffith LG, Swartz MA. Capturing complex 3D tissue physiology in vitro. *Nat Rev Mol Cell*, **2006**, 7, 211-224.
- [117] Sud D, Mehta G, Mehta K, Linderman J, Takayama S, Mycek MA. Optical imaging in microfluidic bioreactors enables oxygen monitoring for continuous cell culture. *J Biomed Opt*, **2006**, 11, 050504.
- [118] Liu RH, Yu Q, Beebe DJ. Fabrication and Characterisation of Hydrogel-Based Microvalves. *J Microelectromech S*, **2002**, 11(1), 45-53.
- [119] Clayton AB, Chirila TV, Lou X. Hydrophilic Sponges Based on 2-Hydroxyethyl Methacrylate. V. Effect of Crosslinking agent reactivity on mechanical properties. *Polym Int*. **1997**, 44, 201-207.
- [120] Liu Q, Hedberg EL, Liu Z, Bahulekar R, Meszlenyi RK, Mikos AG. Preparation of macroporous poly(2-hydroxyethyl methacrylate) hydrogels by enhanced phase separation. *Biomaterials*, **2000**, 21, 2163-2169.
- [121] Wong JY, Bronzino JD. Chapter 5: Biodegradable hydrogels: tailoring properties and function through chemistry and structure, in *Biomaterials*. CRC Press, Boca Raton, **2007**. p.5-12.
- [122] Ogden RW. Large deformation isotropic elasticity on the correlation of theory and experiment for incompressible rubberlike solids. *Proc R Soc Lond A Math Phys Sci*, **1972**, 326, 565-584.
- [123] Roundy D, Rogers M. Exploring the thermodynamics of a rubber band. *Am J Phys*, **2013**, 81, 20-23.

- [124] Marckmann G, Verron E. Comparison of hyperelastic models for rubber-like materials. *Rubber Chem Technol*, **2006**, 79, 835-858.
- [125] Rivlin RS. Large elastic deformations of isotropic materials. In *Further Development of the General Theory*, Philosophical Transactions of the Royal Society, London, **1948**, A 241(835), 379-397.
- [126] Mooney M. A theory of large elastic deformation, *J Appl Phys*, **1940**, 11(9), 582-592.
- [127] Bedalov T, Chevalier Y. Hybrid continuum model for large elastic deformation of rubber. *J Appl Phys*, **2003**, 94, 2701-2706.
- [128] Gent AN, Thomas AG. Forms for the stored (strain) energy function for vulcanized rubber. *J Polym Sci*, **2003**, 28(118), 625-628.
- [129] Mark JE, Polymer Data Handbook. Oxford University Press, New York. **1999**, pp 430.
- [130] Boyce MC, Arruda EM. Constitutive models of rubber elasticity: a review. *Rubber Chem Technol*, **2000**, 73, 504-523.
- [131] Meyers M, Chawla K. Mechanical Behaviour of Materials (2nd ed.). Cambridge University Press, New York. **2009**. pp. 98-103
- [132] Mielke A, Roubicek T. A rate-independent model for inelastic behaviour of shape-memory alloys. *Multiscale Model Simul*, **2003**, 1(4), 571-579.
- [133] Cohen MH, Turnbull D. Molecular transport in liquids and glasses. *J Chem Phys*, **1959**, 31, 1164-1169
- [134] Yasuda H, Peterlin A, Colton CK, Smith KA, Merrill EW. Permeability of solutes through hydrated polymer membranes. III Theoretical background for the selectivity of dialysis membranes. *Makromol Chemie*, **1969**, 126, 177-186.
- [135] Lustig SR, Peppas NA. Solute diffusion in swollen membranes. IX. Scaling laws for solute diffusion in gels. *J Appl Polym Sci*, **1988**, 36(4), 735-747.
- [136] Cukier RI. Diffusion of Brownian spheres in semidilute polymer solutions. *Macromolecules*, **1984**, 17(2), 252-255.
- [137] Phillips RJ, Deen WM, Brady JF. Hindered transport of spherical macromolecules in fibrous membranes and gels. *AIChE J*. **1989**, 35(11), 1761-1769.
- [138] Ogston AG, Preston BN, Wells JD. On the transport of compact particles through solutions of chain-polymers. *Proc R Soc London Ser A*, **1973**, 333, 297-316.
- [139] Johansson L, Elvingston C, Lofroth JE. Diffusion and interaction in gels and solutions (III) Theoretical results on the obstruction effect. *Macromolecules*, **1991**, 24, 6024-6029.
- [140] Ritger PL, Peppas NA. A Simple Equation for Description of Solute Release. I. Fickian and non-Fickian Release from Non-Swellable Devices in the Form of Slabs, Spheres, Cylinders or Discs. *J Control Release*, **1987**, 5, 23-36.

- [141] Rao SS. In *The finite element method in engineering*. 5th ed. Oxford: Butterworth-Heinemann. **2011**, pp. 5.
- [142] Szabo B, Babuska I. In *Introduction to Finite Element Analysis: Formulation, Verification and Validation*, John Wiley & Sons, Ltd, Chichester, UK. **2011**, pp.133.
- [143] Matinez RV, Fish CR, Chen Z, Whitesides GM. Elastomeric origami: Programmable paper elastomer composites as pneumatic actuators. *Adv Funct Mater*, **2012**, 22(7), 1376-1384.
- [144] Official website from COMSOL. URL: <http://www.comsol.com/products>. [Accessed on 06/04/2014]
- [145] Luo X, Copenhagen CV. Mechanical characteristics of poly(2-hydroxyethyl methacrylate) hydrogels crosslinked with various difunctional compounds. *Polym Int*, **2001**, 50, 319–325.
- [146] Antonsen KP, Bohnert JL, Nabeshima Y, Sheu MS, Wu XS, Hoffman AS. Controlled release of proteins from 2-hydroxyethyl methacrylate copolymer gels. *Biomater Artif Cells Immobilization Biotechnol*, **1993**, 21, 1–22.
- [147] Chirila TV, Chen Y, Griffin BJ and Constable IJ. Hydrophilic sponges based on 2-hydroxyethyl methacrylate. I. effect of monomer mixture composition on the pore size. *Polym Int*, **1993**, 32, 221–232.
- [148] Prashantha K, Pai KVK, Yashoda MPG, Sherigara BS. Kinetics of Polymerization of 2-hydroxyethyl methacrylate initiated by a titanium (III)-Dimethylglyoxime redox system. *Turk J Chem*, **2003**, 27, 99–110.
- [149] Anseth KS, Bowman CN, Brannon-Peppas L. Review: mechanical properties of hydrogels and their experimental determination. *Biomaterials*, **1996**, 17, 1647–1657.
- [150] Kono H, Oeda I, Nakamura T. The preparation, swelling characteristics and albumin adsorption and release behaviours of a novel chitosan-based polyampholyte. *React Funct Polym*, **2013**, 73, 97-107.
- [151] Gerrer GG, Sanchez MS, Ribelles JLG, Colomer FJR, Pradas MM. Nanodomains in a hydrophilic-hydrophobic IPN based on poly(2-hydroxyethyl acrylate) and poly(ethyl acrylate). *Eur Polym J*, **2007**, 43(8), 3136-3145.
- [152] Chen J, Liu M, Liu H, Ma L. Synthesis, Swelling and drug release behaviour of poly(NN-diethylacrylamide-co-N-hydroxymethyl acrylamide) hydrogel. *Mater Sci Eng C*, **2009**, 29(7), 2116-2123.
- [153] Teixeira JA, Mota M, Venancio A. A model identification and diffusion coefficients determination of glucose and malic acid in calcium alginate membrane. *Chem Eng J*, **1994**, 56, B9–B14.
- [154] Liu Q, Hedberg EL, Liu Z, Bahulekar R, Meszlenyi RK, Mikos AG. Preparation of macroporous poly(2-hydroxyethyl methacrylate) hydrogels by enhanced phase separation. *Biomaterials*, **2000**, 21, 2163–2169.

- [155] Ganji F., Vasheghani-Farahani S., Vasheghani-Farahani E., Theoretical description of hydrogel swelling: a review. *Iran Polym J*, **2010**, 19 (5), 375-398.
- [156] Li S, Shen Y, Li W, Hao X. A common profile for polymer-based controlled releases and its logical interpretation to general release process. *J Pham Pharmaceut Sci*, **2006**, 9(2), 238-244.
- [157] Korsmeyer RW, Gurny R, Doelker E, Buri P, Peppas NA. Mechanism of solute release from porous hydrophilic polymers. *Int J Pharm*, **1983**, 15, 25-35.
- [158] Tomic SL, Micic MM, Filipovic JM, Suljovrujic EH. Swelling and drug release behaviour of poly(2-hydroxyethyl methacrylate/itaconic acid) copolymeric hydrogels obtained by gamma irradiation. *Radiat Phys Chem*, **2007**, 76, 801-810.
- [159] Sahoo H. Fluorescent labelling techniques in biomolecules: a flashback. *RSC advances*, **2012**, 2, 7017-7029.
- [160] Patel H, Tscheka C, Heerklotz H. Characterizing vesicle leakage by fluorescence lifetime measurements. *Soft Matter*, **2009**, 5, 2849-2851.
- [161] Luo Y, Wang C, Qiao Y, Hossain M, Ma L, Su M. In vitro cytotoxicity of surface modified bismuth nanoparticles. *J Mater Sci Mater Med*, **2012**, 23, 2563-2573.
- [162] Sigma-Aldrich, Biofiles, Vol. 6, No. 5. Available from <http://www.sigmaaldrich.com/life-science/learning-center/biofiles.html> [Accessed on 23rd Sept. 2013]
- [163] Wongpanit P, Sanchavanakit N, Pavasant P, Supaphol P, Tokura S, Rujiravanit R. Preparation and Characterization of Microwave-treated Carboxymethyl Chitin and Carboxymethyl Chitosan Films for Potential Use in Wound Care Application. *Macromol Biosci*, **2005**, 5, 1001-1012.
- [164] Chen XG, Liu CS, Liu CG, Meng XH, Lee CM, Park HJ. Preparation and biocompatibility of chitosan microcarriers as biomaterial. *Biochem Eng J*, **2006**, 27, 269-274.
- [165] Corning Microplate Selection Guide, Corning Incorporated. Available from http://catalog2.corning.com/lifesciences/media/pdf/productselectionguide_microplates11_02_cis_mp_014.pdf [Accessed on 23rd Sept. 2013]
- [166] Weissmanshomer P, Fry M. Chick embryo fibroblasts senescence in vitro: Pattern of cell division and life span as a function of cell density. *Mech Ageing Dev*, **1975**, 4(2), 159-166.
- [167] Park HJ, Zhang Y, Georgescu SP, Johnson KL, Kong D, Galper JB. Human umbilical vein endothelial cells and human dermal microvascular endothelial cells offer new insights into the relationship between lipid metabolism and angiogenesis. *Stem Cell Rev*, **2006**, 2(2), 93-102.
- [168] Toth B, Scholz C, Saadat G, Geller A, Shulze S, Mylonas I, Friese K, Jeschke U. Estrogen receptor modulators and estrogen receptor beta immunolabelling in human umbilical vein endothelial cells. *Acta Histochem*, **2009**, 111, 508-519.
- [169] Niles AL, Moravec RA, Riss TL. Update on in vitro cytotoxicity assays for drug development. *Exper Opin Drug Discou*, **2008**, 3(6), 655-669.

- [170] Xia L, Ng S, Han R, Tuo X, Xiao G, Leo HL, Cheng T, Yu H. Laminar flow immediate overlay hepatocyte sandwich perfusion system for drug hepatotoxicity testing. *Biomaterials*, **2009**, 30, 5927-5936.
- [171] Dobic SN, Filipovic JM, Tomic SL. Synthesis and characterization of poly(2-hydroxyethyl methacrylate/itaconic acid/poly(ethylene glycol) dimethacrylate) hydrogels. *Chem Eng J*, **2012**, 179, 372-380.
- [172] Rocha A, Hahn M, Liang H. Critical fluid shear stress analysis for cell-polymer adhesion. *J Mater Sci*, **2010**, 45(3), 811-817.
- [173] Gibco® Cascade Biologics™, cell data sheet for HUVECs. Available from: http://tools.lifetechnologies.com/content/sfs/manuals/HUVEC_man.pdf [Accessed on 17th Apr. 2014]
- [174] Miller JS, Stevens KR, Yang MT, Baker BM, Nguyen DH, Cohen DM, Toro E, Chen AA, Galie PA, Yu X, Chaturvedi R, Bhatia SN, Chen CS. Rapid casting of patterned vascular networks for perfusable engineered three-dimensional tissues. *Nat Mater*, **2012**, 11, 768-774.
- [175] Jang KJ, Suh KY. A multilayer microfluidic device for efficient culture and analysis of renal tubular cells. *Lab chip*, **2010**, 10, 36-42.
- [176] Lotz MM, Burdsal CA, Erickson HP, McClay DR. Cell adhesion to fibronectin and tenascin: quantitative measurements of initial binding and subsequent strengthening response. *J Cell Biol*, **1989**, 109, 1795-1805.
- [177] Hahn LHE, Yamada KM. Isolation and characterization of active fragments of the adhesive glycoprotein fibronectin. *Cell*, **1979**, 18, 1043-1051.
- [178] Boonen KJ, Van der Schaft DW, Baaijens FP, Post MJ. Interaction between electrical stimulation, protein coating and matrix elasticity: a complex effect on muscle fibre maturation. *J Tissue Eng Regen Med*, **2011**, 5, 60-68.
- [179] Curtis ASG, Forrester JV. The competitive effects of serum proteins on cell adhesion. *J Cell Sci*, **1984**, 71, 17-35.
- [180] Macosko CW. Rheology: Principles, Measurement and Applications. Wiley-VCH, New York, **1994**, p. 37.
- [181] Yavari A, Marsden JE, Ortiz M. On spatial and material covariant balance laws in elasticity, *J Math Phys*, **2006**, 47, 042903, 1-53.
- [182] Adler JH, Dorfmann L, Han D, MacLachlan S, Pabtsch C. Mathematical and computational models of incompressible materials subject to shear. *IMA J Appl Math*, **2005**, 1-27.
- [183] Ogden RW, Non-Linear Elastic Deformations. Ellis Harwood Ltd., Chichester, Halsted Press, New York, **1984**. pp. 204-222.
- [184] Instron Corporation, Reference Manual for Equipment Series 3300 Load Frames. Available from: <http://www.instron.co.uk/wa/library/StreamFile.aspx?doc=78> [17th Apr. 2014].

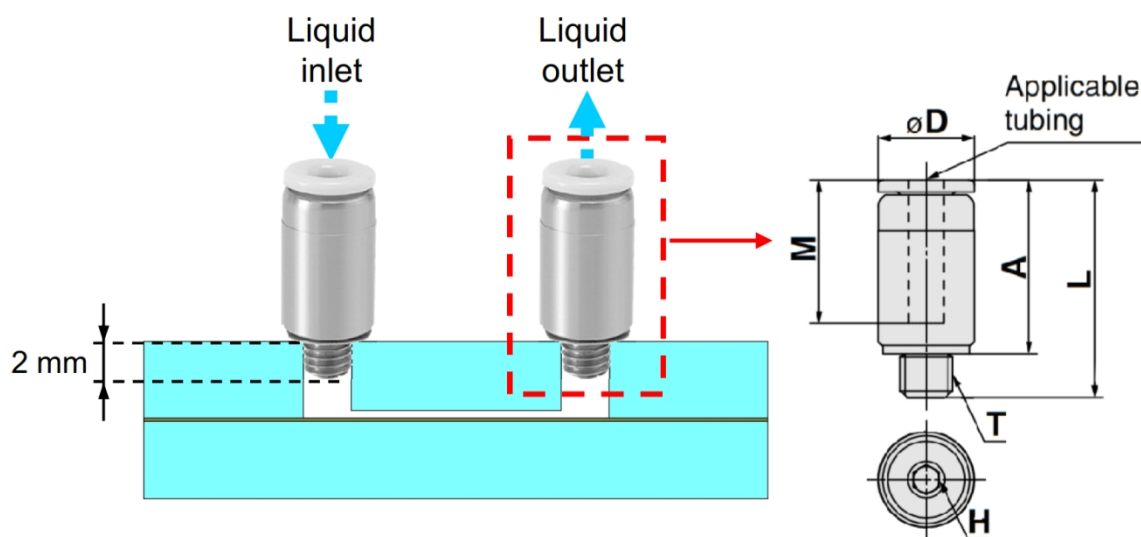
- [185] Beatty MF, Principles of Engineering Mechanics. Springer Science+Business Media Inc., New York, **2006**, pp.151–167.
- [186] Bostan L, Munteanu F, Popa MI, Verestiuc L. Preliminary studies on fatigue analysis of hydrogels based on PHEMA. *Rev Chim (Bucharest)*, **2010**, 61(12), 1235-1238.
- [187] Anssari-Benam A, Bader DL, Screen HRC. A combined experimental and modelling approach to aortic valve viscoelasticity in tensile deformation. *J Mater Sci Mater Med*, **2011**, 22, 253-262.
- [188] Zhang W, Liu S, Wang C, Hu J, Li C, Zhuang Z, Zhou Y, Mathies R, Yang CJ. PMMA/PDMS valves and pumps for disposable microfluidics. *Lab Chip*, **2009**, 9, 3088-3094.
- [189] Liu D, Garimella SV. Investigation on Liquid Flow in Microchannels. *J Thermophys Heat Tr*, **2004**, 18(1), 65-72.
- [190] McDonald JC, Duffy DC, Anderson JR, Chiu DT, Wu H, Schueller OJA, Whitesides GM. Fabrication of microfluidic systems in poly(dimethylsiloxane). *Electrophoresis*, **2000**, 21, 27-40.
- [191] Model type of KJS02-M3 from Automation Distribution Incorporated. Available from: <https://smcpneumatics distributor.com/smc-part-1393/KJS02-M3.html> [Accessed on 30th Sept. 2013].
- [192] Zhao W, Lenardi C, Webb P, Liu C, Santaniello T, Gassa F. A methodology to analyse and simulate mechanical characteristics of poly(2-hydroxyethyl methacrylate) hydrogel. *Polym Int*, **2013**, 62, 1059-1067.
- [193] Handbook of industrial materials. Trade & Technical press LTD. 1st ed. Morden, Surrey, England. **1980**. p344.
- [194] Minsky M. Memoir on Inventing the Confocal Scanning Microscope. *Scanning*, **1988**, 10, 128-138.
- [195] Irgens F. Continuum Mechanics. *Springer Berlin Heidelberg*, **2008**, ISBN: 3-540-74297-2.
- [196] Von Mises R. Mechanik der festen Korper im plastisch deformablen zustand. *Gottin Nachr Math Phys*, **1913**, 1, 582-592.
- [197] Batchelor GK. An Introduction to Fluid Dynamics. Cambridge University Press, Cambridge, UK, **1967**, pp. 211–215.
- [198] Liu D, Garimella SV. Investigation of liquid flow in microchannels. *J Thermophys Heat Tr*, **2004**, 18(1), 65-72.
- [199] Temam R, Navier–Stokes Equations, in *Theory and Numerical Analysis*, American Mathematical Society, Chelsea, **2001**, pp.107–112.
- [200] Masel R. Principles of Adsorption and Reaction on Solid Surfaces. Wiley Interscience, New York. **1996**. p.239-245. ISBN 0471303925.
- [201] BaukalCE, Gershtein VY, Li X. Computational fluid dynamics in industrial combustion. CRC press, **2000**, p.67. ISBN 0849320003

- [202] Menten L, Michaelis MI. Die Kinetic der Invertinwirkung, *Biochem Z*, **1913**, 49, 333-369.
- [203] COMSOL AB, COMSOL Multiphysics User's Guide, version 4.1 COMSOL AB, 2009. Available from 'http://chemelab.ucsd.edu/CAPE/comsol/Comsol_UserGuide.pdf'. [Accessed on 18/04/2014]
- [204] Hill AV. The possible effects of the aggregation of the molecules of haemoglobin on its dissociation curves. *J Physiol*, **1910**, 40, iv-vii.
- [205] Hill AV, The combinations of haemoglobin with oxygen and with carbon monoxide. *Biochem J*, **1913**, 7, 471-480.
- [206] Buchwald P. A local glucose-and oxygen concentration-based insulin secretion model for pancreatic islets. *Theor Biol Med Model*, **2011**, 8(20), 1-25.
- [207] Overview of HPC service of Loughborough University, Available URL: <http://www.lboro.ac.uk/services/it/specialist/hpc/> [accessed on 06/08/2013]
- [208] Foley JE, Cushman SW, Salans LB. Intracellular glucose concentration in small and large rat adipose cells. *Am J Physiol*, **1980**, 238(2), E180-185.
- [209] Tranoudis I, Efron N. Water properties of soft contact lens materials. *Contact Lens & Anterior Eye*, **2004**, 27, 193-208.
- [210] Bashkatov AN, Genina EA, Sinichkin YP, Kochubey VI, Lakodina NA, Tuchin VV. Glucose and mannitol diffusion in human dura mater. *Biophys J*, **2003**, 85(5), 3310-3318
- [211] Li CKN. The glucose distribution in 9L rat brain multicell tumor spheroids and its effect on cell necrosis. *Cancer*, **1982**, 50(10), 2066-2073.
- [212] Casiari JJ, Sotirchos SV, Sutherland RM. Glucose diffusivity in multicellular tumor spheroids. *Cancer Res*, **1988**, 48, 3905-3909.
- [213] Busemeyer J, Vaupel JP, Thews G. Diffusion coefficients of glucose in tumor tissue. *Pflugers Arch*. **1977**, 386, R17.
- [214] Freyer JP and Sutherland RM. Determination of apparent diffusion constants for metabolites in multicellular tumor spheroids. *Adv Exp Med Biol*, **1983**, 159, 463-475.
- [215] Zhang F, Tian J, Wang L, He P, Chen Y. Correlation between cell growth rate and glucose consumption determined by electrochemical monitoring. *Sensor Actuator B*, **2011**, 156, 416-422.
- [216] Voulgaris I, O'Donnell A, Harvey LM, McNeil B. Inactivating alternative NADH dehydrogenases: enhancing fungal bioprocesses by improving growth and biomass yield. *Sci Rep*, **2012**, 2, 322.
- [217] Korin N, Bransky A, Dinnar U, Levenberg S. Periodic "flow stop" perfusion microchannel bioreactors for mammalian and human embryonic stem cell long-term culture. *Biomed Microdevices*, **2009**, 11, 87-94.

- [218] Shah P, Vedarethinam I, Kwasyn D, Andresen L, Dimaki M, Skov S, Svendsen WE. Microfluidic bioreactors for culture of non-adherent cells. *Sensor Actuator B*, **2011**, 156, 1002-1008.
- [219] Liu Q, Hedberg EL, Liu Z, Bahulekar R, Meszlenyi RK, Mikos AG. Preparation of macroporous poly(2-hydroxyethyl methacrylate) hydrogels by enhanced phase separation. *Biomaterials*, **2000**, 21, 2163-2169.
- [220] Horak D. Application of poly(2-hydroxyethyl methacrylate) in Medicine, pp.155-191. In *Leading Edge Research on Polymers and Composites*, edited by Monakov YB, Zaikov GE, Dalinkevich AA. Nova Science Publishers, New York. **2004**, p.157. ISBN 1-59033-975-4.

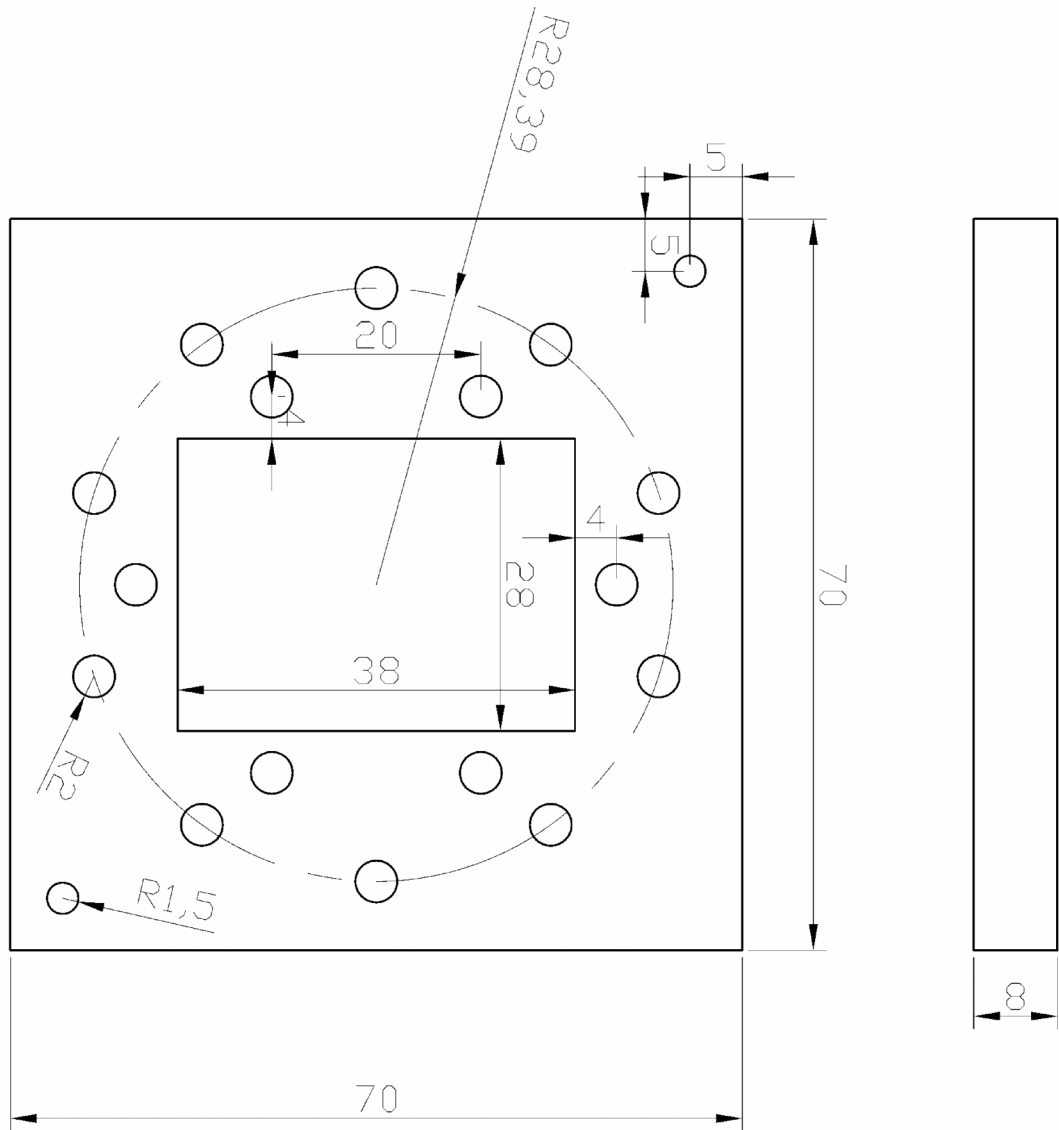
Appendices 1: Dimensions of Connector and Chips

A1.1 Dimensions of connector

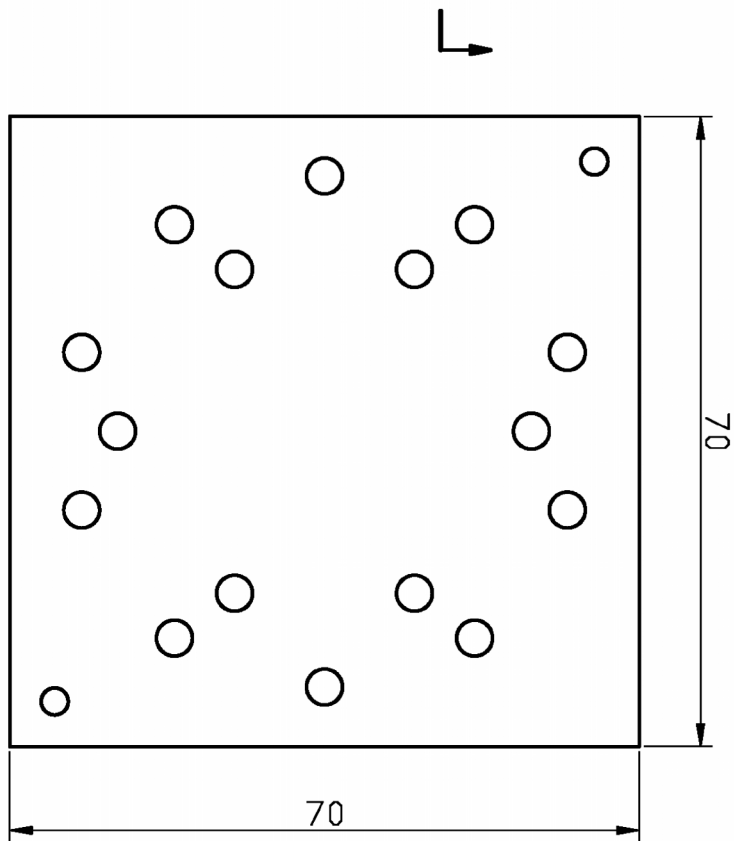
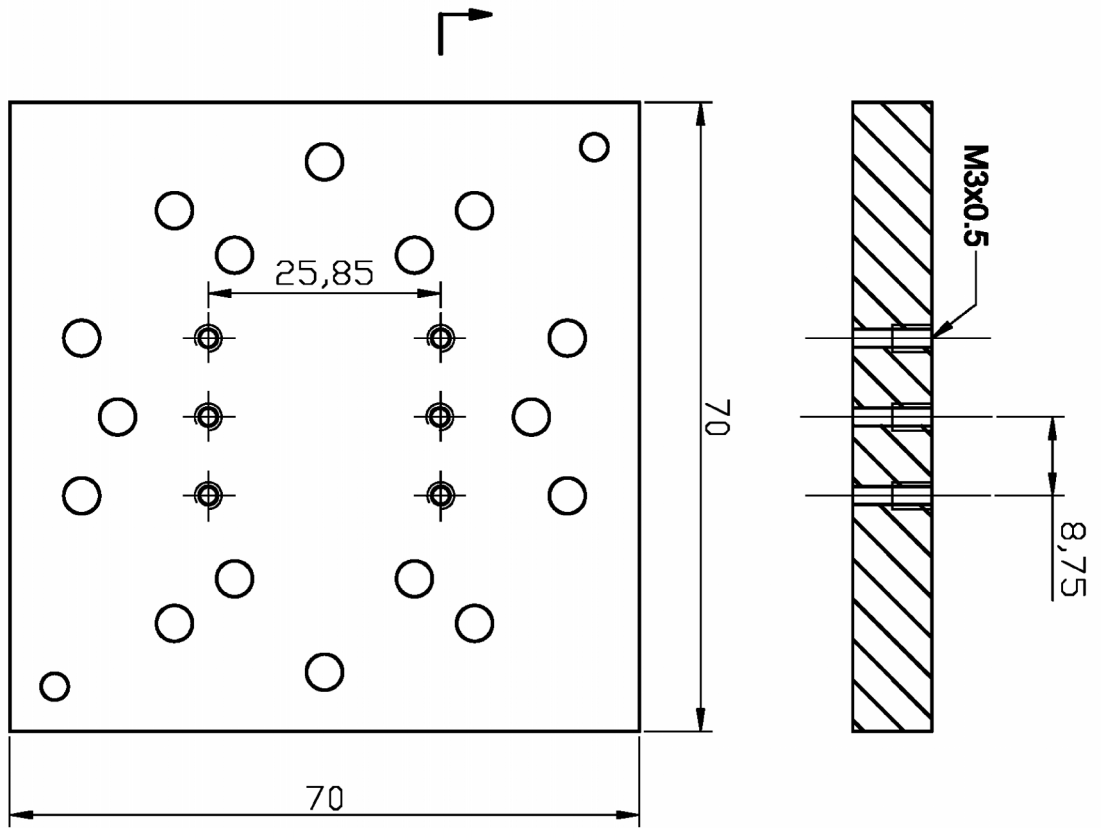


Items	Info.
Applicable tubing. O.D. [mm]	2
Model	KJS02-M3
Connection thread, T [mm]	M3 x 0.5
Width across flats, H [mm]	1.5
Ø D [mm]	5.5
L [mm]	12.5
A [mm]	10
M [mm]	8.8
Effective area [mm ²]	0.9
Weight [g]	1.1

A1.2 Dimensions of Aluminium Rig



A1.3 Dimensions of PMMA Layers



Appendix 2: Calibration Certificate for Compressive Testing Machine

CERTIFICATE OF CALIBRATION ISSUED BY: INSTRON CALIBRATION LABORATORY CERTIFICATE NUMBER: E125052511113337



0019



Instron Calibration Laboratory
 Coronation Road
 High Wycombe, Buckinghamshire HP12 3SY
 Telephone: +44 (0) 1494 456815
 Fax: +44 (0) 1494 456667
 Email: Calibration_Europe@Instron.com

Page 1 of 4 pages

APPROVED SIGNATORY

Digitally signed by Colin Easden
 Reason: I am approving this document
 Date: 2011.05.25 18:13:29 +01'00'

Type of Calibration: Force
Relevant Standard: ISO 7500-1: 2004
Date of Calibration: 25-May-11

Customer

Name: Loughborough University
 Location: Wolfson School, Mechanical&Manufacturing Engineering, Ashby Road
 Loughborough, Leicestershire LE11 3TU
 Country: UK
 Ambient Temperature: 21.9 °C
 P.O./Contract No.: 197210
 Contact: Mr.A.Sandaver Email: a.p.sandaver@lboro.ac.uk

Machine

Manufacturer: Instron
 System ID: 3366J7196
 Type: Electro-Mechanical
 Single Range
 Year of Mfg.: 2004

Transducer

Manufacturer: Instron
 Transducer ID: 2530-443/45147
 Capacity: 10 kN
 Type: Tension/Compression

Classification

The above testing machine has been verified with the indicators and in the modes shown below for increasing force only to ISO 7500-1 using verification equipment calibrated to ISO 376.

Indicator 1. - Digital Readout: Bluehill V2.15 Software (kN)

Range Full Scale (%)	Tested Force Range (kN)	Mode	System Class *
100	0.10375936 to 10.05495	Tension	0.5
	-0.1045002 to -10.12263	Compression	0.5

* System Class for a range is derived from assessment of the following: error, repeatability, return to zero, resolution and proving device classification.

Method of Verification

The calculation of accuracy and repeatability error and the classification of the testing machine's performance was carried out in accordance with the method specified in Annex C of ISO 7500-1.
 The testing machine was verified in the 'as found' condition.

Prior to verification, the machine was inspected for good working order and was found to satisfy the guidelines of section 5 of

Instron CalproCR Version 3.21

This certificate is issued in accordance with the laboratory accreditation requirements of the United Kingdom Accreditation Service. It provides traceability of measurements to recognized national standards, and to units of measurement realized at the National Physical Laboratory or other recognized national standards laboratories. This certificate may not be reproduced other than in full, except with the prior written approval of the issuing laboratory. UKAS is one of the signatories of the International Laboratory Accreditation Cooperation (ILAC) Arrangement for mutual recognition of calibration certificates.

CERTIFICATE OF CALIBRATION

UKAS ACCREDITED CALIBRATION LABORATORY No. 0019

CERTIFICATE NUMBER:
E125052511113337

Page 2 of 4 pages

ISO 7500-1.

No mechanically linked accessories were fitted whilst performing this calibration.

Data Summary - Indicator 1. - Digital Readout: Bluehill V2.15 Software (kN)

TENSION

% of Range	Run 1 Error (%)	Run 2 Error (%)	Run 3 Error (%)	Repeatability Error (%)	Class	Relative Uncertainty* (%)	Uncertainty of Measurement* (± kN)
100% Range (Full Scale: 10.05495 kN)							
0 Return					0.5		
1	0.42	0.42	0.33	0.09	0.5	0.23	0.000
2	0.44	0.41	0.36	0.08	0.5	0.22	0.000
5	0.37	0.38	0.36	0.02	0.5	0.22	0.001
5	0.40	0.43	0.42	0.03	0.5	0.22	0.001
10	0.34	0.43	0.36	0.09	0.5	0.23	0.002
20	0.32	0.35	0.33	0.03	0.5	0.22	0.004
40	0.29	0.31	0.32	0.03	0.5	0.22	0.009
60	0.30	0.29	0.30	0.01	0.5	0.22	0.013
80	0.26	0.29	0.27	0.03	0.5	0.22	0.017
100	0.26	0.25	0.30	0.05	0.5	0.22	0.022

Data Summary - Indicator 1. - Digital Readout: Bluehill V2.15 Software (kN)

COMPRESSION

% of Range	Run 1 Error (%)	Run 2 Error (%)	Run 3 Error (%)	Repeatability Error (%)	Class	Relative Uncertainty* (%)	Uncertainty of Measurement* (± kN)
100% Range (Full Scale: -10.12263 kN)							
0 Return					0.5		
1	-0.04	0.19	0.21	0.25	0.5	0.28	0.000
2	0.04	0.19	0.19	0.15	0.5	0.24	0.000
5	0.18	0.30	0.30	0.12	0.5	0.23	0.001
5	0.41	0.38	0.37	0.04	0.5	0.22	0.001
10	0.44	0.42	0.37	0.07	0.5	0.23	0.002
20	0.36	0.36	0.35	0.01	0.5	0.22	0.004
40	0.37	0.36	0.37	0.01	0.5	0.22	0.009
60	0.36	0.36	0.36	0.00	0.5	0.22	0.013
80	0.34	0.35	0.37	0.03	0.5	0.22	0.017
100	0.33	0.37	0.38	0.05	0.5	0.22	0.022

Worst Resolution Class: 0.5 for 100% Range (Indicator 1: Tension), 0.5 for 100% Range (Indicator 1: Compression).

* The reported expanded uncertainty is based on a standard uncertainty multiplied by a coverage factor $k = 2$, providing a level of confidence of approximately 95%.

The uncertainty stated refers to values obtained during the calibration and makes no allowances for factors such as long term drift, temperature and alignment effects - the influence of such factors should be taken into account by the user of the force-measuring device.

The uncertainty evaluation has been carried out in accordance with UKAS requirements.

Instron CalproCR Version 3.21

CERTIFICATE OF CALIBRATION

UKAS ACCREDITED CALIBRATION LABORATORY No. 0019

CERTIFICATE NUMBER:

E125052511113337

Page 3 of 4 pages

Data - Indicator 1. - Digital Readout: Bluehill V2.15 Software (kN)

TENSION

% of Range	Run 1		Run 2		Run 3	
	Indicated (kN)	Applied (kN)	Indicated (kN)	Applied (kN)	Indicated (kN)	Applied (kN)
100% Range (Full Scale: 10.05495 kN)						
0 Return	-0.0011		-0.0013		-0.0018	
1	0.1042	0.103759360	0.1048	0.104360080	0.1183	0.117911320
2	0.2045	0.203614040	0.2015	0.200680520	0.2025	0.20176683
5	0.5048	0.50295282	0.5047	0.502797630	0.4938	0.492024720
5	0.5186	0.516538	0.5131	0.51092	0.5950	0.59254
10	1.084	1.080299	1.021	1.016646	1.046	1.042298
20	2.002	1.995662	2.036	2.028999	2.011	2.004301
40	4.143	4.130926	4.074	4.061337	4.034	4.021269
60	6.077	6.059119	6.098	6.080637	6.293	6.274193
80	8.115	8.093789	7.996	7.973002	8.030	8.008353
100	9.944	9.917837	10.08	10.054948	10.01	9.979847

Data - Indicator 1. - Digital Readout: Bluehill V2.15 Software (kN)

COMPRESSION

% of Range	Run 1		Run 2		Run 3	
	Indicated (kN)	Applied (kN)	Indicated (kN)	Applied (kN)	Indicated (kN)	Applied (kN)
100% Range (Full Scale: -10.12263 kN)						
0 Return	0.0023		0.0012		-0.0012	
1	-0.1055	-0.105546500	-0.1047	-0.10450025	-0.1073	-0.10707834
2	-0.2048	-0.204725370	-0.2164	-0.215993880	-0.1996	-0.199218770
5	-0.4956	-0.494722950	-0.5028	-0.501280810	-0.5000	-0.49849748
5	-0.5126	-0.510496	-0.5050	-0.503076	-0.5156	-0.513676
10	-1.018	-1.013519	-1.063	-1.058516	-1.016	-1.0123
20	-2.007	-1.999849	-2.026	-2.018717	-2.004	-1.99704
40	-4.047	-4.032081	-4.071	-4.056355	-4.021	-4.006217
60	-6.088	-6.066115	-6.045	-6.023291	-6.027	-6.005218
80	-7.999	-7.971677	-8.054	-8.026002	-8.048	-8.018476
100	-9.993	-9.95976	-10.16	-10.122629	-10.11	-10.071908

Verification Equipment

Equipment ID	Description	Capacity	Cal Date	Cal Due	Certificate Ref.
NHT29	temp. indicator	NA	16-Feb-11	17-Feb-12	20110216B
R85-060	force indicator	NA	08-Jul-09	09-Jul-11	0478/2009070004
N81-10K	load cell	10 kN	06-Apr-11	07-Apr-13	0157/11031583
N81-1K	load cell	1000 N	04-Apr-11	05-Apr-13	0157/11031582

The class of the verification equipment was equal to or better than the class to which this testing machine has been verified.

The average temperature of the equipment during verification was 22.3°C.

CERTIFICATE OF CALIBRATION

UKAS ACCREDITED CALIBRATION LABORATORY No. 0019

CERTIFICATE NUMBER:

E125052511113337

Page 4 of 4 pages

Verification Equipment Usage

Range Full Scale (%)	Equipment ID	Mode	Percent(s) of Range
100	N81-10K	Tension	5/10/20/40/60/80/100
100	N81-1K	Tension	1/2/5
100	N81-10K	Compression	5/10/20/40/60/80/100
100	N81-1K	Compression	1/2/5

Comments

No Comments

Verified by: Chris White
Field Service Engineer

NOTE: Clause 9 of ISO 7500-1 states; The time between verifications depends on the type of testing machine, the standard of maintenance and the amount of use. Unless otherwise specified, it is recommended that verification be carried out at intervals not exceeding 12 months. The machine shall in any case be verified if it is moved to a new location necessitating dismantling or if it is subject to major repairs or adjustments.

The Instron Calibration Laboratory is accredited by UKAS to BS/EN/ISO 17025 (General Requirements for the competence of testing and calibration laboratories) to undertake the calibration reported on this certificate.

Appendix 3: Chemicals Sheets

A3.1 HEMA

A3.2 EGDMA

A3.3 TEMED

A3.4 APS

SAFETY DATA SHEET

according to Regulation (EC) No. 1907/2006

Version 4.2 Revision Date 27.09.2011

Print Date 18.10.2011

1. IDENTIFICATION OF THE SUBSTANCE/MIXTURE AND OF THE COMPANY/UNDERTAKING

1.1 Product identifiers

Product name : 2-Hydroxyethyl methacrylate

Product Number : 477028

Brand : Aldrich

CAS-No. : 868-77-9

1.2 Relevant identified uses of the substance or mixture and uses advised against

Identified uses : Laboratory chemicals, Manufacture of substances

1.3 Details of the supplier of the safety data sheet

Company : Sigma-Aldrich Company Ltd.
The Old Brickyard
NEW ROAD, GILLINGHAM
Dorset
SP8 4XT
UNITED KINGDOM

Telephone : +44 (0)1747 833000

Fax : +44 (0)1747 833313

E-mail address : eurtechserv@sial.com

1.4 Emergency telephone number

Emergency Phone # : +44 (0)1747 833100

2. HAZARDS IDENTIFICATION

2.1 Classification of the substance or mixture

Classification according to Regulation (EC) No 1272/2008 [EU-GHS/CLP]

Skin irritation (Category 2)

Eye irritation (Category 2)

Skin sensitization (Category 1)

Classification according to EU Directives 67/548/EEC or 1999/45/EC

May cause sensitization by skin contact. Irritating to eyes and skin.

2.2 Label elements

Labelling according Regulation (EC) No 1272/2008 [CLP]

Pictogram



Signal word

Warning

Hazard statement(s)

H315

Causes skin irritation.

H317

May cause an allergic skin reaction.

H319

Causes serious eye irritation.

Precautionary statement(s)

P280

Wear protective gloves.

P305 + P351 + P338

IF IN EYES: Rinse cautiously with water for several minutes. Remove contact lenses, if present and easy to do. Continue rinsing.

SAFETY DATA SHEET

according to Regulation (EC) No. 1907/2006

Version 4.1 Revision Date 29.10.2010

Print Date 17.10.2011

1. IDENTIFICATION OF THE SUBSTANCE/MIXTURE AND OF THE COMPANY/UNDERTAKING

Product name : Ethylene glycol dimethacrylate

Product Number : 335681
Brand : Aldrich

Company : Sigma-Aldrich Company Ltd.
The Old Brickyard
NEW ROAD, GILLINGHAM
Dorset
SP8 4XT
UNITED KINGDOM

Telephone : +44 (0)1747 833000
Fax : +44 (0)1747 833313
Emergency Phone # : +44 (0)1747 833100
E-mail address : eurtechserv@sial.com

2. HAZARDS IDENTIFICATION

Classification of the substance or mixture

According to Regulation (EC) No1272/2008

Skin sensitization (Category 1)

Specific target organ toxicity - single exposure (Category 3)

According to European Directive 67/548/EEC as amended.

May cause sensitization by skin contact. Irritating to respiratory system.

Label elements

Pictogram



Signal word

Warning

Hazard statement(s)

H317

May cause an allergic skin reaction.

H335

May cause respiratory irritation.

Precautionary statement(s)

P261

Avoid breathing dust/ fume/ gas/ mist/ vapours/ spray.

P280

Wear protective gloves.

Hazard symbol(s)

Xi

Irritant

R-phrases(s)

R37

Irritating to respiratory system.

R43

May cause sensitization by skin contact.

S-phrases(s)

S24

Avoid contact with skin.

S37

Wear suitable gloves.

Other hazards - none

SAFETY DATA SHEET

according to Regulation (EC) No. 1907/2006

Version 4.1 Revision Date 08.04.2011

Print Date 17.10.2011

1. IDENTIFICATION OF THE SUBSTANCE/MIXTURE AND OF THE COMPANY/UNDERTAKING

1.1 Product identifiers

Product name : *N,N,N',N'*-Tetramethylethylenediamine

Product Number : 411019
Brand : Aldrich
Index-No. : 612-103-00-3
CAS-No. : 110-18-9

1.2 Relevant identified uses of the substance or mixture and uses advised against

Identified uses : Laboratory chemicals, Manufacture of substances

1.3 Details of the supplier of the safety data sheet

Company : Sigma-Aldrich Company Ltd.
The Old Brickyard
NEW ROAD, GILLINGHAM
Dorset
SP8 4XT
UNITED KINGDOM

Telephone : +44 (0)1747 833000
Fax : +44 (0)1747 833313
E-mail address : eurtechserv@sial.com

1.4 Emergency telephone number

Emergency Phone # : +44 (0)1747 833100

2. HAZARDS IDENTIFICATION

2.1 Classification of the substance or mixture

Classification according to Regulation (EC) No 1272/2008 [EU-GHS/CLP]

Flammable liquids (Category 2)
Skin corrosion (Category 1B)
Acute toxicity, Inhalation (Category 4)
Acute toxicity, Oral (Category 4)

Classification according to EU Directives 67/548/EEC or 1999/45/EC

Highly flammable. Causes burns. Harmful by inhalation and if swallowed.

2.2 Label elements

Labelling according Regulation (EC) No 1272/2008 [CLP]

Pictogram



Signal word : Danger

Hazard statement(s)

H225 : Highly flammable liquid and vapour.
H314 : Causes severe skin burns and eye damage.
H302 : Harmful if swallowed.
H332 : Harmful if inhaled.

SAFETY DATA SHEET

according to Regulation (EC) No. 1907/2006

Version 4.0 Revision Date 12.03.2010

Print Date 17.10.2011

1. IDENTIFICATION OF THE SUBSTANCE/MIXTURE AND OF THE COMPANY/UNDERTAKING

Product name : Ammonium persulfate

Product Number : 215589

Brand : Sigma-Aldrich

Company : Sigma-Aldrich Company Ltd.
The Old Brickyard
NEW ROAD, GILLINGHAM
Dorset
SP8 4XT
UNITED KINGDOM

Telephone : +44 (0)1747 833000

Fax : +44 (0)1747 833313

Emergency Phone # : +44 (0)1747 833100

E-mail address : eurtechserv@sial.com

2. HAZARDS IDENTIFICATION

Classification of the substance or mixture

According to Regulation (EC) No1272/2008

Oxidizing solids (Category 3)

Acute toxicity (Category 4)

Eye irritation (Category 2)

Specific target organ toxicity - single exposure (Category 3)

Skin irritation (Category 2)

Respiratory sensitization (Category 1)

Skin sensitization (Category 1)

According to European Directive 67/548/EEC as amended.

Contact with combustible material may cause fire. Harmful if swallowed. Irritating to eyes, respiratory system and skin. May cause sensitization by inhalation and skin contact.

Label elements

Pictogram



Signal word

Danger

Hazard statement(s)

H319

Causes serious eye irritation.

H315

Causes skin irritation.

H272

May intensify fire; oxidiser.

H302

Harmful if swallowed.

H317

May cause an allergic skin reaction.

H334

May cause allergy or asthma symptoms or breathing difficulties if inhaled.

H335

May cause respiratory irritation.

Precautionary statement(s)

P220

Keep/Store away from clothing/ combustible materials.

P261

Avoid breathing dust/fume/gas/mist/vapours/spray.

P280

Wear protective gloves.